

**Catalysed epoxy-sebacic acid
vitrimers: cure kinetics and their
potential for sustainability of
crosslinked polymers**

A thesis submitted to the University of Manchester for the degree of Doctor of
Philosophy in the Faculty of Science and Engineering

2020

QUENTIN-ARTHUR AIMÉ POUTREL

**SCHOOL OF NATURAL SCIENCES,
DEPARTMENT OF MATERIALS**

TABLE OF CONTENTS

Table of Contents	2
List of Figures (Chapters).....	8
List of Figures (Appendices)	17
List of Schemes (Chapters).....	21
List of Schemes (Appendices).....	21
List of Tables (Chapters).....	22
List of Tables (Appendices)	23
List of Equations (Chapters)	24
List of Equations (Appendices).....	24
GLOSSARY.....	25
LIST OF SYMBOLS AND PARAMETERS	28
ABSTRACT.....	29
DECLARATION.....	30
COPYRIGHT STATEMENT	31
ACKNOWLEDGEMENTS	32
THE AUTHOR	34
Chapter 1. Introduction.....	35
1.1 Background.....	35
1.1.1 Epoxy resins: interests and limitations.....	35
1.1.2 Development of reprocessable and healable polymers.....	36
1.1.3 Interest in nanoparticles for enhanced epoxy matrices.....	37
1.1.4 The surge for sustainable solutions.....	37
1.2 Aims and objectives.....	38
1.3 Thesis outline.....	39
1.4 References	42

Chapter 2.	Literature review	45
2.1	Layout of the literature review.....	45
2.2	Vitrimer origin and concept.....	45
2.2.1	Supramolecular networks - Reversible but not covalently bonded crosslinks.....	45
2.2.2	Reversible and covalently bonded crosslinks: dissociative and associative networks.....	47
2.3	Engineering vitrimers.....	49
2.4	Characterisation of vitrimer materials	50
2.4.1	Properties that define vitrimers	50
2.4.2	Additional properties.....	54
2.5	Catalyst based vitrimers	56
2.5.1	Transesterification.....	56
2.5.2	Other catalyst based vitrimer chemistry	64
2.6	Catalyst free vitrimer	65
2.6.1	Transamination.....	65
2.6.2	Imine.....	67
2.6.3	Transalkylation - ionic vitrimers	68
2.6.4	Disulphide metathesis	69
2.6.5	Ester boronic - transesterification and dioxaborolane metathesis.....	71
2.6.6	Transesterification.....	72
2.6.7	Silyl ether chemistry	73
2.6.8	Concluding remarks on vitrimer chemistry and research motivation for the first experimental chapter (Chapter 3).....	74
2.7	Nanocomposites in chemically crosslinked networks	76
2.7.1	The drive towards graphene nanoparticles as fillers	76
2.7.2	Nanoreinforcements in vitrimers - graphene and other nanoparticles	77
2.7.3	Recycling of reinforcement from epoxy composites using vitrimer properties.....	90
2.7.4	Concluding remarks on nanocomposites and research motivation for the 2 nd experimental chapter (Chapter 4).....	93
2.8	“Bio-based” vitrimer and enzymatic catalysis	95
2.8.1	Sustainable vitrimers	96
2.8.2	Enzymatic catalysis - an interesting candidate.....	102
2.8.3	Concluding remarks on sustainable vitrimers and research motivation for the third experimental chapter (Chapter 5).....	108
2.9	Timeline resuming key points of this literature review in the development of vitrimer chemistry and key points for development of this thesis	109
2.10	Conclusion to the literature review.....	110

2.11	References.....	112
Chapter 3.	Dicarboxylic acid-epoxy vitrimers: influence of the off-stoichiometric acid content on cure reactions and thermo-mechanical properties.....	125
	Abstract.....	125
	Graphical abstract.....	126
3.1	Background.....	126
3.2	Materials and methods	128
3.2.1	Sample preparation	129
3.2.2	IR monitoring of the curing process	130
3.2.3	Swelling and soluble fraction.....	130
3.2.4	Mechanical test methods	131
3.3	Results	131
3.3.1	Swelling and soluble fraction analysis	139
3.3.2	Mechanical properties at small and large deformations	140
3.3.3	Stress relaxation of epoxy vitrimers	142
3.3.4	Creep behaviour of epoxy vitrimers	144
3.4	Conclusions.....	146
3.5	Conflicts of interest	147
3.6	Acknowledgement.....	147
3.7	References.....	148
Appendix A.	Supplementary information - Chapter 3.....	154
A.1.	Manufacture of vitrimer networks - mixing, mould casting, degassing and curing.....	154
A.2.	IR analysis method.....	155
A.2.1.	Data collection	155
A.2.2.	Carbonyl peaks assignment	156
A.2.3.	Integration of signals	157
A.2.4.	Complementary FTIR data	159
A.3.	Dynamic mechanical analysis	160
A.4.	Mechanical results.....	161
A.5.	Stress relaxation results	162
A.6.	Creep results for all samples	164
A.7.	References	165

Chapter 4. Graphene epoxy based vitrimer: From matrix properties enhancement to sustainability via nanoparticles recovery	167
Abstract.....	167
Graphical abstract.....	168
4.1 Introduction.....	168
4.2 Material and methods	170
4.2.1 Materials.....	170
4.2.2 Nanoparticles preparation	170
4.2.3 Sample preparation	171
4.2.4 Nanoparticles recycling	172
4.2.5 Swelling and soluble fraction.....	173
4.2.6 Mechanical test methods	173
4.2.7 Spectral characterisation - XRD, Raman, ATR-FTIR, SEM, and XPS.....	174
4.3 Results and discussions	175
4.3.1 Properties of nanoparticles	175
4.3.2 Properties of nanocomposites	177
4.3.3 Properties of recycled particles	186
4.4 Conclusion	192
4.5 Conflicts of interest	194
4.6 Acknowledgement.....	194
4.7 References	195
 Appendix B. Supplementary information - Chapter 4	 203
B.1. Chemical structure of monomers and nanoparticles used in this study.....	203
B.2. Complementary experimental schematics and equations.....	205
B.3. Complementary data for XPS survey of neat particles.....	205
B.4. Swelling samples before and after being soaked in TCB at 135°C for 7 days.....	206
B.5. Complementary information: FT-IR data	206
B.6. Stress relaxation and Creep data: experimental results	207
B.7. Dynamical mechanical analysis results for nanocomposites samples	211
B.8. Complementary information for tensile results.....	211
B.9. Complementary data for XPS	215
B.10. References	217

Chapter 5. Enzymer: sustainable enzymatic catalysis to produce new supramolecular thermoset quenchable to vitrimer material	219
Abstract.....	219
Graphical abstract.....	220
5.1 Introduction.....	220
5.2 Materials.....	222
5.3 Methods	223
5.3.1 Sample preparation	223
5.3.2 Lipase activity assay.....	223
5.3.3 IR monitoring of the curing process and cured samples	224
5.3.4 Swelling and soluble fraction analysis	224
5.3.5 Dissolution experiment	224
5.3.6 Thermomechanical characterisations	225
5.4 Results and discussion	226
5.4.1 Preliminary information regarding NC sample.....	226
5.4.2 Enzyme activity assay	226
5.4.3 Analysis of network formation via ATR-IR.....	227
5.4.4 Polymer characterisation (general properties)	232
5.4.5 Low temperature characterisation.....	239
5.4.6 High temperature characterisation - determination of vitrimer properties.....	243
5.5 Conclusions.....	248
5.6 References	251
 Appendix C. Supplementary information - Chapter 5	 258
C.1. Analysis of network formation via ATR-IR.....	258
C.1.1. Species evolution with raw enzymes and thermally degraded enzymes (3 wt. %)	258
C.1.2. Mechanism of epoxy ring opening via enzyme active site	259
C.2. Polymer characterisation (general properties)	261
C.2.1. Bi-phase polymer without catalyst and with TDL.....	261
C.3. Supramolecular properties.....	263
C.4. Vitrimer properties.....	264
C.5. References	269

Chapter 6. General conclusions	270
Chapter 7. Further work.....	276
7.1 Dicarboxylic acid-epoxy vitrimers: influence of the off-stoichiometric acid content on cure reactions and thermo-mechanical properties.....	276
7.2 Graphene epoxy based vitrimer: From matrix properties enhancement to sustainability via nanoparticles recovery	277
7.3 Enzymer: sustainable enzymatic catalysis to produce new supramolecular thermoset quenchable to vitrimer material	278

Word count (without appendices): 49 517

Word count (with appendices): 54 329

LIST OF FIGURES (CHAPTERS)

Figure 2-1 Schematic of supramolecular polymer bulk based on urea and mix of fatty acids: The mixture of fatty acid and triacid is condensed with diethylene triamine and reacted with urea. The resulting material possesses hydrogen bond acceptors (red) and donors (green) [4].	47
Figure 2-2 Mechanism of covalent adaptive networks: (a) dissociative, and (b) associative [11].	48
Figure 2-3 A thermo-responsive hetero-Diels-Alder reaction [16].	48
Figure 2-4 Reaction of transesterification between two β -hydroxylesters in an epoxy system - adapted from [14].	50
Figure 2-5 Swelling of first vitrimer network and its swelling ratio at different temperatures [19].	51
Figure 2-6 Stress relaxation experiment of initial vitrimer network and its Arrhenius plot (inset), where the slope defines the energy activation of the network [19].	52
Figure 2-7 a-b [22]: Comparison between shear rheology and creep behaviour for a vitrimer network: a) stress relaxation, b) creep compliance; c) Use of birefringence to observe progressive colour fading in a constrained vitrimer at 180°C corresponding to progressive stress relaxation over 20min [20].	52
Figure 2-8 a) Measurement of T_v of graphene vitrimer network using dilatometry experiment[23], b) measurement of T_v using AIE luminogens technique [26].	54
Figure 2-9 Examples of additional vitrimer properties mentioned; a-d) The hard vitrimer network prepared by Leibler and co-workers [19]: reprocessing <i>via</i> injection moulding (a), tensile results of original and reprocessed dogbone specimens (b), temporary shape changing by heating above T_g (c), definitive shape changing by heating above T_v (d); e) healing of epoxidised soybean oil (ESO) fumaropimaric acid (FPA) vitrimer at 180°C [29].	55
Figure 2-10 Example of shape memory behaviour and re-configurability of a vitrimer (a-c): reconfiguration to a new initial shape above 200°C and new temporary shape above 70°C; (d) Schematic of vitrimer programming [23].	56

Figure 2-11 a) Schematic of transcarbonation exchange with formation of an associative intermediate state after hydroxyl reacts with a carbonate, b) Topology rearrangement undergone by the polycarbonate network <i>via</i> transcarbonation [56].	64
Figure 2-12 a) Scheme of transamination process occurring from 100°C[58], b) reprocessing of phenol-carbamate vitrimers and c) their mechanical properties with comparison of initial and reprocessed networks [59].	66
Figure 2-13 Transimination networks: a) associative pathway, b) dissociative pathway, c) PEO vitrimer network and the impact of different solvents on the BER and network malleability [64].	67
Figure 2-14 a) Proposed associative BER mechanism for ionic vitrimers, with b) a comparison of kinetic model and XPS measurement, c) the proposed dissociative mechanism, with d) the corresponding kinetic model and matching of XPS measurement [69].	69
Figure 2-15 Scheme of polymerisation between an epoxy resin and an aromatic disulphide leading to a vitrimer network with BER along the crosslinker units [72].	70
Figure 2-16 a) Schematic of boronic ester transesterification with impact of neighbouring radical on the reaction speed [75], b) crosslinker used to produce the first boronic ester network [75], c) general metathesis scheme [77], d) dioxarbolane metathesis [77].	72
Figure 2-17 a) Silyl ether-hydroxyl exchange compared to b) direct silyl ether metathesis [89].	73
Figure 2-18 a) Alignment of nanoclays during 3D printing by extrusion method [108], b) alignment of COOH-GNP by hot pressing and healing of cracks [109], c) 1 st cycle printing of epoxy nanoclays vitrimer (above dotted line is before curing, below is after curing): (1) hollow skull, (2) Mayan pyramid, (3) phone case, and d) 4 th cycle printing of epoxy nanoclays vitrimer (above dotted line is before curing, below is after curing) into different shape: (1) crab, (2), puckered ring, (3) gear. Scale bar for printed composites is 1 mm [107].	78
Figure 2-19 a) Concept of surface functionalisation to involve nanoparticle in the BER represented here for epoxy functionalised silica nanoparticles [110], b), stress relaxation at 180°C, c) Arrhenius plot, d) energy activation for the disulphide vitrimer matrix and various functionalisation of silica particles (U: neat particles, EP: epoxy functionalised silica, SH: thiol functionalised silica) [111].	80

Figure 2-20 a-d) Healing of crack performed at 180°C for neat disulphide vitrimer matrix (a), non-functionalised silica (b), EP-silica (c) and SH-silica, the scale bar is 50 μm [111]; e) demonstration of CNT extraction from a disulphide matrix using DMF solution of dithiothreitol as a solvent [27].....81

Figure 2-21 a) Restoration and reversible actuation of deformed dynamic 3D structures of a PDA vitrimer. Scale bar: 0.5 cm. (b-e) Examples of different dynamic 3D structures achieved by 2-layered structures. Blank vitrimer films were welded with PDA-NPs vitrimer into different shapes: Light intensity: 1.0 W cm^{-2} . Scale bar: 1 cm [117].83

Figure 2-22 Silver nanowire triboelectric nanogenerator: a) Percolated silver nanowires network embedded in disulphide vitrimer, b) Strategy applied to test healing capacity, c-e) Broken sample optical characterisation (Picture, microscope and SEM), g-i) symmetric characteristic for healed sample, j-i) Electrical performances of original (black) and healed (red) sample [120].....84

Figure 2-23 a) Schematic of the dissolution process for transesterification vitrimer *via* alcohol (EG), b) Normalised weight of vitrimer as function of soaking time for vitrimer samples at 25°C and 180°C, and the non-vitrimer control sample (0% catalyst), c) The residual weight of vitrimer after being soaked for 4 h at 180°C as function of EG weight [130].91

Figure 2-24 a) SEM images of a) original carbon fibres fabric, b) recycled one, c) strain-stress curves of original (blue) carbon fibres fabric and recycled (red), d) strain-stress curve of original (solid black), recycled (dashed blue) and repaired (dashed red) composites, e) mechanical properties of composites over 4 cycles of recycling [130].92

Figure 2-25 a) Tensile properties of original epoxy network (EP, solid black curve), an epoxy sample containing 5% of re-polymerised network (REP5 dashed red curve), and an epoxy sample containing 20% of re-polymerised network (REP20 dotted blue curve), b) DMA results for the same samples [128].93

Figure 2-26 a) Production of eugenol-epoxy monomers, b) Reaction of transesterification in highly branched ester network from eugenol-epoxy and succinic anhydride, c) stress relaxation of the 3 ratio studied, and d) stress relaxation of ratio 1:0.5 at different temperatures [137].97

Figure 2-27 a) General mechanism of reaction between epoxy and anhydride monomers, at the end of the reaction (3rd step) the remaining hydroxyl initiates the opening of a new

anhydride leading to a highly branched network with few hydroxyl groups, b) homopolymerisation of epoxy happening in epoxy excess after the esterification reaction, leaving pendant hydroxyl groups in the cured network [138].98

Figure 2-28 a) Schematic of triepoxy and anhydride hardener monomers cured with a Zn catalyst and mechanism of transesterification in the cured network, b) Stress relaxation of the different ratio prepared for the study at 220°C, c) FTIR spectrum of different ratios with the highest hydroxyl content recorded for 1:0.5 ratio, and d) TGA measurement of the different ratios - the black dotted line has been added to show the initial point of degradation reported for the ratio 1:1 [139].99

Figure 2-29 a) Poly(ethylene glycol) lignin-based vitrimer coating dissolution after 10 min in a 0.1 M NaOH solution for ratio 1:1 and 1:1.2 [28], b) epoxidised sebacic acid lignin-based vitrimer rebinding capacity showing a cohesive fracture, c) mechanical results of lap-shear test after 1st and 2nd bonding [134].100

Figure 2-30 The different reactions catalysed by lipases [148]: I - Hydrolysis of ester (used in biodiesel industry), II - a) Esterification reactions (esterification, amidation, and thioesterification), b) Transesterification reactions (acidolysis, aminolysis, alcoholysis and interesterification).103

Figure 2-31 a) formation of multimeric cluster rich in cationic units able to fix themselves on anionic support; addition of PEI stabilise these clusters onto the substrate, b) Formation of multilayered structure by crosslinking lipases' backbones with PEI [153].105

Figure 2-32 Schematic of epoxy - dicarboxylic anhydrides polymerised by lipases [165].107

Figure 2-33 Schematic of proposed mechanism of epoxy hydrolysis by lipases: In the first the tyrosine amino-acids polarise the oxygen of the epoxy *via* hydrogen bonding facilitating the nucleophilic attack from Asp₃₃₃. Then the activated molecules of water finish the hydrolysis and recover the enzyme active site to restart a new cycle [166].107

Figure 2-34 Timeline overview of the vitrimer development covered in this literature - the top section represents some key studies which were a deciding factor in the development of this thesis; the bottom section represents key studies in the progress of vitrimers as represented in this document.109

Figure 3-1 ATR-FTIR spectral curve of the 100H5CAT sample at the beginning (red curve) and at the end of the reaction (blue curve). The labelled peaks correspond to: (1) C=O stretching of ester related to the polymer network, (2) C=O stretching of sebacic acid, (3)

C-O-C signature of the ether, (4) asymmetric epoxy deformation. The numbers indicate signal integration intervals, see the Appendix A for details of identification and integration procedure.	132
Figure 3-2 Evolution of species for different ratios of polymer network: a) and b) 100H5CAT, c) and d) 30H5CAT. Measurements were performed for 60 min at 125°C; Y-scales for each signal correspond to the values of ATR peak integrals (without normalisation, see Figure 3-1 and Appendix A for details).	133
Figure 3-3 Evolution of IR signals of a reactive composition containing a (100:30) molar excess of epoxy and 5 mol% of 2-PI as the catalyst a) ester and acid signals, b) ether and epoxy signals. Same Y-scales as Figure 3-2.	137
Figure 3-4 Swelling experiment to confirm crosslinking of the structure, mass increase (blue) and mass fraction of the soluble part (green).	139
Figure 3-5 a) Storage moduli for different ratios, obtained by DMA measurements; b) damping response of tested samples.	140
Figure 3-6 Tensile behaviour obtained with ASTM 638 type IV samples. a) Typical stress/strain curves obtained for each epoxy:acid ratio, b) bar chart and curve comparing Young's moduli and tensile strengths of the samples.	141
Figure 3-7 Stress relaxation at different temperatures for three different epoxy/acid ratios: a) 75H5CAT, b) 60H5CAT, and c) 30H10CAT.	143
Figure 3-8 Creep behaviour for different temperatures and three different epoxy/acid ratios: a) 75H5CAT, b) 60H5CAT, and c) 30H10CAT.	145
Figure 3-9 Arrhenius plot from a) stress relaxation and b) creep data of vitrimers with two different epoxy/acid ratios.	146
Figure 4-1 Schematic of the manufacture process to make GNP/GO/GPTS-GO/rGO samples. Neat samples was made from step 3 (Mixing at 250rpm for 24 h) of the process. Adapted from [56].	172
Figure 4-2 Schematic of the process to recycle graphene based nanoparticles from a vitrimer matrix. Adapted from [56].	173
Figure 4-3 Wide survey XPS spectra of neat particles used in this study (GNP, GO, GPTS-GO, and rGO).	175
Figure 4-4 XRD pattern of neat particles used in this study - graphitic impurity of GO and GPTS-GO are indicated by dashed circle.	176

Figure 4-5 XRD pattern of manufactured nanocomposites: a) GNP samples, b) GO samples, c) GPTS-GO samples and, d) rGO samples – Red dotted lines shows the trend of amorphous polymer shift peak for nanocomposites samples, Purple dotted lines shows the position of the top of the amorphous peak of the neat vitrimer, (002) plan is shown by dashed circle; for colours code, reader should refer to online version of this thesis.177

Figure 4-6 Soluble fraction of nanocomposites compared to swelling ratio of vitrimer without nano-reinforcement (purple dotted line) - samples were left at 135°C in TCB for 7 days.179

Figure 4-7 Stress relaxation of different nanocomposites: a) relaxation of 1wt. % samples compared to neat vitrimer at 180°C, b) Relaxation time τ for all samples at 160°C and 180°C, y axis is at log scale, c) Arrhenius plot for GO samples and neat vitrimer, and d) bar chart of activation energy for all nanocomposites compared to neat vitrimer (purple dotted line).181

Figure 4-8 Relaxation time of nanocomposites divided by their own Young's modulus: a) Standard scale, b) y axis in log scale for comparison. 01GO time of relaxation at 180°C is not visible due to its small value (49 s).182

Figure 4-9 DMA results for all samples compared to raw vitrimer: a) GNP samples, b) GO samples, c) GPTS-GO samples, and d) rGO samples.184

Figure 4-10 Young's modulus of nanocomposites calculated between 60-100% strain...185

Figure 4-11 a) Breaking strain of nanocomposites, b) Ultimate strength of nanocomposites - smaller dotted line have been added for the UTS of neat vitrimer to show that lower UTS of nanocomposites (01GO and 05GO) are included in the measured errors of the neat vitrimer's UTS.185

Figure 4-12 High-resolution core-level C_{1s} of original and recycled nanoparticles: a) original GNP, b) recycled GNP, c) original GO, d) recycled GO, e) original GPTS-GO, f) recycled GPTS-GO, g) original rGO, h) recycled rGO - for colours code, reader should refer to online version of this thesis.188

Figure 4-13 XRD patterns for original and recycled nanoparticles: a) GNP, b) GO, c) GPTS-GO and, d) rGO.189

Figure 4-14 Raman spectrum of original and recycled nanoparticles: a) GNP, b) GO, c) GPTS-GO and d) rGO.191

Figure 5-1 UV-Vis spectrum of lipase TL and thermally degraded lipase (TDL) - curve of lipases without NPP have been represented to show that no activity can be recorded without the use of NPP - adapted from [46].227

Figure 5-2 Evolution of ester (red square curve) and epoxy signature (diamond green curve) obtained via ATR-IR for: a) TL3 sample and, b) TDL sample. Values were normalised by the benzene epoxy peak located between 1490-1526 cm^{-1}228

Figure 5-3 Evolution of acid (blue triangle curves) and ether species (purple circle curves) for TL3 sample (a, c) and TDL sample (b, d). The black dotted line represents the maximum peak of acid species and corresponding time in the ether signature evolution. Value were normalised by the benzene epoxy peak located between 1490-1526 cm^{-1}229

Figure 5-4 ATR-IR spectrums of lipases and epoxy at 100°C at a) t = 0 h (blue curve) and b) t = 72 h (red curve). The star shows the C-O stretching from epoxy. In samples with sebacic acid this peak increases due to the formation of esters, rendering the lipases peak nearly indiscernible.230

Figure 5-5 Nucleophile attack of the oxyanion from the Asp₃₃₃ on the epoxy ring. The red dotted circle indicates the free hydroxyl groups possibly detected in the IR curing of lipases and epoxy without dicarboxylic acid.231

Figure 5-6 Schematic of sample phase separation after 72 h curing cycles: NC and TDL exhibit a sediment phase ($\approx 3\text{mm}$) and a clearer top surface ($\approx 2\text{mm}$) and TL3 sample exhibits a homogenous brown colour with a small gradient over its thickness.233

Figure 5-7 FTIR spectra of top and bottom and top surfaces for: a) NC sample, and b) TDL sample.234

Figure 5-8 FTIR spectra of top and bottom and top surfaces for TL3 sample.235

Figure 5-9 Samples after swelling in TCB (7 days at 80°C, followed by 3 days at 135°C): a) NC (delimited by black dotted line), b) TDL, c) TL3. d) Soluble fraction of NC, TDL and TL3 samples after 7 days at 80°C, followed by 3 days at 135°C and the total soluble fraction over 10 days.236

Figure 5-10 DMA results for samples TDL and TL3 compared to TBD and PTL3 (sample PTL3 was added after initial measures to investigate further crosslink mechanism). Inset shows the damping properties of the material with presence of a shoulder for TL3 and TDL sample.237

Figure 5-11 TGA results for NC, TDL and TL3 sample under nitrogen atmosphere. The inset represents the weight derivation of the measurement in function of temperature.	238
Figure 5-12 Reprocessing of TL3 samples at 80°C for 1h under 10MPa pressure - the rough surface observe of the reprocessed product has been induced by the blue peel ply used during the experiment, mould dimension are 55 x 45 x 5 mm.	240
Figure 5-13 Cracks healing of original TL3 sample after 10 min at 80°C.	240
Figure 5-14 Cut healing: TL3 sample cut, b) TL3 sample after 10min at 80°C, c) PTL3 sample cut, d) PTL3 sample after 10min at 80°C - PTL3 shows no cut repair after lipases degradation in the polymer confirming the role of the active site in the healing process	241
Figure 5-15 a) Stress relaxation of NC, TDL and TL3 samples, b-d) dissolution experiment at 80°C (7 days) in ethylene glycol for: NC (b), TDL (c), and TL3 (d) samples - NC sample does not exhibit any relaxation, TDL exhibits faster complex stress relaxation profile while TL3 only relaxes 4% of stress within 10 min. No sample exhibits full relaxation or dissolution in EG indicating that transesterification does not happen in between 80°C-100°C.	242
Figure 5-16 Creep profile of TL3 for: a) second heating cycle, and b) third heating cycle - both creep cycle exhibit a measurable flow to characterise the BER energy activation showing a vitrimer behaviour.	244
Figure 5-17 a) Arrhenius plot of second and third cycle of heating for TL3 sample, b) stress relaxation of TL3 sample ($E_a \approx 55\text{kJ}\cdot\text{mol}^{-1}$).	244
Figure 5-18 Dissolution of samples in ethylene glycol after 24h: a) NC (solvent removed to see sample), b) TDL (fully dissolve in solvent), and c) TL3 (fully dissolved).....	245
Figure 5-19 a) FTIR zoom-in of the hydroxyl range ($3300\text{-}4000\text{ cm}^{-1}$), b) evolution of the $1700\text{-}177\text{ cm}^{-1}$ signature during curing for TLD and TL3. The hydroxyl signature ($\approx 3400\text{-}3600\text{ cm}^{-1}$) exhibits a redshift with temperature indicating less energy bonding of the esters' OH groups. The hydroxyl in the range $1700\text{-}177\text{ cm}^{-1}$ (marked by the 2 dotted lines) coming from the enzymes displays change with temperature. The variation of this signature during the cure looks similar for TDL and TL3 indicating these groups are independent of the active site.....	246
Figure 5-20 Schematic of enzymmer network representing the supramolecular network (left) formed by the lipases active site attacking carbonyl groups to form tetrahedral complex favouring hydrogen bonding with hydroxyl groups. After lipases denaturation ($T > 125\text{-}$	

155°C, right side), the hydrogen bonds are suppressed leading to a polyester network with high proportion of free hydroxyl groups able to reorganise via transesterification.248

LIST OF FIGURES (APPENDICES)

Figure A-1 Schematic of fabrication method used to produce vitrimer samples.....	155
Figure A-2 Schematic of ATR-IR curing experiment to record species evolution over time.	156
Figure A-3 Identification of C=O stretching signals. a) Sebacic acid in the molten state at 145°C in paraffin oil. The signal at 1706 cm ⁻¹ is the regular signal of dimerized H-bonded COOH groups, b) Sebacic acid at different concentrations in PEG600 used as a solvent. The signal at 1735 cm ⁻¹ is due to COOH groups interacting through H-bonds with the ether groups of the solvent. c) Sebacic acid at different concentrations in epoxy resin; the same signals are present. The ether groups of uncured epoxy resin interact with dissolved COOH groups. d) Sebacic acid in epoxy resin after full curing. The C=O stretching signal of the ester is detected at 1735 cm ⁻¹	157
Figure A-4 Typical integration zone for epoxy peak at the beginning (blue curve) and at the end (red curve) of cure process for sample 100H 5CAT.	158
Figure A-5 Evolution of epoxy peak during curing of sample 100H5CAT: beginning (red) and after 60 min (blue) at 145°C.....	159
Figure A-6 Evolution of epoxy peak during curing of sample 50H5CAT: beginning (blue), after 60 min (red) after 8h at 145°C (purple), and 8h at 160°C (green).	159
Figure A-7 Evolution of epoxy peak during curing of sample 30H5CAT: beginning (blue), after 60 min (red) after 8h at 145°C (purple), and 8h at 160°C (green).	160
Figure A-8 Evolution of the glass transition as a function of composition (diamonds) and trace of the fit using the Fox-Flory equation (red solid line).	161
Figure A-9 Stress relaxation results obtained by DMA in shear geometry: a) 100H 5CAT, b) 75H 5 CAT c) 60H5CAT, d) 50H5CAT, e) 30H5CAT, and d) 30H10CAT.	163
Figure A-10 Creep results for all samples.	164
Figure B-1 Chemical structure of nanoparticles: GNP as stack of graphene layers (6-8), Graphene oxide and GPTS-GO - rGO have a similar structure than GO particles but should display lower functionality (acyl and carbonyl function). Adapted from [1].....	203
Figure B-2 Scheme of functionalisation of GO with GPTS - adapted from [2].....	205

Figure B-3 Swelling ratio of nanocomposites compared to swelling ratio of vitrimer without nano-reinforcement (purple dotted line) - samples were left at 135°C in TCB for 7 days.206

Figure B-4 FT-IR spectra of nanocomposites: a) GNP samples, b) GO samples, c) GPTS samples, d) rGO samples - chemicals species are not impacted by nanoparticles addition.206

Figure B-5 Stress relaxation results at different temperature for GNP samples: a) Neat vitrimer, b) 0.1 wt. % GNP, c) 0.5 wt. % GNP, d) 1 wt. % GNP.....207

Figure B-6 Stress relaxation results at different temperature for GO samples: a) Neat vitrimer, b) 0.1 wt. % GO, c) 0.5 wt. % GO, d) 1 wt. % GO.....207

Figure B-7 Stress relaxation results at different temperature for GPTS samples: a) Neat vitrimer, b) 0.1 wt. % GPTS, c) 0.5 wt. % GPTS, d) 1 wt. % GPTS.208

Figure B-8 Stress relaxation results at different temperature for rGO samples: a) Neat vitrimer, b) 0.1 wt. % rGO, c) 0.5 wt. % rGO, d) 1 wt. % rGO.....208

Figure B-9 Creep results after removal of initial elastic strain removal at different temperature for GNP samples: a) Neat vitrimer, b) 0.1 wt. % GNP, c) 0.5 wt. % GNP, d) 1 wt. % GNP.....209

Figure B-10 Creep results after removal of initial elastic strain removal at different temperature for GO samples: a) Neat vitrimer, b) 0.1 wt. % GO, c) 0.5 wt. % GO, d) 1 wt. % GO.....209

Figure B-11 Creep results after removal of initial elastic strain removal at different temperature for GPTS samples: a) Neat vitrimer, b) 0.1 wt. % GPTS, c) 0.5 wt. % GPTS, d) 1 wt. % GPTS.210

Figure B-12 Creep results after removal of initial elastic strain removal at different temperature for rGO samples: a) Neat vitrimer, b) 0.1 wt. % rGO, c) 0.5 wt. % rGO, d) 1 wt. % rGO.210

Figure B-13 Bar chart showing the glass transition temperature of the samples depending of the particles loading type and percentage.211

Figure B-14 Typical strain-stress curve for nanocomposites: a) GNP samples, b) GO samples, c) GPTS samples, d) rGO samples.....213

Figure B-15 SEM micrograph of original and recycled nanoparticles: a) original GNP, b) recycled GNP, c) original GO, d) recycled GO, e) original GPTS-GO, f) recycled GPTS-GO, g) original rGO, and h) recycled rGO.....	214
Figure B-16 XPS survey for original and recycled nanoparticles: a) GNP, b) GO, c) GPTS-GO and d) rGO.....	215
Figure C-1 Spectrum of curing cycle at t = 0h (blue curves) and t = 72h (red curves) for: a) TL3 sample, and b) TDL sample.....	259
Figure C-2 Evolution of hydroxyl groups for: a) TL3 sample, and b) TDL sample.	259
Figure C-3 Evolution of chemical species for the chemical reaction of epoxy and lipases without sebacic acid: a) epoxides, b) ether, and c) hydroxyl groups.	260
Figure C-4 Scheme of the lipase TL active site adapted from [2]. The Ser ₁₀₉ is located in the red dotted circle and the His ₂₇₇ is located in the blue dotted circle.....	260
Figure C-5 DSC of top and bottom faces for: a) NC sample, and b) TDL sample.	261
Figure C-6 Comparison of TL3 DSC measurement with: a) top phases of NC and TDL samples, and b) bottom (sediment) phase of NC and TDL sample - data for NC and TDL are the same that in Figure C-5.....	261
Figure C-7 Swelling ratio of NC, TDL and TL3 samples after 7 days at 80°C, followed by 3 days at 135°C and the total swelling over 10 days. Solvent: TCB.	262
Figure C-8 TGA results for NC, TDL and TL3 sample in air. The inset represents the weight derivation of the measurement in function of temperature.....	262
Figure C-9 Typical tensile curve of original TL3 sample and reprocessed TL3 sample.	263
Figure C-10 Creep result between 60°C and 80°C for: (a) TL3 samples, and (b) TDL sample - The networks do not show any flow behaviour due to transesterification at these temperature.....	263
Figure C-11 First heating cycle of creep for NC sample - The sample do not exhibit any creep behaviour behaving like a thermoset material.....	264
Figure C-12 Creep profile of first heating cycle for: a-b) TDL, and c-d) TL3 - The initial increase of creep between 90°C and 140°C corresponds to potential relaxation phenomenon but the material do not flow enough to be characterised the transesterification. Between 140°C and 245°C, the material creep decreases corresponding to complex degradation of lipases and interaction with the polyester network.	265

Figure C-13 Second and third creep cycle for NC and TDL samples: a) NC (2), b) NC (3), c) TDL (2), and d) TDL(3). - NC samples behaves fully like a classical thermoset, TDL shows little increase of creep at extremely high temperature probably to the amount of initial active lipases.....266

Figure C-14 Fourth creep cycle for samples: a) NC, b) TDL, and c) TL3 - all samples shows similar behaviour indicating that the lipases do not have any impact in this temperature range.266

Figure C-15 Stress relaxation of samples at higher temperature for: a) NC, b) TDL, and c) TL3 - Only TL3 is able to achieved full stress relaxation and show a faster stress relaxation with increased temperature; a higher temperature (250°C) was added for TL3 in order to calculate the energy activation of the sample - $E_a \approx 55 \text{ kJ.mol}^{-1}$267

Figure C-16 FTIR spectrum of TL3 sample from 100°C to 190°C after the 72 h curing cycle - Only difference visible except from hydroxyl groups undergoing a redshift are the C-O vibration $\approx 2100 \text{ cm}^{-1}$ due to atmospheric noise.267

Figure C-17 Zoom-in in the 400-1790 cm^{-1} of the FTIR spectrum of TL3 sample from 100°C up to 190°C after the 72 h curing cycle - no chemical changes is observed.....268

LIST OF SCHEMES (CHAPTERS)

Scheme 3-1 Formation of exchangeable hydroxyl ester links by polyaddition of DE and SA.	135
Scheme 3-2 Branching by the transesterification mechanism, leading to exchangeable cross-links. The scheme illustrates the equilibrium between mono-, di-, tri-, tetraesters and the free diglycol form.....	135
Scheme 3-3 Branching mechanism <i>via</i> anionic ROP of diepoxides-ether bonds thereby formed are not exchangeable.....	137

LIST OF SCHEMES (APPENDICES)

Scheme A-1 Reactants used in the study.....	154
---	-----

LIST OF TABLES (CHAPTERS)

Table 2-1 Networks and properties of catalyst based transesterification vitrimer in literature. NA: Non-applicable, E: Young's modulus, G: Shear modulus, blue shading: <i>influence of hardener and catalyst on vitrimer networks and processing conditions</i> , orange shading: <i>variations from pure epoxy-dicarboxylic hardener formulation</i> , green shading: <i>notion of vitrimer-like materials in transesterification vitrimers – acronym: Zn-PAM is a polymer catalyst corresponding to poly(acrylonitrile-co-zinc methacrylate)</i>	59
Table 2-2 Nanocomposites vitrimer in literature. BER type: (1) transesterification, (2) disulphide metathesis, (3) trans-N-alkylation; NA: Non-applicable, E: Young's modulus, G: Shear modulus, No shading: <i>Processing of vitrimer resins</i> , blue shading: <i>matrices enhancement and its limitation</i> , orange shading: <i>dual triggering of vitrimer matrix</i> , grey shading: <i>nanoparticles used as dynamic crosslinkers</i> , green shading: <i>practical application of nano-vitrimer</i>	86
Table 3-1 Reactant used in this study; <i>eew</i> : epoxy equivalent weight, <i>mw</i> : molecular weight, ROP: ring opening polymerisation.	129
Table 3-2 Sample identification based on the epoxy/sebacic acid ratio and catalyst amount.	130
Table 4-1 Samples denomination.	171
Table 4-2 Calculated yield of recycling for nanoparticles - same recovery yield for GNP and rGO can be found in [75].	187
Table 4-3 Distance between graphene layers calculated using Bragg's law with the top of (002) plane peak.	190
Table 4-4 Calculated I_d/I_g , I_{2d}/I_g ratios, average sp^2 cluster size L_D (average distance between defects) and the defect density n_D for original and recycled nanoparticles.	192
Table 5-1 Samples composition and labelling.	223
Table 5-2 Degradation temperature (5% weight) and maximum peak derivative weight temperature for NC, TDL and TL3 sample.	239

LIST OF TABLES (APPENDICES)

Table A-1 Glass transition temperatures for different ratios taken from the tan delta curves.	160
Table A-2 Tensile properties for different ratios of vitrimer.	161
Table A-3 Relaxation modulus (initial value).	162
Table B-1 Reactant used in this study; eew: epoxy equivalent weight, mw: molecular weight.....	204
Table B-2 Properties of purchased GNP and GO.	204
Table B-3 Summary of the elemental composition determined via XPS survey analysis. The reader would acknowledge that total does not add up to 100% - N _{1s} peak was included in calculation to compare with survey graph of original and recycled particle (results developed later in this manuscript) however N _{1s} content is not relevant for neat particles.	205
Table B-4 Summary of mechanical results for GNP samples.	211
Table B-5 Summary of mechanical results for GO samples.	212
Table B-6 Summary of mechanical results for GPTS-GO samples.	212
Table B-7 Summary of mechanical results for rGO samples.....	212
Table B-8 Summary of the elemental composition calculated from survey XPS data with nitrogen and silicon compounds.....	215
Table B-9 Contributions of individual chemical moieties in the high-resolution C 1s spectra of original and recycled GNP, GO, GPTS-GO and rGO nanoparticles - nitrogen and silicon were removed for fitting to limit artefact.	216

LIST OF EQUATIONS (CHAPTERS)

Equation 2-1 Calculation of swelling ratio of polymers.	51
Equation 2-2 Calculation of soluble fraction of polymers.	51
Equation 3-1 Estimation of gelation by the Flory-Stockmayer model.....	136

LIST OF EQUATIONS (APPENDICES)

Equation A-1 Fox-Flory equation.	160
Equation B-1 Calculation for average sp^2 clusters size.	205
Equation B-2 Calculation for the defect density.	205

GLOSSARY

Acronym	Full term	First call (page number)
2-PI	2-phenylimidazole	125
ACAT	Amine-capped aniline trimer	57
AIE	Aggregation-induced-emission	53
AFT	Addition-fragmentation chain transfer	47
AN\AC	Acetonitrile	67/222
ATR-FTIR	Attenuated total reflection Fourier transform infrared spectroscopy	40
Asp ₃₃₃	Aspartate ₃₃₃	107
BA	Butylamine	57
BARE-silica	Non-functionalised silica nanoparticles	79
BE	Binding energy	174
BER	Bond exchange reaction	39
CALB B	Candida antartica lipase B	105
CAN	Covalent adaptive network	36
CHDA	1,4-cyclohexanedicarboxylic acid	57
CNT	Carbon nanotubes	76
COOH-GNP	Carbonyl functionalised graphene nanoplatelet	78
DA	Diels-Alder	47
DBA	Dibutylamine	57
DE	Diepoxide	129
DGEBA	Diglycidyl ether of bisphenol A	49
DMA	Dynamic mechanical analysis	40
DMF	<i>N,N</i> -dimethylformamide	67
DSC	Differential scanning calorimetry	41
eew	Epoxy equivalent weight	129
EG	Ethylene glycol	39
ENR	Epoxidised natural rubber	57

EP-silica	Epoxy functionalised silica nanoparticles	69
ESO	Epoxidised soybean oil	54
FPA	Fumaropimaric acid	54
FTIR	Fourier transform infrared spectroscopy	40
FRP	Fibres reinforced polymer	35
GLYMO silica	Silane bearing epoxy functionalised silica nanoparticles	79
GO	Graphene oxide	40
GNP	Graphene nanoplatelets	40
3GPTS	3-glycidoxy-propyltrimethoxysilane	170
GPTS-GO	Silane bearing epoxy graphene oxide	40
HCL	Hydrochloric acid	90
HDPE	High density polyethylene glycol	61
His ₂₇₇	Histidine ₂₇₇	231
IR	Infrared	40
Lipase TL	Lipases from <i>Pseudomonas stutzeri</i>	108
mw	Molecular weight	129
NAg	<i>N</i> -acetylglycine	58
NMP	<i>N</i> -methyl-2-pyrrolidone	92
NPP	4-nitrophenylpalmitate	222
NMR	Nuclear magnetic resonance	232
PBT	Poly(butylene terephthalate)	57
PDA-NPs	Polydopamine nanoparticles	82
PDMS	Polydimethylsiloxane	58
PE	polyethylene	61
PEG	Polyethylene glycol	71
PEI	Polyethylenimine	103
PEO	Poly(ethylene oxide)	67
PFPE	Perfluoropolyethers	67
PMMA	Poly(methyl methacrylate)	58
PPh ₃	Triphenylphosphine	57

PPy	Polypyrrole	80
PS	Polystyrene	71
PTMP	Pentaerythriol tetra(3-mercaptopropionate)	70
rGO	Reduced graphene oxide	40
ROP	Ring opening polymerisation	41
SA	Sebacic acid	38
SEM	Scanning electron microscopy	175
Ser ₁₀₉	Serine ₁₀₉	231
SH-silica	Thiol functionalised silica nanoparticles	69
SH-CNT	Thiol functionalised carbon nanotubes	84
SLG	Single layer graphene	76
TBD	1,5,7-triazabicyclo[4.4.0]dec-5-ene	57
TCB	1,2,4-trichlorobenzene	49
TGA	Thermogravimetric analysis	41
THF	Tetrahydrofuran	66
TOL	Toluene	67
Tyr ₅₄	Tyrosine ₅₄	231
UPy	Ureidopyrimidinone	46
UV	Ultra-violet	48
WLF	William-Landel-Ferry	48
xLCE	Liquid crystal elastomer with exchangeable bonds	82
XRD	X-ray diffraction spectroscopy	40
XPS	X-ray photoelectron spectroscopy	40
Zn-PAM	Poly(acrylonitrile-co-zinc methacrylate)	59
Zn(acac) ₂	Zinc acetylacetonate	49
Zn(OAc) ₂	Zinc acetate	58

LIST OF SYMBOLS AND PARAMETERS

Symbol	correspondence
d	Interlayer distance (nm)
E	Young's modulus (Pa)
E_a	Activation energy (kJ.mol ⁻¹)
f_x	Average functionality of the monomer carrying functions x
G	Shear modulus (Pa)
G_0	Initial shear modulus (Pa)
Hz	Hertz (s ⁻¹)
I_D	Intensity of RAMAN D band
I_{2D}	Intensity of RAMAN 2D band
I_G	Intensity of RAMAN G band
λ_L	Wavelength (nm)
L_D	average sp ² cluster size (average distance between defects, nm)
m	Masse (g)
η	Viscosity (Pa.s)
n_D	Defect density (cm ⁻²)
Ω	Ohm
ϕ_x	fractions of polymer x
ρ	Extent of reaction at the gel point
pK_a	Acid dissociation constant
r	Stoichiometric ratio of functional monomers ($r \leq 1$)
τ	Relaxation time (s)
T_α	Glass transition temperature (taken from damping curve) (°C)
T_g	Glass transition temperature (°C)
T_v	Topology freezing temperature/vitrification temperature (°C)
$\tilde{\nu}$	Wavenumber (cm ⁻¹)

ABSTRACT

The development of more sustainable polymers has become a necessity due to the current environmental impact of traditional polymers. The use of thermoset polymers has led to issues regarding their sustainability (not recyclable, healable, or reprocessable). Among those thermosets, epoxy is one of the leading polymers for high-end applications. Vitrimer materials have proved to be an excellent candidate to increase the sustainability of epoxy-based polymers as they exhibit similar properties to the original epoxy network they are derived from, but also have the capability to be reprocessed, healed and recycled. Despite the vast literature available on vitrimer materials, the complete sustainable potential of catalysed epoxy vitrimers and their polymerisation mechanisms has yet to be fully exploited and has driven the current project towards three distinct routes.

First, this research explores the possibility to use a simple and scalable manufacture method to understand the polymerisation mechanism of an epoxy-sebacic acid vitrimer system. The different mechanisms of catalysed polymerisation for off-stoichiometric formulations are used to tune the final thermomechanical properties of the final polymer without drastic changes in the manufacture process. It also explores the limitations of this method to obtain vitrimer or vitrimer-like materials.

Second, the increasing interest of nanotechnology, and more accurately graphene nanoparticles as reinforcements, has also risen concerns about their use in traditional thermosets. Usually difficult to separate from the thermoset matrix, vitrimers show the possibility to be dissolved in mild conditions. Therefore, the extraction and recovery of nanoparticles is the second explored point of this project. After assessment of the effect of nanoparticles addition into the vitrimer system, they are successfully recovered with few structural changes observed.

Finally, various sustainable options are available to replace traditional epoxy or hardener monomers. However, a lot remains unexplored in the case of catalysts. This project shows the possibility to use lipases as sustainable biocatalysts for the polymerisation of epoxy-sebacic acid network. This polymer exhibits vitrimer properties at high temperatures ($> 185^{\circ}\text{C}$) but also a remarkable supramolecular behaviour below 100°C .

DECLARATION

In this work, some paragraphs in section 2.3 and section 2.7 of the literature review (Chapter 2) were adapted from the 1st year report of the author (Quentin-Arthur Poutrel, QAP), therefore, some similarities may be found.

In chapter 4, tensile testing, XRD, DMA and Raman data collecting has been equally split between the author (QAP), Aline Souvignet and Yasmine Baghdadi (YB). Therefore these data have been used for their reports (AS: for Sigma Clermont school, YB: for the University of Manchester). Schematics of experiments were made and used by YB for her report titled *“Enhancement of the Mechanical Properties of Vitrimers using Functionalised Graphene Nanoplatelets”*. Recovery yield values for GNP and rGO can also be found in AS report titled *“Reprocessing of vitrimer composites and recycling of graphene nanoparticles”*. All analysis and other figures were however fully performed and produced by the author (QAP). More details are given before chapter 4 in “Chapter 4 - Preliminary statement”.

In chapter 5, enzyme activity assay and UV-visible data were collected by Auriane Bagur (AG). In a similar way DMA, TGA and DSC data collecting was equally split. Therefore aforementioned data can be found in her report for the University of Bordeaux titled *“Biocatalysed Vitrimers”*. The reprocessing and healing images produced by the author (QAP) were also used in the patent filling report used to obtain the mentioned patent titled *“Vitrimer containing a biocatalyst”* referenced: Blandford, CF, Gresil, M, Poutrel, Q-A & Malone, K Jan. 02 2020, Vitrimer containing a biocatalyst, Patent No. WO2020002904A1. All analysis and figures were, however, fully performed and produced by the author (QAP). More details are given before chapter 5 in “Chapter 5 - Preliminary statement”.

COPYRIGHT STATEMENT

The author of this thesis (including any appendices and/or schedules to this thesis) owns certain copyright or related rights in it (the “Copyright”) and s/he has given The University of Manchester certain rights to use such Copyright, including for administrative purposes.

Copies of this thesis, either in full or in extracts and whether in hard or electronic copy, may be made only in accordance with the Copyright, Designs and Patents Act 1988 (as amended) and regulations issued under it or, where appropriate, in accordance with licensing agreements which the University has from time to time. This page must form part of any such copies made.

The ownership of certain Copyright, patents, designs, trademarks and other intellectual property (the “Intellectual Property”) and any reproductions of copyright works in the thesis, for example graphs and tables (“Reproductions”), which may be described in this thesis, may not be owned by the author and may be owned by third parties. Such Intellectual Property and Reproductions cannot and must not be made available for use without the prior written permission of the owner(s) of the relevant Intellectual Property and/or Reproductions.

Further information on the conditions under which disclosure, publication and commercialisation of this thesis, the Copyright and any Intellectual Property and/or Reproductions described in it may take place is available in the University IP Policy (see <http://documents.manchester.ac.uk/DocuInfo.aspx?DocID=24420>), in any relevant Thesis restriction declarations deposited in the University Library, The University Library’s regulations (see <http://www.library.manchester.ac.uk/about/regulations/>) and in The University’s policy on Presentation of Theses

ACKNOWLEDGEMENTS

First and foremost, I would like to thank my supervisors Dr. Jonny Blaker and Professor Costantinos Soutis. Dr. Blaker has always shown rigor and fairness, whilst displaying humour relating work or personal views. A big thanks for taking a long time correcting thoroughly the English in some sections of this thesis while supporting my French picky side and questions regarding grammar. Prof. Soutis has been an incredible support and pillar of my scientific development, not only through his right balance between guidance and enthusiasm, but also by constantly reminding me to push my knowledge further and to make the most of my time as a PhD student. Also, thank you for your constant faith regarding my funding demands to make the C1 lab great again, allowing other students and me to achieve some quality research.

The second thank you is dedicated to someone who should belong in the paragraph above with Prof. Soutis and Dr. Blaker - Dr. Matthieu Gresil, now working at Monash University (Melbourne, Australia). Dr. Gresil has been the main supervisor of this project until March 2020, and has continued working in the shadows with me to help me finish this project. Dr. Gresil has not only taken me as a PhD student, but also given me an impressive freedom to allow me to develop my ideas, showing trust and respect towards my way of working. For these reasons, thank you 'Dr. Sith'. The three of you have laid the base of the future scientist but also the person I will become in the future, and for that, I am forever indebted to you. You have also reminded me to stay hydrated in appropriate circumstances to preserve my brain cells, and I will continue to apply this advice and transmit to my future entourage.

I would like to acknowledge the University of Manchester and especially the Aerospace Research Institute for financially supporting this project as well as many of the technicians who took time to teach me characterisation techniques required for achieving this work.

I owe a great deal of gratitude to Prof. François Tournilhac, from ESPCI Paris, for giving me the opportunity to work for a few weeks in his laboratory and for helping me understand vitrimer materials in greater depth. Having the chance to work with you was an excellent boost for my project and our discussions developed me both as a scientist and as a human.

A very special thanks goes to some of my friends: Josh Parkin and Jack Saunders for our lunches and president card games where we discovered the French domination many time. Aron Sidhu, for pushing me to get out of work and keep a social – *not too social* – life with our gaming time and life saviour advices to get me out of my stubbornness in trying to make work impossible situations. Thank you to Nawseen Tarannum, for carefully reading my work; you have been of great help in keeping my sanity during the writing period of this document. A huge thanks to our vitrimer student team/family: my work wife Kanokporn Tangthana-Umrung (your kindness and energy has no equal ST!), and our kids Yi Wang and Ruiling Du. Also to my other co-workers, without you all my university life would not have been the same.

I would like to thank and acknowledge all the BSc and MSc students that I had the chance to help throughout their projects. You have helped me through moment of doubts, reminded me that you can learn from anyone, and forced me to develop a patience in explaining over and over while remaining calm! A special mention to Yasmine Baghdadi, Harry Coppock (special thanks for my second most liked FB profile picture), Christopher Bremmer-Stokes and last but not the least Auriane Bagur (Bag), my *Pikachu*, who boosted my mood towards the end of this project and became a real and close friend while teaching Josh and Jack that French people always win. *I will be your Ash forever.*

A small mention for my second house (work being the first one), *Joshua brook* and its staff, which was a core meeting room for all the aforementioned people and me. This place has helped me overcome difficulties but has also being inspirational towards development of many ideas.

Finally, I cannot thank my mom enough, for all her love and support during this thesis and throughout all my life. You have made me the person I am, and I will always be grateful to you for that.

THE AUTHOR

The author of this thesis has a physics and nanomaterials background. After completion of his mathematical and physics BSc at the University of Nantes (France), he completed the MSc “C’nano: Nanosciences, Nanomaterials and Nanotechnologies” at the University of Nantes. For the MSc completion, two internships were required (1st and 2nd year of the MSc), which led the author to start working with epoxy polymer for the dispersion and alignment of graphene nanoplatelets *via* electric field within this polymer matrix at the University of Manchester. Following these projects, the author was initially taken as a PhD student to develop traditional epoxy based material for 3D printing. However, the first months of literature review led to the discovery of vitrimer materials which drove an intense curiosity for these polymers and the development of their incredible potential.

Chapter 1. Introduction

1.1 Background

1.1.1 Epoxy resins: interests and limitations

Over the past 60 years, polymers have been among the most efficient ways to reduce cost of manufacture, weight of structures, and design of complex shapes [1]. Epoxy resins inspire particular interest due to their permanent crosslinks, leading to materials with strong mechanical performance and chemical resistance [2]. Interest in these resins comes from the wide range of chemistry available for tailoring their properties, using a set of commercial monomers and hardeners with almost any possible combination [3]. Furthermore, the polymerisation of epoxy resin relies on the ring opening polymerisation (ROP) mechanism which has the advantage to not create secondary products, leading to a good control over their manufacture and final properties [4], [5]. Therefore, epoxy polymer networks have an important impact on the development of industries and high-performance polymer-based applications [6]. Areas such as electronics, aeronautics, building, and automotive lead to a constant increase of the use of these polymer systems, and the market for epoxy resins is expected to reach a compound annual growth rate of 10 billion by 2025 [7]. Composites are one of the areas where epoxy is used as a matrix for producing fibre reinforced polymer (FRP) matrix to replace metallic counterparts in order to reduce weight, waste during production, or form new shapes [8].

Despite ease of manufacture, being lightweight, and mechanically strong, the permanent network has brought new challenges to solve for industry and researchers [9], [10]. Traditional chemical crosslinked networks (*i.e.* thermosets) cannot be healed, reprocessed and recycled. For example, an epoxy coating undergoing cracks leaves the layer beneath it vulnerable to the external environment and requires patching or replacement [11]. In the composites field, epoxy is the main thermoset used as matrix to produce composite FRP [7]. The drawbacks to these composites are usually related to the epoxy matrix; with poor fracture toughness and poor interface between fibres and epoxy, damages can lead to unexpected failures [12]. In order to prevent these failures, structural health monitoring of composites is compulsory. However, these operations are time

consuming and induce high maintenance costs. Moreover, if damages are too significant, the composites have to be replaced [11], [13].

1.1.2 Development of reprocessable and healable polymers

Efforts towards developing new materials with efficient healing capacity, reprocessability and recyclability have exponentially increased over the past 30 years [14]. Research initially focused on weak reversible bonds (*i.e.* supramolecular networks) [15]–[17]. Despite having good healing efficiency at relatively low temperature (*i.e.* room temperature), these networks usually do not meet the mechanical properties or chemical resistance of thermoset polymers [17]. More recently, a dissociative dynamic bond exchange mechanism was used to create thermoset materials with the ability to be reprocessed or healed under stimuli *via* reversible crosslinks [18]–[20]. Nevertheless, these networks show an important drop in their viscosity and a loss of connectivity once bond exchange starts. This characteristic has limited the use of these materials in structural applications.

In 2011, Leibler and co-workers developed covalently bonded networks based on an associative exchange made from commercially available epoxy and hardeners [21]. By esterification of epoxy and fatty acid in the presence of a chosen catalyst, the network can undergo transesterification of β -hydroxylesters triggered by temperature. These associative covalent adaptive networks (CANs) rely on the transesterification rate increasing with temperature, and display a second transition temperature (different from the glass transition temperature T_g) called T_v . Above T_v , bond exchange becomes fast enough so that the associative CAN exhibited capacity to be healed, reprocessed, and recycled while keeping the initial properties of epoxy (strength and chemical resistance). This new class of polymer was termed vitrimer due to the glassy-like behaviour observed at high temperature, where the viscosity follows Arrhenius behaviour [21]. The surge of eco-friendly solutions in materials science has led to an intense interest and research in vitrimer chemistry. A variety of new networks has since been developed to increase the versatility of vitrimer properties [22], [23].

1.1.3 Interest in nanoparticles for enhanced epoxy matrices

Although these CANs might be the answer to increasing the life cycle of epoxy-based networks, they do not answer underlying problems related to thermoset polymers used as replacements for metallic counterparts (*e.g.* airplane wings). Indeed, most polymers exhibit poor electrical and thermal conductivity when compared with traditional materials [9], [24]. To overcome the limitations of polymer matrices, the impact of nanoreinforcements in epoxy resins have been studied over the past two decades [9], and especially, the reinforcement *via* carbon-based nanoparticles [25], [26]. Vitrimers are a relatively recent class of materials; therefore, limited studies are available showing the influence of nanomaterials on vitrimeric properties or producing multifunctional materials *via* the use of carbon-based particles [27]–[30]. Nonetheless, the similarity between epoxy-based thermoset and epoxy-based vitrimer (due to their structures based on the same polymerisation reactions and chemical bonds) allows to assume similar behaviour regarding mechanical, electrical and thermal conductivity. However, the dynamic network also has another property that was recently exploited: an appropriate solvent can dissolve the crosslinked network when heated above the bond exchange temperature activation. A vitrimer network was entirely dissolved, and the initial monomers were recovered to achieve “close loop recyclability” [31]. Nonetheless, this close loop demonstration does not consider the use of nanomaterials in these polymer networks. Potential to extract the aforementioned reinforcements was demonstrated without characterisation of the recycled particles [32]. Therefore, the potential recovery and re-use of the particles/fibres is yet to be investigated.

1.1.4 The surge for sustainable solutions

Researchers are now focusing on developing more sustainable materials, and there is an interest in bio-based (*i.e.* using sustainable sources for monomers) vitrimer networks. The original epoxy vitrimers, based on transesterification, usually use a range of different catalysts with high activation temperature ($T_v > 140^\circ\text{C}$) [33], [34]. Whereas some networks have been developed to reach lower activation temperature with different chemistry [32], [35], to the author’s knowledge the use of biocatalysts to achieve lower healing

temperature in transesterification networks is, so far, unassessed in the literature. This aspect presents an interesting opportunity towards realising low energy healing polymers.

1.2 Aims and objectives

Despite the large literature regarding vitrimer networks over the past nine years, many fundamentals and potentials of these networks need to be investigated. Epoxy networks are widely used but the polymerisation mechanisms remain debated. Moreover, the sustainability of polymer materials has risen incredible concerns and if the inherent properties of epoxy vitrimer (healing and reprocessing) make them better candidates for a greener alternative, their assessment is still at their early stages. The main aim of this thesis is to develop a better understanding of the polymerisation mechanism of catalysed epoxy vitrimers with a dicarboxylic acid hardener (sebacic acid, SA) and exploration of their potential as sustainable solutions. Toward this goal, a variety of different routes have been developed:

1. A one-pot manufacture method to tune thermomechanical properties by varying the feeding ratio epoxy:SA and studying the crosslinking mechanisms
2. The integration of various functionalised graphitic nanoparticles in the vitrimer matrix and their recovery after integration into a crosslink material
3. The use of a novel biocatalyst to obtain vitrimer properties with lower healing and reprocessing temperature.

The rationale behind the first route was to answer the question about the use of a Lewis base as catalyst for epoxy dicarboxylic acid network which could lead to anionic homopolymerisation of the epoxy. It was hypothesised that the manufacture of different stoichiometry could allow to produce vitrimer networks with increased thermomechanical properties whilst allowing to study the crosslink formation and epoxy homopolymerisation. The one-pot mixture allows to overcome some issues associated with tuning of thermomechanical properties such as change of experimental parameters or initial monomers variation. It also shows the limitation of this method to produce vitrimer networks based on epoxy:SA monomers. This could allow industry to reach for easy manufacture process in the switch to produce vitrimer materials (rather than traditional

thermoset with limited sustainability) with various properties while predicting the material behaviour.

Regarding the second objective, attempts were made to improve the vitrimer properties *via* tuning of the polymer/nanoparticles interface. It was thought that functionalisation with functional groups involved in the bond exchange reaction (BER) would allow better charge transfer between the vitrimer matrix and the nanoparticles while improving vitrimer properties such as stress relaxation. It was hypothesised that the recovery of nanoparticles could be achieved *via* mild dissolution in ethylene glycol (EG) followed by nanoparticles washing in order to obtain new graphitic powder with a potential for being re-used in further applications. This would mean that nanoparticles reinforcement could be environmentally sustainable once the nanocomposite reaches the end of its life.

Finally, the last objective of this work was to explore the possibility of using a biocatalyst (lipase) for epoxy:SA network. So far, sustainable options in vitrimer chemistry have mainly focused on the epoxy and hardener variations. It was believed that the lipase could achieve the same results while being a better sustainable option compared to traditional catalysts due to their low cost and environmentally-friendly production. It was also hypothesised that the enzyme could reach lower healing and processing temperature which leads to lower energy input in the use of vitrimer matrices. The success of the lipases as biocatalyst was achieved and also revealed the possibility to combine supramolecular and vitrimer behaviour without changing the polymer network (hydroxylesters from epoxy:SA polymerisation).

1.3 Thesis outline

This thesis comprises of three experimental chapters (chapter 3, 4, and 5) written in an alternative format to be potentially submitted as journal articles. The related electronic supportive information for each experimental chapter can be respectively found in appendix A, B, and C. Each experimental chapter will be introduced by a 'preliminary statement' located before the titles and the entire document is organised as follow:

Chapter 1 (this chapter) is a general introduction of this research project stating background motivations, aims and objectives and outline of the thesis.

Chapter 2 provides a general background of vitrimers research and opportunities towards their sustainability. It discusses the origin of vitrimer materials, and their main characteristics whilst covering some of their characterisation methods seen in publications, and focuses on the different chemistries used to obtain vitrimer properties. It follows on the use of nanoparticles and discusses the potential to recover fillers reinforcements from the polymer matrix. The potential bio-catalysis of epoxy based vitrimers is then discussed compared to the traditional Lewis acid or base catalysis.

Chapter 3 explores the cure kinetics of an epoxy-SA vitrimer network catalysed by 1,5,7-triazabicyclo[4.4.0]dec-5-ene (TBD). The use of catalyst such as TBD have risen the concern that some secondary reactions such as epoxy homopolymerisation may happen during vitrimer curing. To answer this question, several feeding ratios epoxy:SA were designed and the formation studied via attenuated total reflection Fourier transform infrared spectroscopy (ATR-FTIR). The results allow to consider which polymerisation reaction takes place prior another but also reveal the possibility to use these side reactions to tune the thermomechanical properties of the epoxy:SA system.

Appendix A corresponds to the supplementary information of chapter 3 and includes: manufacture of vitrimer networks, FTIR analysis method, dynamic mechanical analysis, mechanical results, stress relaxation results, and creep results for all samples.

Chapter 4 focuses on designing graphene nanoparticles to interact with the vitrimer bond exchange reaction and their potential recovery. Graphene nanoplatelets (GNP), graphene oxide (GO), silane bearing epoxy graphene oxide (GPTS-GO) and reduced graphene oxide (rGO) were added to epoxy/SA/TBD vitrimer with a loading of 0.1, 0.5, and 1 wt. %. The effect of particle types and loading is discussed and followed by the recovery and characterisation of these nanoparticles. Results of recovery are compared depending on each functionalisation type of nanoparticle, discussing the potential sustainability of graphene nanoparticles uses for catalysed epoxy:SA system.

Appendix B corresponds to the supplementary information of chapter 4 and includes: chemical structures of monomers and nanoparticles, complementary schematics for experiments and equations, X-ray photoelectron spectroscopy (XPS) data for nanoparticles and samples, swelling experiments, FTIR bulk samples data, data for stress relaxation and creep experiments, dynamic mechanical analysis (DMA) results for nanocomposites, tensile results for bulk samples.

Chapter 5 reports the use of a lipase as potential bio-catalyst for the production of more sustainable catalysed vitrimer networks. The cure kinetics of active and denatured lipases are compared, and a mechanism of ring opening polymerisation (ROP) is proposed for the epoxy:SA network. The use of this novel catalyst produces a network exhibiting new properties. Contrary to the TBD catalysed network, this network is able to heal and be reprocessed below 100°C *via* supramolecular interactions. The degradation of lipases in the polymer (between 125°C - 155°C) makes vitrimer behaviour appear above 185°C while quenching the supramolecular network. This behaviour is compared with the FTIR signature in order to propose a mechanism of these new polymers, termed “enzymers”.

Appendix C corresponds to the supplementary information of chapter 5 and includes: complementary information for ATR-IR formation analysis and FTIR bulk analysis, differential scanning calorimetry (DSC) measurements, thermogravimetric analysis (TGA) measurements, as well as complementary creep and stress relaxation data.

Chapter 7 presents an overall conclusion based on experimental results for each chapter as well as a discussion of their limitations.

Chapter 8 suggests recommendations to continue each research point tackled over the experimental parts of this thesis.

1.4 References

- [1] R. F. Gibson, "A review of recent research on mechanics of multifunctional composite materials and structures," *Compos. Struct.*, vol. 92, no. 12, pp. 2793–2810, 2010.
- [2] B. Sreenivasulu, B. R. Ramji, and M. Nagaral, "A Review on Graphene Reinforced Polymer Matrix Composites," *Mater. Today Proc.*, vol. 5, no. 1, Part 3, pp. 2419–2428, 2018.
- [3] K. K. Kar, J. K. Pandey, and S. Rana, *Handbook of Polymer Nanocomposites. Processing, Performance and Application Volume B: Carbon Nanotube Based Polymer Composites*. Springer, 2015.
- [4] J. E. Klee, F. Claussen, and H.-H. Horhold, "High-molecular weight diepoxide-dicarboxylic acid addition polymers," *Polym. Bull.*, vol. 35, pp. 79–85, 1995.
- [5] F. L. Jin, X. Li, and S. J. Park, "Synthesis and application of epoxy resins: A review," *J. Ind. Eng. Chem.*, vol. 29, pp. 1–11, 2015.
- [6] U. Kalsoom, P. N. Nesterenko, and B. Paull, "Recent developments in 3D printable composite materials," *RSC Adv.*, vol. 6, no. 65, pp. 60355–60371, 2016.
- [7] Research&Market, "Epoxy Resins - Global Market Trajectory & Analytics," 2020.
- [8] I. L. Hia, V. Vahedi, and P. Pasbakhsh, "Self-Healing Polymer Composites: Prospects, Challenges, and Applications," *Polym. Rev.*, vol. 56, no. 2, pp. 225–261, 2016.
- [9] S. A. Bello, J. O. Agunsoye, S. B. Hassan, M. G. Z. Kana, and I. A. Raheem, "Epoxy resin based composites, mechanical and tribological properties: A review," *Tribol. Ind.*, vol. 37, no. 4, pp. 500–524, 2015.
- [10] P. D. Mangalgi, "Composite materials for aerospace applications," *Bull. Mater. Sci.*, vol. 22, no. 3, pp. 657–664, 1999.
- [11] K. Diamanti and C. Soutis, "Structural health monitoring techniques for aircraft composite structures," *Prog. Aerosp. Sci.*, vol. 46, no. 8, pp. 342–352, 2010.
- [12] S. Cantoni, F. De Nicola, U. Mercurio, and V. Quaranta, "The role of polymer based composites materials in modern and future aerospace structures," vol. 10, no. 2014, pp. 10–13, 2014.
- [13] T. N. Tallman, S. Gungor, K. W. Wang, and C. E. Bakis, "Damage detection via electrical impedance tomography in glass fiber/epoxy laminates with carbon black filler," *Struct. Heal. Monit.*, vol. 14, no. 1, pp. 100–109, 2015.
- [14] V. K. Thakur and M. R. Kessler, "Self-healing polymer nanocomposite materials: A review," *Polymer*, vol. 69, pp. 369–383, 2015.
- [15] L. Voorhaar and R. Hoogenboom, "Supramolecular polymer networks: Hydrogels and bulk materials," *Chem. Soc. Rev.*, vol. 45, no. 14, pp. 4013–4031, 2016.
- [16] S. J. Rowan, S. J. Cantrill, G. R. L. Cousins, J. K. M. Sanders, and J. F. Stoddart, "Dynamic Covalent Chemistry," *Angew. Chemie Int. Ed.*, vol. 41, no. 6, pp. 898–952, 2002.

- [17] J.-M. Lehn, "Dynamers: dynamic molecular and supramolecular polymers," *Prog. Polym. Sci.*, vol. 30, no. 8, pp. 814–831, 2005.
- [18] A. Gandini, "The furan/maleimide Diels–Alder reaction: A versatile click–unclick tool in macromolecular synthesis," *Prog. Polym. Sci.*, vol. 38, no. 1, pp. 1–29, 2013.
- [19] V. Froidevaux, M. Borne, E. Laborbe, R. Auvergne, A. Gandini, and B. Boutevin, "Study of the Diels–Alder and retro-Diels–Alder reaction between furan derivatives and maleimide for the creation of new materials," *RSC Adv.*, vol. 5, no. 47, pp. 37742–37754, 2015.
- [20] L. Rulisek, P. Sebek, Z. Havlas, R. Hrabal, P. Capek, and A. Svatos, "An experimental and theoretical study of stereoselectivity of furan-maleic and furan-maleide diels-alder reactions," *J. Org. Chem.*, vol. 70, no. 5, pp. 6295–6302, 2005.
- [21] D. Montarnal, M. Capelot, F. Tounilhac, and L. Leibler, "Silica-Like Malleable Materials from permanent organic network," *Science*, vol. 334, pp. 965–968, 2011.
- [22] B. Krishnakumar, R. V. S. P. Sanka, W. H. Binder, V. Parthasarthy, S. Rana, and N. Karak, "Vitrimers: Associative dynamic covalent adaptive networks in thermoset polymers," *Chem. Eng. J.*, vol. 385, no. July 2019, p. 123820, Apr. 2020.
- [23] W. Denissen, J. M. Winne, and F. E. Du Prez, "Vitrimers: permanent organic networks with glass-like fluidity," *Chem. Sci.*, vol. 7, no. 1, pp. 30–38, 2015.
- [24] P. Nordin, "GRAPHENE DE-ICING / ANTI-ICING AND LIGHTNING STRIKE PROTECTION," 2015.
- [25] R. Nadiv *et al.*, "Graphene nanoribbon-Polymer composites: The critical role of edge functionalization," *Carbon*, vol. 99, pp. 444–450, 2016.
- [26] A. Manta, M. Gresil, and C. Soutis, "Infrared thermography for void mapping of a graphene/epoxy composite and its full-field thermal simulation," *Fatigue Fract. Eng. Mater. Struct.*, vol. 42, no. 7, pp. 1441–1453.
- [27] Z. Yang, Q. Wang, and T. Wang, "Dual-Triggered and Thermally Reconfigurable Shape Memory Graphene-Vitrimer Composites," *ACS Appl. Mater. Interfaces*, vol. 8, no. 33, pp. 21691–21699, Aug. 2016.
- [28] Y. Liu, Z. Tang, Y. Chen, S. Wu, and B. Guo, "Programming dynamic imine bond into elastomer/graphene composite toward mechanically strong, malleable, and multi-stimuli responsive vitrimer," *Compos. Sci. Technol.*, vol. 168, pp. 214–223, Nov. 2018.
- [29] J. Chen *et al.*, "Vitrimer Chemistry Assisted Fabrication of Aligned, Healable, and Recyclable Graphene/Epoxy Composites," *Front. Chem.*, vol. 7, p. 632, Sep. 2019.
- [30] B. Krishnakumar *et al.*, "Catalyst free self-healable vitrimer/graphene oxide nanocomposites," *Compos. Part B Eng.*, vol. 184, Mar. 2020.
- [31] H. Memon *et al.*, "Vanillin-Based Epoxy Vitrimer with High Performance and Closed-Loop Recyclability," *Macromolecules*, vol. 53, no. 2, pp. 621–630, 2020.
- [32] F. Zhou *et al.*, "Preparation of self-healing, recyclable epoxy resins and low-electrical resistance composites based on double-disulfide bond exchange," *Compos. Sci. Technol.*, vol. 167, pp. 79–85, 2018.
- [33] A. Demongeot, S.-J. J. Mougner, S. Okada, C. Soulié-Ziakovic, and F. Tournilhac,

- “Coordination and Catalysis of Zn^{2+} in Epoxy-Based Vitrimers,” *Polym. Chem.*, vol. 7, no. 27, pp. 4486–4493, 2016.
- [34] J. H. Chen, X. P. An, Y. D. Li, M. Wang, and J. B. Zeng, “Reprocessable Epoxy Networks with Tunable Physical Properties: Synthesis, Stress Relaxation and Recyclability,” *Chinese J. Polym. Sci. (English Ed.)*, vol. 36, no. 5, pp. 641–648, 2018.
- [35] M. Hayashi, R. Yano, and A. Takasu, “Synthesis of amorphous low: T_g polyesters with multiple COOH side groups and their utilization for elastomeric vitrimers based on post-polymerization cross-linking,” *Polym. Chem.*, vol. 10, no. 16, pp. 2047–2056, 2019.

Chapter 2. Literature review

2.1 Layout of the literature review

This review of literature is structured to cover some of the most important aspects and opportunities in vitrimer research, and can be organised into five distinct parts: (i) the origin of vitrimer networks (Section 2.2) and their mechanisms/properties compared to other types of polymers (thermoplastics, thermosets, supramoleculars, and dissociative CANs, Section 2.3). (ii) The characterisation of key properties in vitrimer networks to be defined for this class of materials, followed by common characterisation of properties which can be performed on any vitrimer networks (Section 2.4). (iii) An overview of the different chemistries of vitrimer and their main characteristics (Section 2.5 and Section 2.6). (iv) The use of carbon nanoparticles in epoxy-based polymers (thermoset or vitrimer), including also other types of reinforcements used in vitrimer matrix and their potential recyclability *via* recovery is discussed (Section 2.7). (v) Finally, an assessment of “sustainable” (term to be defined later in this thesis) vitrimer networks and potential use of lipases as biocatalyst (Section 2.8). A timeline presenting relevant vitrimer works to this thesis and to this literature review is shown in Section 2.9 and conclusion over the literature is presented in Section 2.10.

2.2 Vitrimer origin and concept

2.2.1 Supramolecular networks - Reversible but not covalently bonded crosslinks

The chemistry of vitrimer networks originates from the need to develop polymer materials that are both reprocessable and owe self-healing capacity, enabling higher life expectancy and lower maintenance costs. One of the earliest classes of healable materials are supramolecular networks. These polymers are mainly found in gel form, either as hydrogels or organogels [1]. A supramolecular gel is defined by reversible physical crosslinks (*i.e.* non-covalent). These networks can be swollen, in either water (hydrogel) or solvent (organogel). The reversible crosslinks can be triggered by several parameters such as pH, temperature or the presence of certain compounds (*e.g.* magnetic particles). Their physical crosslinking can be achieved *via* several types of interactions: hydrophobic, π - π^* ,

electrostatic, metal coordination, host-guest, and hydrogen bonding. Supramolecular gels rely on these interactions to achieve two key characteristic properties: self-healing and shear thinning behaviour once the bond exchange occurs. Bulk supramolecular polymers, on the other hand, have more limitations regarding the interactions they rely on [1]. Here, discussion is focused on the interaction within bulk supramolecular polymers – according to the scope of this project. These supramolecular polymers are harder to define as they are not considered thermoplastic materials, nor are they chemically crosslinked. The main distinction with thermoplastics is that bulk supramolecular networks should behave as ‘glassy’ solids even above T_g (if the reversible bond exchange has not been activated). However, the key properties of self-healing and shear thinning and the mechanism behind them remain the same for gels [1]. Whilst gel and polymer bulk supramolecular networks share the same types of interactions, there are limited examples in the literature that rely on hydrophobic, host-guest and π - π^* interactions [1], [2]. Electrostatic and metal coordination interactions have higher potential than those referred to immediately above. Nevertheless, the dominant mechanism used relies on hydrogen bonding.

One of the first examples of a self-healing polymer was realised using urea and ureidopyrimidinone (UPy). The urea formed extended H-bonding arrays while the UPy formed dimers with lower stiffness and those are miscible within the polymer [3]. Later, a poly vinyl alcohol was crosslinked *via* hydrogen bonds with pyrimidine. In 2008, Leibler and co-workers showed that urea and a mixture of fatty acids and triacids (Figure 2-1) can be used to heal rubber with high amount of hydrogen bonding [4].

Supramolecular networks have shown high self-healing capacity and ease of processing within a short range of time [2], [5]. Nevertheless, the weak bonding energy (≈ 1 -5 kcal.mol⁻¹) of these polymer networks gives low mechanical properties compared to chemically crosslinked material with higher energy bonding (≈ 50 -150 kcal.mol⁻¹) which limits the broadening of their application to high performance polymers [1]. Therefore, some researchers have then focused their interests on chemically crosslinked networks able to undergo dynamic exchanges of bonds (*i.e.* covalent adaptive networks, CANs).

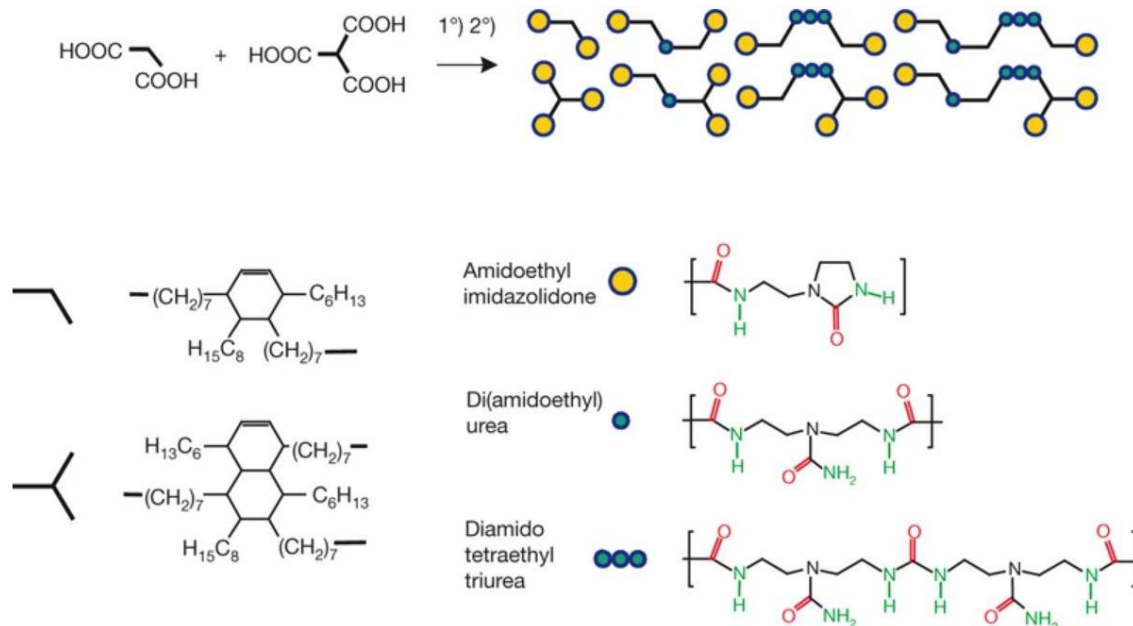


Figure 2-1 Schematic of supramolecular polymer bulk based on urea and mix of fatty acids: The mixture of fatty acid and triacid is condensed with diethylene triamine and reacted with urea. The resulting material possesses hydrogen bond acceptors (red) and donors (green) [4].

2.2.2 Reversible and covalently bonded crosslinks: dissociative and associative networks

Covalent adaptive networks (*i.e.* chemically crosslinked) have been extensively studied for decades [6], [7]; Reviews of these polymers were published by Denissen et al. [8], Bowman et al. [9]. Kloxin et al. [10] and Krishnakumar [11]. CANs are able to relax the stress applied to themselves, and several types of chemistry have been used to reach this aim, such as Diels-Alder reaction (DA) or addition-fragmentation chain transfer (AFT). These chemical reactions are divided in two groups: associative (Figure 2-2a) or dissociative (Figure 2-2b). In dissociative CANs, a temperature increase causes covalent bonds to break, and new bonds are formed as shown in Figure 2-2a.

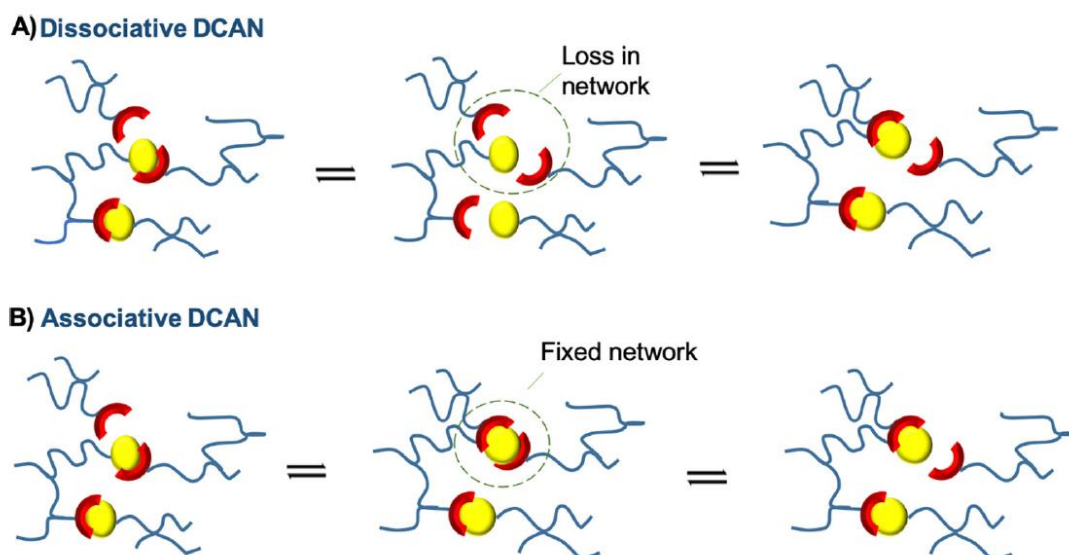


Figure 2-2 Mechanism of covalent adaptive networks: (a) dissociative, and (b) associative [11].

A well-known dissociative CAN is the DA reaction, an organic reaction between an alkene (dienophile) and a conjugated diene to form a cyclohexene. Some of these reactions - *e.g.* between maleimides/maleic anhydride and furans [12] – are reversible upon heating and are named reversible Diels-Alder reactions (rDA) (Figure 2-3). Intensively studied over the last decades, the rDA systems show remarkable potential as covalent adaptive networks due to the large range of reaction possibilities - more than a thousand different reactions are available with the different molecules derivatives - and their renewable characteristics [13]. Although these reactions have promising applications for producing new materials [14], the dissociative aspect of these CANs causes the viscosity to drop significantly beyond the glass transition temperature. Indeed, above T_g , the viscosity follows a William-Landel-Ferry (WLF) law [15] and cannot be controlled without precise modulation of the temperature. This characteristic makes dissociative CANs hard to reprocess without losing the structural integrity of the system.

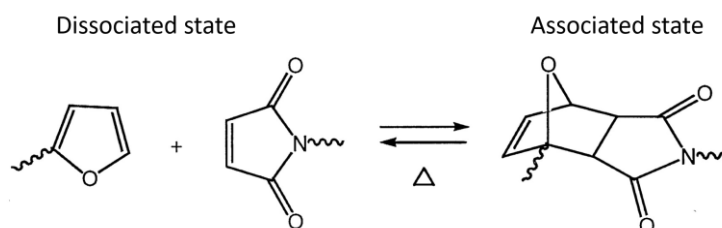


Figure 2-3 A thermo-responsive hetero-Diels-Alder reaction [16].

On the other hand, in associative covalent networks, a bond is broken only when a new one is formed (Figure 2-2b). In other words, the cross-linking density remains constant at each time and temperature. These networks, based on addition-fragmentation chain transfer (ATF), have been studied for more than a decade [17]. The first ATF reactions in bulk polymer were: (i) the thiol radical-mediated addition fragmentation of an allyl sulphide and, (ii) the transesterification reaction between hydroxyl and ester functional group. Scott *et al.* were the first team to complete ATF in sulphide polymer matrix [17]. The team induced photo-ATF *via* radical produced by the photo-cleavage of photo-initiator. Instead of fully curing the polymer, the functionalisation allows stress to be relaxed by light in allyl sulphide based polymers. Some other studies have then explored different radical generators such as trithiocarbonates [18]. However, these systems use highly hazardous chemicals and have a limited lifespan due to termination reaction [8].

2.3 Engineering vitrimers

In 2011, Leibler and co-workers [19], used a metallic salt - zinc acetylacetonate ($\text{Zn}(\text{acac})_2$) - to catalyse the transesterification reaction between epoxy and fatty acid. Based on an associative mechanism, this material is insoluble in water or solvent (*e.g.* trichlorobenzene, TCB). The crosslink density is dynamic, permanent, and possesses an interesting flow and stress relaxation when the bond exchange reaction (BER) is thermally activated. After a temperature - called topology freezing temperature or vitrification temperature (T_v) - the polymer viscosity follows an Arrhenius-like law (similar to strong glass former as vitreous silica), making the epoxy-based polymer able to be reshaped, reprocessed and recycled in other form [19]–[21].

The first vitrimers made by Leibler *et al.* [19] comprised of:

- i) epoxy base: diglycidyl ether of bisphenol A (DGEBA)
- ii) hardener: Pripol 1040 (soft vitrimer with T_g below room temperature)/glutaric anhydride (hard vitrimer, with $T_g \approx 80^\circ\text{C}$)
- iii) catalyst: $\text{Zn}(\text{acac})_2$

In epoxy system used for vitrimers this transesterification happens between two β -hydroxyesters as shown in Figure 2-4.

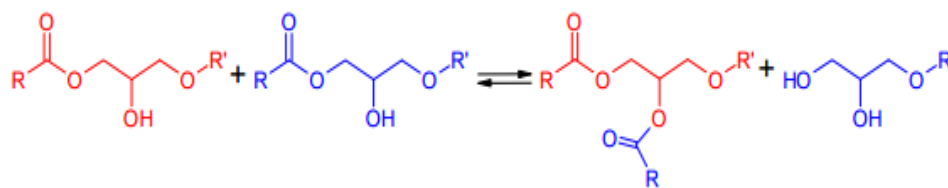


Figure 2-4 Reaction of transesterification between two β -hydroxyesters in an epoxy system - adapted from [14].

These transesterification reactions occur in epoxy systems, however, the rate of this reaction is so slow that networks can be considered as “frozen”. Classic epoxy samples cannot rearrange their topology under stress, being reshaped or self-healed. In vitrimer, the catalyst increases the rate of transesterifications even at a relatively low content (*e.g.* 5 mol% of the acid groups); when the temperature reaches T_v , it allows the stress to be relaxed by the network. This temperature depends on the catalyst nature and its content as studied later by Capelot *et al.* [15]. The first conclusions made by Leibler and co-workers were: (i) insolubility of vitrimers inside trichlorobenzene (TCB) at different temperature (until 180°C for 16 h), (ii) Presence of the topology freezing temperature well separated from the classic glass transition temperature, (iii) Reshaping and reprocessing of epoxy vitrimers samples by simple heating; samples kept their initial mechanical properties even after being reprocessed, (iv) the chemistry of vitrimers is “versatile, relies on readily available ingredients, and does not require any special equipment.”

2.4 Characterisation of vitrimer materials

2.4.1 Properties that define vitrimers

A vitrimer is defined as a crosslink network that has the ability to flow by relaxing stress under the appropriate trigger. From this, the way to characterise a vitrimer can be easily achieved proving two simple properties: (i) assessment of the network chemical crosslinks, and (ii) its capacity to flow. The first property can be demonstrated easily just by immersing the network in an appropriate solvent and measure its swelling capacity and soluble fraction. If the network does not dissolve it is then confirmed that the chemical crosslink has been achieved during polymerisation. The first vitrimer developed by Leibler and co-workers was swollen in TCB for several hours at different temperatures to assess its swelling ratio (Figure 2-5, Equation 2-1) and soluble fraction (Equation 2-2).

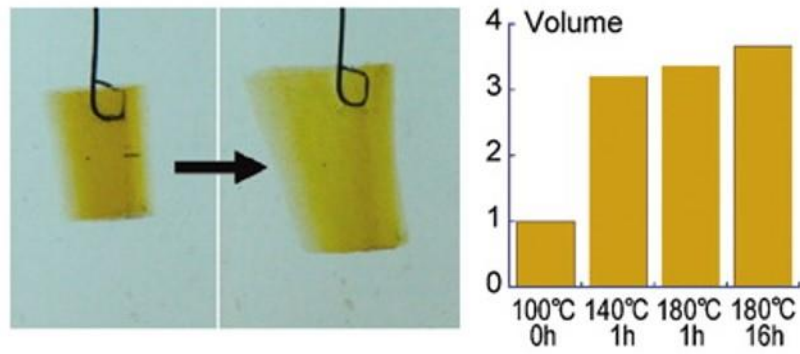


Figure 2-5 Swelling of first vitrimer network and its swelling ratio at different temperatures [19].

These two parameters can be calculated using the following equations:

$$\text{Swelling ratio} = \frac{m_2 - m_3}{m_3} * 100$$

Equation 2-1 Calculation of swelling ratio of polymers.

$$\text{Soluble fraction} = \frac{m_3 - m_1}{m_1} * 100$$

Equation 2-2 Calculation of soluble fraction of polymers.

where m_1 represents the sample initial weight, m_2 is the weight of the swollen sample and m_3 the weight of sample after drying off the solvent.

The second property of flow has been assessed in different ways in the literature. Initially, a stress relaxation experiment was performed over a range of temperatures, then the relaxation time τ was taken at 67% ($1/e$, value chosen arbitrary [22]) of the relaxation process for each temperature. Once τ is acquired for all temperature, the data can be plotted on a logarithmic scale inversely to the temperature (*i.e.* Arrhenius plot). From τ , the viscosity of the network can be calculated and its evolution can also be plotted inversely with the temperature. Vitrimer materials follow a linear trend when plotted within this Arrhenius plot, and the slope of the curve defines their activation energy E_a (*i.e.* the energy required to initiate the bond exchange between chemical moieties) as shown in Figure 2-6.

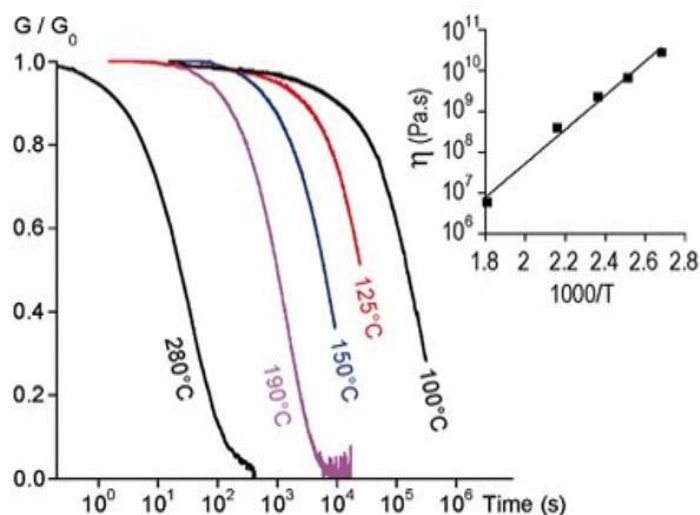


Figure 2-6 Stress relaxation experiment of initial vitrimer network and its Arrhenius plot (inset), where the slope defines the energy activation of the network [19].

Initially performed using rheology with shear geometry, the stress relaxation has then moved towards dynamical mechanical analysis (DMA) with various geometry (*e.g.* tension, compression, *etc.*), and more recently, creep study has been defined as an appropriate method to calculate the vitrimer viscosity at various temperatures and finding their activation energy [22]. An advantage of using DMA rather than rheometer technique is that when a soft material is near 100% relaxation, at relatively high temperature, the sensitivity of the equipment is more stable and allows proper measurement of high deformation (Figure 2-7a,b). So far, these two methods have been used to quantitatively characterise the BER. It should be noted that a simple way to prove stress relaxation of vitrimer material is to use birefringence (Figure 2-7c), however this technique is only qualitative and cannot be used to fully characterise new vitrimer networks [19].

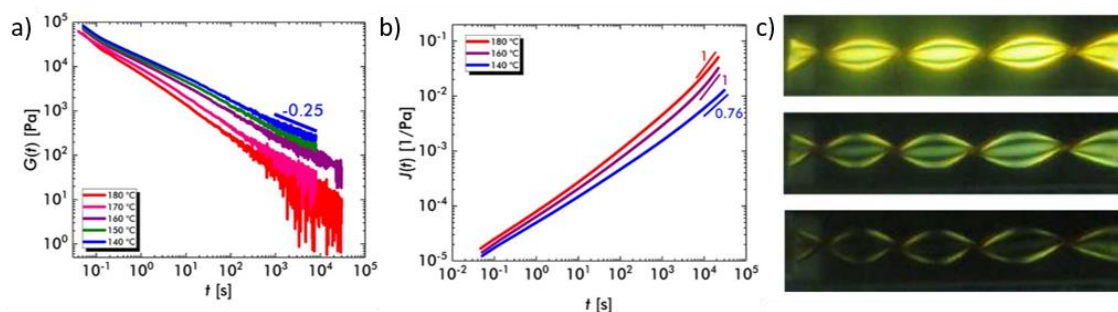


Figure 2-7 a-b [22]: Comparison between shear rheology and creep behaviour for a vitrimer network: a) stress relaxation, b) creep compliance; c) Use of birefringence to observe progressive colour fading in a constrained vitrimer at 180°C corresponding to progressive stress relaxation over 20min [20].

Generally, the vitrification temperature T_v , is determined by the temperature at which the network viscosity reaches 10^{12} Pa.s, or using thermodynamic experiments to observe change in the coefficient of thermal expansion [23]. The former method is heavily dependent on the mechanical properties and crosslink density of the initial network and can induce differences depending on the methods used to calculate viscosity (*i.e.* stress relaxation or creep). Therefore, comparing the T_v of materials with varying properties and across different research groups is challenging and not reliable. The method based on coefficient of thermal expansion allows easy visual interpretation of the T_v , where network viscoelasticity changes from a viscoelastic solid to a viscoelastic melt (Figure 2-8a). This method usually allows for easier discerning between the T_g and T_v , but is limited in terms of accuracy and cannot distinguish between stress relaxation due to bond exchange and other relaxation phenomena [24], [25]. A more effective method has been developed to accurately measure the T_v , using aggregation-induced-emission (AIE) luminogens [26]; their incorporation within an epoxy-unsaturated carboxylic vitrimer network gives the ability to measure T_v *via* fluorescence. These luminogens have high emissivity when agglomerated due to motion restriction and have been proven to be efficient to measure the T_g of other polymers. When vitrimers are in their “glassy” state (*i.e.* below T_v), the luminogens have a high emissivity. Once the bond exchange is activated, the motion of molecular chains allows AIE to move and decreases their agglomerations, making the overall emissivity of the network lower (Figure 2-8b). The T_v of the networks were successfully measured without application of external stress using this method which, to date, seems the most accurate way to obtain this value [26]. Rather than defining the exact T_v , the research community has moved toward focusing on the temperature that can be applied to reshape, heal and reprocess their vitrimer network.

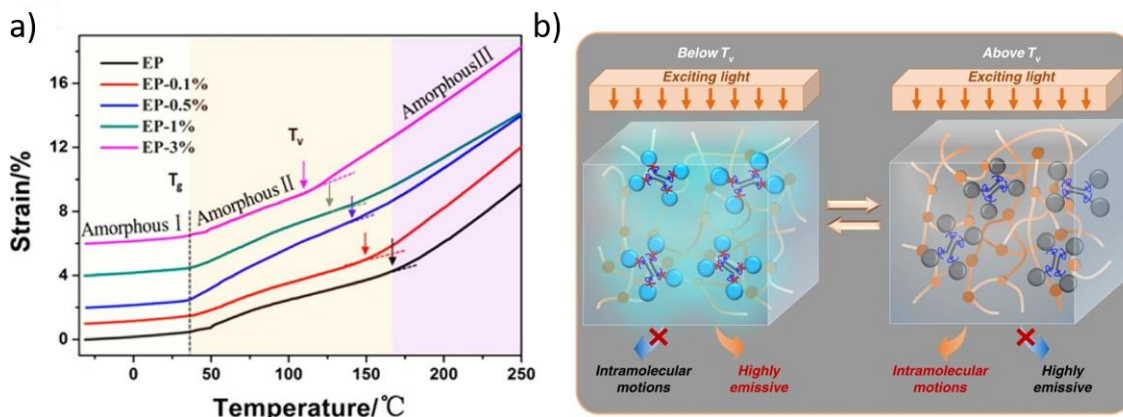


Figure 2-8 a) Measurement of T_v of graphene vitrimer network using dilatometry experiment [23], b) measurement of T_v using AIE luminogens technique [26].

2.4.2 Additional properties

Crack healing can be achieved by using free radicals on the crack surfaces. Once temperature is risen (above the BER activation temperature), these radicals can link with other bonds. It has been demonstrated [27][28], notably, fumaropimaric acid (FPA) has been used as a hardener for epoxidised soybean oil (ESO) resin and $(Zn(acac)^2)$ as catalyst to produce a more bio-based vitrimer that the authors termed ‘*biovitrimer*’ [29]. Their network exhibited crack closure after 60 min at $180^\circ C$ (Figure 2-9a), however crack healing efficiency is likely dependent on the creep behaviour of the vitrimer (higher creep results in better crack closure, QAP’s opinion). It would be safe to assume healing is generally more efficient for elastomeric material than a glassy like polymer.

Reprocessing can also be demonstrated as studies have focused on reprocessing of crushed vitrimer samples *via* extrusion or injection/compression moulding [24], [30], [31]. In the pioneering work of Leibler and co-workers [19], the hard network (*i.e.* high T_g vitrimer made of anhydride) was crushed into pieces and reprocessing was achieved *via* injection moulding (Figure 2-9e). Tensile testing revealed recovery of up to 95% of the initial vitrimer tensile modulus (Figure 2-9b,c).

Shape memory behaviour is characteristic of vitrimers due to their chemical crosslinks. Whilst this property is general for all thermoset polymers, vitrimers have re-programming ability. Shape memory properties of thermosets has attracted a lot of attention, especially for self-unfolding structures for applications such as solar wings in satellites [32], [33], “nano-robots” to enable actions (grabbing, holding and moving) [34].

As aforementioned, thermoset materials can be challenging to process and shape, whereas vitrimers can be re-shaped and have new possibilities for shape memory applications. Vitrimers can be fixed into temporary shapes above their T_g , cooled down, and when the temperature applied reaches T_g again, the vitrimer will come back to its original shape. This operation can be repeated several times due to the covalent bonds, and the initial shape can be reconfigured to a new one by deforming the vitrimer above T_v again. (Figure 2-9d,e). This makes vitrimers not only advantageous for processing of the initial shape but also to reconfigure its shape morphing as shown in Figure 2-10.

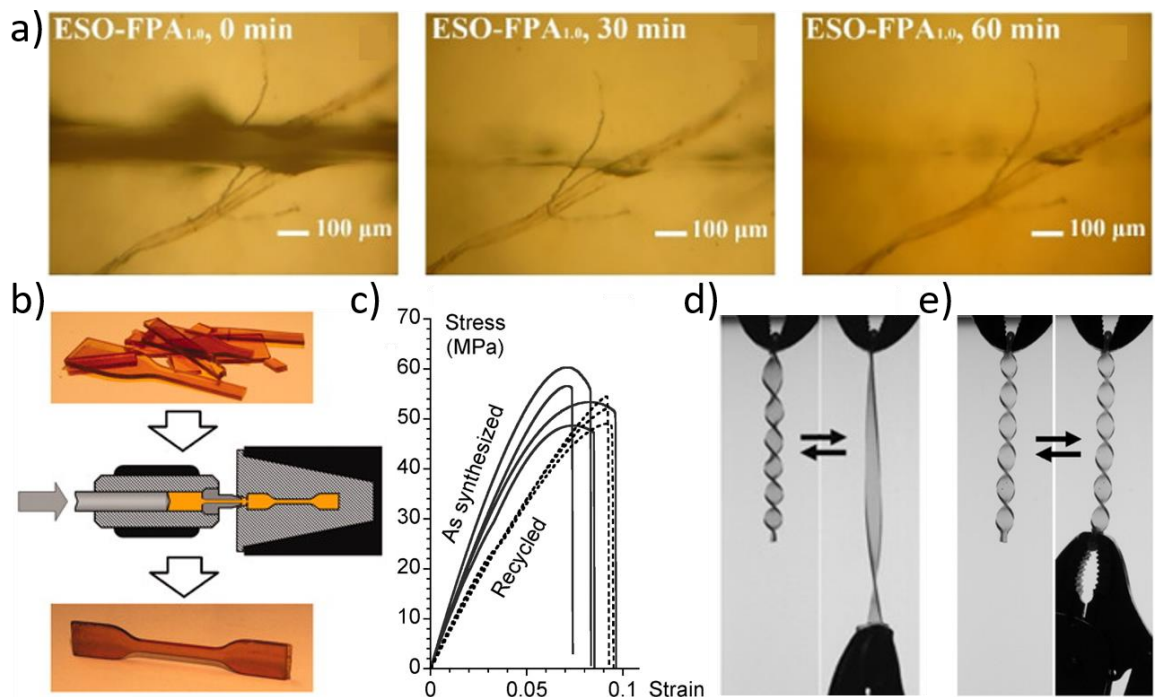


Figure 2-9 Examples of additional vitrimer properties mentioned; a-d) The hard vitrimer network prepared by Leibler and co-workers [19]: reprocessing *via* injection moulding (a), tensile results of original and reprocessed dogbone specimens (b), temporary shape changing by heating above T_g (c), definitive shape changing by heating above T_v (d); e) healing of epoxidised soybean oil (ESO) fumaropimaric acid (FPA) vitrimer at 180°C [29].

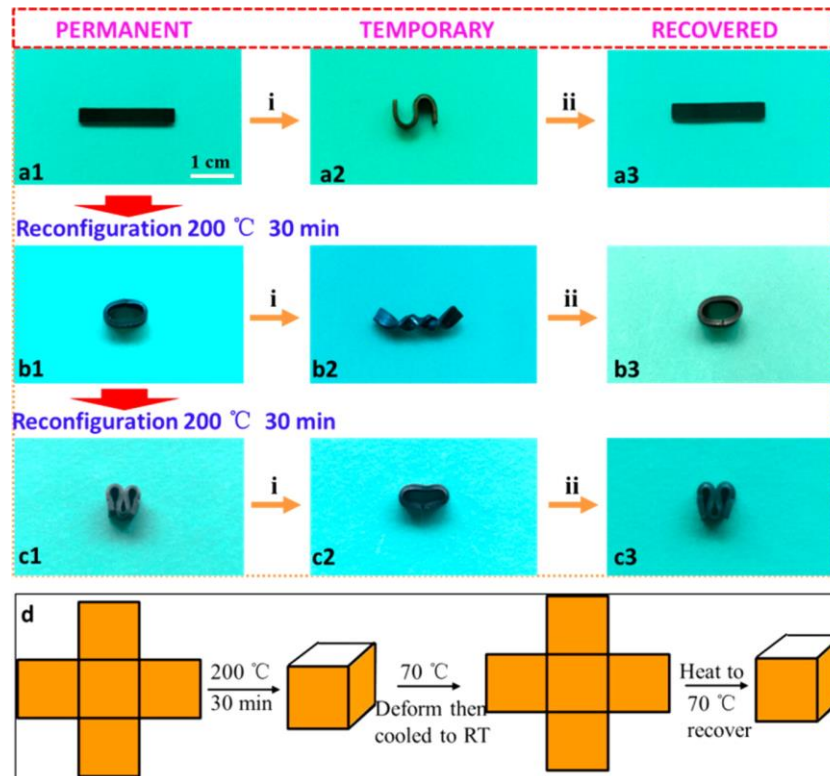


Figure 2-10 Example of shape memory behaviour and re-configurability of a vitrimer (a-c): reconfiguration to a new initial shape above 200°C and new temporary shape above 70°C; (d) Schematic of vitrimer programming [23].

2.5 Catalyst based vitrimers

2.5.1 Transesterification

Since their discovery, transesterification catalysed based vitrimers have been interrogated by a variety of studies to understand their chemistry and behaviours. To understand the current state of literature, this section is divided into three part: (i) Influence of hardener and catalyst on vitrimer networks and processing conditions, (ii) Variations from pure epoxy-dicarboxylic hardener formulation, and (iii) notion of vitrimer-like materials in transesterification vitrimers. The reader can find all the mentioned studies in this section ordered by part in Table 2-1.

The Influence of hardener and catalyst on vitrimer networks and processing conditions has been widely explored. For example, varying the hardener in epoxy-based vitrimers from unsaturated carboxylic acids with different lengths to cyclic anhydride allows tuning of thermochemical properties [19], [26], [35]–[40]. In those works, rubbery and glassy materials can be obtained with T_g below 0°C up to 130°C. Others have studied the impact of blend of hardener such as sebacic acid (SA) and 1,4-cyclohexanedicarboxylic

acid (CHDA), maintaining resin/hardener stoichiometry but varying the relative quantity of each hardener [35]. This study showed that the vitrimer T_g and stiffness can be tuned - the higher the ratio of unsaturated acid, the lower the properties.

An early vitrimer study performed by Leibler and co-workers investigated the effect of three catalysts type on the T_v of vitrimers: triphenylphosphine (PPh_3), triazobicyclodecene (TBD), and $(Zn(acac)_2)$ [15]. The study showed that the T_v of vitrimer networks could be tuned with the catalyst type and content without changing their T_g . Catalysts with certain structures such those with primary amine (butylamine, BA), secondary (dibutylamine, DBA) or tertiary amines, able to bond with the network, are reported to enhance transesterification rate and decrease the activation energy [41]. It is believed that the change of the activation energy is mainly due to variation in the electro-negativity of the surrounding environment and also the nature of the bond between network and catalyst [15], [41]–[44]. The ability of epoxidised natural rubber (ENR) to bond with adjacent surfaces and efficiently relax stress has also been reported to improve compared to traditional ENR *via* catalyst addition [37].

Reprocessing time and temperature of vitrimer blends was studied in function of the particles size of the crushed samples [30]. The study found that smaller particles size (< 1 mm), longer time (> 1 h) and higher temperature (> 160°C) gave the best reprocessing conditions to recover the rubbery modulus and ultimate tensile strength of the initial polymer. A higher pressure applied during reprocessing was also reported to slightly improve the mechanical properties. However, this parameter was of lower importance than the others (particles sizes, time and temperature) [30]. Solvent-induced plastic deformation has also been used to program new shapes from flat vitrimer sheets without the need to heat the sample above its T_g [45].

Variations from pure epoxy-dicarboxylic hardener formulation have been progressively developed. Most epoxy vitrimers reported to this point are amorphous. However, an example of semi crystalline vitrimer was produced using poly(butylene terephthalate) (PBT) as hardener [46]. Towards a different goal, the incorporation of difunctional norbornene with pendant carboxylic and hydroxyl groups allows production of photocurable vitrimer, which was used for nano-scale patterning and printing [47]. Use of a combination of carboxylic acid and amine-capped aniline trimer (ACAT) as hardener led to a vitrimer system responsive to six different triggers (thermal, pH, voltage, metal ions,

light, redox chemicals) [48]. In this work, the presence of the oligoaniline did not disturb the initial properties of the vitrimer network (reprocessing, healing, heat responsive), and also brought to the network the ability to react to the other triggers *via* its inherent redox, photothermal, and electro-activity properties. Aiming to introduce a secondary mechanism of BER, some researchers explored use of different hardeners [49], [50]. For example, *N*-acetylglycine (NAG) used as co-hardener with sebacic acid, allows for extensive hydrogen bonding [49]. In that work the hydrogen bonding acts as “sacrificial bond” to relax stress at a low temperature as well as improves the stiffness of the overall material. 4,4'-dithiodibutyric acid has also been used as co-hardener with sebacic acid to act in synergy with the transesterification *via* disulphide metathesis [50]. The network shows faster relaxation time and two characteristic slopes above T_g in an Angell-fragility plot.

Vitrimer networks based on transesterification were also produced using different resins than epoxidised ones. PBT was crosslinked with glycerol and zinc acetate ($Zn(OAc)_2$) to form semi-crystalline vitrimers from thermoplastics [51]. A hyperbranched polyglycerol has been used as the resin component to produce a vitrimer with UV blocking and fluorescence properties [52]. Polydimethylsiloxane (PDMS) epoxy functionalised particles have been successfully used to produce an emulsion with high “malleability” [53]. The vitrimer network within the emulsion allows better creep resistance and also ease of processing.

Notion of vitrimer-like materials in transesterification vitrimers has appeared recently. The aforementioned networks exhibit ability to fully relax stress with the BER mechanism, however, there are some examples in literature that have demonstrated a capacity to only partially relax [76,77]. These networks have been termed “vitrimer-like” and this property is often due to the imbrication with another polymer network which cannot relax stress itself. For example, the “interfacial broadening” (*i.e.* bicontinuous interface) of polymer made of poly(methyl methacrylate) (PMMA) and epoxy-based vitrimer was studied [54]. A higher content of PMMA was reported to decrease the interfacial broadening due to motion restriction of the vitrimer chains responsible for the bicontinuous interface. Diglycidyl hexahydrophthalate and hydrogenated carboxylated nitrile butadiene rubber also produced a vitrimer like material, where the stress relaxation is limited due to the low amount of free hydroxyl group required for transesterification reactions [55].

Table 2-1 Networks and properties of catalyst based transesterification vitrimer in literature. NA: Non-applicable, E: Young's modulus, G: Shear modulus, blue shading: *influence of hardener and catalyst on vitrimer networks and processing conditions*, orange shading: *variations from pure epoxy-dicarboxylic hardener formulation*, green shading: *notion of vitrimer-like materials in transesterification vitrimers – acronym: Zn-PAM is a polymer catalyst corresponding to poly(acrylonitrile-co-zinc methacrylate)*.

“Resin”	Cross-linker	Catalyst	Mechanical properties	T _g /T _v	E _a (kJ.mol ⁻¹)	Primary aim	Ref
DGEBA	Glutaric anhydride, Pripol 1040	Zn(acac) ₂	9 MPa -1.8 GPa (E)	T _g :15-80°C	80-90	Vitrimer concept and demonstration from commercial epoxy (soft and hard)	[19] 2011
DGEBA	Pripol 1040	PPh ₃ , TBD, Zn(acac) ₂	NA	T _g :40°C T _v : 60-110°C	90	Control of vitrimer T _v by catalyst content/type	[15] 2012
DGEBA	Pripol 1040	Zn(OAc) ₂	NA	NA	NA	Coordination and catalysis of Zn ²⁺	[42] 2016
ENR	Dodecanedioic acid	Zn(OAc) ₂	NA	NA	NA	Adhesion and stress relaxation of ENR vitrimers compared to classic ENR	[37] 2016
DGEBA	Pripol 1040/1025/1252	Zn(OAc) ₂	NA	T _g :-11 to21°C T _v : 70°C	75-130	Curing/viscoelasticity evolution with hardener type and ratio	[38] 2017

DGEBA	Adipic acid	TBD	NA	T _g : 44°C T _v : 105°C	NA	Using solvent to induce BER at low temperature and programming shape morphing from flat structures	[45] 2018
4,4'- bioxepane- 7,7'-dione	4- methylcaprolacton e	Variety of Brønsted acids	NA	T _g : -56 to -52°C	49-67	Studying impact of Bronsted acid on BER	[43] 2018
DGEBA	CHDA, SA	TBD	4 MPa – 1.3 GPa (E)	T _g : 30- 90°C	NA	Tuning the thermomechanical properties of vitrimer by tuning ratio of hardeners	[35] 2018
DGEBA	SA	Zn-PAM	505-649 MPa (E)	T _g : 37- 47°C T _v : 175- 180°C	68-90	Using Zn ²⁺ ionomer to enhance BER and mechanical properties	[44] 2019
DGEBA	SA Citric acid	DBA/BA	NA	T _g : -55°C	90-100	Tuning transesterification rate using bonded primary or tertiary amine catalysts	[41] 2019
1,4- butanediol	Carboxylated polyester	Zn(OAc) ₂	2.9-4.2 MPa (E)	T _g : -39 to -18°C	81-83	Synthesis of low T _g elastomeric vitrimer	[36] 2019

diglycidyl ether				T _v : 138-144°C			
DGEBA	Pripol 1040/ 1,2-Benzoquinone	Zn(OAc) ₂	3 MPa – 1.15 GPa (E)	T _g : -25-85°C	NA	Recycling of vitrimer blend and tuning of thermomechanical properties	[39] 2019
DGEBA	Adipic, dodecanedioic and octadecanedioic acid	TBD	NA	T _g : -11-45°C T _v : 102-144°C	NA	Using AIE luminogen to detect T _v without applying mechanical stress	[26] 2019
methacrylate-grafted high density polyethylene glycol (HDPE)	poly(caprolactone) diol poly(tetrahydrofuran) diol	TBD	NA	T _g : 125-130°C	NA	Reprocessing of HDPE with triple shape memory effect	[40] 2019
DGEBA	Pripol 1040	Zn(OAc) ₂	2-4 MPa (E)	T _g : 23-28°C	NA	Studying the impact of vitrimer particles size, time, pressure and temperature when reprocessing vitrimer	[30] 2020
bisphenol A glycerolate	Pentaerythritol tetrakis(3-	TBD	NA	T _g : 86°C	48-54	Incorporating vitrimer chemistry in Thiol-ene UV curing to obtain	[47] 2016

di(norbornenyl ester) BPAGDN	mercaptopropionate) (PETMP)					remoldable nanoimprint <i>via</i> photopatterning	
DGEBA	Suberic acid/ ACAT	TBD	NA	T _g : 40-55°C T _v : 180°C	NA	Multiple responsive vitrimer (thermal, pH, voltage, metal ions, light, redox chemicals)	[48] 2017
PBT	Glycerol (GLY)	Zn(OAc) ₂	NA	T _g : 50°C	138-163	Semi-crystalline vitrimer made from thermoplastic	[51] 2017
Epoxy and bisphenol ether	PBT	Zn(acac) ₂ + 2MI	NA	T _g : 48-50°C	130-140	Using Zn ²⁺ vitrimer chemistry to crosslink PBT and tune their properties toward extrusion process	[46] 2017
Epoxidised natural rubber	SA NAg	TBD	2-6.5 MPa	T _g : -8 to -7°C	107-113	Integrating H-bonds as reversible low temperature dynamic network to improve toughness and SR	[49] 2019
PDMS epoxy	Fatty dimer acid + CS697	NaOH + Zn(OAc) ₂	0.17-1.13 MPa (G)	T _g : -53 to -23°C T _v : 138-144°C	21-110	Emulsion based vitrimer for improved malleability	[53] 2019

DGEBA	4,4'- Dithiodibutyric acid, SA	TBD	1-2 MPa	T _g : -25- 40°C T _v : 65- 150°C	75-100	Using disulphide bonds to induce synergy between transesterification and disulphide metathesis	[50] 2019
Hyperbranch ed polyglycerol (HPG)	Itaconic anhydride Glutaric anhydride methylcyclohexan e-1,2-dicarboxylic anhydride	Zn(acac) ₂	55-1719 MPa	T _g : 10- 45°C	NA	Producing hyperbranched glycerol vitriimer with adhesion properties, UV blocking and fluorescence properties	[52] 2020
Diglycidyl hexahydrophth alate	hydrogenated carboxylated nitrile butadiene rubber	TBD	2.9-3.5 MPa (E)	T _g : -10 to 0°C	NA	Producing vitriimer-like from hydrogenated carboxylated nitrile butadiene rubber with high thermal and oxidation stability	[55] 2019
PMMA + DGEBA	Dodecanedioic acid	TBD	22-48 MPa (E)	T _g : 29- 110°C T _v : 100- 120°C	NA	Studying the interfacial broadening of PMMA/vitriimer composite as vitriimer like materials and their blends	[54] 2019

2.5.2 Other catalyst based vitrimer chemistry

Initially relying on transesterification mechanism, the chemistry of vitrimer has since adapted to several other types of BER. Transcarbonation chemistry has also been shown to work using a catalyst activated BER. This vitrimer was prepared using bis(6-membered cyclic carbonate) and 1,4-butanediol polymerised together to form a polycarbonate network [56]. This network was prepared with different ratios of C=O and hydroxyl moieties to tune their thermomechanical properties (E_a from 81 to 123 $\text{kJ}\cdot\text{mol}^{-1}$ and T_g ranging from 15°C to 35°C). The polymerisation of the network was catalysed by Ti(IV) alkoxides [56]. Once the network is formed, excess of hydroxyl groups can do nucleophile attack on carbonyl moieties to perform carbonyl substituent exchange (Figure 2-11). Whilst this network exhibits good reprocessability and is reported to recover 80% of the initial monomers, the versatility of efficient catalysts for these reactions are limited. Often, the catalysis leads to secondary products [56], making these networks less reliable than the other networks presented above relying on epoxy ROP reaction.

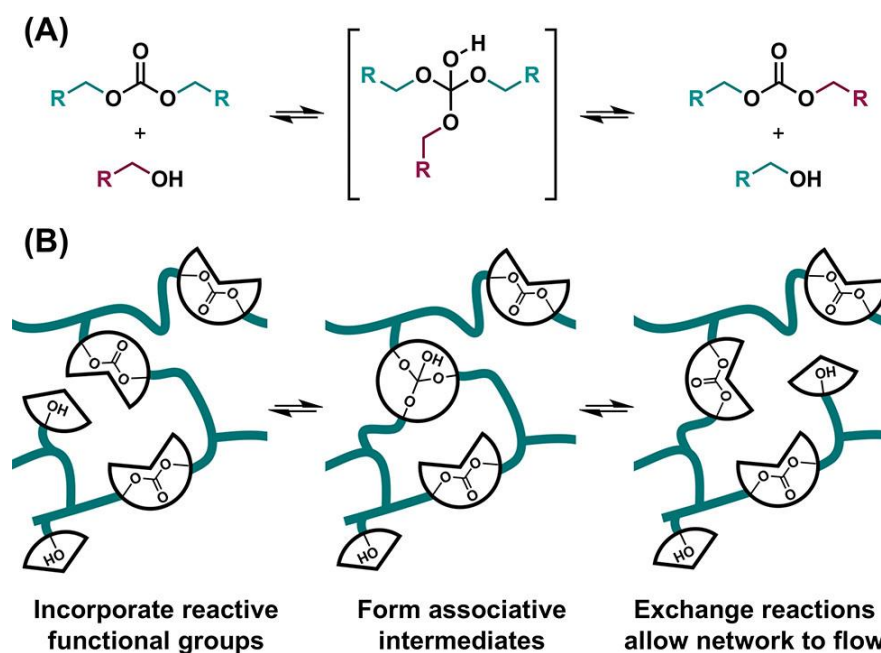


Figure 2-11 a) Schematic of transcarbonation exchange with formation of an associative intermediate state after hydroxyl reacts with a carbonate, b) Topology rearrangement undergone by the polycarbonate network via transcarbonation [56].

Transamination has been reported to be enhanced by catalysts in polyurethane vitrimer [57]. However, these reactions work without the presence of catalyst, and are detailed in section 2.6.

2.6 Catalyst free vitrimer

2.6.1 Transamination

Transamination BER was achieved by Du Prez and co-workers in 2015, using vinylogous urethane vitrimers [58]. The transamination reaction allows transfer of an amine function to a ketoacid (Figure 2-12a). This is usually a slow reaction but was enhanced using Brønsted/Lewis acids or having a high content of free amine functions within the bulk polymer [57]. Contrary to the esterification process which produces free hydroxyl groups for the bond exchange, the vinylogous urethane system does not have this specificity (*i.e.* producing amine groups for the BER). Therefore, the stoichiometry ketone/amine was set to 0.95 in order to remain close to 1:1 stoichiometry while producing crosslinked material with a reasonable amount of residual free amine functions. The network displayed a T_g close to 90°C, an energy activation lower than prior transesterification based vitrimer ($\approx 65 \text{ kJ}\cdot\text{mol}^{-1}$ versus 80-90 $\text{kJ}\cdot\text{mol}^{-1}$ for Leibler's vitrimers system [19]). However, when the T_v of the network was calculated by the viscosity method (temperature at $\eta = 10^{12} \text{ Pa}\cdot\text{s}$), it was found to be 29°C, and the stress relaxation below T_g (90°C) was not dominated by Arrhenius law but rather the WLF law. Du Prez and co-workers stated that a T_v for this network did not, in fact, exist as the network is frozen below its T_g [58].

Following this study, the chemical control of the exchange reaction was investigated comparing uncatalysed reaction with reaction catalysed by Lewis acids or bases [57]. It was found that acids can accelerate the BER, lowering the E_a of vinylogous vitrimer ($\approx 31\text{-}70 \text{ kJ}\cdot\text{mol}^{-1}$ compared to $\approx 80 \text{ kJ}\cdot\text{mol}^{-1}$ for the non-catalysed network), while strong bases such as TBD slowed down the BER ($\approx 120 \text{ kJ}\cdot\text{mol}^{-1}$), acting like a "proton scavenger" of amine functions; the BER was fully stopped with a 5% concentration of TBD. The tuning of BER allows to reduce or increase creep of these materials at their working temperature and compression study showed that TBD samples exhibit higher compression resistance while acid catalysed samples exhibit higher permanent deformation [57]. Since, different networks have been developed using the same BER mechanism. For example a polyurethane based on phenol-carbamate bonds was developed [59], exhibiting high transparency and excellent recovery of tensile properties after reprocessing (up to four

times) at 100°C for 1 min under 5 MPa of applied stress (Figure 2-12b,c), with a reported E_a of $\approx 90 \text{ kJ}\cdot\text{mol}^{-1}$.

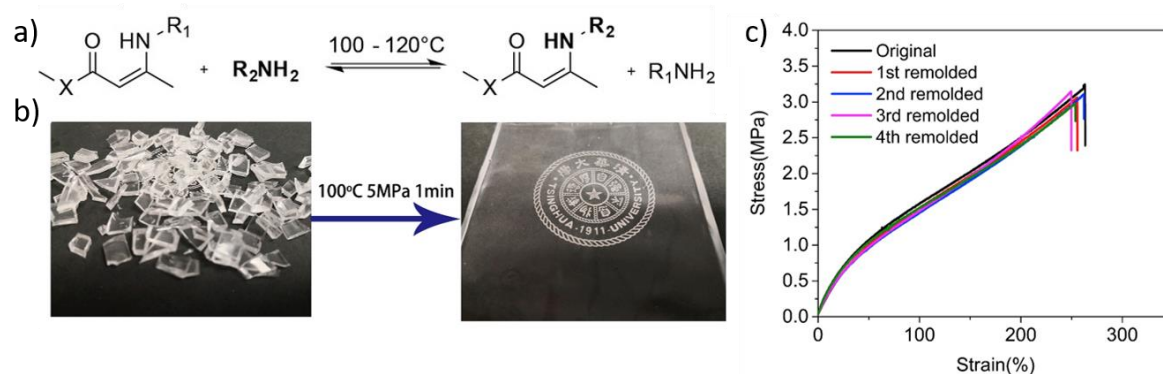


Figure 2-12 a) Scheme of transamination process occurring from 100°C [58], b) reprocessing of phenol-carbamate vitrimers and c) their mechanical properties with comparison of initial and reprocessed networks [59].

In respect of transesterification-based vitrimers, researchers have focused on making thermoplastic-based transamination vitrimers. PDMS was functionalised with amine pendant functions, and crosslinked with bis-vinylous urethane [60]. The resulting network showed no dissolution in tetrahydrofuran (THF), with soluble fraction ranging from 19% to 35%, confirming crosslinking of the network. It should be noted that their vitrimer samples could be quenched by swelling in THF and methyl acetate which condense the free amine radical to vinylous urethane without increasing the crosslink density [60]. PBT was also used to form a vitrimer based on urethane chemistry [24]. By functionalisation with acetoacetyl groups, the PBT was crosslinked with different diamine crosslinkers. The polymer showed T_g varying from 8°C to 24°C with elastic modulus ranging from 4.4 MPa to 43.4 MPa depending on the crosslinker chain lengths and structures [24], providing a facile way to produce crosslinked rubbers with tuneable properties and good processability.

The BER dynamics of a urea system has been investigated to understand the impact of steric hindrance on urea bonds using aminoethanol compounds with secondary amine groups of different bulkiness [61]. A higher degree of steric hindrance resulted in increased BER, although most of the prepared networks were considered dissociative mechanisms, and therefore were labelled as “vitrimer-like” materials. A dual responsive urethane vitrimer was produced by polymerisation of photodimerisable diaminoanthracene and diaminoalkyl linked by a bisacetoacetate [62]. The photodimerisable function allows crosslinking *via* UV and the urea bonds allow healing on application of temperature (80°C, 10 min) [62]. A dual stress relaxation behaviour was observed in a perfluoropolyethers

(PFPE) transamination vitrimer, with two E_a (60 $\text{kJ}\cdot\text{mol}^{-1}$ compared to 130-170 $\text{kJ}\cdot\text{mol}^{-1}$) [63]. Two exchanges pathways (iminium and Michael addition) were found to co-exist in the material, with one another governing the relaxation of the polymer depending on the temperature applied [63].

2.6.2 Imine

Using similar chemistry, BER vitrimers based on transamination reactions have been produced, the first example of which was developed in 2016 [64]. The network was prepared using poly(ethylene oxide) (PEO) and imine crosslinkers; the condensation reaction produces water which remained in the polymer. The imine exchange BER presents two different possible mechanisms: associative with exchange of imine promoted by primary amines, and dissociative with formation of aldehydes and amines, as depicted in Figure 2-13a,b respectively. A kinetic study was performed confirming that the associative mechanism was predominant [64]. Solvents such as acetonitrile (AN), *N,N*-dimethylformamide (DMF) or toluene (TOL) were found to increase the BER, allowing formation of a polymer gel with tuneable malleability (Figure 2-13c) [64].

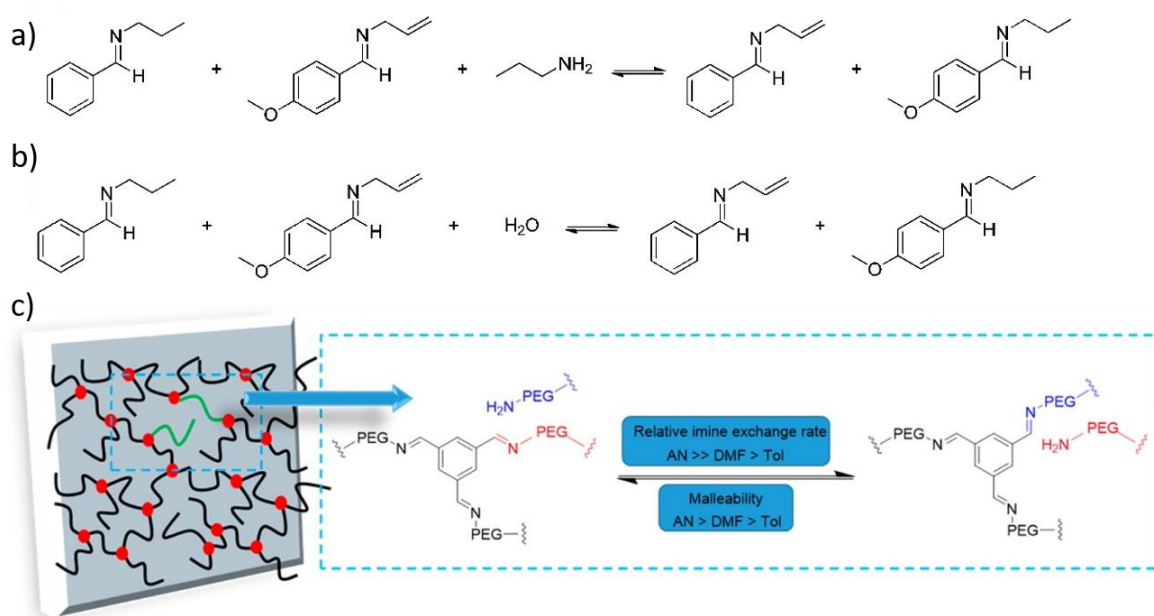


Figure 2-13 Transamination networks: a) associative pathway, b) dissociative pathway, c) PEO vitrimer network and the impact of different solvents on the BER and network malleability [64].

Later, a network comprised of *m*-xylylene diamine, terephthalaldehyde and triethylene tetramine was developed towards a greener version of transamination vitrimers

[65]. The network exhibited high T_g (102°C), good mechanical properties (storage modulus = 1.6 GPa) and an $E_a \approx 80 \text{ kJ.mol}^{-1}$. Due to the two possible exchange pathways of imine based vitrimers, water has significant influence on the network - it can dissolve the network [64], [65], and has also been used to induce malleability at room temperature within an amine functionalised PDMS vitrimer network [66]. The previous examples mentioned above (transamination and transimination) do not rely on the epoxy chemistry. In order to produce transimination vitrimers with high mechanical properties and water insensitivity, an amino capped crosslinker (bearing an amine bond) was synthesised and reacted with an epoxy resin [67]. In this case the BER happens along the crosslinker backbone; the networks produced exhibited T_g ranging from 100°C to 150°C, elastic modulus between 3.5 GPa to 2.7 GPa, depending on the stoichiometry used (ratio epoxy/crosslinker) and an $E_a \approx 60 \text{ kJ.mol}^{-1}$. Immersion in water (up to 15 days - the latest time point investigated) did not impact tensile properties, with water intake $\approx 0.5\%$ of the initial weight.

2.6.3 Transalkylation - ionic vitrimers

Following progress towards catalyst free vitrimer chemistry, transalkylation has been proved to efficiently produce vitrimer and vitrimer like-materials. To the author's knowledge (Quentin-Arthur Poutrel, QAP) the earliest examples of these networks were characterised in 2015 by Drockenmuller and co-workers, using 1,2,3-triazolium salts based crosslinked networks [68]. The chemical reaction allows to have networks that incorporate ions within the bulk material, and therefore, were termed ionic vitrimers. Network relaxation is impacted by the nature of the counter-anions present in the final network (*e.g.* Br⁻, I⁻) with faster relaxation times observed for bromine samples [68]. However, the effect of anion type was not determined. Following this work, a complete study to tune the viscosity profile of ionic vitrimers was performed [69]. That study showed that the nucleophilicity of the counteranion directly impacts the energy activation (140-167 kJ.mol⁻¹) of the network, allowing tuning of stress relaxation profiles. Moreover, the study suggests that a dissociative mechanism takes place rather than an associative one (Figure 2-14) [69]. The authors of that study justified the system to be termed a vitrimer due to the observed Arrhenius relaxation. However, the equilibrium between dissociative and associative mechanism shifts with temperature and seems to be a limited factor for these

networks (the author's view, QAP) as it may induce loss of structure integrity ($\approx 170^\circ\text{C}$ for the related study).

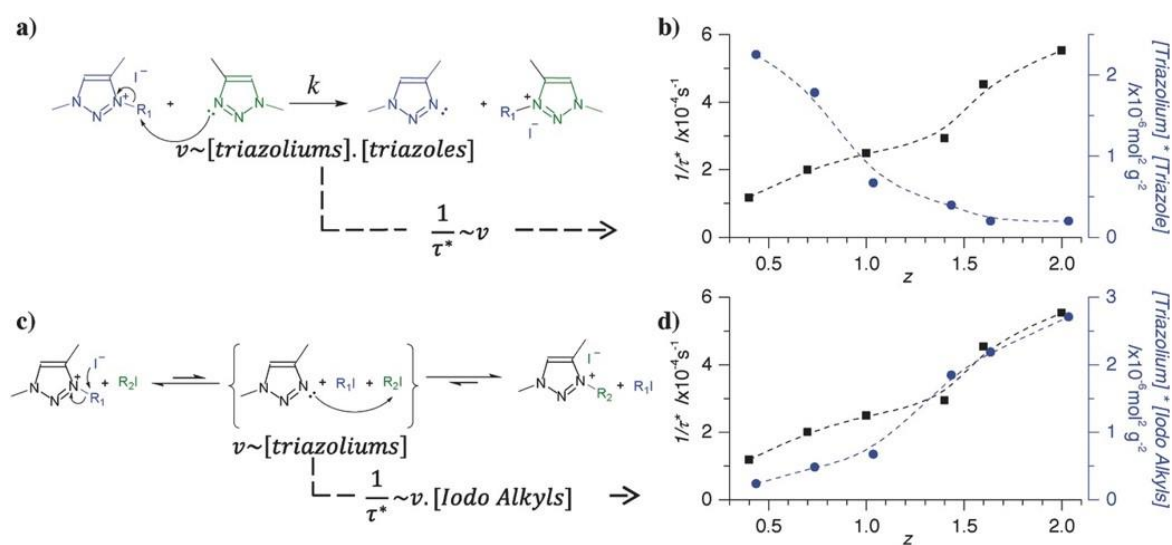


Figure 2-14 a) Proposed associative BER mechanism for ionic vitrimers, with b) a comparison of kinetic model and XPS measurement, c) the proposed dissociative mechanism, with d) the corresponding kinetic model and matching of XPS measurement [69].

A strong adhesive (based on transalkylation) was developed *via* dynamic quaternisation exhibiting adhesive strength up to 23.7 MPa, a $T_g \approx 90^\circ\text{C}$ and $T_v \approx 150^\circ\text{C}$, as well as self-healing ability (maintaining 10 MPa adhesive strength after 20 healing cycles) [70]. A photocurable network was also produced using transalkylation in poly(thioether)-sulfonium salts with an $E_a = 113 \text{ kJ.mol}^{-1}$ [71].

2.6.4 Disulphide metathesis

Disulphide metathesis from aromatic compounds has been used to produce an epoxy vitrimer, *via* bond exchange between the crosslinker units (Figure 2-15) - the network exhibits a high T_g (127°C) with a theoretical T_v below zero (-13°C) with a $E_a = 55 \text{ kJ.mol}^{-1}$ [72]. The same network was then proven to exhibit transient mechanochromism effects after damage (*e.g.* cracks or impactation) [73]. The polymer was reported to become green and this colouration was attributed to the formation of sulphenyl radical formation which was observed to disappear after 24 h at room temperature. Whilst of great interest in the scope of damage detection in composites, the mechanochromism effect was only observed for specific hardener configurations. This fact already limits application as a matrix as the disulphide crosslinker used (4-aminophenyl disulphide) is extremely

expensive (\approx £16.4/g currently) and could not realistically be used on an industrial scale (the author's view, QAP).

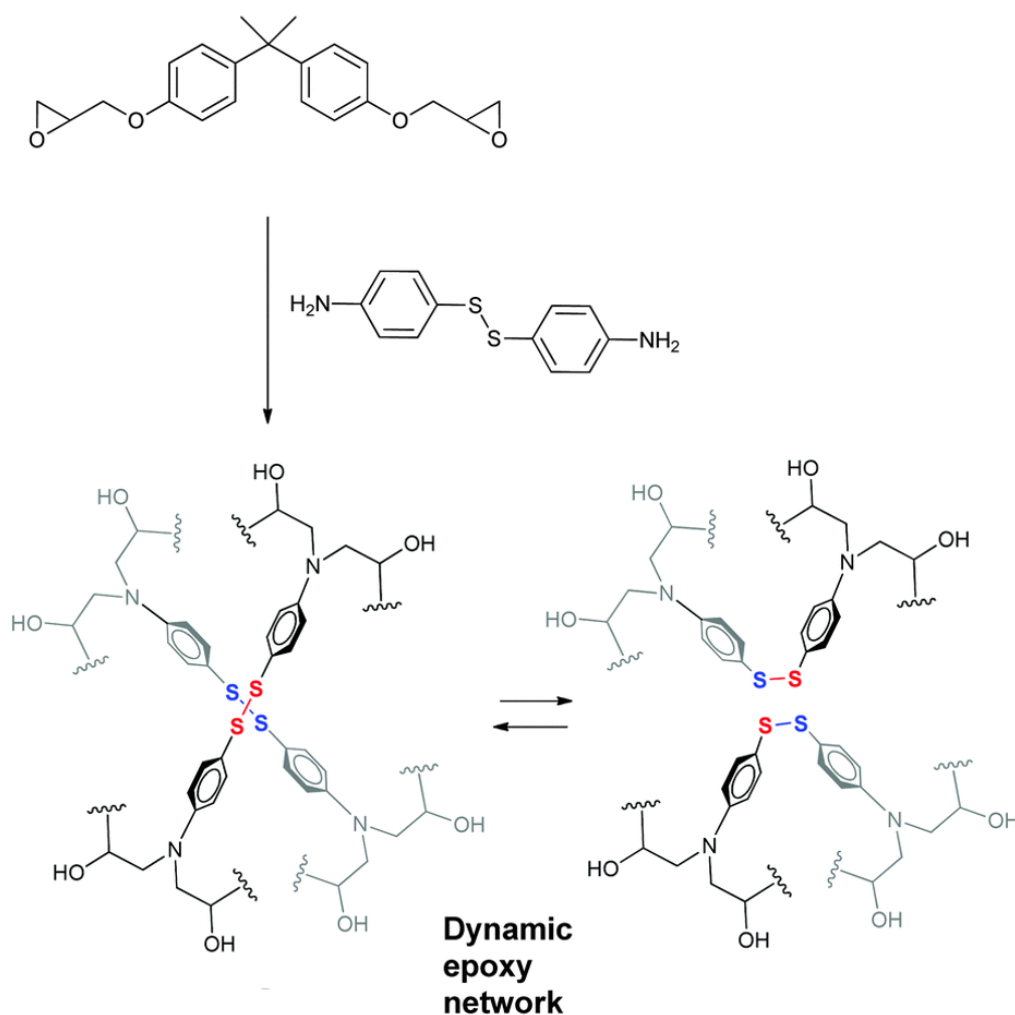


Figure 2-15 Scheme of polymerisation between an epoxy resin and an aromatic disulphide leading to a vitrimer network with BER along the crosslinker units [72].

Sulphur chemistry applied in vitrimers has not been limited to aromatic compounds and a vitrimer has been reported *via* inverse vulcanisation of pentaerythriol tetra(3-mercaptopropionate) (PTMP) with sulphur powder and compression moulding (200°C, 30 min, 10 MPa) [74]. The T_g of the network was varied from 0°C to 30°C by changing the sulphur content (higher content, higher T_g) in the inversed vulcanisation process. Although no relaxation experiments were performed, the polymer exhibited shape memory behaviour and reshaping capability triggered either *via* temperature (40°C) or UV radiation [74].

2.6.5 Ester boronic - transesterification and dioxaborolane metathesis

Boronic ester has also been used to produce vitrimer materials. B-O bonds have a high dissociative energy ($124 \text{ kcal.mol}^{-1}$), allowing formation of networks with good mechanical properties, moreover the rate of bond exchange can be tuned with neighbouring effects [75]. First example of this chemistry relied on transesterification (catalyst free), using two types of boronic acid to produce the network (Figure 2-16a,b), and showed that an ester boronic with neighbouring nitrogen exhibited a relaxation time faster than the hydrogen neighbouring equivalent (five orders of magnitude) [75]. Although both networks exhibit similar mechanical properties ($E = 2.3 \text{ MPa}$ to 4.5 MPa), healing was only observed for the fast exchange polymer (room temperature over 16 h). A similar material was produced by photopolymerisation [76]; although the material was not defined as a vitrimer, its room temperature self-healing mechanism clearly fits vitrimer characteristics, as in the previous example. The boronic ester chemistry is not limited to transesterification. In 2017, Leibler and co-workers produced vitrimers based on dioxaborolane metathesis (Figure 2-16c,d) [77], aiming to transform common thermoplastic to vitrimers for improving their mechanical properties through crosslinking, and also improving the thermal stability of these systems (diol radicals used in transesterification can lead to permanent bonds with high temperature [77]). PMMA, PDMS, high-density PEG (HDPE), and polystyrene (PS) were successfully transformed into dynamic networks either by grafting dioxaborolane onto the polymer backbone or by synthesising copolymers containing pendant function.

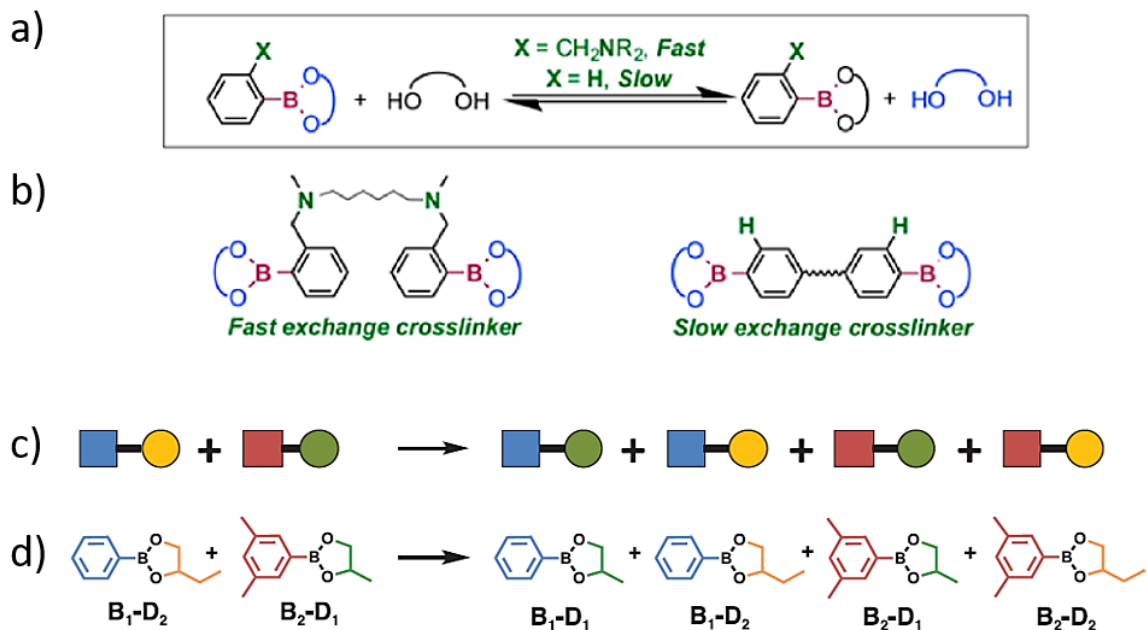


Figure 2-16 a) Schematic of boronic ester transesterification with impact of neighbouring radical on the reaction speed [75], b) crosslinker used to produce the first boronic ester network [75], c) general metathesis scheme [77], d) dioxarbolane metathesis [77].

If the glass transition temperatures of these vitrimers were slightly lower than their reciprocal thermoplastic, the mechanical properties at room temperature could be conserved while allowing reprocessing *via* injection moulding at 180°C and 200°C [77]. This chemistry has since been used to produce PE [78] and PBT [79], [80] vitrimers.

2.6.6 Transesterification

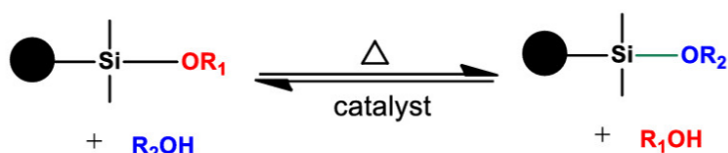
To the author's knowledge, it was only in 2018 that other catalyst free vitrimers based on transesterification (notwithstanding the boronic ester vitrimers presented above) were developed. Using a hyperbranched epoxy polymerised with succinic acid, the networks exhibited T_g ranging from 70°C to 96°C, with tensile modulus above 2 GPa and $E_a \approx 30 \text{ kJ.mol}^{-1}$ [81]. The authors concluded that both stress relaxation and low activation energy originated from the abundant free hydroxyl function within the hyperbranched network [81]. The same system was used to characterise its healing efficiency for epoxy coating, showing complete crack healing and corrosion protection after 200 min at 180°C [82]. A copolymer epoxy/PMMA was claimed to be a vitrimer without catalyst presence [83]. However, in the author's view (QAP), it is unclear if the faster relaxation time obtained at the higher PMMA content (5 to 25% of the polymer composites) was actually due to

PMMA relaxation rather than possible transesterification. Catalyst free transesterification vitrimers were also demonstrated using phthalate monoester (similar to the previously mentioned imine networks cf. section 2.6.2, the BER can be dissociative or associative, and high temperatures favour the dissociative pathway), with $E_a \approx 120 \text{ kJ.mol}^{-1}$ for the associative mechanism [84]. Poly(oxime-ester) systems have been photo-polymerised *via* UV and exhibited vitrimer properties with $T_g \approx 10^\circ\text{C}$ and T_v (measured by dilatometry) ranging from 109°C to 134°C [85].

2.6.7 Silyl ether chemistry

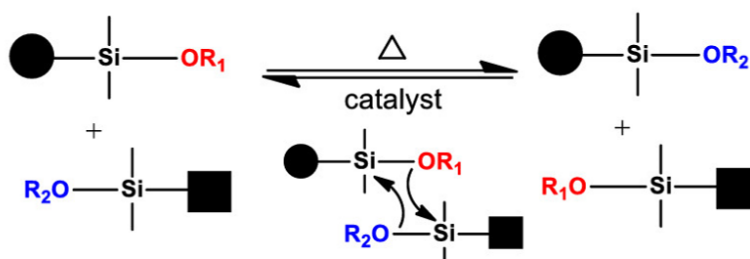
Silyl ether metathesis has been recently performed with epoxy in order to produce networks with high thermal stability without a catalyst [86]. After precursor preparation, the network exhibits stress relaxation with $E_a \approx 75 \text{ kJ.mol}^{-1}$ and Young's modulus ranging from 1.3 GPa to 1.7 GPa, values close to traditional epoxy networks [87]. Similar networks have been developed using potassium hydroxide to catalyse silyl ether metathesis [88], but this network can undergo side reactions with the free hydroxyl groups such as dehydration, oxidation or transesterification (Figure 2-17a) [89]. Another catalysed network has been produced to achieve direct silyl ether metathesis (Figure 2-7b) [89], showing good thermal stability even after being reprocessed three times ($E \approx 101 \text{ MPa}$).

a) Silyl ether-hydroxyl exchange



Limitations: side reactions of free alcohols (dehydration, oxidation, transesterification, etc.)

b) Direct silyl ether metathesis



Advantages: no free alcohol is required and silyl ether motif is thermally and oxidatively stable

Figure 2-17 a) Silyl ether-hydroxyl exchange compared to b) direct silyl ether metathesis [89].

2.6.8 Concluding remarks on vitrimer chemistry and research motivation for the first experimental chapter (Chapter 3)

The aforementioned networks (in sections 2.5 and 2.6) demonstrate the versatility of vitrimer chemistry, adaptable to different thermosets (and crosslinks). Many thermoplastics can be transformed into vitrimers either by grafting functional groups along the polymer backbone or implementing these exchangeable groups within the chain structure. The initial vitrimer based on commercial formulation of epoxy from Leibler and co-workers has been reproduced and extended outside of epoxy chemistry. Recently 'vitrimer-like' materials have been posited (section 2.6). Yet, the classification of 'vitrimer-like' remains unclear; dissociative mechanisms exhibiting Arrhenius behaviour have been reported, but also associative mechanisms, where full stress relaxation was not achieved. Many researchers have focused on developing these new polymer networks, tuning thermomechanical behaviour in parallel. However, simplifying the process required to tune the properties of vitrimer is an attractive prospect. An interesting study focusing on 3D printing of different traditional thermoset polymers, showed a tailorable T_g just by changing the hardener type from unsaturated to cyclic crosslinker and by adjusting the ratio of resin/hardener [90]. The change of hardener type is widely covered in vitrimer system, but the change of ratio between resins and hardener was only briefly mentioned in epoxy network without further investigation [91], [92]. A reduction in creep has been reported for a network composed by $\approx 40\%$ permanent crosslinks in a disulphide epoxy matrix [93]. On the other hand, studies performed by Altuna *et al.* on epoxy excess with carboxylic acid, reported that the catalyst could induce anionic homopolymerisation of the epoxy [94], [95].

Catalyst induced BER is often cited as a potential drawback of the material (justifying research towards catalyst free vitrimers). Toxic catalysts, and/or degradation of the catalyst are factors behind these claims. Although true, it should be pointed out that the use of a catalyst may also favour one reaction over another, and is useful to control network polymerisation and final properties. Favouring the esterification and transesterification of epoxy with carboxylic acid, followed by the network reinforcement with permanent covalent bond formation may have some beneficial aspects. This hypothesis (formulated by QAP) forms the first experimental chapter (Chapter 3) of this thesis.

In order to tune the thermomechanical properties of a catalyst-based transesterification vitrimer only by varying the epoxy/hardener ratio, a range of samples were produced with different stoichiometry. Network formation was monitored to understand the catalyst impact on epoxy based system especially on the anionic homopolymerisation as indicated by Altuna *et al.* [94], [95]. The limit of ratio variation was also studied to observe transition from vitrimer to 'vitrimer-like' and then to a classical thermoset material.

2.7 Nanocomposites in chemically crosslinked networks

2.7.1 The drive towards graphene nanoparticles as fillers

As presented earlier (in section 1.1.3), graphene and its derivatives are a recurrent type of nanoparticle used as reinforcement in polymer materials. Obtained by isolation of one sheet of graphite, the single layer graphene (SLG) was first characterised by Geim and Nosovlov [96]. With the "scotch tape" method - considered as mechanical exfoliation - they proved theoretical properties of graphene such as its bands structure and linear relation of dispersion. Since this discovery further research was done to exploit this material and to use it with its exceptional properties. A single layer graphene (SLG) comprises of sp^2 carbon atoms which form a honeycomb structure of ≈ 0.345 nm thick. By hybridisation of its atoms, it possesses a huge carrier charge (≈ 250000 $cm^2.V.s$) and thermal conductivity (≈ 5000 W/m.K). Due to its morphology, graphene possesses a large theoretical mechanical capacity (1 TPa Young's modulus and strength of 130 GPa) [97]. It is also ultra-light, with a density close to 0.77 mg/m^2 , and therefore, could be embedded in almost any polymer without dramatically increasing the structure's density. Previously cited properties are however valid for a perfect SLG. Nowadays, it is nearly impossible to produce a graphene monolayer with no defects in ambient air [98]; and interaction with surrounding environment lead to decrease of properties, for example the calculated strength of SLG in polymer matrices was found $\approx 11 \pm 6.7$ GPa [99]. This is why derived forms of graphene are used, which have lowered properties (*e.g.* carbon nanotubes CNT, or graphene nanoplatelets GNP). GNPs are generally composed of 10-100 layers of graphene, which lead to lower mechanical properties. However, they retain high electron mobility, high mechanical properties and high thermal conductivity whilst keeping low density for use in polymer matrices [99].

GNP influence is widely studied on epoxy material to enhance their mechanical, electrical, and thermal properties [100]. Commonly, CNTs are the preferred filler choice to create percolated networks within epoxy matrices to obtain lower electrical resistance [101], but alignment of GNP allows to similar behaviour to be obtained [87]. Tensile mechanical properties are shown to improve with addition of GNP particles, yet a limiting

GNP concentration is quickly obtained before exhibiting a decrease in the same mechanical properties [102], [103]. This behaviour is due to two key factors: (i) the high tendency of graphene particle to form agglomerates and, (ii) once the particle concentration is too high, significant free volume of the polymer is filled with agglomerates which start acting as local stress points within the polymer network. Researchers have tackled the former issue of particle agglomeration by functionalising their surfaces with different chemical groups. Initial focus was placed on functionalisation to improve dispersion [87], improvement of the connection with the polymer matrix and to tune nanocomposite properties (*e.g.* mechanical [104], thermal [105] or electrical [106]). Vast literature exists for the use of graphitic particles in traditional epoxy networks (> 3000 publications between 2015 and end 2019, source: *web of science*), and the development of vitrimers has led to innovative studies relating to the use of nanoparticles. These studies have not only focused on improving matrix properties but also exploited vitrimer properties and understanding the effect of nano-reinforcement inclusion (*e.g.* healing capacity, shape morphing, and reprocessability). This part of the literature review covers the achievements realised to date with nanoreinforcements in vitrimer matrices. It focuses on all kinds of nanoparticles - not only graphitic nanoparticles - then, examples of fibres recycling (*e.g.* carbon or glass) from FRP composites comprising a vitrimer as a matrix are presented. This underpins the second experimental chapter of this thesis (Chapter 4).

2.7.2 Nanoreinforcements in vitrimers - graphene and other nanoparticles

The current literature on vitrimer nanocomposites can be broken down into five main categories: (i) processing of vitrimers, (ii) vitrimer property enhancements and limitations, (iii) dual triggering networks, (iv) nanoparticles as dynamic crosslinkers, and (v) the practical applications of vitrimer matrix nanocomposites. It is worth noting that whilst most studies cross the above categories, the principal focus of each study can be predominantly fit into a single category. The different studies mentioned here are summarised and categorised in order, as shown in Table 2-2.

Processing of vitrimer resins has been explored in 3D printing with nanoclays used as thickeners for an epoxy based vitrimer [107]. This method was previously used for the 3D printing of a traditional epoxy thermoset [108]; the increased of viscosity allows the structural integrity to be maintained between printing and curing. On the other hand,

extrusion printing allows for nanoparticle alignment (Figure 2-18a) leading to improved tensile properties along the travel direction of the nozzle. Compared to traditional epoxy thermoset systems, the vitrimer matrix showed recyclability (*i.e.* re-printing into a new shape after first cure, Figure 2-18c,d). After solubilisation in ethylene glycol (EG), the solvent was then evaporated to re-tune the resin's viscosity. The Young's modulus increased from 3.5 MPa to 12.5 MPa between moulded vitrimer and 3D printed parts. Young's modulus remains stable after four printing cycles, although a progressive decrease in the material strength is observed (from ≈ 6 MPa to ≈ 5 MPa), in this author's view (QAP) this was probably induced by residual solvent molecules and solvated vitrimer. Another type of processing was used to achieve alignment of carbonyl functionalised GNP (COOH-GNP) within vitrimer [109]. The nanocomposites were first cured, and then hot pressed above the reprocessing temperature (T_v) of the vitrimer matrix. The compression induced COOH-GNP alignment while the matrix was assuming its new definitive shape (Figure 2-18b). The alignment improved the tensile modulus from 0.25 MPa to 2 MPa, and cracks healing and reprocessing were also proved to work with either IR light or temperature.

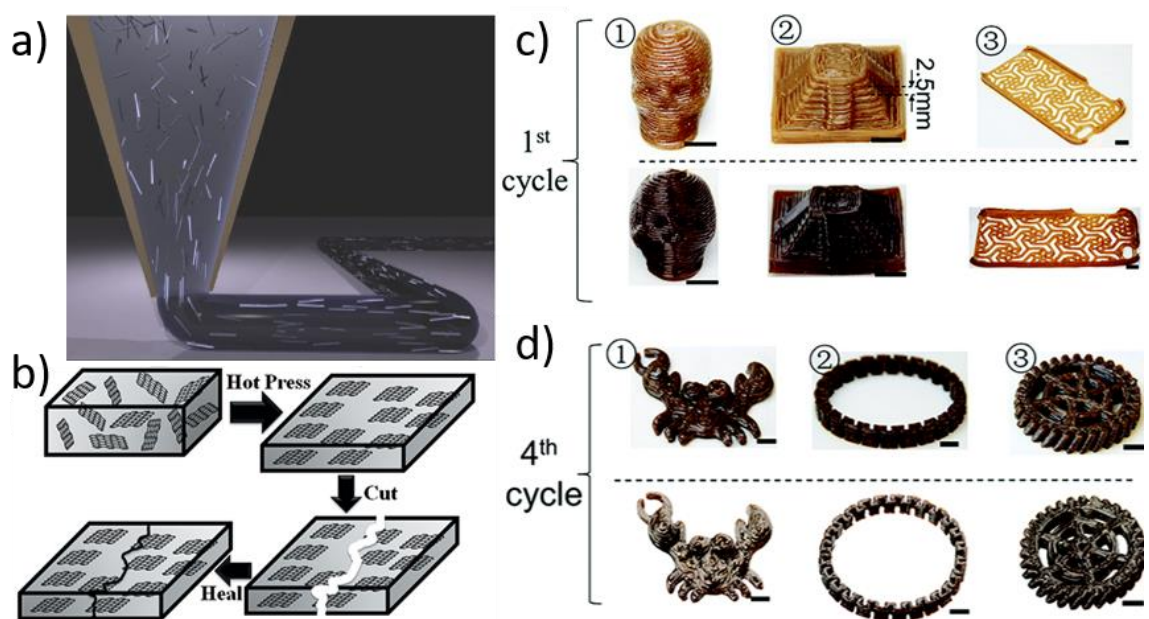


Figure 2-18 a) Alignment of nanoclays during 3D printing by extrusion method [108], b) alignment of COOH-GNP by hot pressing and healing of cracks [109], c) 1st cycle printing of epoxy nanoclays vitrimer (above dotted line is before curing, below is after curing): (1) hollow skull, (2) Mayan pyramid, (3) phone case, and d) 4th cycle printing of epoxy nanoclays vitrimer (above dotted line is before curing, below is after curing) into different shape: (1) crab, (2), puckered ring, (3) gear. Scale bar for printed composites is 1 mm [107].

Vitrimer matrix enhancement and its limitation was firstly studied using nanosilica particles as reinforcements [110]. Two kind of nanoparticles were used: non-functionalised (BARE-silica) and silane bearing epoxy functionalised groups (GLYMO, as labelled in the publication, Figure 2-19a) with 25 wt. % and 40 wt. % loading. The GLYMO nanocomposites exhibited the highest tensile modulus (44 MPa, 40 wt. %) compared to BARE (35 MPa, 40% wt. %), but both were higher than the neat vitrimer (12 MPa). However, the relaxation time at 190°C of both nanocomposites was longer than the neat vitrimer (1.6 min). The relaxation time of the nanocomposites increased with particle loading increment and GLYMO silica exhibited faster relaxation than BARE silica (5.4 min and 7.4 min respectively at 40 wt. %). It was suggested that the nanoparticles were hindering the relaxation process by decreasing the motion of polymer chains. However, the epoxy functionalised particles allowed to partially counteract this drawback by involving the nanoparticles in the relaxation process while improving the mechanical properties. Another functionalisation of nanosilica particles was performed in a disulphide vitrimer system with either epoxy (EP) or thiol (SH) functions (10 wt. % to 40 wt. %) [111]. The Young's modulus of the vitrimer increased from ≈ 600 MPa to ≈ 700 MPa between neat matrix and functionalised nanoparticles (EP exhibited the highest value but error bars of SH and EP overlap). Non-functionalised particles exhibited an intermediate value at ≈ 640 MPa. Similarly, relaxation time at 180°C increased with particle loading, and the functional group involved in the BER (here, SH-silica) displayed lower relaxation time than the other nanocomposites (Figure 2-19b). Healing of crack was demonstrated to be faster with SH-silica than for the neat vitrimer, however EP-silica showed incomplete crack closure after 120 min at 180°C (Figure 2-20a).

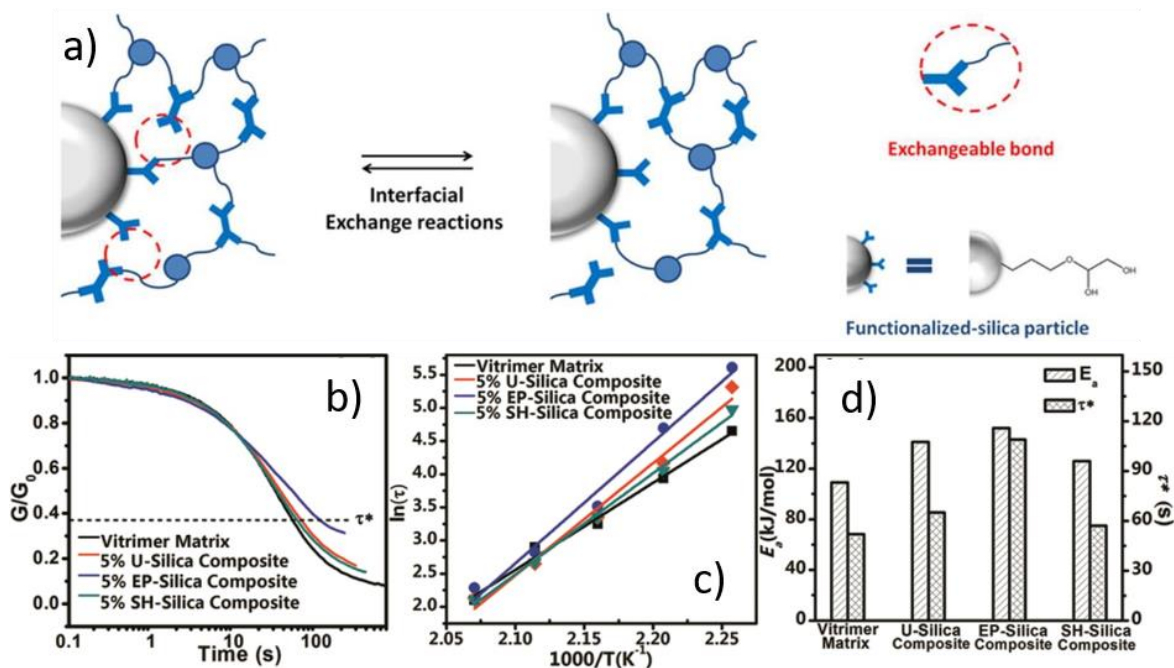


Figure 2-19 a) Concept of surface functionalisation to involve nanoparticle in the BER represented here for epoxy functionalised silica nanoparticles [110], b), stress relaxation at 180°C, c) Arrhenius plot, d) energy activation for the disulphide vitrimer matrix and various functionalisation of silica particles (U: neat particles, EP: epoxy functionalised silica, SH: thiol functionalised silica) [111].

Carbonyl functionalised CNTs were used for an epoxidised natural rubber (ENR) and sebacic acid (SA) vitrimer catalysed by TBD [112]. The tensile properties (Young's modulus) of the network were enhanced by 10 MPa (from ≈ 1 MPa to ≈ 11 MPa), preserved after three cycles of reprocessing (sample cut into pieces and hot pressed at 180°C) and the electrical conductivity of the polymer increased by four orders of magnitude with CNT inclusion. It was noticed that the E_a of the nanocomposites was 150 $\text{kJ}\cdot\text{mol}^{-1}$ compared to previous similar a vitrimer network without CNT (80 $\text{kJ}\cdot\text{mol}^{-1}$ [15], [19]). However no analyses were shown on the impact of nanoparticle loading/functionalisation on vitrimer properties (such as E_a , T_v , or relaxation time). CNT-filled vitrimers were furthermore produced to design low electrical resistance nanocomposites [27], [113]. One study was based on an epoxy vitrimer and polypyrrole (PPy) functionalised CNT system [27]. Electrical conductivity was increased up to four orders of magnitude with a loading of 1.2 vol. %. Reinforcement with PPy-CNT showed a higher conductivity than their non-functionalised counterparts. It is worth noting that contrary to silica particles, the CNTs were reported to decrease E_a (106 $\text{kJ}\cdot\text{mol}^{-1}$ to 95 $\text{kJ}\cdot\text{mol}^{-1}$) and T_v (96°C to 78°C) of the vitrimer matrix compared to the neat vitrimer. This fact is possibly due to their better thermal conductivity

of CNTs compared to silica particles and also lower loading allowing more chains motion (in the author's view, QAP). The second study was based on a disulphide vitrimer, and does not focus on vitrimer properties enhancement (such as relaxation time, T_v , E_a) with nanoparticles [27]. It demonstrates that these nanocomposites can be ground and then reprocessed by hot pressing, and that the surface conductivity of the nanocomposites decreases after reprocessing (from $4.9 \times 10^9 \Omega$ to $3.39 \times 10^9 \Omega$). From their study, a point worth noting is that similar to transesterification-based catalyst vitrimers, the network can be dissolved in an appropriate solvent (EG for transesterification and DMF solution with dithiothreitol for disulphide metathesis networks). Once the network was degraded, CNT powder extraction was reported (Figure 2-20b) although no further characterisation or exploration of this point was performed.

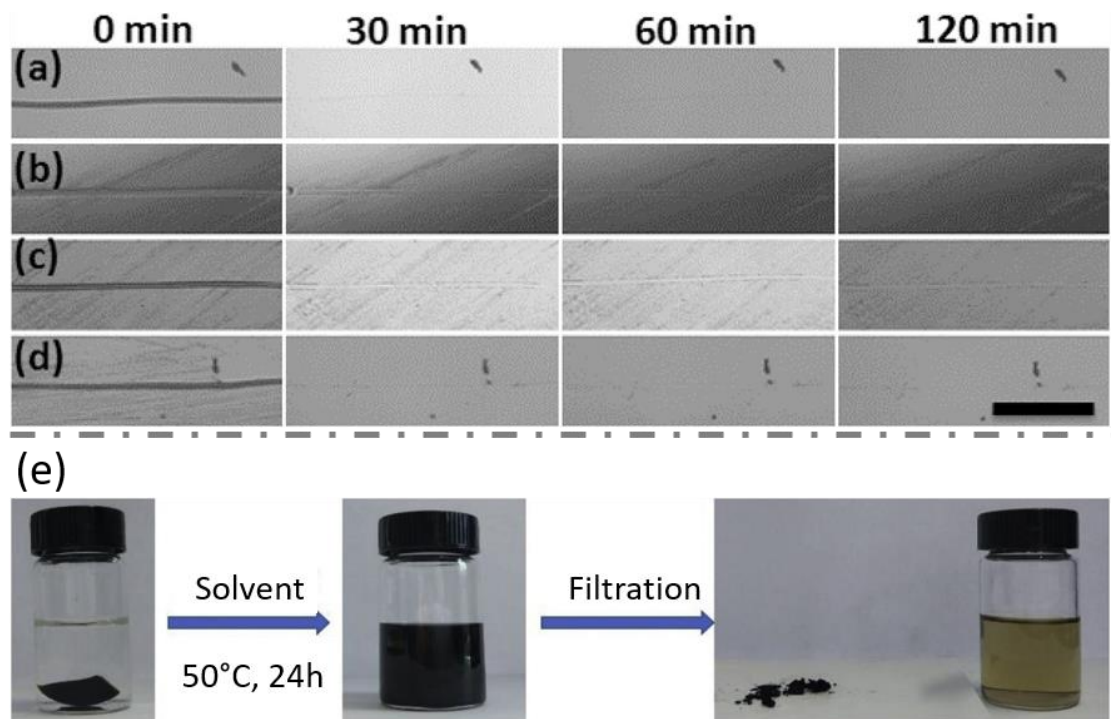


Figure 2-20 a-d) Healing of crack performed at 180°C for neat disulphide vitrimer matrix (a), non-functionalised silica (b), EP-silica (c) and SH-silica, the scale bar is 50 μm [111]; e) demonstration of CNT extraction from a disulphide matrix using DMF solution of dithiothreitol as a solvent [27].

Dual triggering of vitrimer matrix was the earliest example to the author's knowledge of a nanocomposite vitrimer with embedded CNTs in 2014 [114]. Using the photothermal properties of graphitic particles - the characteristic to absorb light and convert as thermal energy - epoxy nanocomposites showed a dual trigger (heat and light) ability. In fact, healing of cracks was improved when triggered by IR light exposure

compared to direct heat exposure (full healing was achieved after 10 s of laser exposure, while only partial healing was reached after 1 h at 180°C). The CNT vitrimer also displayed the ability to be welded after laser exposure to either a vitrimer network or a classical thermoset. Another similar system (previously mentioned in part 2.4.2-Figure 2-10), based on transesterification showed successful shape memory behaviour and reconfiguration *via* IR light [23]. A very similar network was produced using reduced graphene oxide (rGO) to demonstrate again the possibility to obtain dual-responsive shape memory behaviour and reconfigurability *via* light and heat [115]. For that study, the mechanical properties of the network increased gradually when increasing particles loading (From 32 MPa to 51 MPa between 0 and 3 wt. %). Nevertheless, complete reduction of graphene oxide also claimed was not sufficiently demonstrated in this author's opinion (QAP), and could possibly have led to uncontrolled ratios of rGO/GO depending on the particle loading in their vitrimer samples.

Two interesting studies reportedly used organic nanoparticles (able to be dispersed more readily in polymers in general without surface treatment, contrary to inorganic particles such as GNP) to achieve dual triggered vitrimer [116], [117]. Using their previous study with PPy-CNT [27], researchers developed "ordered polypyrrole nanorings", with high photo-thermal conversion performance [116]. The properties of these nanorings allow the vitrimer to be dual-responsive without the use of CNTs. The other study used polydopamine nanoparticles (PDA-NPs) to achieve the dual responsive behaviour [117]. Used in a liquid crystal elastomer vitrimer (xLCE, a polymer having the ability to undergo shape change without programming phase(s) by network rearrangement at a certain temperature), the PDA-NPs exhibited the capability to produce several dynamic 3D structures triggered *via* IR light (Figure 2-21).

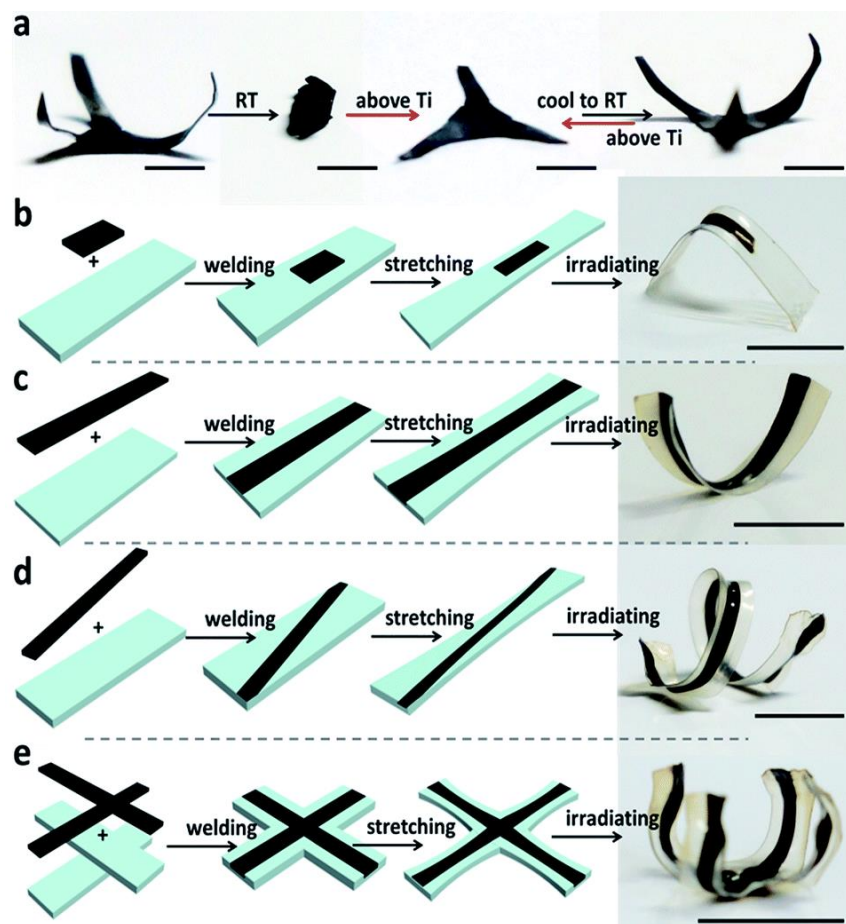


Figure 2-21 a) Restoration and reversible actuation of deformed dynamic 3D structures of a PDA vitrimer. Scale bar: 0.5 cm. (b-e) Examples of different dynamic 3D structures achieved by 2-layered structures. Blank vitrimer films were welded with PDA-NPs vitrimer into different shapes: Light intensity: 1.0 W cm^{-2} . Scale bar: 1 cm [117].

Nanoparticles used as dynamic crosslinkers refers to studies focusing on the nanoparticles surface to be used as BER medium. The group working on these networks focuses on malleable styrene-butadiene rubber and silica nanoparticles [111], [118]. Two ways to achieve the BER solely at the interface between the polymer matrix and the nanoparticles have been explored: (i) functionalising the rubber chains with carbonyl functions to interact with the hydroxyl functionalised silica *via* transesterification [135] and, (ii) functionalising the rubber chains with pyridium to interact with the bromide functionalised silica particle *via* transalkylation [142]. Both networks exhibit reprocessability up to 3 times with stable tensile properties, and T_v decreasing with concomitant increase in nanoparticle loading ($155\text{-}160^\circ\text{C}$ for the pyridium system and $170\text{-}180^\circ\text{C}$ for the carbonyl system). It was reported that the E_a of the pyridium vitrimer was lower than other vitrimers based on similar BER from literature, but that difference is likely

due to the differences between functional moieties used rather than the use of nanoparticles (author's view, QAP) [118].

Practical applications of nano-vitrimerers are for now scarce, but the potential of vitrimer has been emphasised as a triboelectric generator for self-wearable electronics [119], [120]. The first reported example reported used a disulphide vitrimer matrix with embedded silver nanowires [120]. A challenge in flexible electronics is to use body motion to produce electricity; often the flexible conductive material can undergo damage, rendering the device useless. Here the proposed material can be cut and healed due to the vitrimer properties, showing recovery of electrical conductivity after being healed (Figure 2-22). Silver nanowires have been explored as potential transparent conductive fillers [121], but the concept was also demonstrated with SH-CNTs [119]. This latter network showed similar conducting and healing properties, but the embedded CNT allowed triggering of the network healing *via* near-IR light.

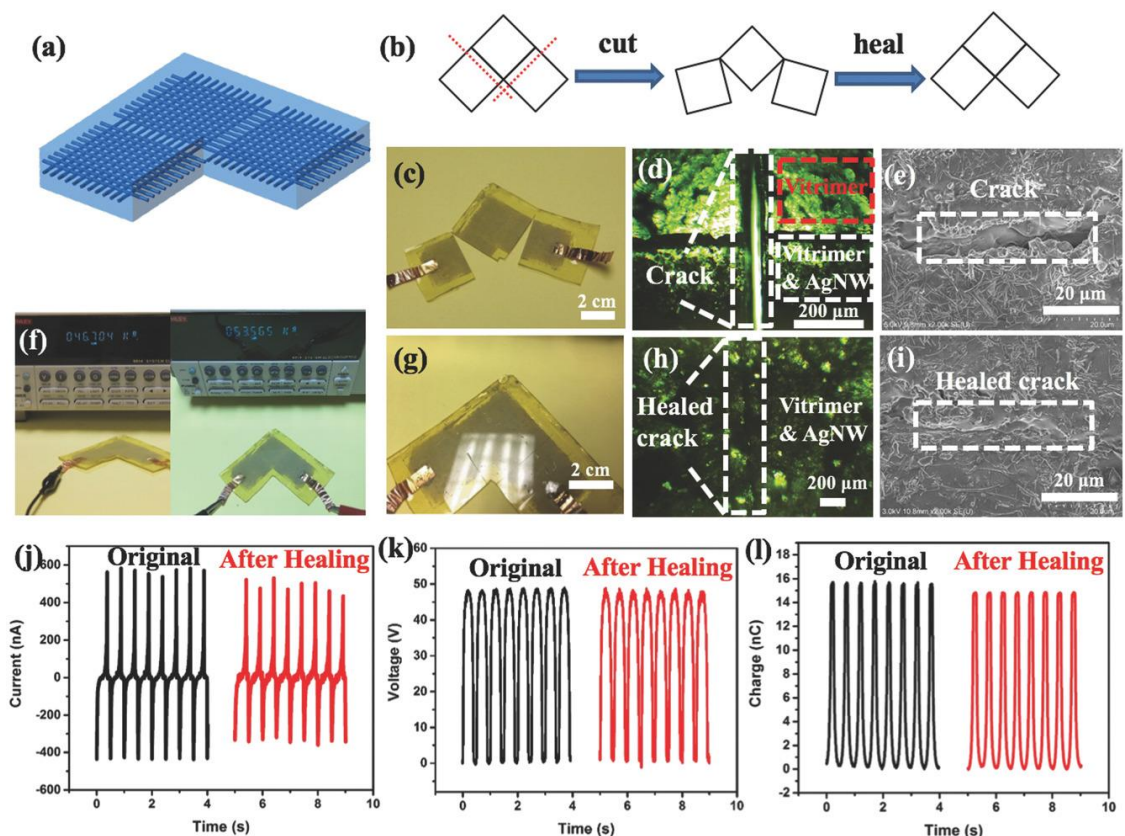


Figure 2-22 Silver nanowire triboelectric nanogenerator: a) Percolated silver nanowires network embedded in disulphide vitrimer, b) Strategy applied to test healing capacity, c-e) Broken sample optical characterisation (Picture, microscope and SEM), g-i) symmetric characteristic for healed sample, j-i) Electrical performances of original (black) and healed (red) sample [120].

From the different examples above, the potential use of nanoparticles in vitrimer matrix is apparent - especially, the epoxy chemistry known to pursue nanoparticles reinforcement but also development of multifunctional materials using graphitic nanoparticles. Nonetheless, the properties of vitrimer polymers to be dissolved in an appropriate solvent (as mentioned in part 1.1.3) have barely been explored for nanocomposites; the only example showing possibility to extract nanoparticles from vitrimer was limited to a single photograph [34]. Therefore, before introducing the motivation behind the second experimental chapter of this thesis, a short overview of some work performed on fibre reinforced vitrimer composite system is necessary.

Table 2-2 Nanocomposites vitrimer in literature. BER type: (1) transesterification, (2) disulphide metathesis, (3) trans-*N*-alkylation; NA: Non-applicable, E: Young's modulus, G: Shear modulus, No shading: *Processing of vitrimer resins*, blue shading: *matrices enhancement and its limitation*, orange shading: *dual triggering of vitrimer matrix*, grey shading: *nanoparticles used as dynamic crosslinkers*, green shading: *practical application of nano-vitrimer*.

Monomers	Catalyst	BER	Reinforcements	Mechanical properties	T _g /T _v	E _a (kJ.mol ⁻¹)	Primary aim	Ref
DGEBA, Pripol 1040	Zn(acac) ₂	1	COOH-GNP	0.25-2 MPa (E)	T _g : 0-16°C	84-96	Inducing alignment of GNP <i>via</i> hot press curing with healing and reprocessing capability	[109] 2019
DGEBA, Pripol 1040	Zn(acac) ₂	1	Nanoclays	3.5 -12.5 MPa (E)	T _g : 30-40°C	70-78	Tuning viscosity of vitrimer to print and reprint 3D structure	[107] 2017
DGEBA/DER, Pripol 1040	Zn(acac) ₂	1	Nanosilica and epoxy functionalised nanosilica	10-46 MPa (E)	T _g : 30-37°C	NA	Studying the impact of neat nanosilica particles and functionalised nanosilica particles on vitrimer	[110] 2016
DGEBA, 4-Aminophenyl disulfide (4-AFD)	NA	2	Functionalised silica (epoxy or thiol)	586-772 MPa (E)	T _g : 151-156°C	109-152	Engineering the surface of nanosilica particles to study effect on vitrimer matrix	[122] 2017

DGEBA, citric acid	TBD	1	PPy-CNT	NA	T _g : 60-85°C T _v : 78-96°C	95-106	Using PPy's functionalisation to improve electrical conductivity and BER	[113] 2017
(4-hydroxyphenyl) disulphide, 4-AFD	NA	2	PPy-CNT	2.2 GPa (G)	T _g : 133°C T _v : 86°C	38	Using CNT to produce vitrimer with low electrical resistance and suggestion method to extract nanoparticles	[27] 2018
Epoxidised natural rubber	TBD	1	Carbonyl functionalised CNT	0.55 – 10 MPa (E)	T _g : 10-20°C T _v : 200-225°C	166-216	Using functionalised CNT to produce robust rubber vitrimer with low electrical resistance	[112] 2018
carboxyl group-grafted styrene-butadiene rubber	TBD	1	Epoxy functionalised silica	1.6-3.4 MPa (E)	T _g : -20 to 0°C T _v : 170-180°C	80-85	Using epoxy functionalisation to crosslink with SBR without use of hardener	[111] 2018
butadiene-styrene-	NA	3	(3-	1.3-3 MPa (E)	T _g : -22°C and 40°C	45-88	Using silica modified surface to use it as crosslinker to produce vitrimer matrix	[118] 2018

vinylpyridine rubber			bromopropyl)tri methoxysilane modified silica		T _v : 155-160°C			
Epoxy monomer named "TMBPDGE", adipic acid	TBD	1	GO to rGO	31-54 MPa (E)	T _g : 60-80°C	NA	Dual responsive SMP using light and heat	[115] 2019
DGEBA, adipic acid	TBD	1	PPy nanorings	NA	T _g : 30°C	NA	Using polypyrrole nanorings to induce NIR absorption and photothermal conversion	[116] 2019
DGEBA, SA	TBD	1	GNP	NA	T _g : 35-45°C T _v : 120-175°C	NA	Using graphene reinforcements to obtain dual triggered SMP	[23] 2016
DGEBA, SA	TBD	1	CNT	NA	T _g : 35-45°C T _v : 175°C	NA	Using CNT for welding and healing of nanocomposites vitrimer with IR light	[123] 2014
4,4'-dihydroxybiphenyl, SA	TBD	1	CNT and PDA-NPs	NA	T _g : 70°C	NA	Using PDA to replace CNT in shape morphing vitrimer (xLCE) triggered by light	[117] 2017

DGEBA, AFD	NA	2	CNT	2.6 MPa (E)	T _g : 66 -73°C	NA	Using CNT photothermal effect to induce near IR healing in triboelectric generator	[119] 2018
DGEBA, Polysulphide	NA	2	Silver nanowire	NA	NA	146	Using vitrimer properties to produce healable self-wearable nanogenerator	[120] 2018

2.7.3 Recycling of reinforcement from epoxy composites using vitrimer properties

Leibler and co-workers were the first to introduce example of composite materials comprised of glass fibres and an epoxy vitrimer matrix back in 2016 [92]. Their study only focused on the welding of glass fibre composites made of vitrimer with different composites (non-epoxy, traditional epoxy thermoset and vitrimer). It was demonstrated that the vitrimer samples were able to bond with high mechanical strength to all other types of composites, displaying a cohesive fracture after 1 h 30 at 160°C (lap shear test). Others have exploited the reprocessing ability of vitrimer to produce composites from dry powder of vitrimer *via* compression moulding [124]. However none of the above studies investigated composite end of the life (*e.g.* recycling, repurposing, reprocessing), which is known to be a concern in the field [125].

Demand for carbon fibres used in composites is expected to reach 140 000 tons by 2020 [125]. Constant rise in their demand has led to intensive research towards recycling carbon fibres (or other fibres such as glass and aramid). An informative review written in an accessible style for non-technical readers of proposed solutions (for degradable thermoset polymer in composites) was recently published [126]. Among those solutions, vitrimers have proven an efficient constituent towards recycling carbon fibres for further use. To the author's knowledge only a few vitrimer studies (five) have been performed towards fibres recovery of composites. All of them, with the exception of one (using the boronic ester metathesis [127]), relied on the epoxy vitrimer chemistry [72], [128]–[130]. Among those epoxy vitrimers, the extraction of carbon fibres was achieved by dissolving the disulphide network within a thiol-solution [72]; for the transimination vitrimer, the network dissolution was performed in 0.1M HCl [129].

Of particular relevance to this thesis, interest resides in epoxy vitrimers based on transesterification (following work performed in Chapter 3). In 2016, a study focused on the dissolution and re-polymerisation of a vitrimer based on Leibler and co-workers' first vitrimer formulation (DGEBA, pripol 1040 and Zn(acac)₂) [130]. Using an alcohol as solvent (EG), they managed to fully dissolve the vitrimer matrix at 180°C for 4 h. The idea was to involve the hydroxyl group of the solvent in the transesterification mechanism above the vitrimer's T_v (Figure 2-23a). As the solvent molecule chains are not connected to the

network they allow the network to be progressively solvated (Figure 2-23b); a high excess of solvent allows to reach full dissolution of the vitrimer network (Figure 2-23c).

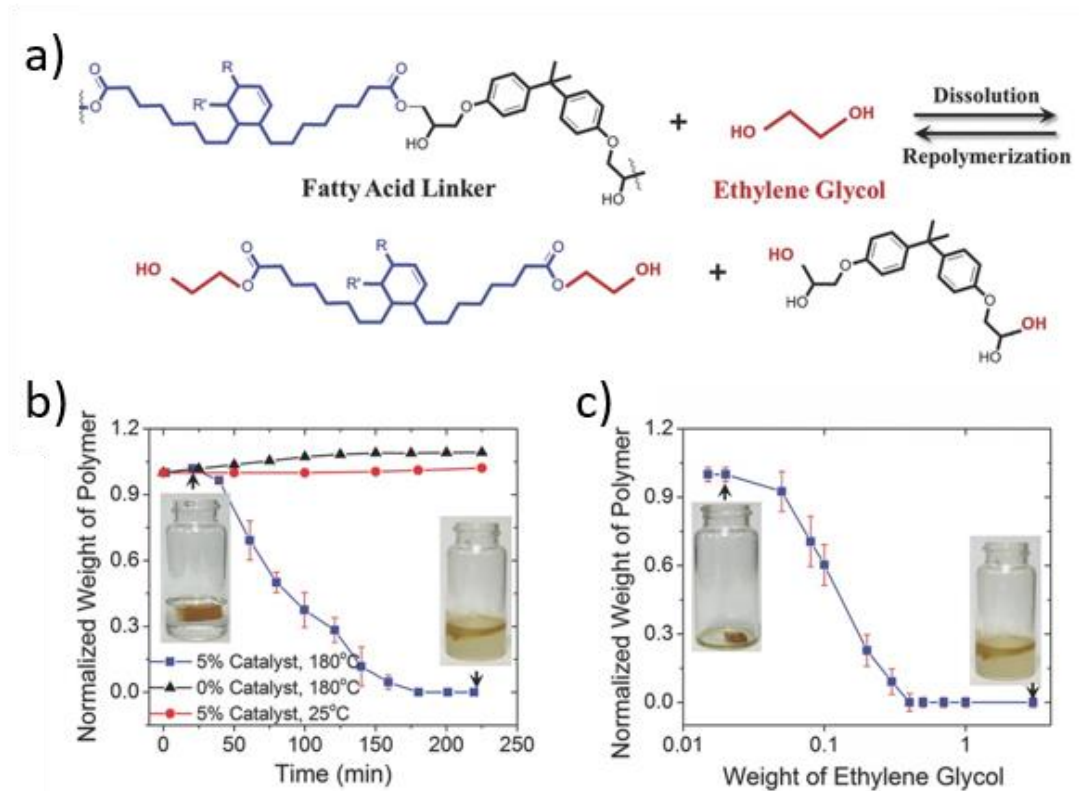


Figure 2-23 a) Schematic of the dissolution process for transesterification vitrimer *via* alcohol (EG), b) Normalised weight of vitrimer as function of soaking time for vitrimer samples at 25°C and 180°C, and the non-vitrimer control sample (0% catalyst), c) The residual weight of vitrimer after being soaked for 4 h at 180°C as function of EG weight [130].

It was demonstrated that the recycled carbon fibres had similar morphology (Figure 2-24a,b) and mechanical properties (Figure 2-24c) to the original ones, and could be used to reform a new composite made as well from the solvated vitrimer. By adding monomers and evaporating the solvent, the recycled matrix produced composites with similar strength in their tensile properties (Figure 2-24d,e). However it is actually questionable (QAP opinion) if the re-polymerisation process reproduces similar vitrimers polymer than its original. Evaporating the solvent surely favours transesterification towards higher crosslinking density, but no characterisations of the re-polymerised vitrimer were performed (only as FRP composite) [130]. Once the crosslinking increases, remaining solvent molecules will be harder to extract with the increased viscosity, likely leaving residual EG in the final vitrimer. The mechanical data from recycled composites performed in ref [130] are insufficient to affirm recovery of the mechanical properties of the matrix

(the tensile strength of a composite along the fibre direction is mostly due to the fibre components, and their Young's modulus is so high next to the resin's one that it is not possible to distinguish a small decrease in the polymer performances).

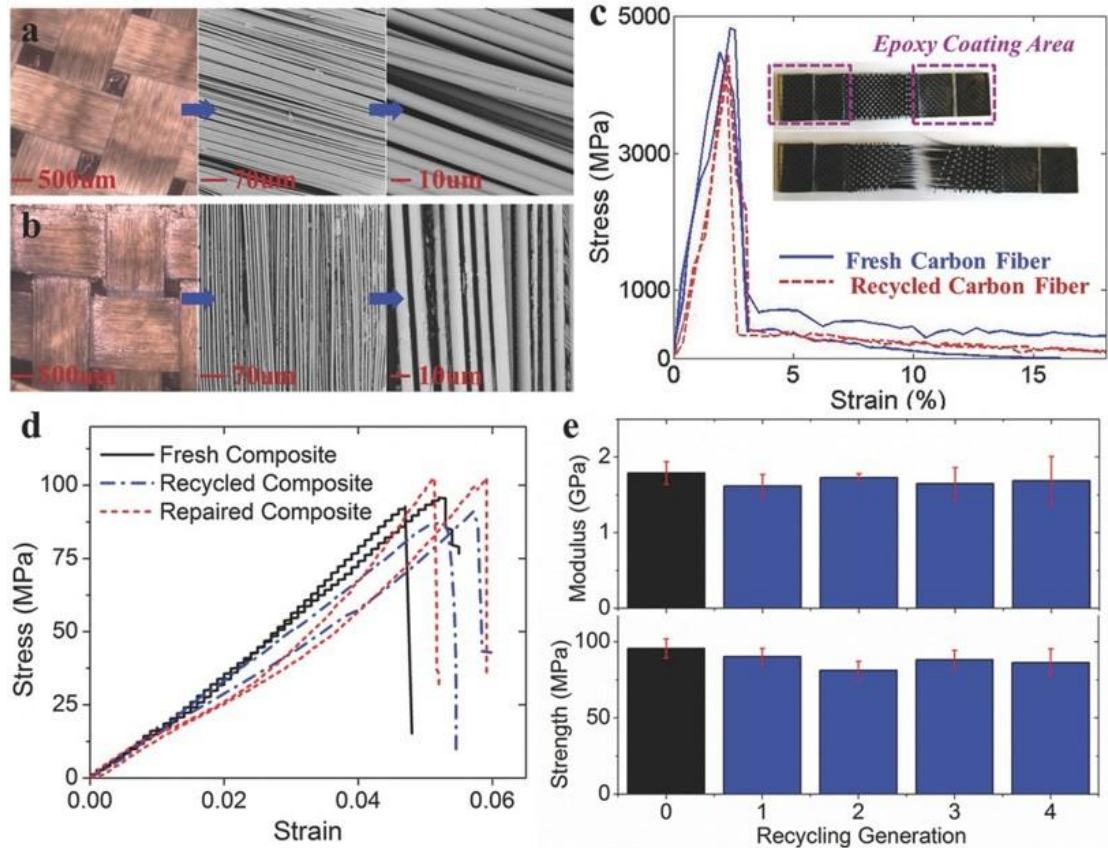


Figure 2-24 a) SEM images of a) original carbon fibres fabric, b) recycled one, c) strain-stress curves of original (blue) carbon fibres fabric and recycled (red), d) strain-stress curve of original (solid black), recycled (dashed blue) and repaired (dashed red) composites, e) mechanical properties of composites over 4 cycles of recycling [130].

Following this work, the same group demonstrated that a traditional epoxy thermoset (*i.e.* permanent polyester network) composite could also be dissolved by swelling the network in a mix of solvent (EG or EG+ *N*-methyl-2-pyrrolidone NMP) with a transesterification catalyst (TBD) [131]. In their work, the hardener used was a cyclic anhydride (hexahydro-4-methylphthalic anhydride), producing a network with higher mechanical properties than their previous study ([130]). A follow up work from the same group studied the re-polymerised network thermomechanical properties (tensile and T_g) and a gradual decrease of these properties was observed with increasing content of re-polymerised vitrimer (Figure 2-25) [128]. This fact confirms the question risen above regarding their previous work: it is likely that full evaporation cannot be re-obtained while

re-polymerising the vitrimer, leaving solvent molecules and solvated oligomers which ultimately lead to lower thermomechanical properties.

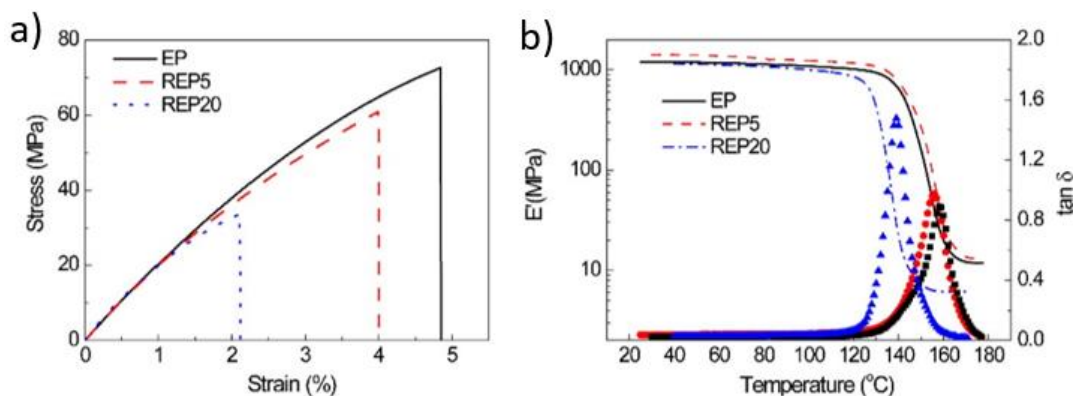


Figure 2-25 a) Tensile properties of original epoxy network (EP, solid black curve), an epoxy sample containing 5% of re-polymerised network (REP5 dashed red curve), and an epoxy sample containing 20% of re-polymerised network (REP20 dotted blue curve), b) DMA results for the same samples [128].

2.7.4 Concluding remarks on nanocomposites and research motivation for the 2nd experimental chapter (Chapter 4)

From the penultimate section (2.7.2), some uses of nanoparticles in vitrimers matrix to form nanocomposites materials are overviewed. These nanoparticles can be used just as reinforcements but also as a route to produce multifunctional materials with vitrimer properties (*i.e.* healing, reprocessing capability). The growth of studies on nanocomposite vitrimers demonstrates huge interest in these materials; for epoxy-based vitrimer systems, graphitic nanoparticles such as CNTs and GNPs allow remote triggering of the vitrimer BER by light. Many researchers focused on this aspect, and it is likely that in the future, the number of “graphene vitrimer” studies will see a similar growth to that of graphene epoxy nanocomposites (*i.e.* traditional epoxy). This raises concerns regarding the sustainability of this kind of nanocomposite - especially at the end-of-life. The recycling of carbon fibres from traditional composites, although in its early stage, demonstrates the huge potential associated with vitrimer matrix to achieve “closed-loop” recyclability. The method used for recycling is considered mild (< 180°C), and has been claimed to be suitable for other fibres types (*e.g.* aramid and glass fibres) [125]. Interestingly recovery of nanoparticles from polymer matrix was shown to be feasible but limited to a single picture. Therefore, the second chapter (chapter 4) of this thesis focuses on studying the effect of graphitic particles with several types of functionality on the stoichiometric formulation of the vitrimer

developed in the first experimental chapter (Chapter 3). It is determined how the type of nanoparticles influences the thermomechanical properties of the polymer network but also some of its vitrimer properties (*i.e.* relaxation times). Then, extraction of the nanoparticles are studied following the dissolution procedure seen above; after washing, chemical characterisation of the recovered particles is performed to compare them with their original counterparts. It is believed that this method could lead to re-use of the nanoparticles to produce new nanocomposites but could also be adapted to several other types of nanoparticles and vitrimers.

2.8 “Bio-based” vitrimer and enzymatic catalysis

The last section of this literature is the premise to the third experimental chapter (Chapter 5): it focuses on the exploration of sustainable chemistry for vitrimer, especially in epoxy vitrimer based. The first requirement is to properly introduce the term sustainable in the context of this thesis, starting by a proper definition of bio-inspired and bio-sourced material. Etymologically, a bio-inspired material should refer to a material with a mechanism copying some natural aspect (*e.g.* bi-layered materials able to change shape with difference of coefficient of thermal expansion copying pine cone structure [132]). In this case, the developed material does not require its component(s) to originate from natural or sustainable sources. On the other hand, a bio-sourced/bio-based materials have the requirement to have its components (*i.e.* monomers, reinforcements, *etc.*) originating from sources which are bio-based, in other words, a “greener” version than the previous materials from which they replicate the properties [56], [133].

However, in literature, the term bio is often used with an adjunct of the monomer name made from renewable sources (*e.g.* bioepoxy [31]) which can lead to potential confusion between bio-based or bio-inspired. If bio-based monomers are potentially a better option regarding their environmental impact, they can hardly be classified as fully “bio”, as sometimes their production include the use of harsh chemical with potential wastes (*e.g.* epoxidised sebacic acid using epichlorohydrin [134]). Therefore (and to avoid potential confusion with bio-inspired), in terms of this work, the term ‘sustainable vitrimers’ was chosen rather than bio-based/biovitimer. This section is organised as follow: (i) some examples of bio-based monomers used to produce sustainable transesterification based vitrimer, (ii) some examples of sustainable vitrimer for other BER types, (iii) a short discussion on catalyst for producing sustainable vitrimers, (iv) the presentation of enzyme (lipases) as biocatalyst, and (v) their potential use in polymer network or epoxy vitrimer networks.

2.8.1 Sustainable vitrimers

Sustainable transesterification based vitrimers - resins and hardener from bio-based sources

The literature regarding sustainable vitrimers concerns mostly transesterification based vitrimers. Among those, a majority focuses on epoxidised chemicals. Effectively, the epoxy market is in constant growth [135], and demand for more sustainable solution has driven research efforts in this direction as mentioned in section 1.1.4. A few of these networks were already covered throughout the previous sections of this document [29], [31], [56], [136] and are not all covered in more detail, as the idea of sustainable vitrimer remains the same (despite differences of monomers used): they use bio-sourced/bio-based monomers (one or all monomers) for their production.

Zhang's group has been focusing on developing sustainable vitrimers [28][134], [137] and studied various feeding ratio of epoxy: hardener. These networks displayed limitation depending of the feeding ratio which are discussed in the following paragraphs for their relevance regarding Chapter 3 of this thesis.

To manufacture an epoxy vitrimer not originating from petro-chemistry, eugenol-derived epoxy was produced by dissolving eugenol in ethanol with potassium iodine to form a eugenol diene [137]. The diene was then epoxidised in dichloromethane with *m*-chloroperoxybenzoic acid to obtain eugenol-epoxy monomers (Figure 2-26a). This monomer was then reacted with succinic anhydride and three ratios (epoxy:anhydride) were studied: 1:1, 1:0.75, and 1:0.5 (Figure 2-26b). Properties such as shape memory, crack healing and reprocessing (physical *via* grinding and compression moulding or chemical *via* dissolution in ethanol) were demonstrated. Interestingly the study claimed (proven with data) that the best healing, faster relaxation time, more efficient healing, and reprocessing was observed in sample with ratio 1:0.5 (Figure 2-26c,d) [137].

The authors of the study reported this fact to be something to take into account in the development of some vitrimer formulations. This point was, however, already studied and explained in early vitrimer study and is due to a simple difference between the epoxy carboxylic acid reaction and epoxy anhydride reaction [138]. In a reaction with dicarboxylic acids, a hydroxyl group reacts with the epoxy ring to form the ester, in this case, one epoxy

group reacts with only one carbonyl group, and the epoxy ring opening leaves a pendant hydroxyl group which is required for the transesterification reaction. However, the reaction with anhydride compound is slightly different; the general accepted reaction is that the anhydride is opened by a hydroxyl (or catalyst) to form an acid [138]. This acid can then react with an epoxy group, producing a pendant hydroxyl group. This hydroxyl group can then initiate the opening of a new anhydride to propagate the polymerisation (Figure 2-27a). In this model, in a ratio 1:1, this leads to a highly branched network with few pendant hydroxyl groups. Therefore, when the ratio is fixed to 1:0.5, the epoxy can homopolymerise after the esterification process, which leaves pendant hydroxyl groups (Figure 2-27b), allowing faster stress relaxation and better vitrimer properties.

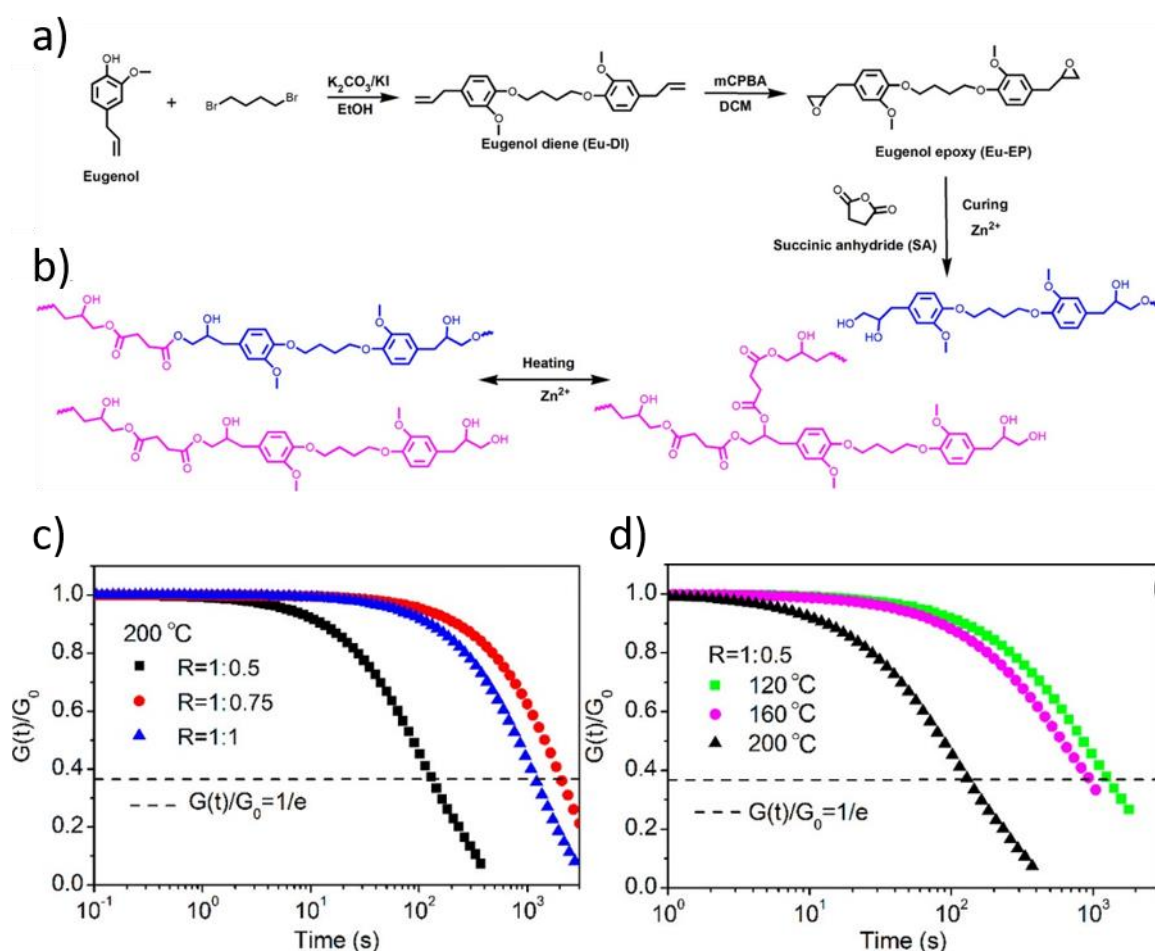


Figure 2-26 a) Production of eugenol-epoxy monomers, b) Reaction of transesterification in highly branched ester network from eugenol-epoxy and succinic anhydride, c) stress relaxation of the 3 ratio studied, and d) stress relaxation of ratio 1:0.5 at different temperatures [137].

anhydride hardener to have enough ester and hydroxyl groups available in the network while avoiding too much etherification *via* epoxy homopolymerisation [138].

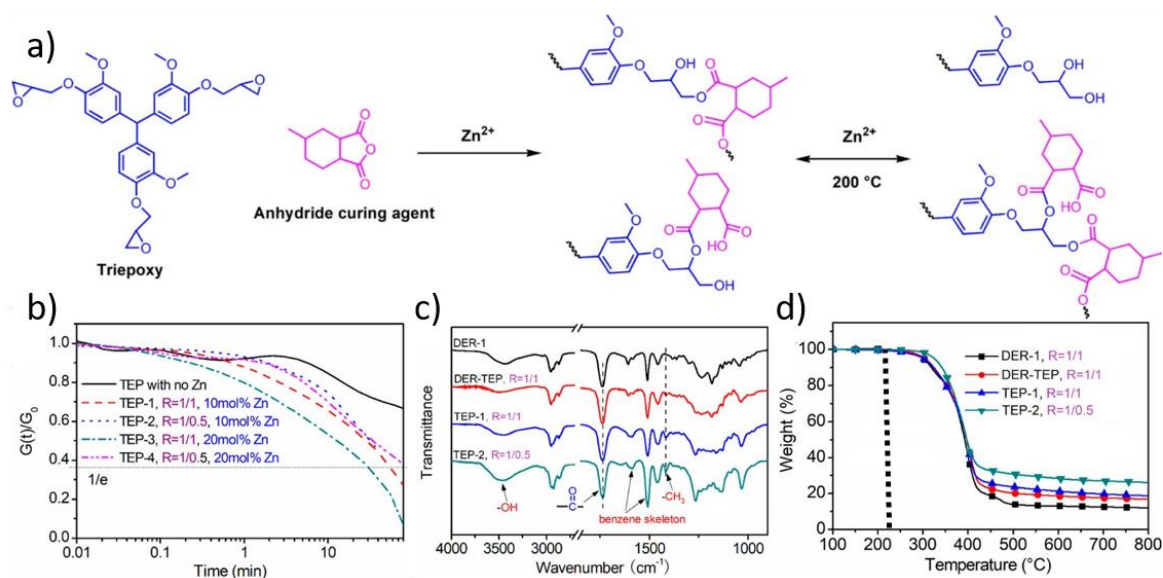


Figure 2-28 a) Schematic of triepoxy and anhydride hardener monomers cured with a Zn catalyst and mechanism of transesterification in the cured network, b) Stress relaxation of the different ratio prepared for the study at 220°C, c) FTIR spectrum of different ratios with the highest hydroxyl content recorded for 1:0.5 ratio, and d) TGA measurement of the different ratios - the black dotted line has been added to show the initial point of degradation reported for the ratio 1:1 [139].

Later, this group developed other vitrimer networks derived from lignin [28][134]. The first network was manufactured by crosslinking a poly(ethylene glycol)-epoxy with a carbonyl functionalised lignin catalysed by $Zn(acac)_2$ [28]. It was used to produce a healable and removable epoxy-based coating (Figure 2-29a) and an excess of carbonyl content was reported to decrease performance of healing after 1:1.2 ratio (epoxy:carbonyls). The other study used similar modified lignin but was crosslinked with an epoxidised sebacic acid monomer (epoxy groups were added *via* epichlorohydrin treatment) catalysed with $Zn(acac)_2$ [134]. The study demonstrated that the vitrimer network (prepared with 1:0.75, 1:1 and 1:1.5 ratios epoxy:carbonyl) was able to reach a cohesive failure while performing lap-shear test proving its potential for recoverable adhesives (Figure 2-29b,c).

It should be noted that, in the aforementioned studies of this group, 100% stress relaxation was never demonstrated, raising the concern that these network should more accurately be classified as “vitrimer-like” materials, having the capacity to be healed and reprocessed partially, while remaining soluble in appropriate solvent, rather than be termed vitrimers.

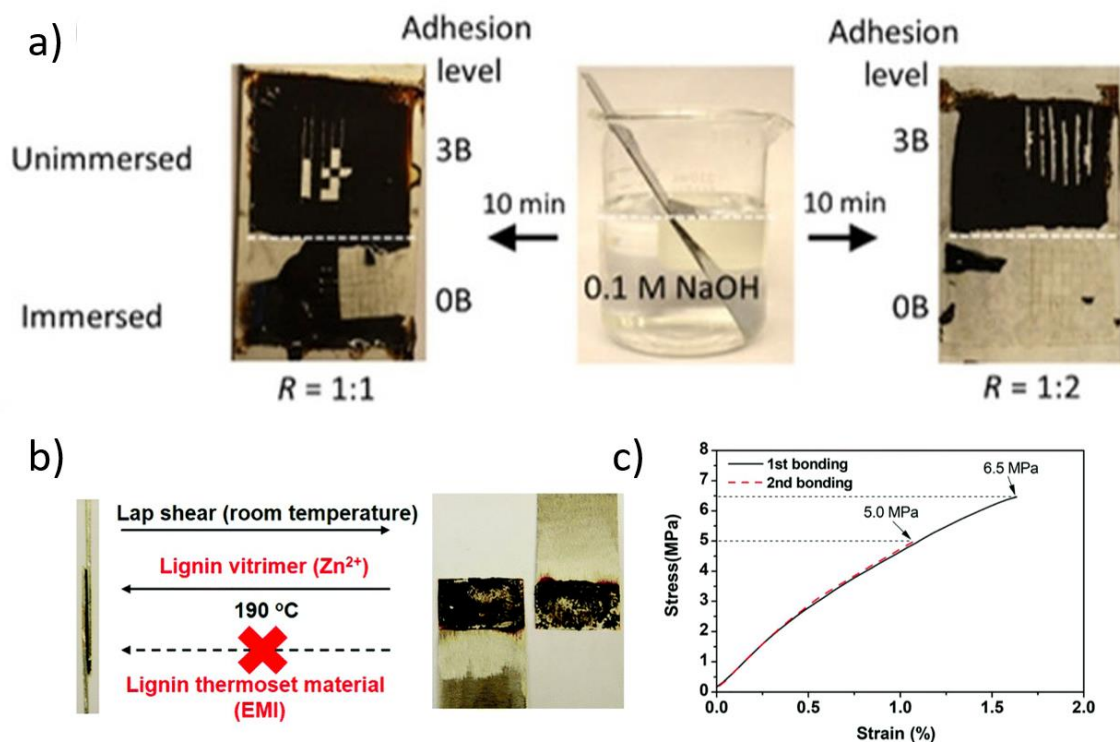


Figure 2-29 a) Poly(ethylene glycol) lignin-based vitrimer coating dissolution after 10 min in a 0.1 M NaOH solution for ratio 1:1 and 1:1.2 [28], b) epoxidised sebacic acid lignin-based vitrimer rebinding capacity showing a cohesive fracture, c) mechanical results of lap-shear test after 1st and 2nd bonding [134].

Studies from different groups regarding sustainable transesterification vitrimers included: a biocompatible vitrimer film was produced *via* crosslinking of poly(acrylonitrile-co-butadiene) with polyhedral oligomeric silsesquioxane catalysed by $Zn(acac)_2$ [140]. By transesterifications, the network can be patterned several times and folds into a variety of complex structures and was reported to be a potential candidate for tissue engineering applications. A dual triggered sustainable vitrimer was produced using ENR crosslinked with dodecanoic acid and a various amount of ACAT (monomer previously reported to produce a multifunctional vitrimer in section 2.5.1) catalysed by $Zn(acac)_2$ [141]. This network exhibited good crack healing using heat (30 min, 200°C) and IR light in 15 min (due to an increase of the temperature sample to 225°C after 1 min irradiation). An ethylene propylene-diene monomer was epoxidised without the help of epichlorohydrin (using performic acid) for a “greener” epoxidation method [142]. The monomer was then crosslinked with dodecanoic acid and $Zn(acac)_2$ as catalyst to produce a vitrimer network with an $E_a \approx 74 \text{ kJ.mol}^{-1}$.

Sustainable vitrimer based on different BER mechanisms - resins and hardener from bio-based sources

Recently, transimination sustainable vitrimers have been developed [136], [143]. A fully sustainable imine network was produced with a furan dialdehyde derived from fructose crosslinked with a mix of di- and tri-amines prepared from fatty acid [143]. This network exhibited conservation of mechanical properties up to three recycling steps (E ranging from 4.4 to 5.1 MPa) with an $E_a = 80 \text{ kJ.mol}^{-1}$ (from stress relaxation experiment). A vanillin-based monomer (two different monomers produced from vanillin *via* reaction in ethanol at 60°C for 3 h) was crosslinked with epoxy to form vitrimers [136]. This network achieved “closed-loop” recyclability; after dissolution in ethanol the network was fully reformed after distillation of ethanol and the mechanical properties were conserved ($E \approx 2.5\text{-}2.8 \text{ GPa}$).

A disulphide sustainable poly(ester amide) vitrimer was produced after preparation of a polyamide salt, sebacic acid, castor oil monomers crosslinked with 4-aminophenyl disulphide [144]. Several feeding ratios of monomers were used, showing a Young's modulus ranging from 1.4 MPa to 106 MPa, and an $E_a \approx 96 \text{ kJ.mol}^{-1}$ was reported for the only ratio able to fully relax stress with the others being characterised as ‘vitrimer-like’.

Case of catalysts: what are the choices for sustainable vitrimer manufacture?

From the examples above, it is possible to see that most of the sustainable vitrimers studies have focused on finding bio-based monomers. Some route for epoxidation has been demonstrated to be working while being more sustainable compared to the epichlorohydrin process. Monomers other than epoxy can also be used to produce vitrimer materials or other catalyst-free BER mechanism may be exploited for these systems. However, this thesis focuses on an epoxy vitrimer network based on transesterifications. The variety of dicarboxylic acid used in these vitrimer allows to readily find bio-based compound (*e.g.* the SA is derived from castor oil). However, there is no solution proposed regarding the catalyst. Transesterification based-vitrimers have been catalysed by a wide range of catalysts such as $\text{Zn}(\text{OAc})_2$, $\text{P}(\text{Ph})_3$ or TBD [15] among others, but production and purification of these chemicals is usually time consuming. A further challenge to enhance vitrimer systems is to incorporate environmental and economical components in their

synthesis. The biodiesel industry has been looking into sustainable transesterification catalysts for over two decades, aiming for bio-based materials but also economically-feasible production [145]. One type of catalyst is not found in the vitrimer studies and remains to be investigated: enzymes, and more accurately lipases (for transesterifications networks).

2.8.2 Enzymatic catalysis - an interesting candidate

Enzymes - short overview

Enzymes are proteins that are present in biological systems ranging from viruses to mammals [146]. They are able to catalyse a wide variety of reactions including the hydrolysis of ester functions, such as the transformation of glycerides into glycerol and fatty acids [147]. In the biodiesel industry, they are used for the separation of esters from waste oils while avoiding secondary reactions such as saponification of free fatty acid [147]. Enzymes contain an active site, composed of a base, an acid, and a nucleophile. These active sites are clefts or grooves at the enzyme surface, usually composed of amino acids from different parts of the polypeptide chain that are brought together in the tertiary structure of the folded protein [146]. Substrates initially bind to the active site by noncovalent interactions, including hydrogen bonds, ionic bonds, and hydrophobic interactions [146]. Among biocatalysts, lipase is an enzyme that is able to catalyse reactions such as esterification, amidation and transesterification among others (Figure 2-30) [148]. Lipase accepts a wide variety of substrates while maintaining a high regioselectivity [146], [149]–[151]. The regioselectivity is determined by the enzyme active shape and size, but also interactions with other amino-acids surrounding the active site which interact with the rest of the molecule chains *via* weak interactions (*e.g.* hydrogen bonding).

The enzyme immobilisation mechanism is yet to be fully understood and controlled. It was reported that lipases can be immobilised *via* their active site, and also their backbones [152]–[154]. The huge variety of enzymes produced over the past decades has makes it difficult to fully grasp the specific behaviour of one enzyme compared to another, especially when put in interaction with different solvents or polymer chains. For example, once immobilised, Novozym 435 lipases will be moderately released from the substrate in

solvent after temperature application [152]. A more efficient release was obtained after addition of detergent-like or substrate products in the solvent (*e.g.* diglycerides, free fatty acid, *etc.*). In the other way, for keeping Novozym 435 immobilised on the substrate, it was reported to crosslink the lipase backbone using multifunctional polymers such as aldehyde dextran or polyethylenimine (PEI) [152].

I. Hydrolysis



II. Synthesis

a Esterification

Esterification



Amidation



Thioesterification



b Transesterification

Acidolysis reaction



Aminolysis reaction



Alcoholysis reaction



Interesterification reaction



Figure 2-30 The different reactions catalysed by lipases [148]: I - Hydrolysis of ester (used in biodiesel industry), II - a) Esterification reactions (esterification, amidation, and thioesterification), b) Transesterification reactions (acidolysis, aminolysis, alcoholysis and interesterification).

Some lipases are reported to form multimeric enzyme clusters (*i.e.* agglomeration of enzymes on the substrate) which produces second free functional groups inside the cluster [153]. PEI was reported to stabilise these clusters to avoid separation of the lipases *via* interactions with their backbones leading to the formation of structures very rich in cationic groups able to be immobilised on anionic supports (Figure 2-31a) [153]. These interactions may lead to potential degradation of the catalytic properties (by reducing the lipase's motion or inducing conformational changes) but they also stabilise their quaternary structures which allows the production of layered structures (Figure 2-31b).

It is possible to see from these few examples that working with lipases can lead to difficulty towards deep understanding of their mechanisms and interactions with their surrounding environment. However, the catalytic properties of lipases (high regioselectivity and low temperature activation) associated to this complexity can produce interesting results when applied to polymers while keeping an incredible sustainability benefit compared to conventional catalysts.

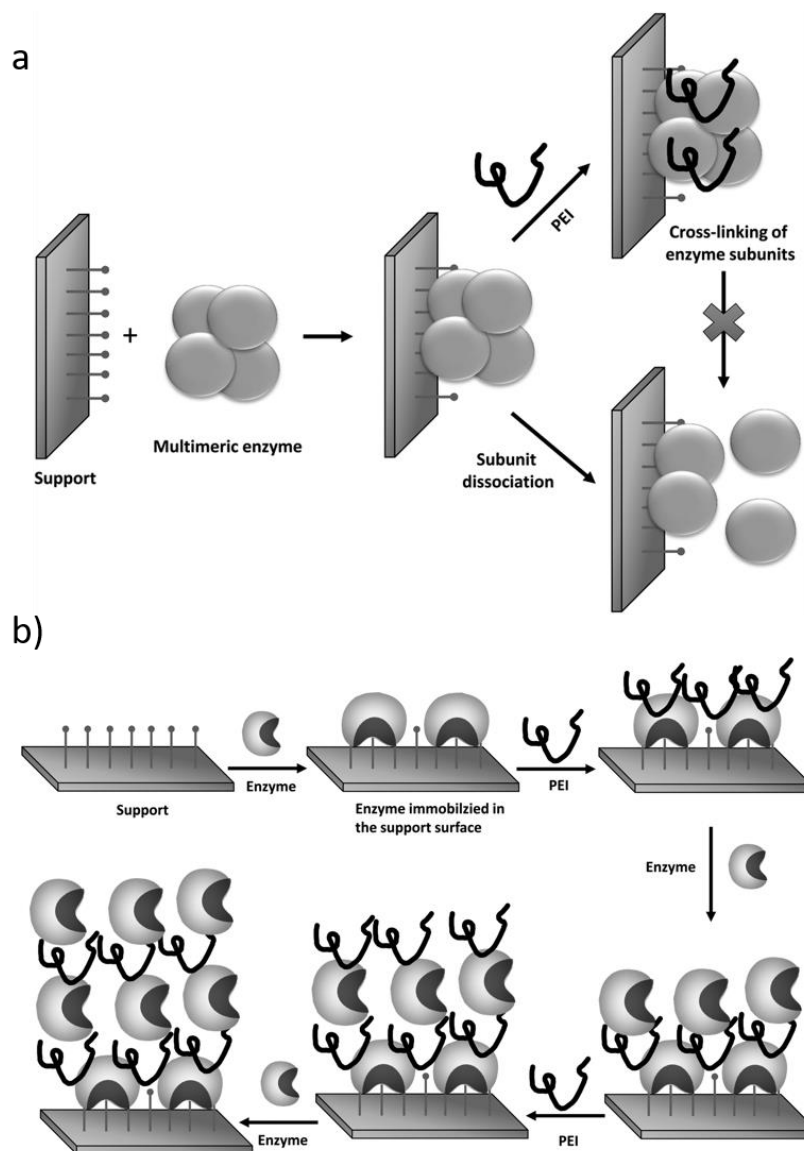


Figure 2-31 a) formation of multimeric cluster rich in cationic units able to fix themselves on anionic support; addition of PEI stabilise these clusters onto the substrate, b) Formation of multilayered structure by crosslinking lipases' backbones with PEI [153].

Lipases and their uses for polymers

Lipases have been used to catalyse various monomers preparation and polymerisation reactions using their high regioselectivity property [155]. Investigation of cure kinetics and better conversion of monomers to polymers or block copolymers has been proven with various lipases. CALB B (Candida Antarctica lipase B) lipases were shown to efficiently produce PDMS-PEG amphiphilic block copolymer reaching a high molecular weight [156]. The use of these lipases to produce supramolecular (as these copolymers are known to assemble into supramolecular structures in specific solvents) networks without

using metallic catalyst was reported to be interesting for biomedical use. A similar study proved the possibility to replace PEG by poly(ϵ -caprolactone) to produce triblock copolymers [157]. CALB B was also reported to produce semi-crystalline copolyester by polymerising the reaction of poly(hexamethylene γ -ketopimelate) with poly(hexamethylene γ -ketopimelate-co-hexamethylene adipate) [158]. The network can be functionalised post-polymerisation with amioxy or hydrazide agent by grafting in mild conditions (24 h, room temperature). Recently (2020), CALB B was used to produce vinyl glycolate derivatives of polydydic alcohol with high functionalities [159]. The lipases' catalytic properties were compared to Lewis acid and base demonstrating again a higher conversation rate without side reactions. The thermal stability of lipases can also be improved *via* subtraction on some monomers [160]. Usually, enzymes are active within a specific temperature range (\approx 20-80°C [161]) and beyond this, the enzyme's tertiary structure unfolds causing loss of catalytic properties. However, CALB B was reported to be stabilised up to 160°C *via* subtraction on macroporous acrylic resin particles [160].

Studies related to epoxy compounds are versatile and meagre and the lipases were initially used to epoxidise monomers [148], [162]. On the other hand, lipases were also shown to have an increase in their catalytic activity when immobilised on epoxy substrate which led to faster polymerisation *via* ROP with a higher conversion rate of monomers [163]. The ROP of lactone was demonstrated and models were proposed to explain the mechanism triggered by the active site [164] which was then used to understand possible polymerisation mechanisms of epoxide networks. The polymerisation of epoxy compounds with different dicarboxylic anhydrides was then investigated [165]. From this study, the proposed mechanism showed an opening of the anhydrides by the lipases to form a complex, which then reacts with "water which may be contained in the enzyme" (from the authors' study terms) and epoxy compound to form an ester (Figure 2-32). By propagation the system allowed to produce polyester polymers with high conversion of monomers.

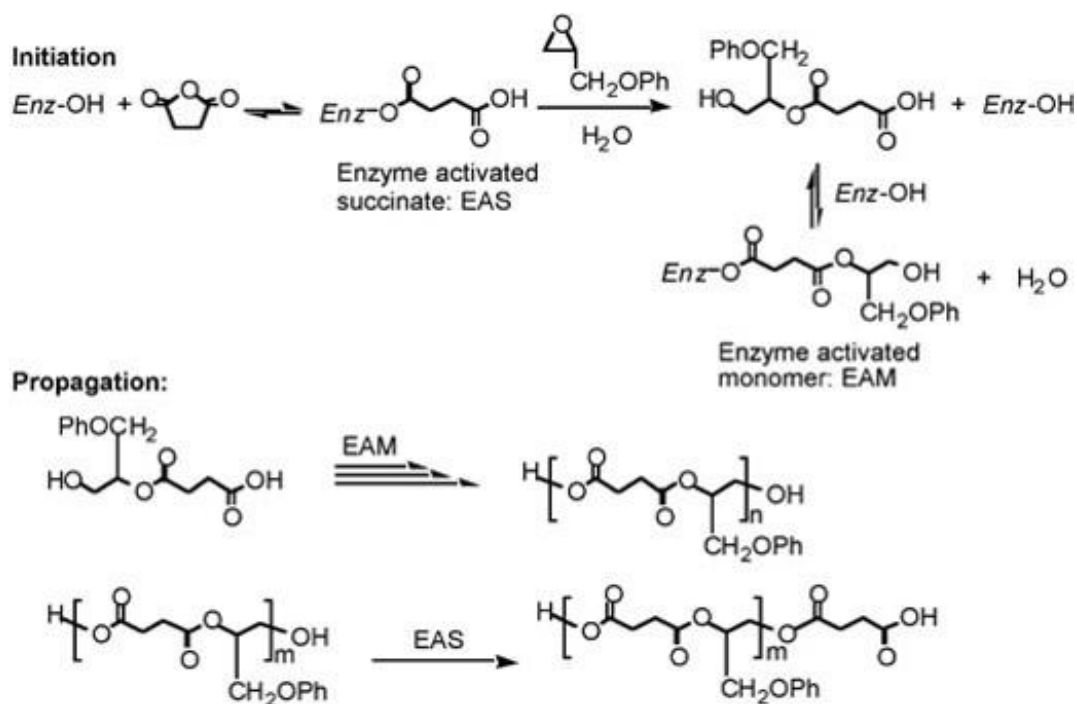


Figure 2-32 Schematic of epoxy - dicarboxylic anhydrides polymerised by lipases [165].

A previous study on the hydrolysis of epoxy posited that the ring opening was triggered by the nucleophilic attack of the aspartate₃₃₃ (Asp₃₃₃) facilitated by two tyrosine amino-acids polarising the epoxy moiety [166]. This attack results in the formation of a hydroxylalkyl covalent intermediate. Another aspartate with histidine activates a molecule of water which hydrolyses the covalent intermediate to finish the epoxy hydrolysis (Figure 2-33).

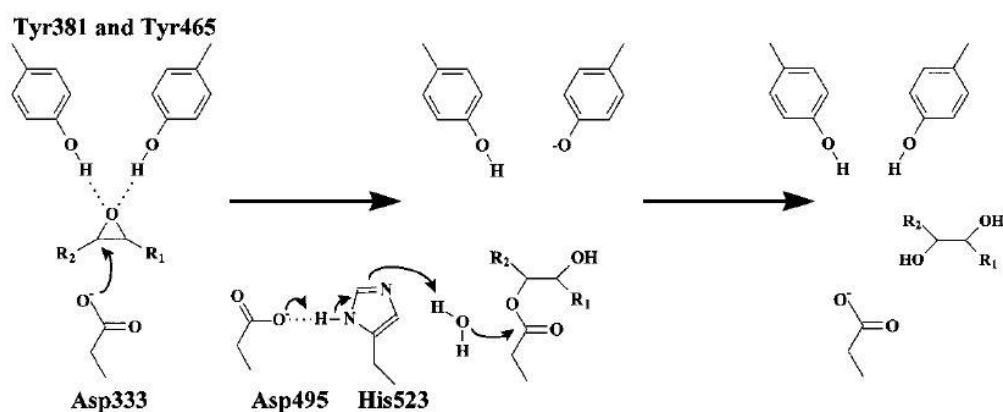


Figure 2-33 Schematic of proposed mechanism of epoxy hydrolysis by lipases: In the first the tyrosine amino-acids polarise the oxygen of the epoxy *via* hydrogen bonding facilitating the nucleophilic attack from Asp₃₃₃. Then the activated molecules of water finish the hydrolysis and recover the enzyme active site to restart a new cycle [166].

2.8.3 Concluding remarks on sustainable vitrimers and research motivation for the third experimental chapter (Chapter 5)

As for their development into new chemistries or nanocomposites, the concept of vitrimers allowed a quick adaptation toward sustainable approaches. Research corresponding to the use of bio-based components, either as resins or hardeners, can easily be integrated to vitrimers as the BER is happening at the crosslink units (or is directly induced by the monomers structure as in disulphide networks). This fact, combined with researchers working intensively towards greener alternatives allowed to swiftly adapt toward producing vitrimer networks from their traditional thermoset matrices.

However, to the knowledge of the author, these efforts focused only to produce networks based on similar catalysed reactions: either by using a Lewis base or acid (case of transesterification), or using 'natural' BER catalysed by free functional groups (imine networks). Non-catalysed BER have the potential to be fully bio-based using natural compounds and their preparation. Even epoxidation can be achieved using better alternatives than epichlorohydrin [139]. For catalysed networks, we have seen that catalysts can lead to secondary reactions which can be either beneficial or detrimental to the network, and degradation of the catalyst can also lead to loss of network properties [89], [91], [94], [95].

From biodiesel research, enzymes seem to be a good catalyst choice with potential to achieve vitrimer systems. Their high regioselectivity could achieve a significant conversion of monomers to ester with pendant hydroxyl groups. Moreover, they would be, in theory, able to catalyse the BER at the temperature range of the enzyme activation (*i.e.* < 100°C) leading to epoxy vitrimer systems with low healing and reprocessing temperature. Lipases used as catalyst for epoxy vitrimer networks could be the next step to produce these vitrimers from a fully bio-based viewpoint. This idea led the research motivation for the third experimental chapter of this thesis. A lipase termed TL from *Pseudomonas stutzeri* (a bacteria from soil commercialized by Meito Sangyo Co., Ltd), known to selectively recognise bulky secondary alcohol [167], [168], is used to catalyse the esterification of the epoxy/SA system. The kinetic reaction (at 100°C) is observed between an active and deactivated lipase (thermally degraded) system. The bulk polymer is then characterised a low temperature (80°C), to observe its reprocessing and healing capability as well as

relaxation characteristic. The network is then tested at high temperature (125°C-250°C) to observe if the network produced can be categorised as a vitrimer.

2.9 Timeline resuming key points of this literature review in the development of vitrimer chemistry and key points for development of this thesis

To remind the readers some of the information covered in the previous sections, an overview of the timeline of the vitrimers development is shown in Figure 2-34. The associated key studies that oriented the choices of this research project are shown above the timeline, and the key studies that have developed the vitrimer field are located below it. The author (QAP), would like to point out that most studies mentioned have their place in each side of the timeline. Moreover, many other studies are not represented in this figure to keep some clarity but would have also deserve a potential mention.

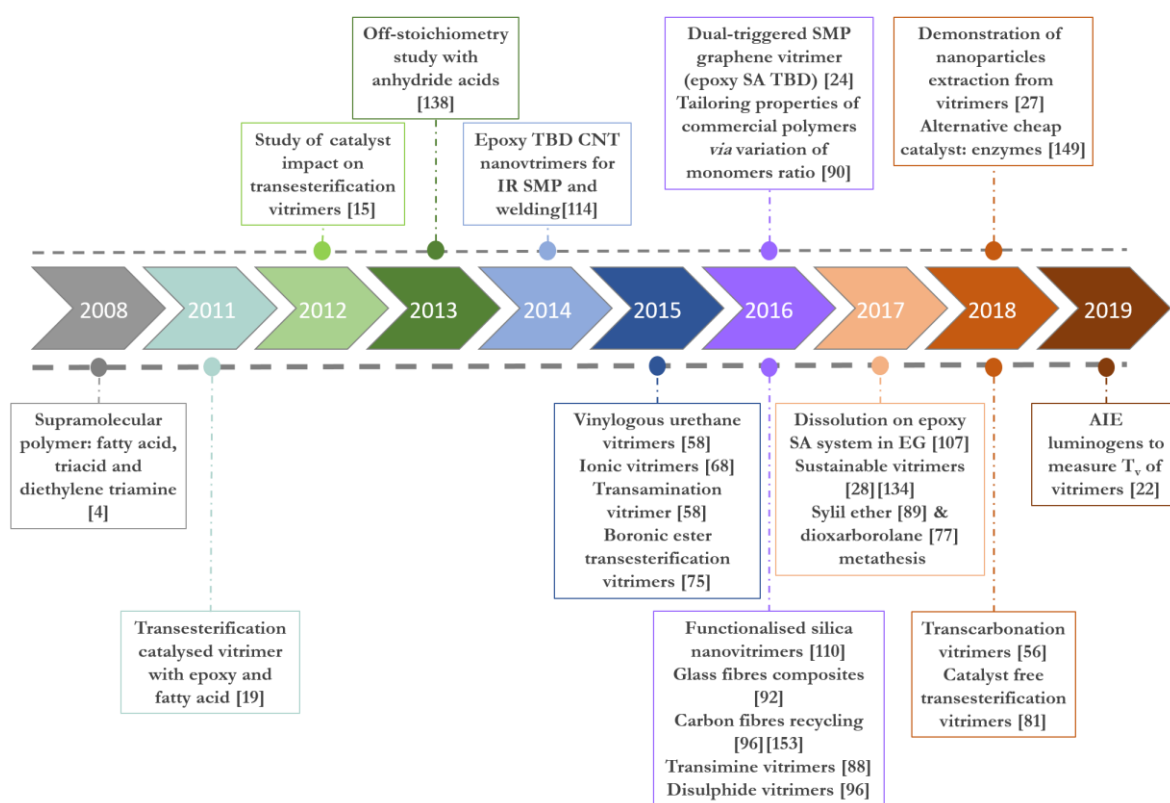


Figure 2-34 Timeline overview of the vitrimer development covered in this literature - the top section represents some key studies which were a deciding factor in the development of this thesis; the bottom section represents key studies in the progress of vitrimers as represented in this document.

2.10 Conclusion to the literature review

This literature review has covered several topics related to the aims and goals of this thesis to explore the potential of the vitrimer matrix: epoxy/sebacic acid. The choice of epoxy as a resin originates from its intense use and large variety of monomers available in industry. However, traditional thermosets have many drawbacks, and the apparition of vitrimer matrices (following a large quest for healable materials such as supramolecular and Diels-alder networks) opens new possibilities toward design, application and use of thermosets.

The choice of the initial vitrimer matrices developed by Leibler and co-workers (epoxy/carboxylic acid or anhydride), led to a quick attraction of the research community to develop newer chemistries on similar bond exchange mechanism. If these networks can find relevant applications, they are still no match to easily fit as potential replacement of traditional epoxy thermoset in terms of ease of production, availability and acceptance in industries. Therefore, it is important to understand, in better depth, how the network formation can be controlled in the presence of a catalyst. Off-stoichiometry formulations are of great interest and the understanding of their mechanism is in growth. Related to these points, Chapter 3 of this thesis focuses on the cure kinetic linked to these formulations and impact on the mechanical properties of these polymers while keeping a manufacture process easily scalable.

Graphene nanocomposites is a 'hot' topic and the combination with vitrimer properties has led to innovative properties to produce multifunctional materials. The understanding of nanoparticles and vitrimers is still in its beginning and many studies are building the way towards control of these properties. However, the end product life of nanocomposites and their environmental impact has always been a concern since the conference on convergent technologies in Paris (14th-15th December 2004). Therefore, the demonstration of traditional fibres (glass or carbon) opened the way towards the possibility of recovering the nanoparticles from these nanocomposites and assess their modification for potential post-utilisation (topic of the Chapter 4 of this thesis).

In regard of more sustainable solutions, bio-based materials always remain an interesting choice. Vitrimers properties already tend to make these materials a greener alternative than their thermoset counterparts. However, to the author's knowledge (QAP),

enzymes were not considered as a potential catalyst replacement to produce vitrimer network. This fact led to investigate lipases as catalysts for low temperature (100°C) curing vitrimers using the epoxy/sebacic acid network (Chapter 5).

2.11 References

- [1] L. Voorhaar and R. Hoogenboom, "Supramolecular polymer networks: Hydrogels and bulk materials," *Chem. Soc. Rev.*, vol. 45, no. 14, pp. 4013–4031, 2016.
- [2] A. Campanella, D. Döhler, and W. H. Binder, "Self-Healing in Supramolecular Polymers," *Macromol. Rapid Commun.*, vol. 39, no. 17, pp. 1–19, 2018.
- [3] R. F. M. Lange, M. Van Gurp, and E. W. Meijer, "Hydrogen-bonded supramolecular polymer networks," *J. Polym. Sci. Part A Polym. Chem.*, vol. 37, no. 19, pp. 3657–3670, 1999.
- [4] P. Cordier, F. Tournilhac, C. Soulié-Ziakovic, and L. Leibler, "Self-healing and thermoreversible rubber from supramolecular assembly," *Nature*, vol. 451, no. 7181, pp. 977–980, 2008.
- [5] Y. Yang and M. W. Urban, "Self-healing polymeric materials," *Chem. Soc. Rev.*, vol. 42, no. 17, pp. 7446–7467, 2013.
- [6] L. Leibler, M. Rubinstein, and R. H. Colby, "Dynamics of telechelic ionomers. Can polymer diffuse large distance without relaxing stress?," *J. Phys. II*, vol. 3, pp. 1581–1590, 1993.
- [7] R. D. Andrew, A. V. Tobolsky, and E. E. Hanson, "The theory of Permanent Set at Elevated Temperatures in Natural and Synthetic Rubber Vulcanizates," *Rubber Chem. Technol.*, vol. 4, pp. 1099–1112, 1946.
- [8] W. Denissen, J. M. Winne, and F. E. Du Prez, "Vitrimers: permanent organic networks with glass-like fluidity," *Chem. Sci.*, vol. 7, no. 1, pp. 30–38, 2015.
- [9] C. N. Bowman and C. J. Kloxin, "Covalent adaptable networks: Reversible bond structures incorporated in polymer networks," *Angew. Chemie - Int. Ed.*, vol. 51, no. 18, pp. 4272–4274, 2012.
- [10] C. J. Kloxin and C. N. Bowman, "Covalent adaptable networks: smart, reconfigurable and responsive network systems.," *Chem. Soc. Rev.*, vol. 42, no. 17, pp. 7161–73, 2013.
- [11] B. Krishnakumar, R. V. S. P. Sanka, W. H. Binder, V. Parthasarthy, S. Rana, and N. Karak, "Vitrimers: Associative dynamic covalent adaptive networks in thermoset polymers," *Chem. Eng. J.*, vol. 385, no. July 2019, p. 123820, Apr. 2020.
- [12] L. Rulisek, P. Sebek, Z. Havlas, R. Hrabal, P. Capek, and A. Svatos, "An experimental and theoretical study of stereoselectivity of furan-maleic and furan-maleide diels-alder reactions," *J. Org. Chem.*, vol. 70, no. 5, pp. 6295–6302, 2005.
- [13] A. Gandini, "The furan/maleimide Diels-Alder reaction: A versatile click-unclick tool in macromolecular synthesis," *Prog. Polym. Sci.*, vol. 38, no. 1, pp. 1–29, 2012.
- [14] V. Froideveaux, M. Borne, E. Laborbe, R. Auvergne, A. Gandini, and B. Boutevin, "Study of the Diels-Alder and retro-Diels-Alder reaction between furan derivatives and maleimides for the creation of new materials," *RSC adv.*, vol. 5, pp. 37742–37754, 2015.
- [15] M. Capelot, M. M. Unterlass, F. Tournilhac, and L. Leibler, "Catalytic control of the

- vitriimer glass transition," *ACS Macro Lett.*, vol. 1, no. 7, pp. 789–792, 2012.
- [16] X. Chen *et al.*, "A Thermally Re-mendable Cross-Linked Polymeric Material," *Science*, vol. 295, no. 5560, pp. 1698–1702, 2002.
- [17] T. F. Scott, A. D. Schneider, W. D. Cook, and C. N. Bowman, "Photoinduced Plasticity in Cross-Linked Polymers," *Science*, vol. 308, no. 5728, pp. 1615–1617, 2005.
- [18] Y. Amamoto, H. Otsuka, A. Takahara, and K. Matyjaszewski, "Self-healing of covalently cross-linked polymers by reshuffling thiuram disulfide moieties in air under visible light," *Adv. Mater.*, vol. 24, no. 29, pp. 3975–3980, 2012.
- [19] D. Montarnal, M. Capelot, F. Tounilhac, and L. Leibler, "Silica-Like Malleable Materials from permanent organic network," *Science*, vol. 334, pp. 965–968, 2011.
- [20] E. Chabert, "Materiaux composites a matrices vitrimere et polymere," Université Pierre et Marie Curie - Paris VI, 2015.
- [21] D. Montarnal, "Use of reversible covalent and non-covalent bonds in new recyclable and reprocessible polymer materials," Université Pierre et Marie Curie - Paris VI, 2011.
- [22] R. G. Ricarte, F. Tournilhac, M. Cloître, and L. Leibler, "Linear Viscoelasticity and Flow of Self-Assembled Vitrimers: The Case of a Polyethylene/Dioxaborolane System," *Macromolecules*, vol. 53, no. 5, pp. 1852–1866, 2020.
- [23] Z. Yang, Q. Wang, and T. Wang, "Dual-Triggered and Thermally Reconfigurable Shape Memory Graphene-Vitriimer Composites," *ACS Appl. Mater. Interfaces*, vol. 8, no. 33, pp. 21691–21699, Aug. 2016.
- [24] Z. Liu, C. Zhang, Z. Shi, J. Yin, and M. Tian, "Tailoring vinylogous urethane chemistry for the cross-linked polybutadiene: Wide freedom design, multiple recycling methods, good shape memory behavior," *Polymer*, vol. 148, pp. 202–210, 2018.
- [25] C. He *et al.*, "Conformational Entropy as a Means to Control the Behavior of Poly(diketoenamine) Vitrimers In and Out of Equilibrium," *Angew. Chemie*, vol. 132, no. 2, pp. 745–749, 2020.
- [26] Y. Yang, S. Zhang, X. Zhang, L. Gao, Y. Wei, and Y. Ji, "Detecting topology freezing transition temperature of vitrimers by AIE luminogens," *Nat. Commun.*, vol. 10, no. 1, 2019.
- [27] F. Zhou *et al.*, "Preparation of self-healing, recyclable epoxy resins and low-electrical resistance composites based on double-disulfide bond exchange," *Compos. Sci. Technol.*, vol. 167, pp. 79–85, 2018.
- [28] C. Hao *et al.*, "A High-Lignin-Content, Removable, and Glycol-Assisted Repairable Coating Based on Dynamic Covalent Bonds," *ChemSusChem*, vol. 12, no. 5, pp. 1049–1058, 2019.
- [29] X. Yang, L. Guo, X. Xu, S. Shang, and H. Liu, "A fully bio-based epoxy vitriimer: Self-healing, triple-shape memory and reprocessing triggered by dynamic covalent bond exchange," *Mater. Des.*, vol. 186, p. 108248, Jan. 2020.
- [30] H. Li *et al.*, "Influence of treating parameters on thermomechanical properties of recycled epoxy-acid vitrimers," *Soft Matter*, vol. 16, no. 6, pp. 1668–1677, 2020.

- [31] Z. Ma, Y. Wang, J. Zhu, J. Yu, and Z. Hu, "Bio-based epoxy vitrimers: Reprocessability, controllable shape memory, and degradability," *J. Polym. Sci. Part A Polym. Chem.*, vol. 55, no. 10, pp. 1790–1799, 2017.
- [32] R. Wu *et al.*, "Rigidisation of deployable space polymer membranes by heat-activated self-folding," *Smart Mater. Struct.*, vol. 27, no. 10, p. 105037, 2018.
- [33] J. Matovic and K. Reichenberger, "Two - way SMA actuators for space application: Performances and reliability," in *Procedia Engineering*, 2010, vol. 5, pp. 1372–1375.
- [34] Y. Shen and T. Fukuda, "State of the art: micro-nanorobotic manipulation in single cell analysis," *Rend. Lincei*, vol. 1, no. 1, pp. 1–13, 2014.
- [35] J. H. Chen, X. P. An, Y. D. Li, M. Wang, and J. B. Zeng, "Reprocessable Epoxy Networks with Tunable Physical Properties: Synthesis, Stress Relaxation and Recyclability," *Chinese J. Polym. Sci. (English Ed.)*, vol. 36, no. 5, pp. 641–648, 2018.
- [36] M. Hayashi, R. Yano, and A. Takasu, "Synthesis of amorphous low: T_g polyesters with multiple COOH side groups and their utilization for elastomeric vitrimers based on post-polymerization cross-linking," *Polym. Chem.*, vol. 10, no. 16, pp. 2047–2056, 2019.
- [37] L. Imbernon, S. Norvez, and L. Leibler, "Stress Relaxation and Self-Adhesion of Rubbers with Exchangeable Links," *Macromolecules*, vol. 49, no. 6, pp. 2172–2178, 2016.
- [38] F. Snijkers, R. Pasquino, and A. Maffezzoli, "Curing and viscoelasticity of vitrimers," *Soft Matter*, vol. 13, no. 1, pp. 258–268, 2017.
- [39] B. Zhang *et al.*, "Recycling of vitrimer blends with tunable thermomechanical properties," *RSC Adv.*, vol. 9, no. 10, pp. 5431–5437, 2019.
- [40] F. Ji *et al.*, "Reprocessable and Recyclable Crosslinked Polyethylene with Triple Shape Memory Effect," *Macromol. Mater. Eng.*, vol. 304, no. 3, 2019.
- [41] F. I. Altuna, C. E. Hoppe, and R. J. J. Williams, "Epoxy vitrimers with a covalently bonded tertiary amine as catalyst of the transesterification reaction," *Eur. Polym. J.*, vol. 113, pp. 297–304, 2019.
- [42] A. Demongeot, S.-J. J. Mougner, S. Okada, C. Soulié-Ziakovic, and F. Tournilhac, "Coordination and Catalysis of Zn^{2+} in Epoxy-Based Vitrimers," *Polym. Chem.*, vol. 7, no. 27, pp. 4486–4493, 2016.
- [43] J. L. Self, N. D. Dolinski, M. S. Zayas, J. Read de Alaniz, and C. M. Bates, "Brønsted-Acid-Catalyzed Exchange in Polyester Dynamic Covalent Networks," *ACS Macro Lett.*, vol. 7, no. 7, pp. 817–821, 2018.
- [44] X. Niu, F. Wang, X. Li, R. Zhang, Q. Wu, and P. Sun, "Using Zn^{2+} Ionomer to Catalyze Transesterification Reaction in Epoxy Vitrimer," *Ind. Eng. Chem. Res.*, vol. 58, no. 14, pp. 5698–5706, 2019.
- [45] Y. Yang, E. M. Terentjev, Y. Wei, and Y. Ji, "Solvent-assisted programming of flat polymer sheets into reconfigurable and self-healing 3D structures," *Nat. Commun.*, vol. 9, no. 1, p. 1906, 2018.
- [46] A. Demongeot, R. Groote, H. Goossens, T. Hoeks, F. Tournilhac, and L. Leibler, "Cross-

Linking of Poly(butylene terephthalate) by Reactive Extrusion Using Zn(II) Epoxy-Vitrimer Chemistry," *Macromolecules*, vol. 50, no. 16, pp. 6117–6127, 2017.

- [47] G. B. Lyon, L. M. Cox, J. T. Goodrich, A. D. Baranek, Y. Ding, and C. N. Bowman, "Remoldable Thiol–Ene Vitrimers for Photopatterning and Nanoimprint Lithography," *Macromolecules*, vol. 49, no. 23, pp. 8905–8913, 2016.
- [48] Q. Chen, X. Yu, Z. Pei, Y. Yang, Y. Wei, and Y. Ji, "Multi-stimuli responsive and multi-functional oligoaniline-modified vitrimers," *Chem. Sci.*, vol. 8, no. 1, pp. 724–733, 2017.
- [49] Y. Liu, Z. Tang, S. Wu, and B. Guo, "Integrating Sacrificial Bonds into Dynamic Covalent Networks toward Mechanically Robust and Malleable Elastomers," *ACS Macro Lett.*, vol. 8, no. 2, pp. 193–199, 2019.
- [50] M. Chen, L. Zhou, Y. Wu, X. Zhao, and Y. Zhang, "Rapid Stress Relaxation and Moderate Temperature of Malleability Enabled by the Synergy of Disulfide Metathesis and Carboxylate Transesterification in Epoxy Vitrimers," *ACS Macro Lett.*, vol. 8, no. 3, pp. 255–260, 2019.
- [51] Y. Zhou, J. G. P. Goossens, R. P. Sijbesma, and J. P. A. Heuts, "Poly(butylene terephthalate)/Glycerol-based Vitrimers *via* Solid-State Polymerization," *Macromolecules*, vol. 50, no. 17, pp. 6742–6751, 2017.
- [52] Y. Shan *et al.*, "A renewable dynamic covalent network based on itaconic anhydride crosslinked polyglycerol: Adaptability, UV blocking and fluorescence," *Chem. Eng. J.*, vol. 385, Apr. 2020.
- [53] R. R. Vaidyula, P. Y. Dugas, E. Rawstron, E. Bourgeat-Lami, and D. Montarnal, "Improved malleability of miniemulsion-based vitrimers through *in situ* generation of carboxylate surfactants," *Polym. Chem.*, vol. 10, no. 23, pp. 3001–3005, 2019.
- [54] K. Hu *et al.*, "Interfacial Broadening Kinetics between a Network and a Linear Polymer and Their Composites Prepared by Melt Blending," *Macromolecules*, vol. 52, no. 24, pp. 9759–9765, 2019.
- [55] S. Kaiser, S. Wurzer, G. Pilz, W. Kern, and S. Schlögl, "Stress relaxation and thermally adaptable properties in vitrimer-like elastomers from HXNBR rubber with covalent bonds," *Soft Matter*, vol. 15, no. 30, pp. 6062–6072, 2019.
- [56] R. L. Snyder, D. J. Fortman, G. X. De Hoe, M. A. Hillmyer, and W. R. Dichtel, "Reprocessable Acid-Degradable Polycarbonate Vitrimers," *Macromolecules*, vol. 51, no. 2, pp. 389–397, 2018.
- [57] W. Denissen, M. Driesbeke, R. Nicolaÿ, L. Leibler, J. M. Winne, and F. E. Du Prez, "Chemical control of the viscoelastic properties of vinylogous urethane vitrimers," *Nat. Commun.*, vol. 8, p. 14857, 2017.
- [58] W. Denissen, G. Rivero, R. Nicolaÿ, L. Leibler, J. M. Winne, and F. E. Du Prez, "Vinylogous urethane vitrimers," *Adv. Funct. Mater.*, vol. 25, no. 16, pp. 2451–2457, 2015.
- [59] J. Shi, T. Zheng, B. Guo, and J. Xu, "Solvent-free thermo-reversible and self-healable crosslinked polyurethane with dynamic covalent networks based on phenol-carbamate bonds," *Polymer*, vol. 181, Oct. 2019.

- [60] T. Stukenbroeker, W. Wang, J. M. Winne, F. E. Du Prez, R. Nicolaÿ, and L. Leibler, "Polydimethylsiloxane quenchable vitrimers," *Polym. Chem.*, vol. 8, no. 43, pp. 6590–6593, 2017.
- [61] L. Zhang and S. J. Rowan, "Effect of Sterics and Degree of Cross-Linking on the Mechanical Properties of Dynamic Poly(alkylurea-urethane) Networks," *Macromolecules*, vol. 50, no. 13, pp. 5051–5060, 2017.
- [62] T. Wright, T. Tomkovic, S. G. Hatzikiriakos, and M. O. Wolf, "Photoactivated Healable Vitrimeric Copolymers," *Macromolecules*, vol. 52, no. 1, pp. 36–42, 2019.
- [63] M. Guerre, C. Taplan, R. Nicolaÿ, J. M. Winne, and F. E. Du Prez, "Fluorinated Vitriimer Elastomers with a Dual Temperature Response," *J. Am. Chem. Soc.*, vol. 140, no. 41, pp. 13272–13284, 2018.
- [64] A. Chao, I. Negulescu, and D. Zhang, "Dynamic Covalent Polymer Networks Based on Degenerative Imine Bond Exchange: Tuning the Malleability and Self-Healing Properties by Solvent," *Macromolecules*, vol. 49, no. 17, pp. 6277–6284, 2016.
- [65] H. Zheng, Q. Liu, X. Lei, Y. Chen, B. Zhang, and Q. Zhang, "A conjugation polyimine vitriimer: Fabrication and performance," *J. Polym. Sci. Part A Polym. Chem.*, vol. 56, no. 22, pp. 2531–2538, 2018.
- [66] Z. Feng *et al.*, "Multifunctional Vitriimer-Like Polydimethylsiloxane (PDMS): Recyclable, Self-Healable, and Water-Driven Malleable Covalent Networks Based on Dynamic Imine Bond," *Ind. Eng. Chem. Res.*, vol. 58, no. 3, pp. 1212–1221, 2019.
- [67] H. Liu, H. Zhang, H. Wang, X. Huang, G. Huang, and J. Wu, "Weldable, malleable and programmable epoxy vitrimers with high mechanical properties and water insensitivity," *Chem. Eng. J.*, vol. 368, pp. 61–70, Jul. 2019.
- [68] M. M. Obadia, B. P. Mudraboyina, A. Serghei, D. Montarnal, and E. Drockenmuller, "Reprocessing and Recycling of Highly Cross-Linked Ion-Conducting Networks through Transalkylation Exchanges of C–N Bonds," *J. Am. Chem. Soc.*, vol. 137, no. 18, pp. 6078–6083, 2015.
- [69] M. M. Obadia, A. Jourdain, P. Cassagnau, D. Montarnal, and E. Drockenmuller, "Tuning the Viscosity Profile of Ionic Vitrimers Incorporating 1,2,3-Triazolium Cross-Links," *Adv. Funct. Mater.*, vol. 27, no. 45, p. 1703258, 2017.
- [70] J. Tang, L. Wan, Y. Zhou, H. Pan, and F. Huang, "Strong and efficient self-healing adhesives based on dynamic quaternization cross-links," *J. Mater. Chem. A*, vol. 5, no. 40, pp. 21169–21177, 2017.
- [71] B. Hendriks, J. Waelkens, J. M. Winne, and F. E. Du Prez, "Poly(thioether) Vitrimers *via* Transalkylation of Trialkylsulfonium Salts," *ACS Macro Lett.*, vol. 6, no. 9, pp. 930–934, 2017.
- [72] A. Ruiz De Luzuriaga *et al.*, "Epoxy resin with exchangeable disulfide crosslinks to obtain reprocessable, repairable and recyclable fiber-reinforced thermoset composites," *Mater. Horizons*, vol. 3, no. 3, pp. 241–247, 2016.
- [73] A. Ruiz de Luzuriaga *et al.*, "Transient mechanochromism in epoxy vitriimer composites containing aromatic disulfide crosslinks," *J. Mater. Chem. C*, vol. 4, no. 26, pp. 6220–6223, 2016.

- [74] S. Zhang, L. Pan, L. Xia, Y. Sun, and X. Liu, "Dynamic polysulfide shape memory networks derived from elemental sulfur and their dual thermo-/photo-induced solid-state plasticity," *React. Funct. Polym.*, vol. 121, pp. 8–14, 2017.
- [75] O. R. Cromwell, J. Chung, and Z. Guan, "Malleable and Self-Healing Covalent Polymer Networks through Tunable Dynamic Boronic Ester Bonds," *J. Am. Chem. Soc.*, vol. 137, no. 20, pp. 6492–6495, 2015.
- [76] J. J. Cash, T. Kubo, A. P. Bapat, and B. S. Sumerlin, "Room-temperature self-healing polymers based on dynamic-covalent boronic esters," *Macromolecules*, vol. 48, no. 7, pp. 2098–2106, 2015.
- [77] M. Röttger, T. Domenech, R. Van Der Weegen, A. Breuillac, R. Nicolaÿ, and L. Leibler, "High-performance vitrimers from commodity thermoplastics through dioxaborolane metathesis," *Science*, vol. 356, no. 6333, pp. 62–65, 2017.
- [78] F. Caffy and R. Nicolaÿ, "Transformation of polyethylene into a vitrimer by nitroxide radical coupling of a bis-dioxaborolane," *Polym. Chem.*, vol. 10, no. 23, pp. 3107–3115, 2019.
- [79] A. Breuillac, A. Kassalias, and R. Nicolaÿ, "Polybutadiene Vitrimers Based on Dioxaborolane Chemistry and Dual Networks with Static and Dynamic Cross-links," *Macromolecules*, vol. 52, no. 18, pp. 7102–7113, 2019.
- [80] H. Guo, L. Yue, G. Rui, and I. Manas-Zloczower, "Recycling Poly(ethylene-vinyl acetate) with Improved Properties through Dynamic Cross-Linking," *Macromolecules*, vol. 53, no. 1, pp. 458–464, 2020.
- [81] J. Han, T. Liu, C. Hao, S. Zhang, B. Guo, and J. Zhang, "A Catalyst-Free Epoxy Vitrimer System Based on Multifunctional Hyperbranched Polymer," *Macromolecules*, vol. 51, no. 17, pp. 6789–6799, 2018.
- [82] J. Han *et al.*, "Hyperbranched Polymer Assisted Curing and Repairing of an Epoxy Coating," *Ind. Eng. Chem. Res.*, vol. 58, no. 16, pp. 6466–6475, 2019.
- [83] H. Han and X. Xu, "Poly(methyl methacrylate)–epoxy vitrimer composites," *J. Appl. Polym. Sci.*, vol. 135, no. 22, pp. 1–5, 2018.
- [84] M. Delahaye, J. M. Winne, and F. E. Du Prez, "Internal Catalysis in Covalent Adaptable Networks: Phthalate Monoester Transesterification As a Versatile Dynamic Cross-Linking Chemistry," *J. Am. Chem. Soc.*, vol. 141, no. 38, pp. 15277–15287, 2019.
- [85] C. He, S. Shi, D. Wang, B. A. Helms, and T. P. Russell, "Poly(oxime-ester) Vitrimers with Catalyst-Free Bond Exchange," *J. Am. Chem. Soc.*, vol. 141, no. 35, pp. 13753–13757, 2019.
- [86] Z. Ding, L. Yuan, G. Liang, and A. Gu, "Thermally resistant thermadapt shape memory crosslinked polymers based on silyl ether dynamic covalent linkages for self-folding and self-deployable smart 3D structures," *J. Mater. Chem. A*, vol. 7, no. 16, pp. 9736–9747, 2019.
- [87] Q.-A. Poutrel, Z. Wang, D. Wang, C. Soutis, and M. Gresil, "Effect of pre and Post-Dispersion on Electro-Thermo-Mechanical Properties of a Graphene Enhanced Epoxy," *Appl. Compos. Mater.*, vol. 24, no. 2, pp. 313–336, 2017.

- [88] Q. Liu, L. Jiang, Y. Zhao, Y. Wang, and J. Lei, "Reprocessable and Shape Memory Thermosetting Epoxy Resins Based on Silyl Ether Equilibration," *Macromol. Chem. Phys.*, vol. 220, no. 13, p. 1900149, May 2019.
- [89] C. A. Tretbar, J. A. Neal, and Z. Guan, "Direct Silyl Ether Metathesis for Vitrimers with Exceptional Thermal Stability," *J. Am. Chem. Soc.*, vol. 141, no. 42, pp. 16595–16599, 2019.
- [90] Q. Ge, A. H. Sakhaei, H. Lee, C. K. Dunn, N. X. Fang, and M. L. Dunn, "Multimaterial 4D Printing with Tailorable Shape Memory Polymers," *Sci. Rep.*, vol. 6, no. April, p. 31110, 2016.
- [91] F. I. Altuna, C. E. Hoppe, and R. J. J. Williams, "Shape memory epoxy vitrimers based on DGEBA crosslinked with dicarboxylic acids and their blends with citric acid," *RSC Adv.*, vol. 6, no. 91, pp. 88647–88655, 2016.
- [92] E. Chabert, J. Vial, J.-P. Cauchois, M. Mihaluta, and F. Tournilhac, "Multiple welding of long fiber epoxy vitrimer composites," *Soft Matter*, vol. 12, no. 21, pp. 4838–4845, 2016.
- [93] L. Li, X. Chen, K. Jin, and J. M. Torkelson, "Vitrimers Designed Both To Strongly Suppress Creep and To Recover Original Cross-Link Density after Reprocessing: Quantitative Theory and Experiments," *Macromolecules*, vol. 51, no. 15, pp. 5537–5546, 2018.
- [94] F. I. Altuna, C. E. Hoppe, and R. J. J. Williams, "Epoxy vitrimers: The effect of transesterification reactions on the network structure," *Polymers*, vol. 10, no. 1, p. 43, 2018.
- [95] F. I. Altuna, U. Casado, I. E. Dell'Erba, L. Luna, C. E. Hoppe, and R. J. J. Williams, "Epoxy vitrimers incorporating physical crosslinks produced by self-association of alkyl chains," *Polym. Chem.*, vol. 11, no. 7, pp. 1337–1347, 2020.
- [96] K. S. Novoselov *et al.*, "Electric Field Effect in Atomically Thin Carbon Films," *Science*, vol. 306, no. 5696, pp. 666–669, 2004.
- [97] L. Yue, G. Pircheraghi, S. A. Monemian, and I. Manas-Zloczower, "Epoxy composites with carbon nanotubes and graphene nanoplatelets - Dispersion and synergy effects," *Carbon*, vol. 78, pp. 268–278, 2014.
- [98] F. Banhart, J. Kotakoski, and A. V. Krasheninnikov, "Structural Defects in Graphene," *Am. Chem. Soc. Nano*, vol. 5(1), pp. 26–41, 2011.
- [99] D. G. Papageorgiou, I. A. Kinloch, and R. J. Young, "Mechanical properties of graphene and graphene-based nanocomposites," *Prog. Mater. Sci.*, vol. 90, pp. 75–127, 2017.
- [100] M. Gresil, Z. Wang, Q.-A. Poutrel, and C. Soutis, "Thermal Diffusivity Mapping of Graphene Based Polymer Nanocomposites," *Sci. Rep.*, vol. 7, no. 1, p. 5536, 2017.
- [101] Y. Geng, M. Y. Liu, J. Li, X. M. Shi, and J. K. Kim, "Effects of surfactant treatment on mechanical and electrical properties of CNT/epoxy nanocomposites," *Compos. Part A Appl. Sci. Manuf.*, vol. 39, no. 12, pp. 1876–1883, 2008.
- [102] S. Chandrasekaran, C. Seidel, K. Schulte, and Schulte K., "Preparation and

- characterization of graphite nano-platelet (GNP)/epoxy nano-composite: Mechanical, electrical and thermal properties,” *Eur. Polym. J.*, vol. 49, no. 12, pp. 3878–3888, 2013.
- [103] C. M. Hadden *et al.*, “Mechanical properties of graphene nanoplatelet/carbon fiber/epoxy hybrid composites: Multiscale modeling and experiments,” *Carbon*, vol. 95, pp. 100–112, 2015.
- [104] B. Ahmadi-Moghadam *et al.*, “Functionalization of Graphene Nanoplatelets on the Mechanical Response of Graphene/Epoxy Composites,” *Mater. Des.*, vol. 66, pp. 142–149, 2015.
- [105] S. Quiles-Díaz *et al.*, “Influence of the chemical functionalization of graphene on the properties of polypropylene-based nanocomposites,” *Compos. Part A Appl. Sci. Manuf.*, vol. 100, pp. 31–39, 2017.
- [106] S. G. Prolongo, B. G. Meliton, G. Del Rosario, and A. Ureña, “New alignment procedure of magnetite-CNT hybrid nanofillers on epoxy bulk resin with permanent magnets,” *Compos. Part B Eng.*, vol. 46, pp. 166–172, 2013.
- [107] Q. Shi *et al.*, “Recyclable 3D printing of vitrimer epoxy,” *Mater. Horizons*, vol. 4, no. 4, pp. 598–607, 2017.
- [108] B. G. Compton and J. A. Lewis, “3D-printing of lightweight cellular composites,” *Adv. Mater.*, vol. 26, no. 34, pp. 5930–5935, 2014.
- [109] J. Chen *et al.*, “Vitrimer Chemistry Assisted Fabrication of Aligned, Healable, and Recyclable Graphene/Epoxy Composites,” *Front. Chem.*, vol. 7, p. 632, Sep. 2019.
- [110] A. Legrand and C. Soulié-Ziakovic, “Silica-Epoxy Vitrimer Nanocomposites,” *Macromolecules*, vol. 49, no. 16, pp. 5893–5902, 2016.
- [111] Y. Liu, Z. Tang, Y. Chen, C. Zhang, and B. Guo, “Engineering of β -Hydroxyl Esters into Elastomer-Nanoparticle Interface toward Malleable, Robust, and Reprocessable Vitrimer Composites,” *ACS Appl. Mater. Interfaces*, vol. 10, no. 3, pp. 2992–3001, 2018.
- [112] M. Qiu, S. Wu, Z. Tang, and B. Guo, “Exchangeable interfacial crosslinks towards mechanically robust elastomer/carbon nanotubes vitrimers,” *Compos. Sci. Technol.*, vol. 165, pp. 24–30, 2018.
- [113] H. Zhang and X. Xu, “Improving the transesterification and electrical conductivity of vitrimers by doping with conductive polymer wrapped carbon nanotubes,” vol. 99, pp. 15–22, Aug. 2017.
- [114] Y. Yang, Z. Pei, X. Zhang, L. Tao, Y. Wei, and Y. Ji, “Carbon nanotube-vitrimer composite for facile and efficient photo-welding of epoxy,” *Chem. Sci.*, vol. 5, no. 9, pp. 3486–3492, 2014.
- [115] G. kang Chen, K. Wu, Q. Zhang, Y. cen Shi, and M. geng Lu, “Dual-Responsive Shape Memory and Thermally Reconfigurable Reduced Graphene Oxide-Vitrimer Composites,” *Macromol. Res.*, vol. 27, no. 6, pp. 526–533, Jun. 2019.
- [116] G. Qin and J. Qiu, “Ordered polypyrrole nanorings with near-infrared spectrum absorption and photothermal conversion performance,” *Chem. Eng. J.*, pp. 652–661,

2019.

- [117] Z. Li *et al.*, "Polydopamine nanoparticles doped in liquid crystal elastomers for producing dynamic 3D structures," *J. Mater. Chem. A*, vol. 5, no. 14, pp. 6740–6746, 2017.
- [118] J. Huang, L. Zhang, Z. Tang, S. Wu, and B. Guo, "Reprocessable and robust crosslinked elastomers *via* interfacial C–N transalkylation of pyridinium," *Compos. Sci. Technol.*, vol. 168, no. July, pp. 320–326, 2018.
- [119] Q. Guan, Y. Dai, Y. Yang, X. Bi, Z. Wen, and Y. Pan, "Near-infrared irradiation induced remote and efficient self-healable triboelectric nanogenerator for potential implantable electronics," *Nano Energy*, vol. 51, pp. 333–339, 2018.
- [120] J. Deng *et al.*, "Vitrimer Elastomer-Based Jigsaw Puzzle-Like Healable Triboelectric Nanogenerator for Self-Powered Wearable Electronics," *Adv. Mater.*, vol. 30, no. 14, pp. 1–10, 2018.
- [121] R. Zhang and M. Engholm, "Recent progress on the fabrication and properties of silver nanowire-based transparent electrodes," *Nanomaterials*, vol. 8, no. 8, pp. 1–17, 2018.
- [122] Z. Huang, Y. Wang, J. Zhu, J. Yu, and Z. Hu, "Surface engineering of nanosilica for vitrimer composites," *Compos. Sci. Technol.*, vol. 154, pp. 18–27, 2018.
- [123] Y. Yang, Z. Pei, X. Zhang, L. Tao, Y. Wei, and Y. Ji, "Carbon nanotube–vitrimer composite for facile and efficient photo-welding of epoxy," *Chem. Sci.*, vol. 5, no. 9, pp. 3486–3492, 2014.
- [124] L. Yu *et al.*, "Rapid Fabrication of Malleable Fiber Reinforced Composites with Vitrimer Powder," *ACS Appl. Polym. Mater.*, vol. 1, no. 9, pp. 2535–2542, 2019.
- [125] G. Oliveux, L. O. Dandy, and G. A. Leeke, "Current status of recycling of fibre reinforced polymers: Review of technologies, reuse and resulting properties," *Prog. Mater. Sci.*, vol. 72, pp. 61–99, 2015.
- [126] A. Li, J. Fan, and G. Li, "Recyclable thermoset shape memory polymers with high stress and energy output *via* facile UV-curing," *J. Mater. Chem. A*, vol. 6, no. 24, pp. 11479–11487, 2018.
- [127] S. Wang, X. Xing, X. Zhang, X. Wang, and X. Jing, "Room-temperature fully recyclable carbon fibre reinforced phenolic composites through dynamic covalent boronic ester bonds," *J. Mater. Chem. A*, vol. 6, no. 23, pp. 10868–10878, 2018.
- [128] X. Kuang, Y. Zhou, Q. Shi, T. Wang, and H. J. Qi, "Recycling of Epoxy Thermoset and Composites *via* Good Solvent Assisted and Small Molecules Participated Exchange Reactions," *ACS Sustain. Chem. Eng.*, vol. 6, no. 7, pp. 9189–9197, 2018.
- [129] S. Wang *et al.*, "Facile *in situ* preparation of high-performance epoxy vitrimer from renewable resources and its application in nondestructive recyclable carbon fiber composite," *Green Chem.*, vol. 21, no. 6, pp. 1484–1497, 2019.
- [130] K. Yu, Q. Shi, M. L. Dunn, T. Wang, and H. J. Qi, "Carbon Fiber Reinforced Thermoset Composite with Near 100% Recyclability," *Adv. Funct. Mater.*, vol. 26, no. 33, pp. 6098–6106, 2016.

- [131] X. Kuang, Q. Shi, Y. Zhou, Z. Zhao, T. Wang, and H. J. Qi, "Dissolution of epoxy thermosets *via* mild alcoholysis: The mechanism and kinetics study," *RSC Adv.*, vol. 8, no. 3, pp. 1493–1502, 2018.
- [132] A. R. Studart and R. M. Erb, "Bioinspired materials that self-shape through programmed microstructures," *Soft Matter*, vol. 10, no. 9, pp. 1284–1294, 2014.
- [133] S. Ghaffari Mosanenzadeh, M. W. Liu, H. G. Palhares, and H. E. Naguib, "Design of thermal hybrid composites based on liquid crystal polymer and hexagonal boron nitride fiber network in polylactide matrix," *J. Polym. Sci. Part B Polym. Phys.*, vol. 54, no. 4, pp. 457–464, 2016.
- [134] S. Zhang *et al.*, "Preparation of a lignin-based vitrimer material and its potential use for recoverable adhesives," *Green Chem.*, vol. 20, no. 13, pp. 2995–3000, 2018.
- [135] Research&Market, "Epoxy Resins - Global Market Trajectory & Analytics," 2020.
- [136] H. Memon *et al.*, "Vanillin-Based Epoxy Vitrimer with High Performance and Closed-Loop Recyclability," *Macromolecules*, vol. 53, no. 2, pp. 621–630, 2020.
- [137] T. Liu *et al.*, "Eugenol-Derived Biobased Epoxy: Shape Memory, Repairing, and Recyclability," *Macromolecules*, vol. 50, no. 21, pp. 8588–8597, 2017.
- [138] M. Capelot, "Chimie de Polycondensation, Polymere supramoleculaire et vitrimere," Universite Pierre et Marie Curie - Paris VI, 2013.
- [139] T. Liu *et al.*, "A Self-Healable High Glass Transition Temperature Bioepoxy Material Based on Vitrimer Chemistry," *Macromolecules*, vol. 51, no. 15, pp. 5577–5585, 2018.
- [140] N. K. Kim *et al.*, "3D hierarchical scaffolds enabled by a post-patternable, reconfigurable, and biocompatible 2D vitrimer film for tissue engineering applications," *J. Mater. Chem. B*, vol. 7, no. 21, pp. 3341–3345, 2019.
- [141] Z. Feng *et al.*, "Photothermal-Induced Self-Healable and Reconfigurable Shape Memory Bio-Based Elastomer with Recyclable Ability," *ACS Appl. Mater. Interfaces*, vol. 11, no. 1, pp. 1469–1479, 2019.
- [142] G. Zhang *et al.*, "Mechanically Robust and Recyclable EPDM Rubber Composites by a Green Cross-Linking Strategy," *ACS Sustain. Chem. Eng.*, vol. 7, no. 13, pp. 11712–11720, 2019.
- [143] S. Dhers, G. Vantomme, and L. Avérous, "A fully bio-based polyimine vitrimer derived from fructose," *Green Chem.*, vol. 21, no. 7, pp. 1596–1601, 2019.
- [144] J. H. Chen, W. Q. Yuan, Y. D. Li, Y. X. Weng, and J. B. Zeng, "Malleable and Sustainable Poly(ester amide) Networks Synthesized via Melt Condensation Polymerization," *ACS Sustain. Chem. Eng.*, vol. 7, no. 18, pp. 15147–15153, 2019.
- [145] I. M. Rizwanul Fattah *et al.*, "State of the Art of Catalysts for Biodiesel Production," *Front. Energy Res.*, vol. 8, no. June, pp. 1–17, 2020.
- [146] N. N. Gandhi, N. S. Patil, S. B. Sawant, J. B. Joshi, P. P. Wangikar, and D. Mukesh, "Lipase-Catalyzed Esterification," *Catal. Rev. - Sci. Eng.*, vol. 42, no. 4, pp. 439–480, 2000.
- [147] E. L. Almeida, C. M. G. Andrade, and O. Andreo Dos Santos, "Production of Biodiesel

Via Catalytic Processes: A Brief Review," *Int. J. Chem. React. Eng.*, vol. 16, no. 5, 2018.

- [148] L. Casas-Godoy, F. Gasteazoro, S. Duquesne, F. Bordes, A. Marty, and G. Sandoval, "Lipases: An Overview," in *Lipases and Phospholipases: Methods and Protocols, Methods in Molecular Biology*, Georgina S., no. 1835, Springer Nature, 2018, pp. 3–38.
- [149] B. Norjannah, H. C. Ong, H. H. Masjuki, J. C. Juan, and W. T. Chong, "Enzymatic transesterification for biodiesel production: A comprehensive review," *RSC Adv.*, vol. 6, no. 65, pp. 60034–60055, 2016.
- [150] U. Schuchardt, R. Sercheli, and R. M. Vargas, "Transesterification of vegetable oils: A review," *Journal of the Brazilian Chemical Society*, vol. 9, no. 3. Sociedade Brasileira de Quimica, pp. 199–210, 1998.
- [151] A. Gog, M. Roman, M. Toşa, C. Paizs, and F. D. Irimie, "Biodiesel production using enzymatic transesterification - Current state and perspectives," *Renew. Energy*, vol. 39, no. 1, pp. 10–16, 2012.
- [152] C. Ortiz *et al.*, "Novozym 435: The 'perfect' lipase immobilized biocatalyst?," *Catal. Sci. Technol.*, vol. 9, no. 10, pp. 2380–2420, 2019.
- [153] J. J. Virgen-Ortíz, J. C. S. Dos Santos, Á. Berenguer-Murcia, O. Barbosa, R. C. Rodrigues, and R. Fernandez-Lafuente, "Polyethylenimine: A very useful ionic polymer in the design of immobilized enzyme biocatalysts," *J. Mater. Chem. B*, vol. 5, no. 36, pp. 7461–7490, 2017.
- [154] O. Barbosa, R. Torres, C. Ortiz, Á. Berenguer-Murcia, R. C. Rodrigues, and R. Fernandez-Lafuente, "Heterofunctional supports in enzyme immobilization: From traditional immobilization protocols to opportunities in tuning enzyme properties," *Biomacromolecules*, vol. 14, no. 8, pp. 2433–2462, 2013.
- [155] R. A. Gross, A. Kumar, and B. Kalra, "Polymer synthesis by in vitro enzyme catalysis," *Chem. Rev.*, vol. 101, no. 7, pp. 2097–2124, 2001.
- [156] Y. Poojari and S. J. Clarson, "Lipase catalyzed synthesis and thermal properties of poly(dimethylsiloxane)-poly(ethylene glycol) amphiphilic block copolymers," *J. Inorg. Organomet. Polym. Mater.*, vol. 20, no. 1, pp. 46–52, 2010.
- [157] Y. Poojari and S. J. Clarson, "Lipase catalyzed synthesis of poly(ϵ -Caprolactone)-poly(Dimethylsiloxane)-poly(ϵ -Caprolactone) triblock copolymers," *Silicon*, vol. 1, no. 3, pp. 165–172, 2009.
- [158] W. Wu, "Lipase - catalyzed synthesis and post - polymerization modification of new fully bio-based poly(hexamethylene γ -ketopimelate) and poly(hexamethylene γ -ketopimelate-co-hexamethylene adipate) copolyesters," *e-polymer*, no. 20, pp. 214–225, 2020.
- [159] M. B. Buendia, A. E. Daugaard, and A. Riisager, "Catalytic Transesterification Routes to Novel Vinyl Glycolate Derivatives of Polyhydric Alcohols," *Catal. Letters*, no. 0123456789, 2020.
- [160] Y. Poojari and S. J. Clarson, "Thermal stability of *Candida antarctica* lipase B immobilized on macroporous acrylic resin particles in organic media," *Biocatal. Agric. Biotechnol.*, vol. 2, no. 1, pp. 7–11, 2013.

- [161] J. Guo, C. P. Chen, S. G. Wang, and X. J. Huang, "A convenient test for lipase activity in aqueous-based solutions," *Enzyme Microb. Technol.*, vol. 71, pp. 8–12, 2015.
- [162] C. Aouf *et al.*, "The use of lipases as biocatalysts for the epoxidation of fatty acids and phenolic compounds," *Green Chem.*, vol. 16, no. 4, pp. 1740–1754, 2014.
- [163] B. Chen, J. Hu, E. M. Miller, W. Xie, M. Cai, and R. A. Gross, "Candida antarctica Lipase B chemically immobilized on epoxy-activated micro- and nanobeads: Catalysts for polyester synthesis," *Biomacromolecules*, vol. 9, no. 2, pp. 463–471, 2008.
- [164] A. M. Gumel, M. S. M. Anuar, Y. Chisti, and T. Heidelberg, "Ultrasound assisted lipase catalyzed synthesis of poly-6-hydroxyhexanoate," *Ultrasoun. Sonochem.*, vol. 19, no. 3, pp. 659–667, 2012.
- [165] Y. Soeda, T. Okamoto, K. Toshima, and S. Matsumura, "Enzymatic ring-opening polymerization of oxiranes and dicarboxylic anhydrides," *Macromol. Biosci.*, vol. 2, no. 9, pp. 429–436, 2002.
- [166] T. Yamada, C. Morisseau, J. E. Maxwell, M. A. Argiriadi, D. W. Christianson, and B. D. Hammock, "Biochemical evidence for the involvement of tyrosine in epoxide activation during the catalytic cycle of epoxide hydrolase," *J. Biol. Chem.*, vol. 275, no. 30, pp. 23082–23088, 2000.
- [167] M. J. Kim *et al.*, "Highly enantioselective dynamic kinetic resolution of 1,2-diarylethanol by a lipase-ruthenium couple," *Org. Lett.*, vol. 10, no. 6, pp. 1295–1298, 2008.
- [168] A. Marañón, P. Hoyos, J. D. Carballeira, Á. C. Cabrera, M. B. Ansorge-Schumacher, and A. R. Alcántara, "Lipase from *Pseudomonas stutzeri*: Purification, homology modelling and rational explanation of the substrate binding mode," *J. Mol. Catal. B Enzym.*, vol. 87, pp. 88–98, 2013.

CHAPTER 3 - PRELIMINARY STATEMENT

This chapter has been published in *Polymer chemistry* and can be found online at: <https://doi.org/10.1039/D0PY00342E>. Initially submitted in April 2018, it was rejected; however, reviewers suggested resubmission under intensive re-work of the manuscript and emphasis on the polymerisation mechanisms and addition of ratio 1:0.6. Thanks to their helpful comments, the manuscript was entirely re-worked and submitted in March 2020 to be accepted with corrections. As the UK laboratory was closed (due to the COVID-19 situation), 2-PI curing suggested by reviewer 2 was performed in Paris at the ESPCI by Francois Tournilhac (FT) to answer reviewers' comments. The graphical abstract was also produced by FT but its design was discussed as a team work. Original study idea, manufacture method, FTIR analysis method, and rest of the testing are all originated from QAP. The related electronic supplementary information of this chapter is in appendix A.

Polymer chemistry, as part of the Royal Society of Chemistry (RSC), requires a specific submitting layout (two columns, 600DPI figures, font sizes, *etc.*) which have been judged by the author (QAP) not well-suited for a thesis presentation. Therefore, all the layout has been adapted to a better format to fit the presentation of this work. All texts and figures are, however, similar to the online version of this manuscript.

Chapter 3. Dicarboxylic acid-epoxy vitrimers: influence of the off-stoichiometric acid content on cure reactions and thermo-mechanical properties

Quentin-Arthur Poutrel^{a,b}, Jonny J Blaker^a, Constantinos Soutis^b, François Tournilhac^{*c}, and Matthieu Gresil^{*d}

^a Bio-Active Materials Group, Department of Materials, The University of Manchester, Manchester, UK

^b Aerospace Research Institute, The University of Manchester, Manchester, UK

^c Molecular, Macromolecular Chemistry, and Materials, ESPCI Paris, PSL University, CNRS, 10 rue Vauquelin, 75005 Paris, France

^d i-Composites Lab, Department of Materials Science and Engineering, Monash University, Clayton, Australia

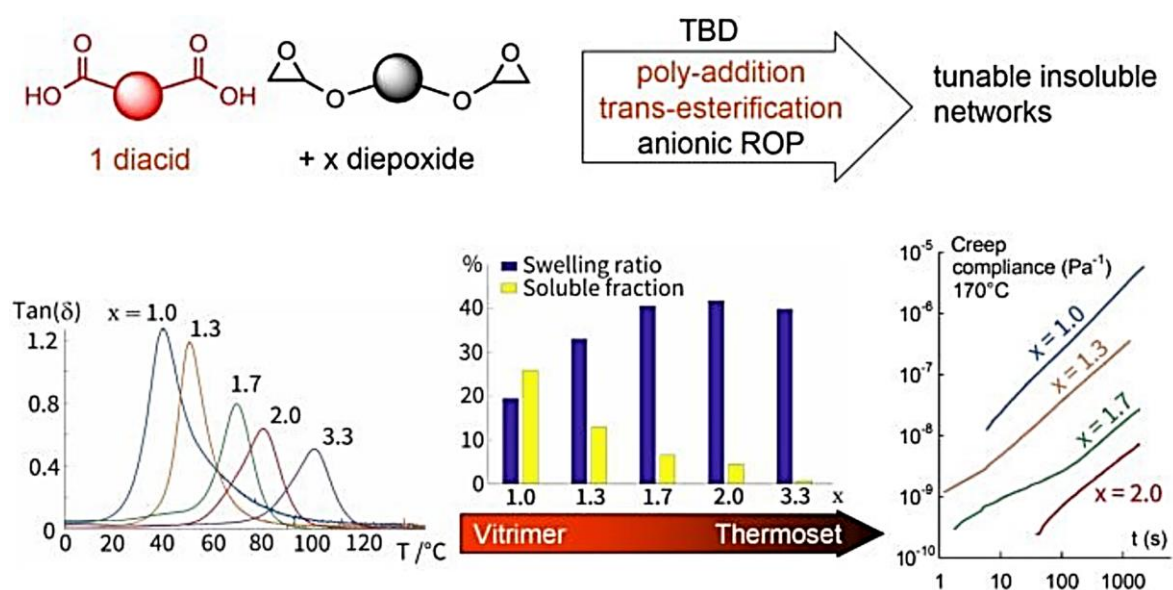
*corresponding authors: francois.tournilhac@espci.fr, matthieu.gresil@monash.edu

Abstract

The present study explores a broad range of stoichiometry, with the [epoxy]/[acyl] ratio ranging from excess to unity for commercial diepoxide/sebacic acid vitrimer formulations, with 1,5,7-triazabicyclo[4.4.0]dec-5-ene (TBD) used as the catalyst. In particular, it investigates to what extent side reactions promoted by off-stoichiometry mixtures can help achieve desirable thermomechanical properties (*i.e.* glass transition T_g , Young's modulus, strain at break, and strength) for an optimised vitrimer that behaves like a stiff material at room temperature, retaining its capacity to flow at high temperature while remaining insoluble. The possible role of TBD as an anionic initiator is tested in the homopolymerisation of epoxy and compared to a known anionic initiator, 2-phenylimidazole (2-PI). Attenuated total reflection infrared (ATR-IR) spectroscopy reveals different reaction speeds, but an identical scenario for either 2-PI or TBD. The acid + epoxy addition occurs first, then epoxy homopolymerisation takes place after di-carboxylic acid consumption; an ester typically forms in less than 20 min at 125°C with TBD, while the formation of ether takes several hours. For all [epoxy]/[acyl] ratios ranging from 1:1 to 1:0.3, it is found that the integrity of the network is retained when subjected to 1,2,4

trichlorobenzene (TCB) solvent treatment. From the 1 : 1 to 1 : 0.75 epoxy to acyl ratio, the material retains full ability to flow and relax stresses under thermal stimulation, showing a 10 fold increase in viscosity and unchanged activation energy of about 100 kJ.mol⁻¹. Beyond 1 : 0.6 stoichiometry, a gradual transition from vitrimer to non-exchangeable crosslinked materials is observed as these networks show only partial stress relaxation due to interpenetration in the polyether network.

Graphical abstract



3.1 Background

Polymer networks with reversible covalent links have been investigated as systems that are capable of topology rearrangement in response to excitation [1], [2] (thermal or photochemical activation), as reviewed in the last 6 years [3], [4]. Systems where reversibility involves chemical reactions occurring through a dissociative mechanism such as the Diels–Alder reaction [5] were first studied due to the wide range of chemical reactions available [6], [7]. In these systems, the dissociative mechanism means that whenever topology rearrangement is desired, existing links have to be broken before new links can be established, leading to a temporary drop in viscosity and loss of structural integrity once bond reversibility is activated. In contrast, a different family of reversible covalent networks can be envisioned where the formation of new bonds takes place before existing ones are broken, thus maintaining the integrity of the network throughout the exchange process. In 2005, Bowman and co-workers [8] described photo-induced plasticity

in crosslinked polymers based on reversible chain-transfer reactions involving an associative mechanism, and, in 2011, Leibler and co-workers [9] introduced the concept of vitrimers - a class of polymer networks with dynamic links and/or crosslinks that became the example of associative exchange reactions upon thermal excitation. Vitrimers are insoluble thermoset-like polymers. Under thermal stimulation, bond exchanges are rapid, especially in the presence of a well-chosen catalyst. Thereby, the material can flow through reorganisation of the network topology; thus they have been proven to be heat-processable, recyclable and weldable, akin to thermoplastics [10]–[12].

The present concept (*i.e.* covalent bond exchange) is not linked to any particular chemistry. In vitrimer prototypes, the possibility of building dynamic polyhydroxyl ester networks by thermoset chemistry has been demonstrated [9]. Since then, numerous examples of vitrimers based on various skeletons and involving a wide choice of exchange reactions, with and without catalysts, have been described [13]–[22]. Nonetheless, the epoxy chemistry used in the initial vitrimers remains appealing since it is based on the choice of industrially relevant monomers. Epoxy resins are heavily used in transport-, health-, electronic-, and energy-related technologies. Currently, a wide range of epoxy monomers and hardeners are commercially available or at least well described in the literature [23], [24], and virtually any combination of each is possible. Epoxy curing is an ensemble of ring-opening reactions with the ability to operate without solvent, without by-products - not even a molecule of water - and with low shrinkage [25], [26]. Esterification and transesterification are among the most common reactions of organic chemistry, used on a large scale to produce [27] (and recycle) polyesters [28] and, more recently, in bio-diesel production [29], for which vast literature on reaction conditions and catalysts is available [30]–[34].

Epoxy based vitrimers are relatively new material systems that can be employed as matrix in fibre reinforced composite materials [35], [36]. However, so far, the glass transition - an intrinsic property of thermosets, designated as T_g (measured by DSC) or T_α (measured by DMA) - has remained difficult to predict by any method other than trial and error. Often efforts made to increase the T_g (or T_α) above a certain value (depending on network compounds and curing conditions) lead to issues with the entire formulation in terms of compatibility, processing, degassing, and curing cycles [37].

Epoxy-carboxylic acid vitrimer formulations reported in the literature to date [9], [38]–[40] have mostly used a 1:1 epoxy to acyl ratio. The addition of one -COOH group to the epoxy ring generates one hydroxide for each ester formed, resulting in an equal concentration of both reactants for further exchanges by transesterification. Decreasing the epoxy to acyl ratio to 1:2 has been reported for some epoxy–anhydride formulations, and in all cases a decrease in weldability was observed [10], [35]. The present work explores the effect of varying the stoichiometric ratio in the opposite direction, *i.e.* towards increasing the epoxy to acyl content. Altuna *et al.* [41], [42] have shown that decreasing the acid content could lead to the formation of ethers through anionic homopolymerisation of the remaining epoxy as suggested by Matějka *et al.* [43] in the early 80s. Torkelson and co-workers [44] synthesised vitrimers containing a maximum of 40% fraction of permanent crosslinks to increase the creep resistance. Hoppe *et al.* [45] analysed the reaction of bisphenol-A diglycidyl ether, DGEBA with a stoichiometric amount of monocarboxylic acid and also with a variable excess of epoxy groups with a conventional tertiary amine as the catalyst. They obtained a gel when the ratio of epoxy to acid groups was higher than 3, but with a drop in the T_g from 90 to 0°C. Recently, Altuna *et al.* [46] synthesised poly hydroxy-ester vitrimer networks with a fraction of non-exchangeable amine links as internal catalysts in the network; they developed a statistical analysis of the network structure to estimate the partition of the tertiary amine between sol and gel fractions.

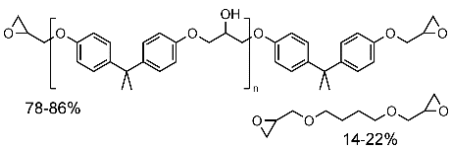
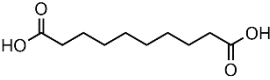
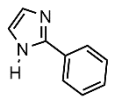
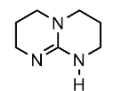
Here, the effect of non-stoichiometry on vitrimer properties is investigated. In our experiments, epoxy vitrimer samples have been manufactured, using a commercial epoxy resin (mixture of diepoxide monomers) and sebacic acid (SA) as a hardener, with different stoichiometries (from 1:0.3 to 1:1 epoxy/acyl ratio), and 1,5,7-triazabicyclo[4.4.0]dec-5-ene (TBD) as the organic catalyst.

3.2 Materials and methods

Araldite LY 564 was chosen for its versatility as a low-viscosity resin for a variety of applications, including materials for electronics or structural composites. Sebacic acid is a classic bio-based molecule used as a monomer in polyamide chemistry and already proven in epoxy vitrimer formulations [41], [46]–[48]. TBD is a well-known transesterification catalyst with a guanidine structure, including secondary, tertiary amine, and imine functions [49]. Its structure makes it a strong base, potentially initiating anionic ring-

opening polymerisation (ROP) [50] of epoxides. For comparison, mixtures of the diepoxide with 2-phenyl-imidazole (2-PI), which is known as an effective anionic initiator, were also investigated. The structures of the monomers and catalysts are shown in Table 3-1 and in the Appendix A, Scheme A-1.

Table 3-1 Reactant used in this study; *eew*: epoxy equivalent weight, *mw*: molecular weight, ROP: ring opening polymerisation.

Chemical structure	Compound	Acronym	M (g/mol)
	Diepoxide monomer (LY564)	DE	172-176 (<i>eew</i>)
	Diacyl monomer (sebacic acid)	SA	202.2 (<i>mw</i>)
	Initiator of anionic ROP (2-phenylimidazole)	2-PI	144.2 (<i>mw</i>)
	Transesterification catalyst (1,5,7-triazabicyclo[4.4.0]dec-5-ene)	TBD	139.2 (<i>mw</i>)

3.2.1 Sample preparation

The diepoxide monomer (DE) - Araldite LY564 - was purchased from Huntsman Ltd; sebacic acid (SA) 2-phenylimidazole (2-PI) and 1,5,7-triazabicyclo[4.4.0]dec-5-ene (TBD) were supplied by Tokyo Chemical Industry Ltd Belgium. Sebacic acid and TBD were added to epoxy as received and mixed for 24 h at 50°C until a white homogeneous liquid was obtained. The final mixture was then poured into moulds, to give rectangular 60 mm × 60 mm × 5 mm, and dog-bone shaped specimens measuring 115 mm × 33 mm × 6 mm, according to the ASTM standard 638 Type IV. The samples were degassed under vacuum for 2 h at 90°C to ensure the removal of possible air bubbles formed during mixing. The samples were cured at 145°C for 8 h (ramp 1.7°C min⁻¹ from room temperature to 145°C), and then post-cured at 160°C for 8 h. A schematic of sample fabrication is shown in Figure A-1.

A series of samples was produced with different epoxy/SA ratios (summarised in Table 3-2). The reaction was performed using a 1:1 ratio of functional groups of epoxy to sebacic acid in the presence of TBD added as a 5% molar equivalent (meq.) of the epoxy

group. The resulting material system was labelled 100H5CAT. Samples were prepared with different epoxy/SA ratios to explore the effect of reducing acid content in the vitrimer, as follows: 1:0.75, 1:0.6, 1:0.5, and 1:0.3, the respective materials were labelled as 75H, 60H, 50H and 30H. All reactive mixtures in this series were prepared using 5% meq. TBD relative to the epoxy group, except the one with 10% meq. TBD, following the work of Leibler and co-workers [31], and labelled as 5CAT and 10CAT, respectively (Table 3-2).

Table 3-2 Sample identification based on the epoxy/sebacic acid ratio and catalyst amount.

Samples label						
	100H5CAT	75H5CAT	60H5CAT	50H5CAT	30H5CAT	30H10CAT
DE (meq)	100	100	100	100	100	100
SA (meq)	100	75	60	50	30	30
TBD (meq)	5	5	5	5	5	10

3.2.2 IR monitoring of the curing process

Attenuated total reflection infrared spectroscopy (ATR-IR) was performed using a Specac high-temperature Golden Gate ATR cell mounted on a Bruker Tensor 37 IR spectrometer. Curing took place at 125°C and the IR data were collected during the first 60 minutes of the process, showing the change in the mixture composition. Samples with 5% catalyst were studied with different epoxy/acid ratio (100H, 50H and 30H). For this study, most relevant information was found in the 900-2000 cm^{-1} wavenumber range shown in Figure A-2. Due to the overlapping of signals, monitoring was performed through the integration of absorbance over well-defined intervals. The method of analysis for ATR IR curing and integration of relevant IR signatures can be found in the ESI (Figure A-2 to Figure A-7).

3.2.3 Swelling and soluble fraction

Swelling studies were performed using samples measuring approximately 5 mm × 5 mm × 3 mm. The samples were weighed and their dimensions measured before immersion in 1,2,4-trichlorobenzene (TCB) at 135°C (well above the T_g of the samples), after 3 days and 1 week to ensure that swelling equilibrium has been reached. TCB was chosen for its high vaporisation temperature (214°C). Swollen samples were extracted, wiped with a

tissue, and stabilised at room temperature for 2 days to avoid any thermal expansion effect; swelling ratio and soluble fraction were calculated by gravimetry for all samples.

3.2.4 Mechanical test methods

Dynamic mechanical analysis (DMA) and creep experiments were performed using a Q800 DMA (TA Instruments, USA) operating in the dual cantilever mode on rectangular samples (55 mm × 15 mm × 4 mm) with a heating regime of -30°C to 200°C at 3°C.min⁻¹, and a measurement frequency of 1 Hz following standard procedures to measure the glass transition temperature (T_g).

Stress relaxation experiments were conducted using a Q800 DMA (TA Instruments, USA) operating in the shear mode on rectangular samples (50 mm × 50 mm × 4 mm) with 1% strain applied and allowed to relax for 500 min at each temperature level. Temperature parameters have been adapted for each sample type according to their mechanical properties.

Creep testing was performed on rectangular samples (55 mm × 15 mm × 4 mm) cut from larger plates to observe bulk relaxation. A dual cantilever clamping system was chosen to minimise the noise due to measurement. Measurements were performed at several temperatures (from 110°C to 190°C every 10°C). The samples were heated and left to equilibrate at 110°C for 10 min prior to applying a stress of 10 kPa (100H5CAT), 1 MPa (30H10CAT) or 100 kPa (others) for 30 min to reach the regime of linear time variation [31]. They were then left to relax for 10 min and heated to the next temperature level.

Quasi-static tensile tests were performed using 3 dog-bone specimens (115 mm × 33 mm × 6 mm) for each composition, using an Instron 5969 model testing machine, equipped with a 2 kN load cell, following the ASTM standard 638 Type IV. The samples were tested at 25°C at a displacement rate of 3 mm min⁻¹ to obtain the entire stress-strain response and elastic modulus.

3.3 Results

In an effort to gain better understanding of the network formation, infrared spectral analysis of sample curing was performed *via* ATR-IR. A typical IR spectrum of test sample 100H5CAT during curing is presented in Figure 3-1, where the peaks of interest are highlighted. At the beginning of the experiment, two C=O stretching bands are already

detected at $\tilde{\nu} \approx 1705 \text{ cm}^{-1}$ and $\tilde{\nu} \approx 1735 \text{ cm}^{-1}$. The first is the conventional signal of a carboxylic acid in the molten state. The second, whose relative intensity increases with dilution (see appendix A) is due to interaction with the solvent (here, the epoxy resin plays the role of the solvent) [51]. Once the reaction with epoxy starts, the absorption peak at 1705 cm^{-1} diminishes, while that at 1735 cm^{-1} increases, due to the C=O stretching signal of the ester (overlapped with the solvated COOH one). In parallel, the decay of the characteristic epoxy peak ($\tilde{\nu} \approx 914 \text{ cm}^{-1}$) was observed. The measurement of this signal is particularly important in samples with low acid content since it helps in understanding how the epoxide groups react with an off stoichiometric amount of acyl groups.

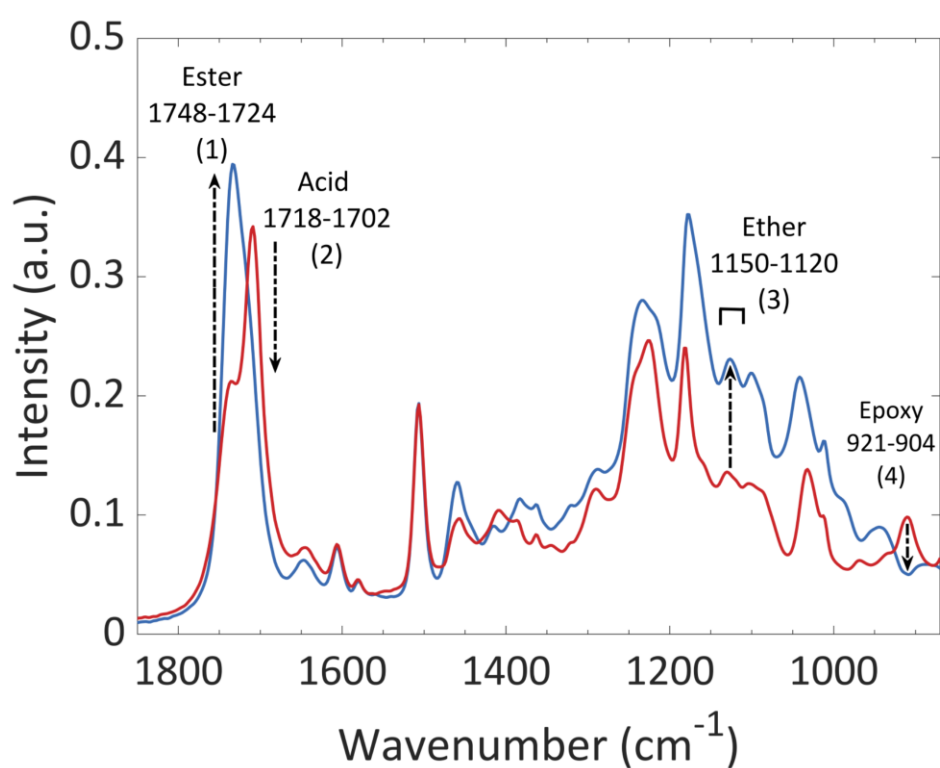


Figure 3-1 ATR-FTIR spectral curve of the 100H5CAT sample at the beginning (red curve) and at the end of the reaction (blue curve). The labelled peaks correspond to: (1) C=O stretching of ester related to the polymer network, (2) C=O stretching of sebacic acid, (3) C-O-C signature of the ether, (4) asymmetric epoxy deformation. The numbers indicate signal integration intervals, see the Appendix A for details of identification and integration procedure.

As for polyether formation, it is challenging to identify a single peak to characterise the homopolymerisation of epoxide due to the complexity of the infrared absorption pattern, especially when several single C–O bonds are present. However, by analysing the whole range of C-O stretching vibration ($\tilde{\nu} \approx 1000\text{-}1200 \text{ cm}^{-1}$) it is possible to extract a C-O-C signature and follow its relative change in different reactive mixtures (see Appendix A).

The relative change of the defined peaks over time is shown in Figure 3-2 (100H5CAT and 30H5CAT). In Figure 3-2a, it can be seen that acid (blue curve, triangles) and ester (red curve, squares) signals follow complementary evolutions. The acid signal shows rapid conversion to ester during the first fifteen minutes, but the reaction continues and is still not completed after 60 min of curing at 125°C. In Figure 3-2b, the signal from the epoxy (green curve, diamonds) decreases regularly throughout the first hour of curing. The ether signal (purple curve and disks) increases slowly over the time. Thus, under the conditions of 1:1 stoichiometry, the acid + epoxy → ester addition is predominant. Figure 3-2c,d, shows the evolution of the same signals for 30H5CAT. For this off-stoichiometric formulation, the acid + epoxy → ester addition reaction is clearly accelerated by an excess of epoxy; a horizontal asymptote is reached after 12-15 min. Interestingly, the etherification (Figure 3-2d) does not start until the addition reaction is completed and ultimately it reaches a higher level than in the 100H5CAT compound. In parallel, the signal from the epoxy (Figure 3-2d) which participates in both reactions shows a regular decrease, slower than that in 100H5CAT as expected from the law of mass action.

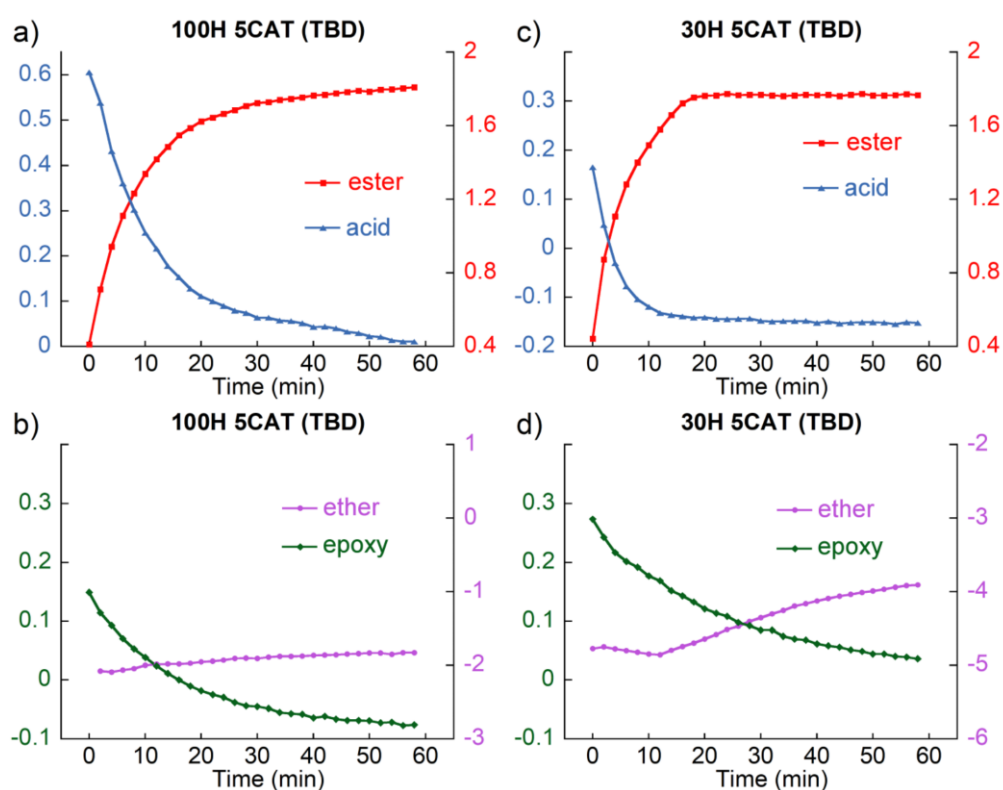


Figure 3-2 Evolution of species for different ratios of polymer network: a) and b) 100H5CAT, c) and d) 30H5CAT. Measurements were performed for 60 min at 125°C; Y-scales for each signal correspond to the values of ATR peak integrals (without normalisation, see Figure 3-1 and Appendix A for details).

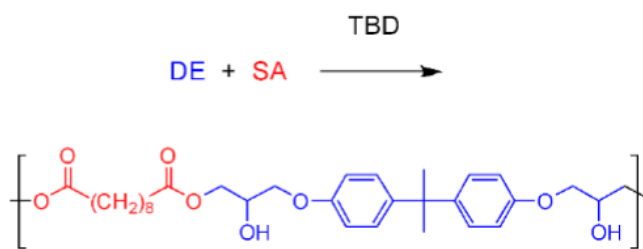
At 125°C, the conversion is less than complete after 1 h of curing. A long curing time of 8 h at 145°C was applied to all samples to achieve optimal conversion. Analysis of epoxy residues for different stoichiometric ratios is reported in the Appendix A, Figure A-5 to - Figure A-7. It appears that even at a low acid content (1:0.3), almost all epoxy groups have been consumed at the end of the reaction as shown in Figure A-7. This suggests that even at highly unbalanced stoichiometry, residual unreacted monomers concentration remains constantly low.

In all formulations, a postcure is then necessary (*e.g.* 3000 s at 150°C) [52] to allow equilibration of the network by transesterification reactions as reported by Altuna *et al.* [41], [42] but this cannot be detected by IR spectroscopy as it does not change the nature of chemical bonds.

The question then arises whether such unbalanced systems can form a network. In our system, four main polymerisation reactions can be considered:

1. Polyaddition acid + epoxy forming a linear polyhydroxy ester (accelerated by TBD as shown in Figure 3-2a).
2. Fischer esterification between free hydroxyl group and acid forming ester with the release of water (not detected in our experiments).
3. Transesterification reaction between the ester bonds and hydroxyl radicals (catalysed by TBD, not detectable by FTIR but demonstrated in the literature on small molecules) [52], [53].
4. Anionic ring opening polymerisation (ROP) between epoxy groups forming ether bonds [41], [42] (initiated here by TBD).

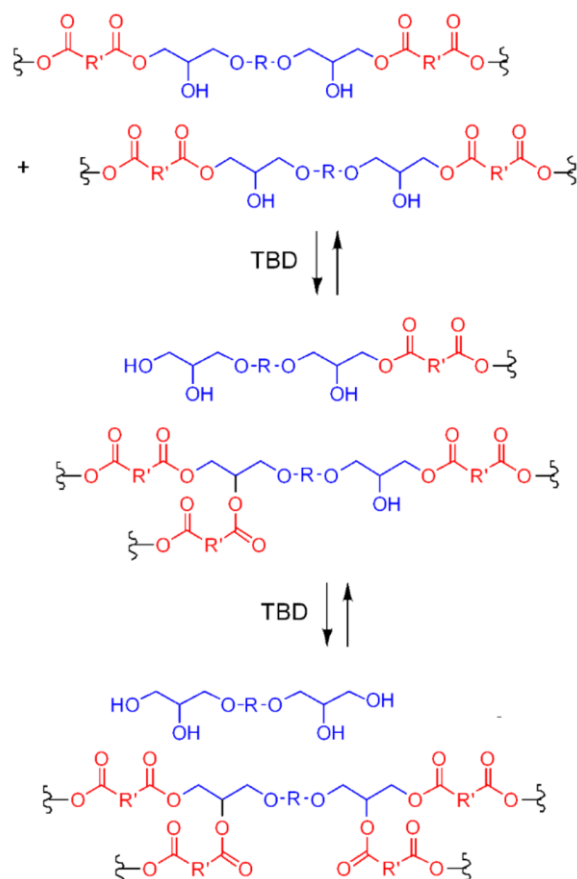
Regarding reaction (1) (illustrated in Scheme 3-1), the two monomers are bifunctional (diacid and diepoxy). This reaction essentially leads to linear products, whose molar mass is determined from the conversion and feed ratio values; virtually infinite molar masses are achievable only at exact stoichiometry. If reaction (1) (polyaddition) was the only one to occur, the gel point would not be reachable, even more, under off-stoichiometry conditions. In this case, the material properties would be expected to range from low viscous oil to entangled thermoplastic polymer ones.



Scheme 3-1 Formation of exchangeable hydroxyl ester links by polyaddition of DE and SA.

Reactions (2)–(4) are all expected to produce branching, potentially leading to a crosslinked polymer. Reaction (2) would require opposite off-stoichiometry conditions (excess of SA) and an acidic environment to take place. It is unlikely to occur with reactive mixtures catalysed by TBD (inducing a basic environment).

Branching by reaction (3) (transesterification), as illustrated in Scheme 3-2, is likely to occur in the presence of TBD but the occurrence of gelation through this process is less than obvious because each time a new branching is created by transesterification exchange, another link is broken somewhere.



Scheme 3-2 Branching by the transesterification mechanism, leading to exchangeable cross-links. The scheme illustrates the equilibrium between mono-, di-, tri-, tetraesters and the free diglycol form.

Under this circumstance, the relationship between composition and the possibility of gelation may be estimated using the Flory-Stockmayer model (Equation 3-1) [54], [55]:

$$p = \frac{1}{\sqrt{r(1-f_A)(1-f_B)}}$$

Equation 3-1 Estimation of gelation by the Flory-Stockmayer model.

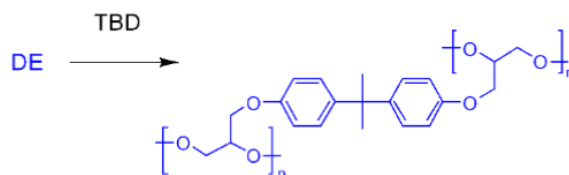
where p is the extent of reaction at the gel point, f_A and f_B the average functionality of the monomers carrying functions A and B respectively and r the stoichiometric ratio of functions A and B ($r \leq 1$). This model was developed for polycondensation, it assumes equireactivity throughout the process and the absence of loops but makes no hypothesis with regards to the chronology of forming bonds. For gelation to take place, Equation 3-1 must have a solution with $p < 1$.

Once transesterification is activated, the diglycol units generated by opening the diepoxide monomers can exist in the form of mono-, di- tri- and tetra-esters as well as in the free diglycol form (Scheme 3-2).

The diglycol unit therefore expresses a functionality $f_B = 4$, while it remains bifunctional in the absence of transesterification. When assuming equireactivity of all alcohol groups, transesterification of the (1:1) composition would reach the same equilibrium as condensation of one mol diacid with one mole diglycol where Equation 3-1 with $f_A = 2$, $f_B = 4$ and $r = 0.5$ predicts gelation [52]. For the (1:0.75) composition, $r = 0.375$, gelation is still predicted but requires a high value of conversion ($p = 0.94$). For compositions farther from stoichiometry, 1:0.6, 1:0.5, and 1:0.3 gelation would not take place if additions and transesterifications were the only reactions to occur. Gelation of polyhydroxyesters formed by 1:1 amounts of diepoxides and dicarboxylic acids has been investigated both theoretically and experimentally [41], [42], [52], [56], [57]. Further statistical study, based on the branching theory [57] also confirms the passage of the gel point in a diacid-diepoxide system able to reorganise.

Reaction (4) (chain polymerisation by anionic ROP), illustrated in Scheme 3-3, is likely to occur in a basic environment and promote gelation whenever epoxy is in excess. Additional links thereby formed are not ester linkages but non-exchangeable ether links. Regarding this reaction, the diepoxide monomer is tetrafunctional and able to form crosslinks. Previous observations [41], [42] demonstrate that epoxy vitrimer formulations

containing 1:2 excess of epoxy and 1-methyl imidazole as an initiator form networks through this reaction.



Scheme 3-3 Branching mechanism *via* anionic ROP of diepoxides-ether bonds thereby formed are not exchangeable.

With TBD, reaction (3) (transesterification) is known to be fast [49], [52], [53] and allows the gel point to be passed quickly, while reaction (2) (Fischer esterification) and reaction (4) are slow but increase the crosslink density of the 3D network. Reactions (1) and (2) terminate when there is no more acid, whereas reaction (4) continues until there is no epoxy left and slows down with a decrease in the epoxy concentration. Therefore, in all samples with TBD and excess epoxy the formation of the network is associated with reactions (1), (3) and (4).

Curing in the presence of a catalyst, which is at the same time a strong base, still raises questions whether the epoxy homopolymerisation can take place rather than the addition reaction between acid and epoxy. Hence, curing of epoxy was investigated by comparing the differences in the evolution of IR signals for 30H5CAT-type compositions containing an (100:30) excess of epoxy mixed with 5% meq. of either TBD or 2-PI. 2-PI is known to be an effective initiator of anionic ROP of epoxides [37].

Variations in the IR signals of TBD and 2-PI based samples are plotted in Figure 3-2c,d and in Figure 3-3 respectively, using the same scales as Figure 3-2.

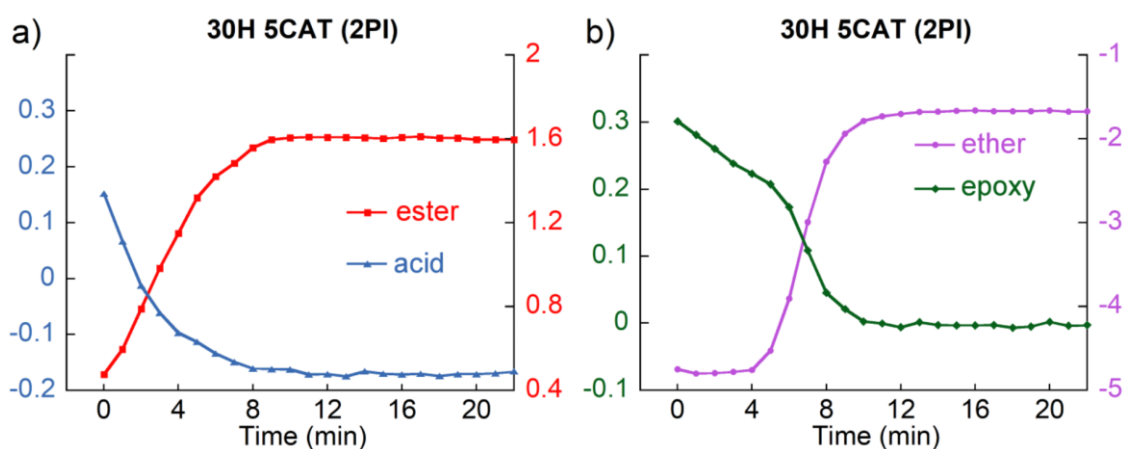


Figure 3-3 Evolution of IR signals of a reactive composition containing a (100:30) molar excess of epoxy and 5 mol% of 2-PI as the catalyst a) ester and acid signals, b) ether and epoxy signals. Same Y-scales as Figure 3-2.

With 2-PI, the ester and acid traces mirror each other (Figure 3-3a) and reach complete conversion within about 8 minutes. As for the ether signal, first it shows an induction period of about 5 min, then a steep increase correlated with the disappearance of the COOH functions and eventually saturation after about 12 min. As for the epoxy signal, it clearly shows two different slopes for both of the above reactions, first a slow conversion stage during the reaction with the acid then a faster stage during anionic homopolymerisation.

If we compare with 2-PI, the overall speed of reactions is slower than with TBD, the two reactions are more clearly decoupled with 2PI but in both cases, the scenario is the same: a first wave is observed, corresponding to the addition reactions (Figure 3-2a,b) then a second wave due to anionic homopolymerisation. The proposed mechanism is very similar to that depicted in scheme 2 and scheme 3 in ref. [58] for a thiol–epoxy system. The base (either TBD or 2-PI) deprotonates the COOH function, producing a carboxylate anion which can attack the epoxy group and produce an alkoxide anion. In the presence of excess acid groups, a rapid proton exchange between the alkoxide anion and the acid takes place (because of the difference in pK_a of the alcohol/alkoxide and acid/carboxylate pairs) leading to the formation of another carboxylate anion and a hydroxyester group. In off-stoichiometric formulations, once the acid is depleted this proton transfer does not take place and epoxy homopolymerisation propagates as long as alkoxide anions are present.

Once the acid is exhausted (after approx. 4 min for 2-PI, 12 min for TBD) the conversion of epoxy accelerates with 2-PI (Figure 3-3b) while nothing similar happens with TBD (Figure 3-2a). 2-PI is known to be a nucleophile, which can directly attack the epoxy through the formation of a zwitterionic adduct [59] and is regenerated after ROP propagation [60], [61], a mechanism consistent with acceleration after the consumption of the acid. In TBD, the nucleophilic imine function neighbours with a H-bonding secondary amine function. This capping property is favourable to complex alkoxide and activated acyl functions at a suitable position for transesterification [50], but may deactivate nucleophilic species involved in the anionic ROP of epoxy.

On the other hand, TBD is significantly more basic than an imidazole (pK_a of the conjugate acid > 20 for TBD [62] compared to a value of 6.48 of 2-PI [63]). TBD potentially attacks epoxy *via* the formation of oxygenated anions: alkoxide or carboxylate, rather than directly.

The fact that homopolymerisation is slower with TBD increases the probability of hydrolytic terminations *e.g.* with water molecules, conducive to the appearance of additional hydroxyl groups able to participate in the exchange reactions.

3.3.1 Swelling and soluble fraction analysis

The results of swelling experiments are summarised in Figure 3-4. All samples swelled in TCB and remained insoluble indicating that network polymer chains are indeed in a good solvent environment and chemically bound to the rest of the network.

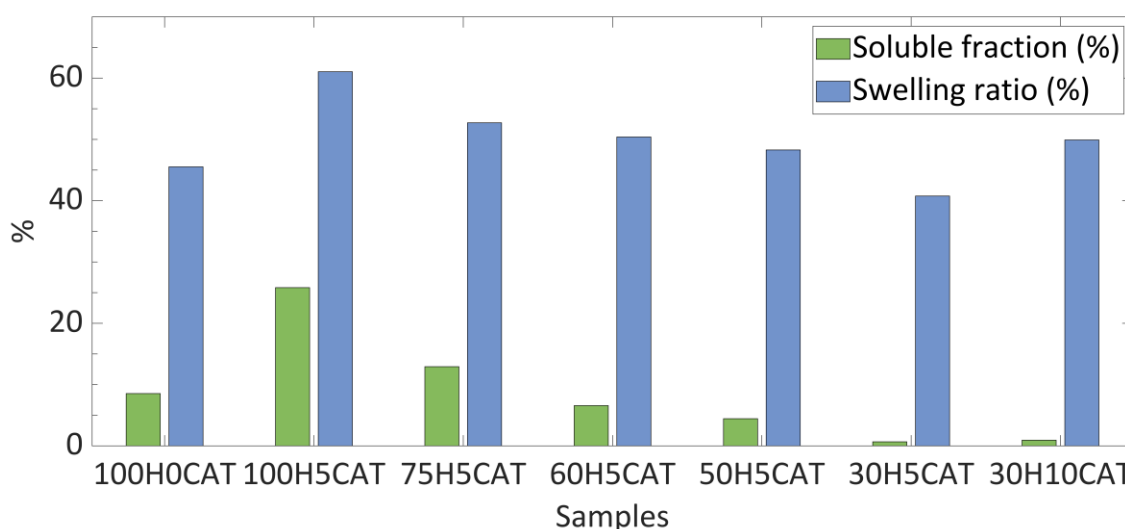


Figure 3-4 Swelling experiment to confirm crosslinking of the structure, mass increase (blue) and mass fraction of the soluble part (green).

For 100H5CAT, the soluble fraction $\approx 25\%$ is close to the predicted value [57]. The obtained network shows a decrease in its soluble fraction, concomitant with a decrease in the acyl content of the samples due to an increased crosslinking density and epoxy homopolymerisation. Similarly, the swelling ratio decreases as the soluble fraction decreases with the acyl content. It is notable that the 30H10CAT sample exhibited a slightly higher swelling ratio than 30H5CAT ($\approx 49\%$ against $\approx 40\%$). As shown below in the DMA data, this difference correlates with a slightly lower elastic modulus of the former. This indicates a higher crosslink density upon decreasing the amount of initiator for these off-stoichiometric compositions, where formation of the network is dominated by chain-wise polymerisation. Overall, none of these samples were dissolved and are considered to have crosslinked beyond the gel point.

3.3.2 Mechanical properties at small and large deformations

DMA results, summarised in Figure 3-5, show that when the acid content of the prepared vitrimers decreases (from 1:1 meq. to 1:0.3 meq. epoxy:acid), the glass transition temperature (tan delta peak values, Table A-1) gradually increases, from $\approx 40^\circ\text{C}$ (sample 100H) to $\approx 100^\circ\text{C}$ (samples 30H). This variation follows the rule of mixtures described by the Fox-Flory equation, as also observed in the off-stoichiometry thiol-epoxy formulation [64], [65], thus demonstrating the homogeneity of the networks (Figure A-8). The catalyst loading (5% or 10% meq. of epoxy) did not change the T_α of the 30H sample type but rubbery plateau modulus was lower with a higher catalyst content. To summarise, it appears that the T_α and the rubbery plateau can be tuned by changing the stoichiometric ratio between the epoxy and hardener. It is worth noting that in our system the term “soft crosslinker” would be more appropriate than hardener.

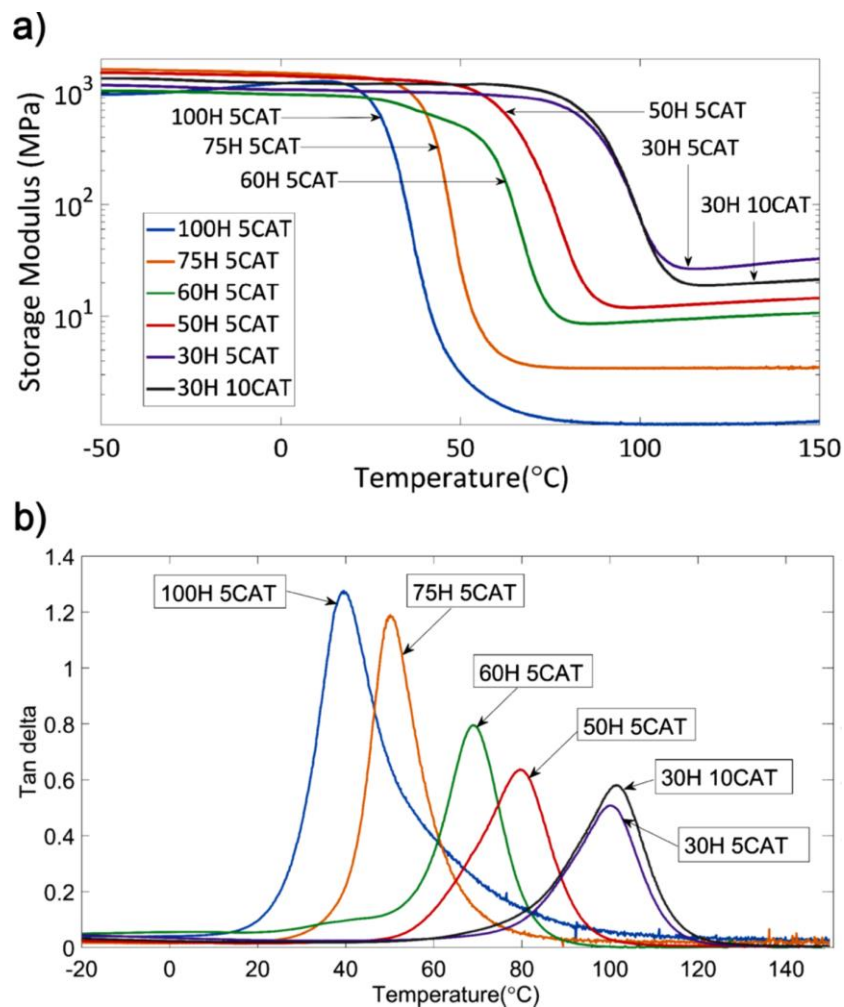


Figure 3-5 a) Storage moduli for different ratios, obtained by DMA measurements; b) damping response of tested samples.

The maximum of the loss tangent peak (Figure 3-5b) gradually decreases concomitantly with the sebacic acid content. This observation should be correlated with the evolution of a soluble fraction in the same series. Higher damping ability is related to the amount of network defects (*i.e.* dangling chains, isolated microgel fragments, and oligomers). The presence of such defects in samples close to stoichiometry proves a crosslinking mechanism mostly related to exchanges by transesterification as illustrated in Scheme 3-3. Whereas, off-stoichiometric compounds appear to be more tightly crosslinked, due to crosslinking mechanism by anionic ROP as illustrated in Scheme 3-2.

Tensile tests were conducted and representative stress/strain curves for different stoichiometric ratios investigated are presented in Figure 3-6. Sample 100H5CAT exhibited significant elongation (> 300%) and low stress at break (< 2 MPa), and Young's modulus (0.5 MPa) corresponding to a lightly crosslinked elastomer. Once the content of acid is decreased (75H5CAT sample), the tensile response shows an increase of initial Young's modulus (1.6 MPa) and strength (> 10 MPa), and concomitant decrease in the strain at break (\approx 140%). At lower acid contents (50H5CAT and 30H5CAT), the materials behave like a stiff epoxy thermoset with Young's modulus in the GPa range, and strength around 50 MPa.

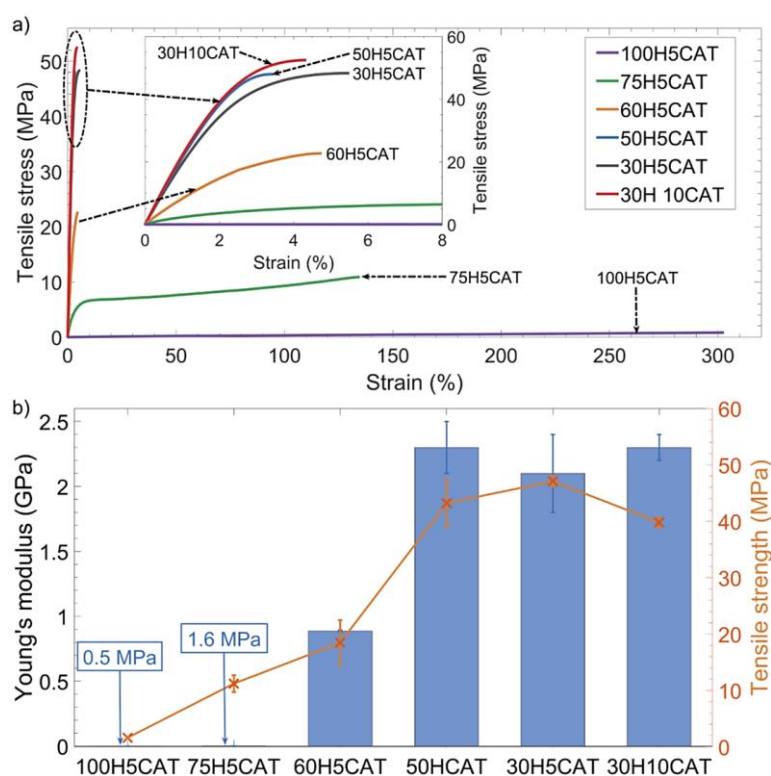


Figure 3-6 Tensile behaviour obtained with ASTM D 638 type IV samples. a) Typical stress/strain curves obtained for each epoxy:acid ratio, b) bar chart and curve comparing Young's moduli and tensile strengths of the samples.

100H5CAT behaves like a low-density crosslinked elastomer due to the length and size of the SA fragment and its relatively low T_{α} ($\approx 40^{\circ}\text{C}$). When the acid content is reduced, the homopolymerisation of epoxy leads to lower average distance between hard fragments of the epoxy backbone closely connected by glycerol units (Scheme 3-2). In contrast to SA/epoxy bonding that regularly introduced a flexible spacer between them (Scheme 3-1 and Scheme 3-3).

Performance of off-stoichiometric samples are very similar to conventional epoxies used in industries, with sebacic acid being a relatively cheap and safe “hardener” to handle. Mechanical data are summarised in Table A-2.

3.3.3 Stress relaxation of epoxy vitrimers

The capacity of relaxing stress was measured to ascertain the impact of off-stoichiometric formulation. The difference in mechanical properties required adapting the testing temperature for each sample examined (the stronger the network is, the higher the temperature must be). Sample type 100H5CAT and 75H5CAT exhibit complete stress relaxation as shown in Figure 3-7a and Figure A-9b. For 60H5CAT, at 180°C , the stress hardly relaxes down to 10% of the initial value after 20000 s (Figure 3-7b) and application of higher temperature caused observable chemical degradation of the network and significant deviation from exponential decay at this time scale (Figure A-9c). Similar behaviour is observed for the 50H5CAT sample with stress relaxed down to 20% of the initial value (Figure A-9d). 30H samples (5CAT and 10CAT) both exhibit a tendency to relax down to a value of $G/G_0 \approx 0.2$ (Figure 3-7c). These results are in line with the findings of Torkelson and co-workers [44], where vitrimers with $< 50\%$ of non-exchangeable covalent bonds were found to exhibit a near full relaxation. When the network is composed of more than 50% of irreversible bonds, it is only able to relax about 70% of the applied strain (30H5CAT and 10CAT samples correspond to 70% irreversible covalent bond content in the network).

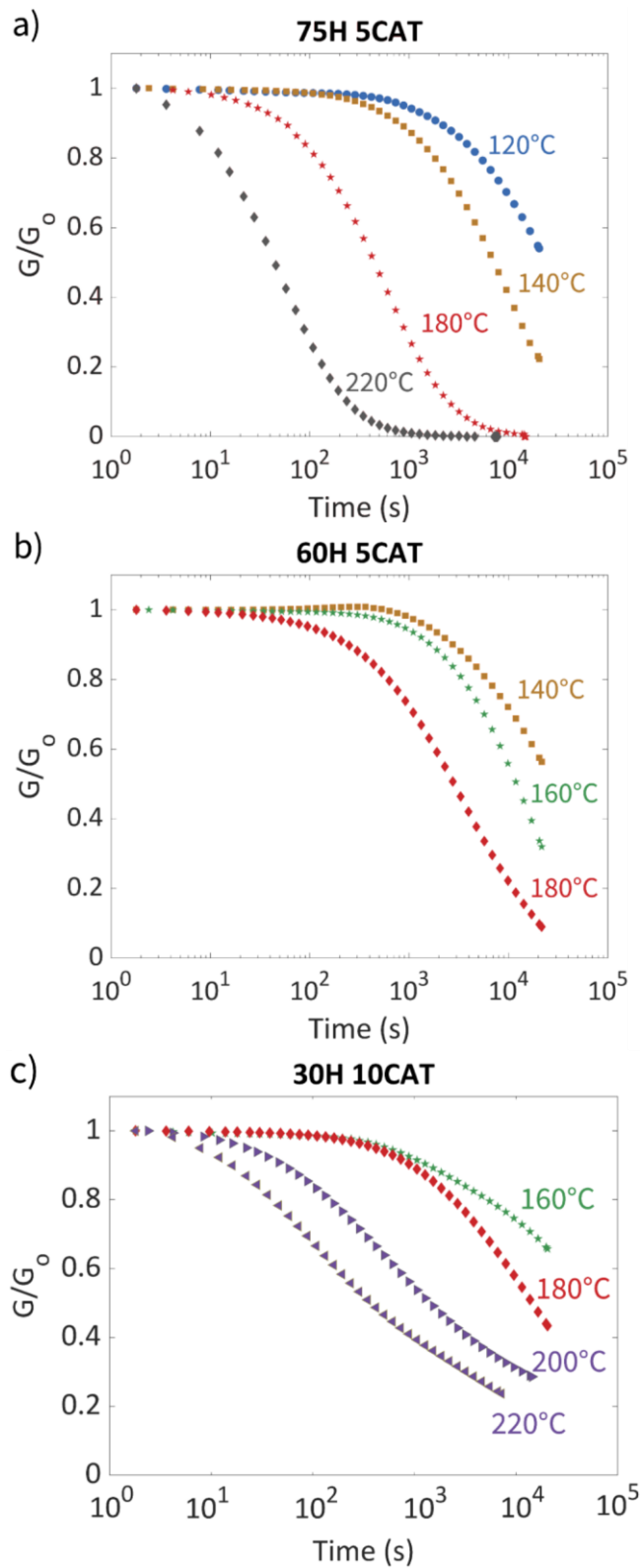


Figure 3-7 Stress relaxation at different temperatures for three different epoxy/acid ratios: a) 75H5CAT, b) 60H5CAT, and c) 30H10CAT.

3.3.4 Creep behaviour of epoxy vitrimers

The flow properties of the materials were also evaluated using creep experiments. As pointed out recently, this method is useful for characterising vitrimers with very slow dynamics [66], and avoids the shortcoming of low force measurements. Creep data of the same three samples under an applied stress of 0.1 MPa (75H5CAT and 60H5CAT), and 1 MPa (30H10CAT) are presented in Figure 3-8. Evidently, the sample closest to stoichiometry (75H5CAT, Figure 3-8a) flows like a liquid with the deformation increasing linearly with time, as also observed for the 100H5CAT sample (Figure A-10b). Moving further towards off-stoichiometry samples (60H5CAT), creep data do not exhibit a capacity to flow as the acquired deformation after 30 min is still well below 1% and the overall variation is not linear with time. This demonstrates that despite its capacity to nearly relax full stress under 1% applied deformation, 60H5CAT is, however, unable to flow like a liquid. Such observations lead to the conclusion that this material cannot be recognised as a vitrimer, but rather as a vitrimer-like material as defined in ref. [67], [68], showing the ability to be welded or healed but not entirely reshaped. Moving further to using an acyl content of 50% and lower (50H5CAT, 30H5CAT and 30H10CAT), any ability to flow disappears from creep profiles (Figure A-10d,e and Figure 3-8c) and the data rather suggest shape fixity of an essentially permanent network.

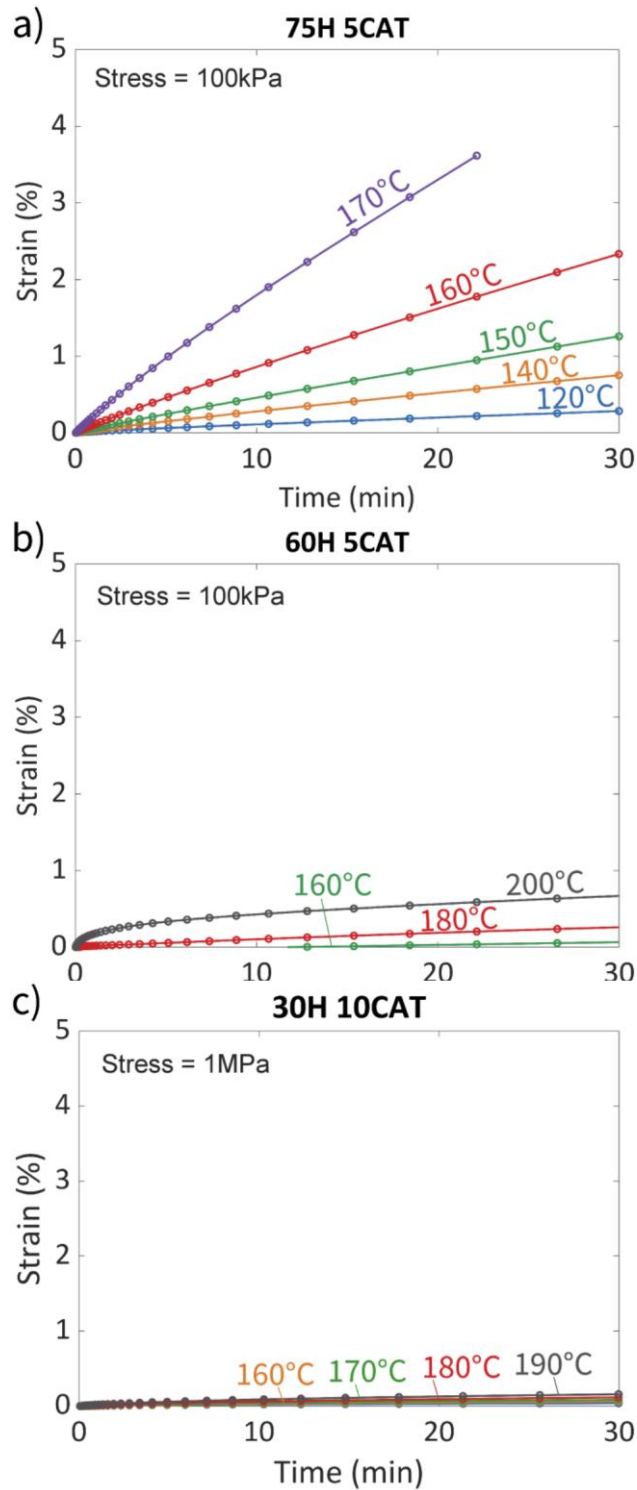


Figure 3-8 Creep behaviour for different temperatures and three different epoxy/acid ratios: a) 75H5CAT, b) 60H5CAT, and c) 30H10CAT.

Fitting stress relaxation data of 100H5CAT by a single exponential decay allows one to determine the relaxation time, *e.g.* at 180°C: $\tau \approx 90$ s. The value of τ at any temperature deduced from stress relaxation data is represented as Arrhenius plot in Figure 3-9a. The slope gives an activation energy of about 100 kJ.mol⁻¹.

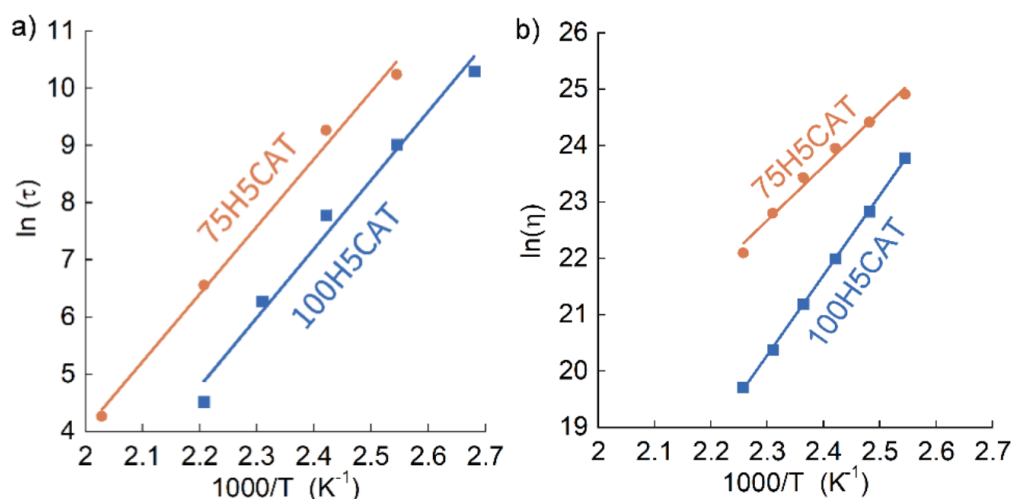


Figure 3-9 Arrhenius plot from a) stress relaxation and b) creep data of vitrimers with two different epoxy/acid ratios.

The same treatment on 75H5CAT stress relaxation data affords significantly longer relaxation times *e.g.* $\tau \approx 700$ s at 180°C and a similar activation energy. In addition, experimental data do not completely overlap the fit, suggesting that more than one relaxation time had to be considered.

In Figure 3-9b the Arrhenius plots of the same samples are calculated from the creep data. In this figure, the activation energy for 75h5CAT is lower and viscosity higher than that of the stoichiometric one. This indicates that the presence of sequences comprising a large number of non-exchangeable bonds induce slower relaxation modes which is not detectable by a monoexponential fit and decrease the thermoresponsivity of the system.

In other samples 50H5CAT, 30H5CAT (Figure A-9d,e), 60H5CAT, and 30H10CAT (Figure 3-7b,c), the extent of stress relaxation progressively decreases concomitantly with acid content and fitting by a single exponential model can no longer be achieved.

3.4 Conclusions

The present work demonstrates that full conversion of epoxy functions is achieved despite using a relatively low acyl content compared to the epoxy amount (down to 30% of the epoxy functions). The side reactions involved in the curing of non-stoichiometric systems are not necessarily detrimental to properties of materials. Effectively, TBD promotes anionic ROP in off-stoichiometric samples, leading to branching and crosslinking of the network. However, this reaction remains slow compared to the polyaddition of epoxy and acyl functions and promotes the formation of non-exchangeable

polyether chains. At any stoichiometry, the epoxy acyl curing in the presence of TBD produces an insoluble crosslinked polymer (> 75% of insoluble fraction). The samples closer to stoichiometry present more defects compared to the samples with a strong off-stoichiometry composition, which explains the improvement of thermomechanical properties in the elastomeric range. The rubbery plateau and mechanical strength of the materials both increase, when departing from stoichiometry and a transition from elastomeric to glassy behaviour is observed. This transition of the thermomechanical properties with the hardener content leads to the conclusion that sebacic acid acts more as a “soft crosslinker” for this network. When decreasing the acyl content of the formulation, the network undergoes a progressive transition from a vitrimer material (100H5CAT and 75H5CAT), to a vitrimer-like [67], [68] material (60H5CAT), and finally, to a permanently crosslinked material. The present study shows the potential to produce a tunable vitrimer formulation, without changing any of the manufacturing process parameters other than stoichiometry. This tuning aspect could raise practical interests for applications requiring tailored thermomechanical properties, without the need of altering the chemical formulation or handling processes.

3.5 Conflicts of interest

There are no conflicts to declare.

3.6 Acknowledgement

We thank Polly Greensmith and Mickael Pomes-Hadda for their technical assistance with DMA. F. T. acknowledges financial support from the ANR through the MATVIT project (ANR-18-CE06-0026-01) and the European Union’s Horizon 2020 research and innovation program under grant agreement No. 828818.

3.7 References

- [1] L. Leibler, M. Rubinstein, and R. H. Colby, "Dynamics of telechelic ionomers. Can polymer diffuse large distance without relaxing stress?," *J. Phys. II*, vol. 3, pp. 1581–1590, 1993.
- [2] R. D. Andrew, A. V. Tobolsky, and E. E. Hanson, "The theory of Permanent Set at Elevated Temperatures in Natural and Synthetic Rubber Vulcanizates," *Rubber Chem. Technol.*, vol. 4, pp. 1099–1112, 1946.
- [3] C. N. Bowman and C. J. Kloxin, "Covalent adaptable networks: Reversible bond structures incorporated in polymer networks," *Angew. Chemie - Int. Ed.*, vol. 51, no. 18, pp. 4272–4274, 2012.
- [4] C. J. Kloxin and C. N. Bowman, "Covalent adaptable networks: smart, reconfigurable and responsive network systems.," *Chem. Soc. Rev.*, vol. 42, no. 17, pp. 7161–73, 2013.
- [5] X. Chen *et al.*, "A Thermally Re-mendable Cross-Linked Polymeric Material," *Science*, vol. 295, no. 5560, pp. 1698–1702, 2002.
- [6] V. Froidevaux, M. Borne, E. Laborbe, R. Auvergne, A. Gandini, and B. Boutevin, "Study of the Diels–Alder and retro-Diels–Alder reaction between furan derivatives and maleimide for the creation of new materials," *RSC Adv.*, vol. 5, no. 47, pp. 37742–37754, 2015.
- [7] A. Gandini, "The furan/maleimide Diels–Alder reaction: A versatile click–unclick tool in macromolecular synthesis," *Prog. Polym. Sci.*, vol. 38, no. 1, pp. 1–29, 2013.
- [8] T. F. Scott, A. D. Schneider, W. D. Cook, and C. N. Bowman, "Photoinduced Plasticity in Cross-Linked Polymers," *Science*, vol. 308, no. 5728, pp. 1615–1617, 2005.
- [9] D. Montarnal, M. Capelot, F. Tounilhac, and L. Leibler, "Silica-Like Malleable Materials from permanent organic network," *Science*, vol. 334, pp. 965–968, 2011.
- [10] M. Capelot, D. Montarnal, F. Tournilhac, and L. Leibler, "Metal-catalyzed transesterification for healing and assembling of thermosets," *J. Am. Chem. Soc.*, vol. 134, no. 18, pp. 7664–7667, 2012.
- [11] R. L. Snyder, D. J. Fortman, G. X. De Hoe, M. A. Hillmyer, and W. R. Dichtel, "Reprocessable Acid-Degradable Polycarbonate Vitrimers," *Macromolecules*, vol. 51, no. 2, pp. 389–397, 2018.

- [12] Y. Spiesschaert, M. Guerre, L. Imbernon, J. M. Winne, and F. Du Prez, "Filler reinforced polydimethylsiloxane-based vitrimers," *Polymer*, vol. 172, pp. 239–246, 2019.
- [13] I. Azcune and I. Odriozola, "Aromatic disulfide crosslinks in polymer systems: Self-healing, reprocessability, recyclability and more," *Eur. Polym. J.*, vol. 84, pp. 147–160, 2016.
- [14] L. Zhang and S. J. Rowan, "Effect of Sterics and Degree of Cross-Linking on the Mechanical Properties of Dynamic Poly(alkylurea-urethane) Networks," *Macromolecules*, vol. 50, no. 13, pp. 5051–5060, 2017.
- [15] S. Zhang, L. Pan, L. Xia, Y. Sun, and X. Liu, "Dynamic polysulfide shape memory networks derived from elemental sulfur and their dual thermo-/photo-induced solid-state plasticity," *React. Funct. Polym.*, vol. 121, pp. 8–14, 2017.
- [16] B. Hendriks, J. Waelkens, J. M. Winne, and F. E. Du Prez, "Poly(thioether) Vitrimers via Transalkylation of Trialkylsulfonium Salts," *ACS Macro Lett.*, vol. 6, no. 9, pp. 930–934, 2017.
- [17] M. M. Obadia, A. Jourdain, P. Cassagnau, D. Montarnal, and E. Drockenmuller, "Tuning the Viscosity Profile of Ionic Vitrimers Incorporating 1,2,3-Triazolium Cross-Links," *Adv. Funct. Mater.*, vol. 27, no. 45, p. 1703258, 2017.
- [18] A. Demongeot, R. Groote, H. Goossens, T. Hoeks, F. Tournilhac, and L. Leibler, "Cross-Linking of Poly(butylene terephthalate) by Reactive Extrusion Using Zn(II) Epoxy-Vitrimer Chemistry," *Macromolecules*, vol. 50, no. 16, pp. 6117–6127, 2017.
- [19] J. Tang, L. Wan, Y. Zhou, H. Pan, and F. Huang, "Strong and efficient self-healing adhesives based on dynamic quaternization cross-links," *J. Mater. Chem. A*, vol. 5, no. 40, pp. 21169–21177, 2017.
- [20] T. Stukenbroeker, W. Wang, J. M. Winne, F. E. Du Prez, R. Nicolaÿ, and L. Leibler, "Polydimethylsiloxane quenchable vitrimers," *Polym. Chem.*, vol. 8, no. 43, pp. 6590–6593, 2017.
- [21] A. Arnebold, S. Wellmann, and A. Hartwig, "Network dynamics in cationically polymerized, crosslinked epoxy resins and its influence on crystallinity and toughness," *Polymer*, vol. 91, pp. 14–23, 2016.
- [22] A. Arnebold, S. Wellmann, and A. Hartwig, "Covalent integration of differently structured polyester polyols improves the toughness and strength of cationically

- polymerized, amorphous epoxy networks,” *J. Appl. Polym. Sci.*, vol. 133, no. 38, pp. 1–11, 2016.
- [23] V. R. Sastri and G. C. Tesoro, “Reversible Crosslinking in Epoxy Resins. II. New Approaches,” *J. Appl. Polym. Sci.*, vol. 39, pp. 1439–1457, 1990.
- [24] J.-P. Pascault and R. J. J. Williams, *Epoxy Polymers: New Materials and innovations*. Wiley-VCH Verlag, 2010.
- [25] M. Holst, K. Schänzlin, M. Wenzel, J. Xu, D. Lellinger, and I. Alig, “Time-resolved method for the measurement of volume changes during polymerization,” *J. Polym. Sci. Part B Polym. Phys.*, vol. 43, no. 17, pp. 2314–2325, 2005.
- [26] X. Fernández-Francos, S. G. Kazarian, X. Ramis, and À. Serra, “Simultaneous monitoring of curing shrinkage and degree of cure of thermosets by attenuated total reflection fourier transform infrared (ATR FT-IR) spectroscopy,” *Appl. Spectrosc.*, vol. 67, no. 12, pp. 1427–1436, 2013.
- [27] J. Scheirs and T. E. Long, *Modern Polyesters: Chemistry and Technology of Polyesters and Copolyesters*. Chichester: John Wiley and Sons LTd., 2013.
- [28] M. Delahaye, J. M. Winne, and F. E. Du Prez, “Internal Catalysis in Covalent Adaptable Networks: Phthalate Monoester Transesterification As a Versatile Dynamic Cross-Linking Chemistry,” *J. Am. Chem. Soc.*, vol. 141, no. 38, pp. 15277–15287, 2019.
- [29] M. Hanna and M. Fangrui, “Biodiesel production: a review 1,” *Bioresour. Technol.*, vol. 70, pp. 1–15, 1999.
- [30] W. Liu, D. F. Schmidt, and E. Reynaud, “Catalyst Selection, Creep, and Stress Relaxation in High-Performance Epoxy Vitrimers,” *Ind. Eng. Chem. Res.*, vol. 56, no. 10, pp. 2667–2672, 2017.
- [31] M. Capelot, M. M. Unterlass, F. Tournilhac, and L. Leibler, “Catalytic control of the vitrimer glass transition,” *ACS Macro Lett.*, vol. 1, no. 7, pp. 789–792, 2012.
- [32] A. S. Hoffman, “Stimuli-responsive polymers: Biomedical applications and challenges for clinical translation,” *Adv. Drug Deliv. Rev.*, vol. 65, no. 1, pp. 10–16, 2013.
- [33] J. Otera, “Transesterification,” *Chem. Rev.*, vol. 93, no. 4, pp. 1449–1470, Jun. 1993.
- [34] A. Demongeot, S.-J. J. Mougner, S. Okada, C. Soulié-Ziakovic, and F. Tournilhac, “Coordination and Catalysis of Zn²⁺ in Epoxy-Based Vitrimers,” *Polym. Chem.*, vol. 7, no. 27, pp. 4486–4493, 2016.
- [35] E. Chabert, J. Vial, J.-P. Cauchois, M. Mihaluta, and F. Tournilhac, “Multiple welding

- of long fiber epoxy vitrimer composites," *Soft Matter*, vol. 12, no. 21, pp. 4838–4845, 2016.
- [36] A. Ruiz De Luzuriaga *et al.*, "Epoxy resin with exchangeable disulfide crosslinks to obtain reprocessable, repairable and recyclable fiber-reinforced thermoset composites," *Mater. Horizons*, vol. 3, no. 3, pp. 241–247, 2016.
- [37] V. Rebizant *et al.*, "Chemistry and mechanical properties of epoxy-based thermosets reinforced by reactive and nonreactive SBMX block copolymers," *Macromolecules*, vol. 37, no. 21, pp. 8017–8027, Oct. 2004.
- [38] Q. Shi *et al.*, "Recyclable 3D printing of vitrimer epoxy," *Mater. Horizons*, vol. 4, no. 4, pp. 598–607, 2017.
- [39] Y. Yang, Z. Pei, X. Zhang, L. Tao, Y. Wei, and Y. Ji, "Carbon nanotube-vitrimer composite for facile and efficient photo-welding of epoxy," *Chem. Sci.*, vol. 5, no. 9, pp. 3486–3492, 2014.
- [40] K. Yu, P. Taynton, W. Zhang, M. L. Dunn, and H. J. Qi, "Influence of stoichiometry on the glass transition and bond exchange reactions in epoxy thermoset polymers," *RSC Adv.*, vol. 4, no. 89, pp. 48682–48690, 2014.
- [41] F. I. Altuna, C. E. Hoppe, and R. J. J. Williams, "Shape memory epoxy vitrimers based on DGEBA crosslinked with dicarboxylic acids and their blends with citric acid," *RSC Adv.*, vol. 6, no. 91, pp. 88647–88655, 2016.
- [42] F. I. Altuna, C. E. Hoppe, and R. J. J. Williams, "Epoxy vitrimers: The effect of transesterification reactions on the network structure," *Polymers*, vol. 10, no. 1, p. 43, 2018.
- [43] L. Matějka, S. Pokomý, and K. Dušek, "Network formation involving epoxide and carboxyl groups," *Polym. Bull.*, vol. 7, no. 2, pp. 123–128, 1982.
- [44] L. Li, X. Chen, K. Jin, and J. M. Torkelson, "Vitrimeres Designed Both To Strongly Suppress Creep and To Recover Original Cross-Link Density after Reprocessing: Quantitative Theory and Experiments," *Macromolecules*, vol. 51, no. 15, pp. 5537–5546, 2018.
- [45] C. E. Hoppe, M. J. Galante, P. A. Oyanguren, and R. J. J. Williams, "Epoxyes modified by palmitic acid: From hot-melt adhesives to plasticized networks," *Macromol. Mater. Eng.*, vol. 290, no. 5, pp. 456–462, 2005.
- [46] F. I. Altuna, C. E. Hoppe, and R. J. J. Williams, "Epoxy vitrimers with a covalently

- bonded tertiary amine as catalyst of the transesterification reaction," *Eur. Polym. J.*, vol. 113, pp. 297–304, 2019.
- [47] Z. Pei, Y. Yang, Q. Chen, E. M. Terentjev, Y. Wei, and Y. Ji, "Mouldable liquid-crystalline elastomer actuators with exchangeable covalent bonds," *Nat. Mater.*, vol. 13, no. 1, pp. 36–41, 2014.
- [48] Z. Pei, Y. Yang, Q. Chen, Y. Wei, and Y. Ji, "Regional Shape Control of Strategically Assembled Multishape Memory Vitrimers," *Adv. Mater.*, vol. 28, no. 1, pp. 156–160, 2016.
- [49] B. G. G. Lohmeijer *et al.*, "Guanidine and amidine organocatalysts for ring-opening polymerization of cyclic esters," *Macromolecules*, vol. 39, no. 25, pp. 8574–8583, Dec. 2006.
- [50] R. C. Pratt, B. G. G. Lohmeijer, D. A. Long, R. M. Waymouth, and J. L. Hedrick, "Triazabicyclodecene: A simple bifunctional organocatalyst for acyl transfer and ring-opening polymerization of cyclic esters," *J. Am. Chem. Soc.*, vol. 128, no. 14, pp. 4556–4557, 2006.
- [51] E. Cazares-Cortes, B. C. Baker, K. Nishimori, M. Ouchi, and F. Tournilhac, "Polymethacrylic Acid Shows Thermoresponsivity in an Organic Solvent," *Macromolecules*, vol. 52, no. 15, pp. 5995–6004, 2019.
- [52] M. Capelot, "Chimie de Polycondensation, Polymere supramoleculaire et vitrimere," Universite Pierre et Marie Curie - Paris VI, 2013.
- [53] U. Schuchardt, R. Sercheli, and R. M. Vargas, "Transesterification of vegetable oils: A review," *Journal of the Brazilian Chemical Society*, vol. 9, no. 3. Sociedade Brasileira de Quimica, pp. 199–210, 1998.
- [54] P. J. Flory, "Molecular Size Distribution in Three Dimensional Polymers. VI. Branched Polymers Containing A-R-Bf-1 Type Units," *J. Am. Chem. Soc.*, vol. 63, pp. 3083–3090, 1941.
- [55] W. H. Stockmayer, "Theory of molecular size distribution and gel formation in branched-chain polymers," *J. Chem. Phys.*, vol. 11, no. 2, pp. 45–55, 1943.
- [56] J. E. Klee, F. Claussen, and H.-H. Horhold, "High-molecular weight diepoxide-dicarboxylic acid addition polymers," *Polym. Bull.*, vol. 35, pp. 79–85, 1995.
- [57] K. Dusek and L. Matejka, "Transesterification and Gelation of Polyhydroxy Esters Formed From Diepoxides and Dicarboxylic Acids," *Adv. Chem. Ser.*, pp. 15–26, 1984.

- [58] X. Fernández-Francos, A. O. Konuray, A. Belmonte, S. De La Flor, À. Serra, and X. Ramis, "Sequential curing of off-stoichiometric thiol-epoxy thermosets with a custom-tailored structure," *Polym. Chem.*, vol. 7, no. 12, pp. 2280–2290, 2016.
- [59] M. S. Heise and G. C. Martin, "Curing Mechanism and Thermal Properties of Epoxy-Imidazole Systems," *Macromolecules*, vol. 22, no. 1, pp. 99–104, 1987.
- [60] X. Fernández-Francos, "Theoretical modeling of the effect of proton donors and regeneration reactions in the network build-up of epoxy thermosets using tertiary amines as initiators," *Eur. Polym. J.*, vol. 55, no. 1, pp. 35–47, 2014.
- [61] S. K. Ooi, W. D. Cook, G. P. Simon, and C. H. Such, "DSC studies of the curing mechanisms and kinetics of DGEBA using imidazole curing agents," *Polymer*, vol. 41, no. 10, pp. 3639–3649, 2000.
- [62] I. Kaljurand *et al.*, "Extension of the self-consistent spectrophotometric basicity scale in acetonitrile to a full span of 28 pKa units: Unification of different basicity scales," *J. Org. Chem.*, vol. 70, no. 3, pp. 1019–1028, 2005.
- [63] H. Walba and W. Isensee, "Acidity Constants of Some Arylimidazoles and Their Cations," *J. Org. Chem.*, vol. 26, no. 8, pp. 2789–2791, 1961.
- [64] T. G. Fox and P. J. Flory, "Second-order transition temperatures and related properties of polystyrene. I. Influence of molecular weight," *J. Appl. Phys.*, vol. 21, no. 6, pp. 581–591, 1950.
- [65] A. Belmonte, C. Russo, V. Ambroggi, X. Fernández-Francos, and S. D. la Flor, "Epoxy-based shape-memory actuators obtained *via* dual-curing of off-stoichiometric 'thiol-epoxy' mixtures," *Polymers*, vol. 9, no. 3, 2017.
- [66] R. G. Ricarte, F. Tournilhac, M. Cloître, and L. Leibler, "Linear Viscoelasticity and Flow of Self-Assembled Vitrimers: The Case of a Polyethylene/Dioxaborolane System," *Macromolecules*, vol. 53, no. 5, pp. 1852–1866, 2020.
- [67] L. Imbernon, S. Norvez, and L. Leibler, "Stress Relaxation and Self-Adhesion of Rubbers with Exchangeable Links," *Macromolecules*, vol. 49, no. 6, pp. 2172–2178, 2016.
- [68] S. Kaiser, S. Wurzer, G. Pilz, W. Kern, and S. Schlögl, "Stress relaxation and thermally adaptable properties in vitrimer-like elastomers from HXNBR rubber with covalent bonds," *Soft Matter*, vol. 15, no. 30, pp. 6062–6072, 2019.

Appendix A. Supplementary information - Chapter 3

Quentin-Arthur Poutrel^{a,b}, Jonny J Blaker^a, Constantinos Soutis^b, François Tournilhac^{*c}, and Matthieu Gresil^{*d}

^a Bio-Active Materials Group, Department of Materials, The University of Manchester, Manchester, UK

^b Aerospace Research Institute, The University of Manchester, Manchester, UK

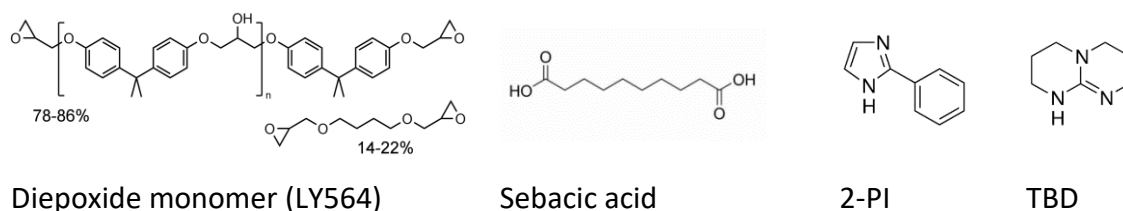
^c Molecular, Macromolecular Chemistry, and Materials, ESPCI Paris, PSL University, CNRS, 10 rue Vauquelin, 75005 Paris, France

^d i-Composites Lab, Department of Materials Science and Engineering, Monash University, Clayton, Australia

*corresponding authors: francois.tournilhac@espci.fr, matthieu.gresil@monash.edu

A.1. Manufacture of vitrimer networks - mixing, mould casting, degassing and curing

Reactants used in this study are presented in Scheme A-1.



Scheme A-1 Reactants used in the study.

Sebacic acid and TBD were added to the epoxy as received, and mixed for 24 h at 50°C until obtaining a white homogeneous mixture. The final mixture was then placed into an open mould, degassed under vacuum for 2 h at 90°C to ensure removal of air inadvertently added during mixing. Samples were then cured at 145°C for 8 h (ramp 1.7°C/min from room temperature to 145°C), a post-cure was then completed at 160°C for 8 h (Figure A-1).

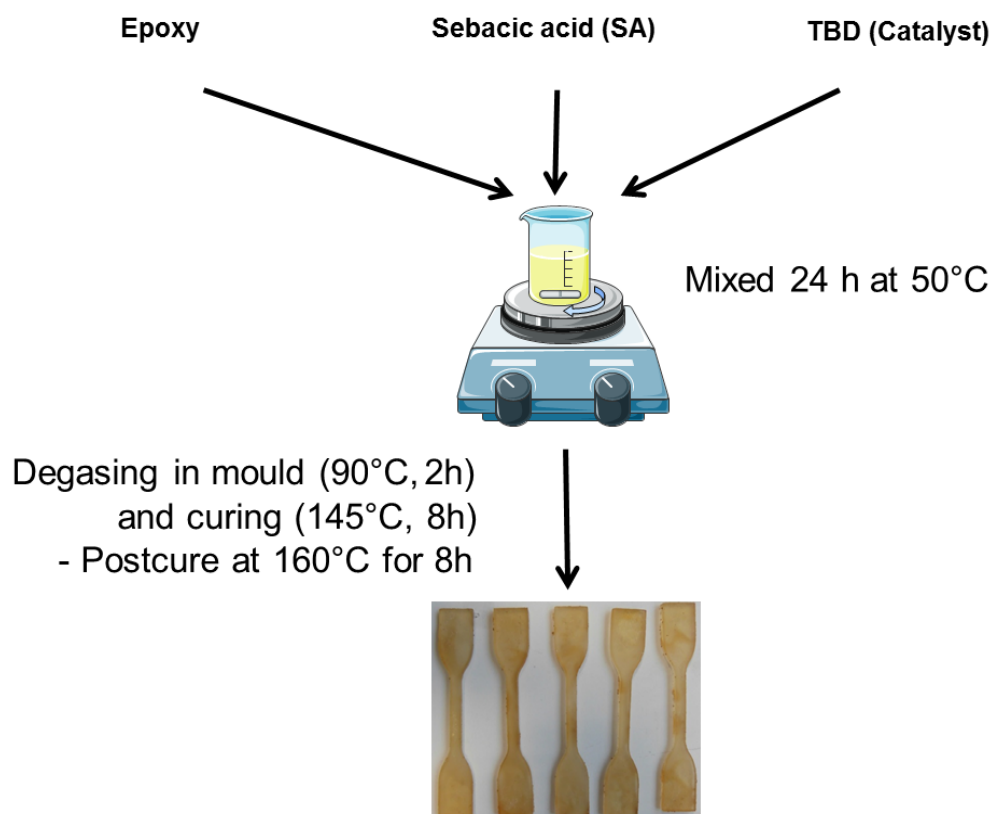


Figure A-1 Schematic of fabrication method used to produce vitrimer samples.

A.2. IR analysis method

A.2.1. Data collection

Data were collected using a Bruker Tensor 37 spectrometer equipped with a Specac GoldenGate thermalized ATR stage. Components of reactive mixtures were weighed and mixed together at room temperature in a mortar before placing a drop of the mixture on the golden gate cell preheated to 125°C. Spectra were then recorded at regular 2 min intervals (resp. 1 min. intervals with 2-PI). CO₂/water vapour correction and noise reduction were applied through the Opus software. Data were then analysed using integration tools in the Opus 3D module. Data were then analysed using integration tools in the Opus 3D module. Figure A-2 shows a typical collection of spectra (one hour curing of 100H5CAT at 125°C), obtained in the 2000-600 cm⁻¹ range. Identification of signals in the 1600-1800 cm⁻¹ range is shown in Figure A-3. Area ranges for integration of signals of interest are shown in Figure A-4.

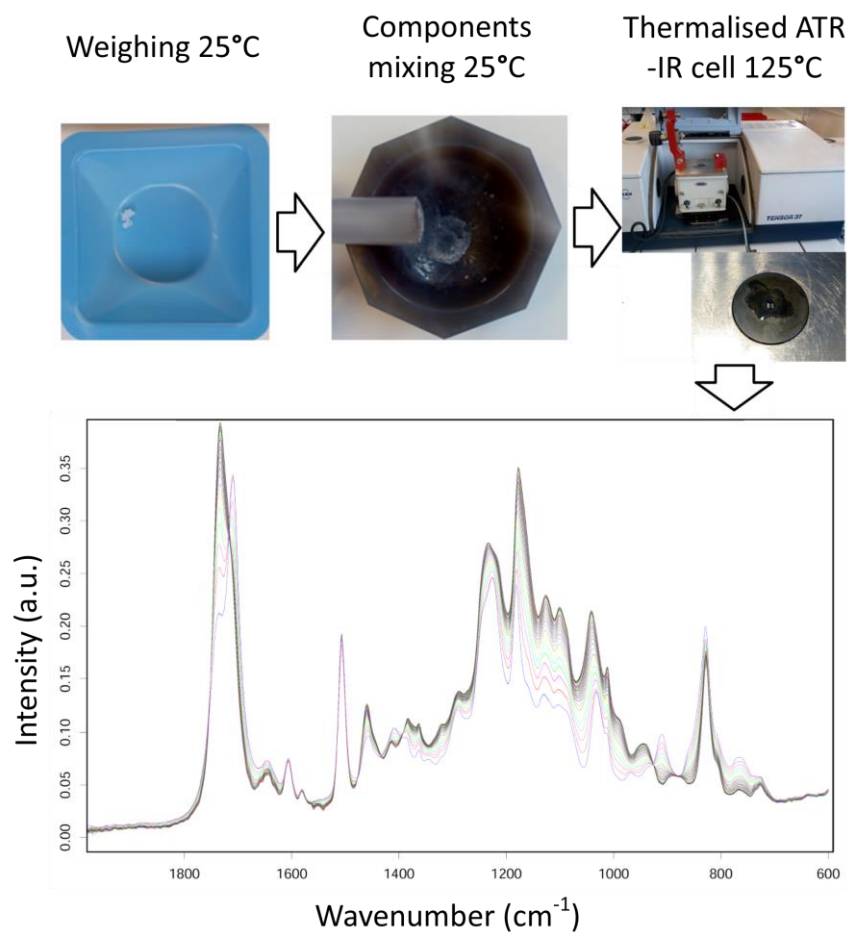


Figure A-2 Schematic of ATR-IR curing experiment to record species evolution over time.

A.2.2. Carbonyl peaks assignment

In Figure A-2, major changes are observed in the 1600-1800 cm⁻¹ region during curing. The signal detected at 1706 cm⁻¹ is attributed to the C=O stretching of H-bonded dimerised carboxylic acid groups [1]. Another signal, detected at 1735 cm⁻¹ is attributable to the C=O stretching of the ester. However, for all investigated formulations, a signal at 1735 cm⁻¹ was already present before starting the cure cycle while no ester was yet present. Spectra of sebacic acid recorded in various liquid environments and concentrations (Figure A-3) lead to the conclusion that the C=O stretching signal of solvated COOH groups (forming an H-bond to surrounding ether groups) overlaps the signal of ester at 1735 cm⁻¹.

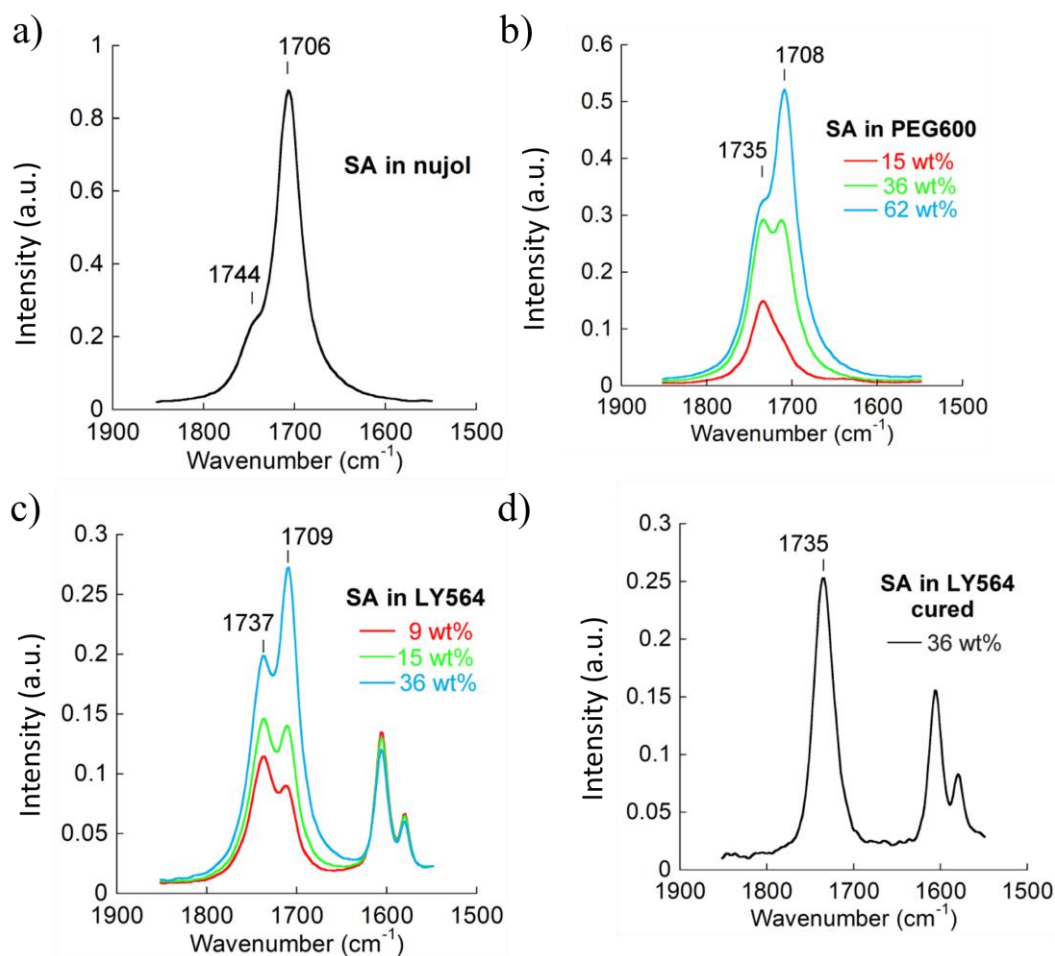


Figure A-3 Identification of C=O stretching signals. a) Sebacic acid in the molten state at 145°C in paraffin oil. The signal at 1706 cm^{-1} is the regular signal of dimerized H-bonded COOH groups, b) Sebacic acid at different concentrations in PEG600 used as a solvent. The signal at 1735 cm^{-1} is due to COOH groups interacting through H-bonds with the ether groups of the solvent. c) Sebacic acid at different concentrations in epoxy resin; the same signals are present. The ether groups of uncured epoxy resin interact with dissolved COOH groups. d) Sebacic acid in epoxy resin after full curing. The C=O stretching signal of the ester is detected at 1735 cm^{-1} .

A.2.3. Integration of signals

Integration of ATR signals was used for monitoring of curing reactions. The method of integration is illustrated in Figure A-4. The result of integration (either positive or negative) as a function of time is plotted without any post treatment or normalization in Figure 3-2 and Figure 3-3:

- **Esters:** Monitoring was performed by integration of the C=O stretching peak (1735 cm^{-1}) over the 1748–1724 cm^{-1} interval.
- **Carboxylic acids:** Monitoring was performed by integration of the C=O stretching peak (1705 cm^{-1}) over the 1718–1703 cm^{-1} interval.

- **Epoxides:** Monitoring was performed by integration of the asymmetric epoxy ring deformation [2] (914 cm^{-1}) over the $921\text{--}904\text{ cm}^{-1}$ interval.
- **Ethers:** According to literature [2], the following signals are expected for the ether:
 - Characteristic C–O stretching signals:
 - Aliphatic ether functions: several signals in the $1140\text{--}1100\text{ cm}^{-1}$ range.
 - Interfering C–O stretching signals:
 - Aryl-alkyl ether functions: two signals around 1250 cm^{-1} and 1040 cm^{-1} .
 - Primary and secondary alcohol functions: two signals around 1065 cm^{-1} and 1100 cm^{-1} .
 - Ester functions: several signals in the $1280\text{--}1160\text{ cm}^{-1}$ range.

In order to extract a specific signal of ethers formed by the anionic polymerization of the epoxy with minimum interference with other functions present, the ether signature was isolated by integration of the ATR trace between 1150 and 1120 cm^{-1} . Baseline for integration was taken by connecting the maximums of the neighboring peaks (1182 cm^{-1} and 1033 cm^{-1}) which showed little change during the reaction.

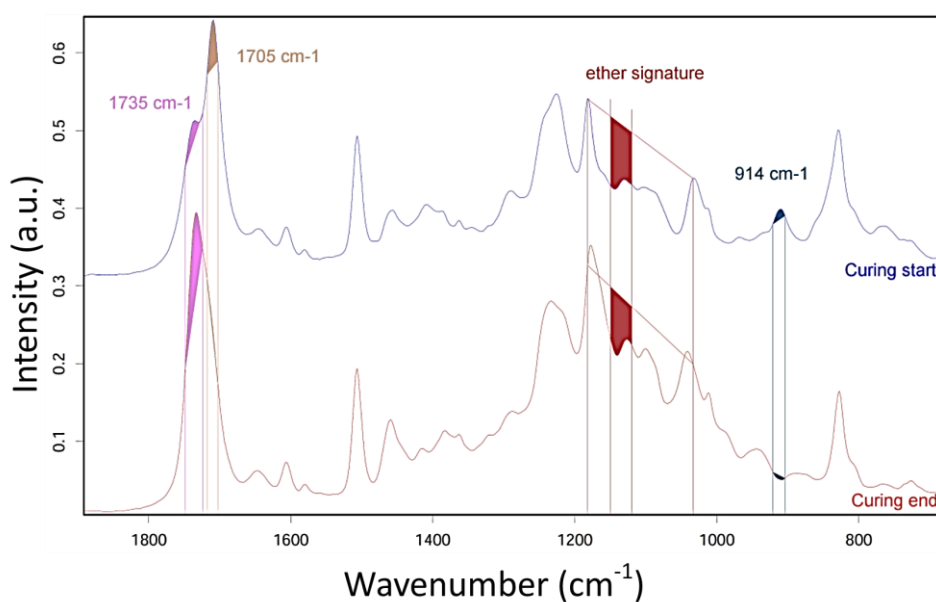


Figure A-4 Typical integration zone for epoxy peak at the beginning (blue curve) and at the end (red curve) of cure process for sample 100H 5CAT.

A.2.4. Complementary FTIR data

To ensure that all epoxy groups were consumed at the end of the curing cycle, a postcure was applied to all samples. Figure A-5 shows that epoxy groups of 100H samples are virtually exhausted after the cure cycle of 60 min at 145°C. Samples 50H and 30H (Figure A-6 and Figure A-7 respectively) were still containing some epoxy after 60 min at 145°C. Therefore, the reaction was carried out for 8 h at 145°C and then 160°C for 8 h for all samples. The figure shows small remaining absorption at 914 cm⁻¹ did not change for several hours at 160°C indicating that the eventual small fraction of remaining epoxy groups is no longer reactive (probably due to reduced mobility after crosslinking).

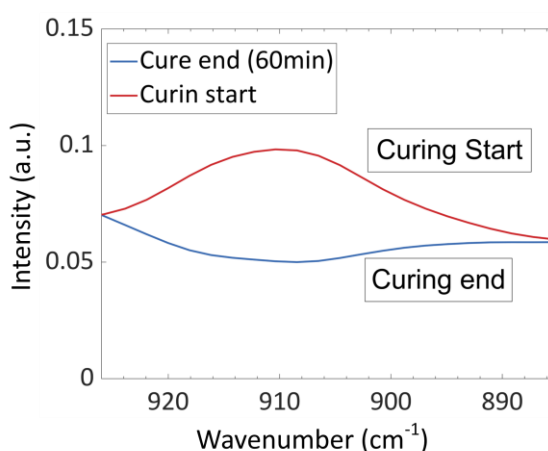


Figure A-5 Evolution of epoxy peak during curing of sample 100H5CAT: beginning (red) and after 60 min (blue) at 145°C.

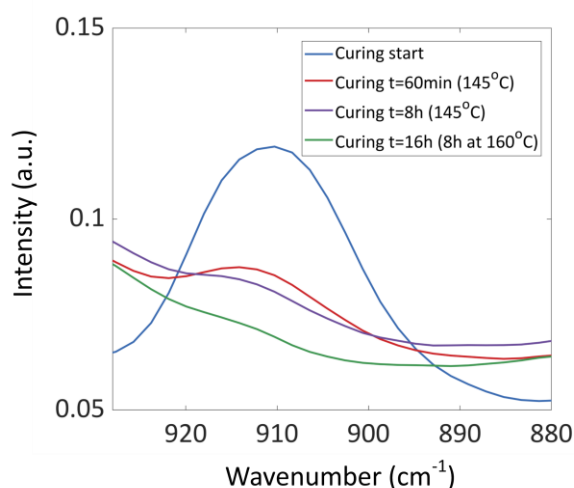


Figure A-6 Evolution of epoxy peak during curing of sample 50H5CAT: beginning (blue), after 60 min (red) after 8h at 145°C (purple), and 8h at 160°C (green).

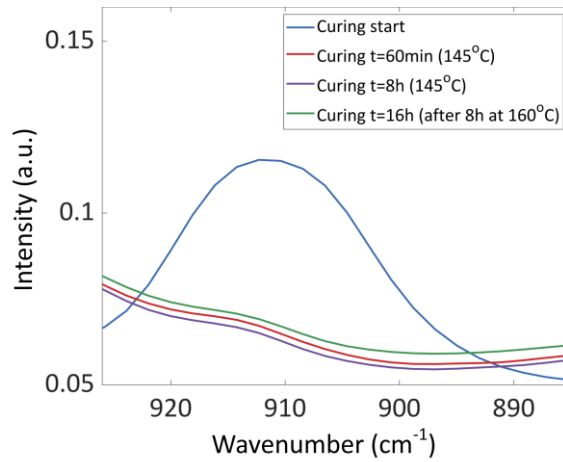


Figure A-7 Evolution of epoxy peak during curing of sample 30H5CAT: beginning (blue), after 60 min (red) after 8h at 145°C (purple), and 8h at 160°C (green).

A.3. Dynamic mechanical analysis

The values of T_{α} taken at maximum value of the tan delta curves are given in Table A-1. The data are fitted using the Fox-Flory equation:

$$\frac{1}{T_{\alpha}} = \frac{\phi_1}{T_{\alpha 1}} + \frac{\phi_2}{T_{\alpha 2}}$$

Equation A-1 Fox-Flory equation.

where ϕ_1 , ϕ_2 are the volume fractions of polymer 1 and polymer 2 and $T_{\alpha 1}$, $T_{\alpha 2}$ their respective glass transition temperatures. The results are presented in Figure A-8; ϕ_1 and ϕ_2 are approximated respectively by the weight fractions of excess epoxy and the weight fraction of stoichiometric epoxy + acid monomers in the composition. $T_{\alpha 2}$ and $T_{\alpha 1}$ are taken as adjustable parameters and represent respectively the glass transitions of epoxy homopolymer and that of a 1:1 adduct of epoxy + sebacic acid. The trace of the fitting curve is shown in Figure A-8. Best fit was achieved with $T_{\alpha 1} = 39^{\circ}\text{C}$, $T_{\alpha 2} = 160^{\circ}\text{C}$. The latter value is close to the one commonly reported for the epoxy homopolymer [3], [4].

Table A-1 Glass transition temperatures for different ratios taken from the tan delta curves.

Samples						
	100H5CAT	75H5CAT	60H5CAT	50H5CAT	30H5CAT	30H10CAT
T_{α} (°C)	40	50	69	80	100	101

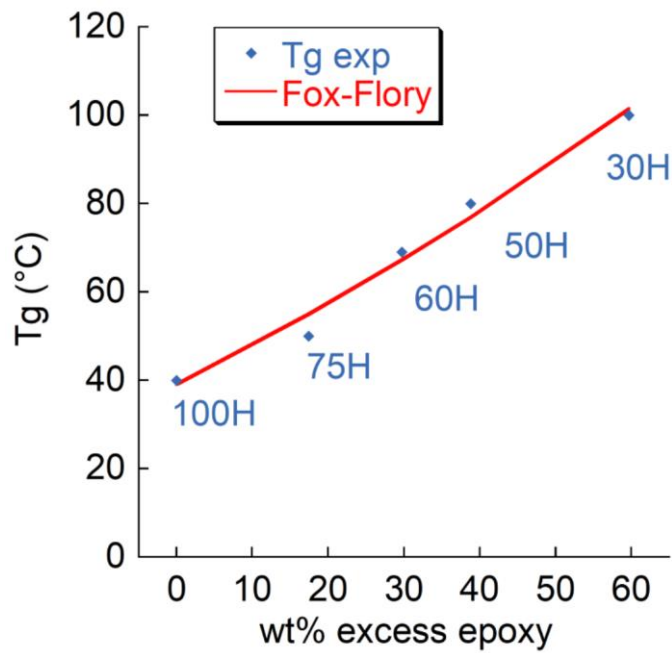


Figure A-8 Evolution of the glass transition as a function of composition (diamonds) and trace of the fit using the Fox-Flory equation (red solid line).

A.4. Mechanical results

Mechanical properties of vitrimers at different ratios is reported in Table A-2.

Table A-2 Tensile properties for different ratios of vitrimer.

Samples						
	100H 5CAT	75H 5CAT	60H5CAT	50H5CAT	30H5CAT	30H10CAT
Young modulus (MPa)	0.471 ± 0.14	1.63 ± 21	886 ± 8	2300 ± 200	2100 ± 300	2300 ± 100
Breaking strain (%)	328.1 ± 19	143.6 ± 36.6	6.4 ± 0.9	7.2 ± 0.1	13.42 ± 0.1	12.7 ± 0.1
Ultimate tensile strength (MPa)	0.83 ± 0.02	11.2 ± 1.5	18.46 ± 4	43.2 ± 4.2	47.1 ± 1	39.8 ± 0.9

A.5. Stress relaxation results

Figure A-9 shows the results of stress relaxation experiments for each ratio. For compounds 100H5CAT and 75H5CAT, the solid red lines indicate the results of fitting by a monoexponential decay. The values of relaxation time thereby determined are plotted in Arrhenius axes in Figure 3-9, initial value of the shear relaxation modulus G_0 for these two samples are reported in Table A-3.

Table A-3 Relaxation modulus (initial value).

Samples	100°C	120°C	140°C	160°C	180°C	220°C
100H5CAT G_0 (MPa)	0.57	0.63	0.69	0.55	0.58	
75H5CAT G_0 (MPa)		4.40	5.05		5.80	5.30

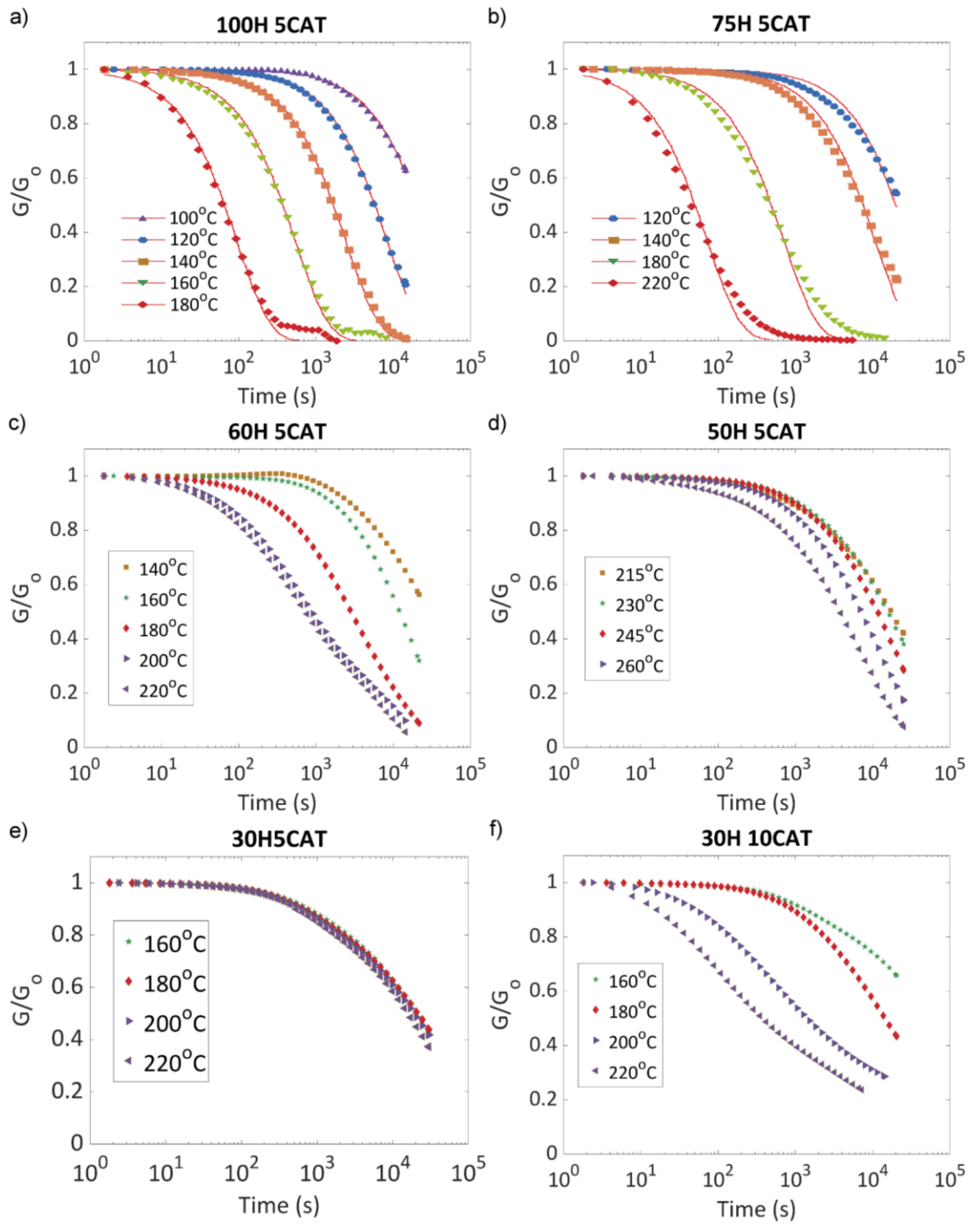


Figure A-9 Stress relaxation results obtained by DMA in shear geometry: a) 100H 5CAT, b) 75H 5 CAT c) 60H5CAT, d) 50H5CAT, e) 30H5CAT, and d) 30H10CAT.

A.6. Creep results for all samples

Figure A-10 shows the results of creep experiments for each ratio. The value of applied stress is indicated. Compound 100H5CAT and compound 75H5CAT flow under application of stress whereas other compounds only show very limited values of creep.

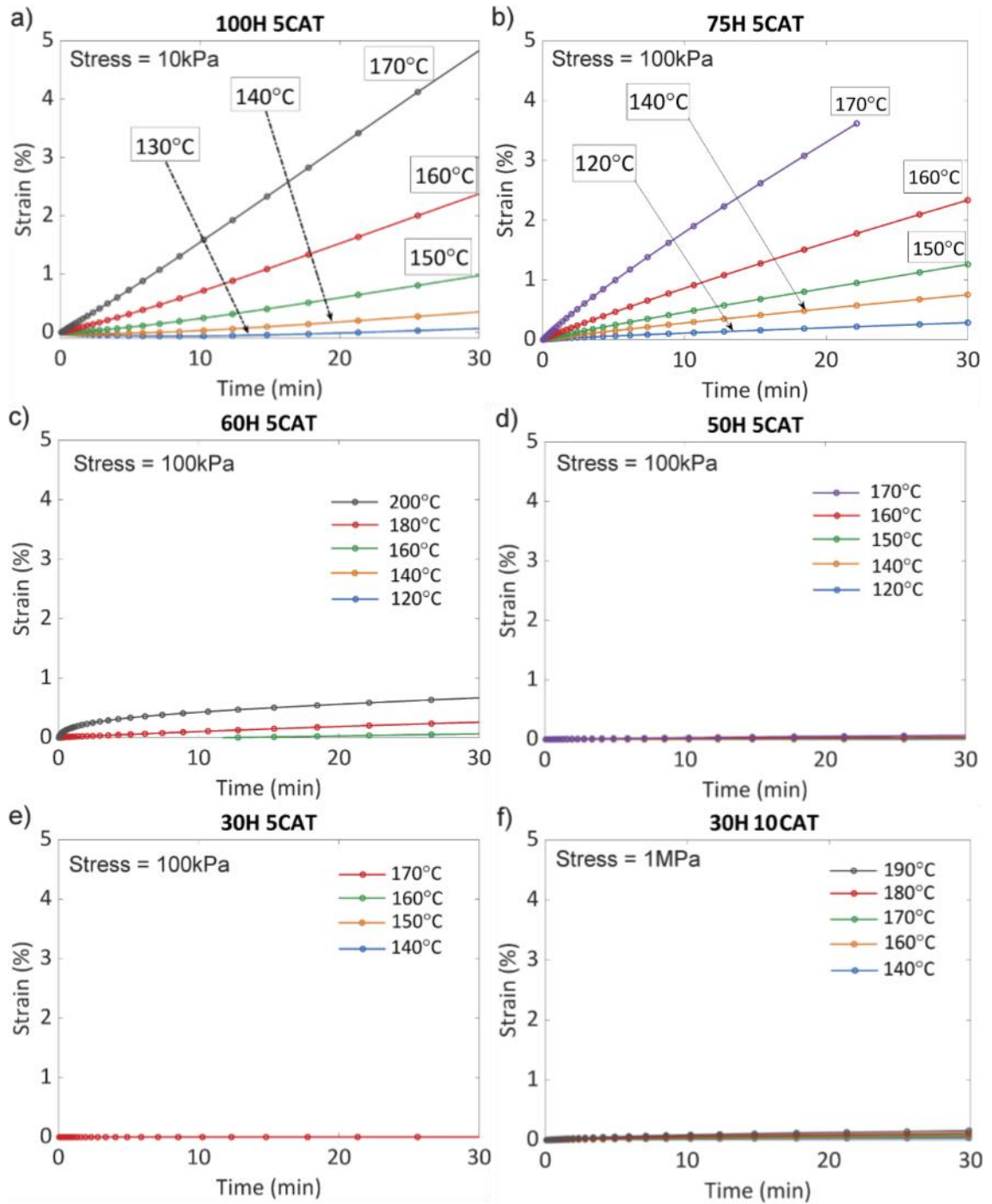


Figure A-10 Creep results for all samples.

A.7. References

- [1] V. Rebizant *et al.*, "Chemistry and mechanical properties of epoxy-based thermosets reinforced by reactive and nonreactive SBMX block copolymers," *Macromolecules*, vol. 37, no. 21, pp. 8017–8027, Oct. 2004.
- [2] R. A. Nyquist, Ed., "Epoxides and Ethers," in *Interpreting Infrared, Raman, and Nuclear Magnetic Resonance Spectra*, vol. 2, 2001, pp. 1–26.
- [3] M. S. Heise and G. C. Martin, "Curing Mechanism and Thermal Properties of Epoxy-Imidazole Systems," *Macromolecules*, vol. 22, no. 1, pp. 99–104, 1987.
- [4] S. K. Ooi, W. D. Cook, G. P. Simon, and C. H. Such, "DSC studies of the curing mechanisms and kinetics of DGEBA using imidazole curing agents," *Polymer*, vol. 41, no. 10, pp. 3639–3649, 2000.

CHAPTER 4 - PRELIMINARY STATEMENT

This chapter was initially submitted to *Carbon* in April 2020. After rejection in June 2020 (short comments from reviewers indicated confusing layout and requirement of higher quality figures) - an intense re-work of the manuscript layout and figures improvement were performed to improve its clarity and quality. This manuscript is now under review for the journal *Composite Structures*. The related electronic supplementary information of this chapter is in appendix B.

This chapter is a collaboration between the MSc students (AS and YB, see declaration for full name) and the author (QAP) supervised by Matthieu Gresil. Original idea of functionalisation of nanoparticles and recovery of nanoparticles originate from QAP. Manufacture of samples was taught by QAP to AS and YB and most of their samples done with the help of QAP. XRD and TGA data is a service run by the University of Manchester; therefore, samples were left by one of the authors to the service and data collected by a technician. Raw data was shared but plotting and analysis were performed individually (by QAP for this project and submitted paper). Swelling and soluble fraction experiments were performed as a team between AS and QAP, and measured data shared equally. In the same way, plotting and analysis was fully performed by the author (QAP). In a similar way, tensile testing of samples was performed as a team or alternatively by YB, AS and QAP; however, plotting and analysis for this work was performed by QAP. Nanoparticles recovery yields for GNP and rGO originate from AS under QAP supervision; other yields (GO and GPTS-GO) originate from QAP. Raman and stress relaxation data were collected by QAP and raw data shared with AS for her report. Rest of the non-mentioned data are originated from QAP. All plotting and analysis performed in this chapter (and submitted paper) are an original production of QAP with exception of Figure 4-1 and Figure 4-2 which have been produced by YB. Figure B-1 has been adapted from AS report.

Chapter 4. Graphene epoxy based vitrimer: From matrix properties enhancement to sustainability via nanoparticles recovery

Quentin-Arthur Poutrel^{a,b}, Yasmine Baghdadi^b, Aline Souvignet^b, Matthieu Gresil^{c,*}

^a Aerospace Research Institute, The University of Manchester, Manchester, UK

^b Department of Materials, The University of Manchester, Oxford Road, Manchester, UK

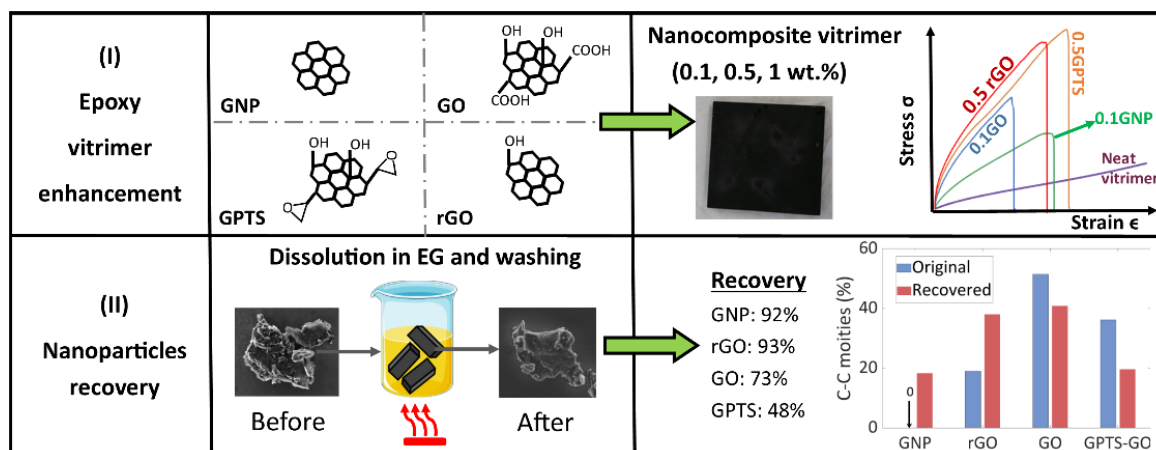
^c i- Composites Lab, Department of Materials Science and Engineering, Monash University, 20 Research Way, Clayton, Australia

*corresponding authors: matthieu.gresil@monash.edu

Abstract

The present study explores the effect of different graphitic nanoparticles (graphene nanoplatelets (GNP), graphene oxide (GO), reduced graphene oxide (rGO) and silane bearing epoxy functionalised graphene nanoplatelets (GPTS-GO)) on an epoxy vitrimer formulations. The mechanical properties (Young's modulus, strain at break, and tensile strength) are investigated with different loading of nanoparticles: 0.1, 0.5 and 1 wt. % of the total nanocomposites mass. Overall, mechanical property are greatly increased for all nanoparticles type, up to 2 time (0.5 wt. % rGO). Spectral characterisation reveals that the nanoparticles seem to bond with the vitrimer matrix when functionalised (GO, rGO and GPTS-GO). Stress relaxation demonstrates that inclusion of nanoparticles decreases the time of relaxation concomitantly with particles loading when normalised by their mechanical properties. All nanoparticles are successfully extracted *via* a simple dissolution/washing method from the vitrimer matrix, and chemical investigation (XPS, RAMAN, and XRD) of recovered particles shows no traces of remaining polymer. These characterisations also provide information over the chemicals change undergone by nanoparticles during recovery process. Low functionality particles (GNP and rGO) displays some added functional groups (hydroxyl compounds) after recycling. Reversibly, highly functionalised particles (GO and GPTS-GO) undergo cleaving of functional units during extraction process.

Graphical abstract



4.1 Introduction

With the first confirmation of graphene properties by Geim and Novoselov in 2004 [1], graphene is intensively studied in many areas such as electronics [2]–[4], the building industry [5], [6], opto-electronic [7]–[10] and widely used in polymer research [11]–[17]. Graphene exhibits excellent mechanical, thermal and electrical properties while, on the other hand, most polymers exhibit poor conductivities [18]. Therefore, the effect of graphene and its derivative, such as graphene nanoplatelets (GNP), graphene oxide (GO), reduced graphene oxide (rGO), or other functionalisation, on epoxy polymers is a very important research focus (≈ 36 peered review journals between 2000-2009, ≈ 603 between 2010-2014, and ≈ 3345 between 2015-2019, source: *Web of Science*).

The discovery of vitrimers by Leibler and Coll. in 2011 opened a new area of research, focusing on covalent adaptive networks (CANs) [19]. Vitriimer is a new class of polymer material which gained its place between traditional thermosets and thermoplastics. These dynamic covalent networks are able to flow by bond exchange reaction (BER) under excitation (*e.g.* heat, light, *etc.*) [20], [21]. The bond exchange is associative, meaning that a new bond is formed before breaking the previous one. Due to this associative nature, vitriimer can relax stress, flow at high temperature, while keeping their structure integrity (*i.e.* crosslink density constant), and their chemical resistance to solvent [21]. These networks exhibit two transition temperatures: (i) the glass transition temperature T_g and (ii) the topology freezing temperature, also called vitrification temperature T_v . The latter, compared to the former one, is a unique characteristic of

vitriimer networks. At T_v , the bond exchange is fast enough to enable flow and full stress relaxation of the network which permits to heal, reprocess, and recycle the crosslinked polymer [22]–[26]. Vitriimer network was initially based on commercially available epoxy networks relying on transesterification BER mechanism and several studies focused on tuning their mechanical behaviour *via* hardener types and its feeding ratio [22], [23], [27], [28]. Since then, many other researchers have demonstrated that other chemistry is possible [29]–[38]. Despite the versatility of chemistry to produce vitriimer networks, few studies show the impact of functionalised graphene nanoparticles on their properties. Initial work on carbon based nanoparticles focused on dual shape memory actuation [39], [40], efficient welding or fast curing of vitriimer network [41], [42], improved electrical conductivity [43], and alignment of nanoreinforcements using structural reconfiguration [24], [44], [45]. These works demonstrate the potential of nanocomposite vitrimers to manufacture and design multifunctional materials. One interesting feature of vitriimer networks is their capacity to be diluted in appropriate solvents compared to traditional thermoset networks. Recycling of carbon fibre from vitriimer matrix was demonstrated, allowing fibres to be recovered and used to produce new composites with similar mechanical behaviour than the former ones [46]–[48]. Catalysts used in epoxy-based vitriimer are generally not bonded to the covalent network. Since the recycling *via* depolymerisation has been achieved onto vitriimer, the recycling of traditional thermoset network has been demonstrated *via* swelling in alcohol loaded with catalyst selected to cleave covalent bonds [49]. However, these works do not address underlying problems rising from the use of nanoparticles in crosslinked networks: the extraction and recycling of these nanofillers.

The increase use of nanoparticles - including carbon based - in polymer leads to new environmental issues (*e.g.* air, water, and soil pollution) [50]. For example, researchers have shown that release of titanium dioxide (TiO_2) nanoparticles in water results in biological accumulation and affects food chain [51]. If the impact of the TiO_2 nanoparticles on the environment is still under study, it was shown their toxicity change depending of their size, aspect ratio and UV irradiation, and this effect is enhanced at the nanoscale [52]. It is known that carbon-based nanoparticles are constantly released into air, however, the degree of their toxicity on cell and ecosystem is widely debated among several studies [53]. Researchers, nonetheless, reach a consensus on the limitation of nanoparticles

release in the environment. It was demonstrated that a nanocomposite with 2wt. % CNT incorporation release 12.6% particles than its neat counterpart under abrasion test [54]. In vitrimer networks, potential recovery of graphene was demonstrated from on disulphide BER [55], however, only extraction of powder was shown without further analysis of the recycled nanoparticles.

Herein, the effect of four types of graphene (GNP, GO, rGO, and silane epoxy bearing functionalised GO (GPTS-GO)) on an epoxy-based vitrimer is quantified. Nanoparticles are then extracted from the vitrimer matrix and their morphology and chemical change is characterised. Despite potential structural changes, reduction of chemical groups, or potential exfoliation/agglomeration, all nanoparticles are successfully recovered.

4.2 Material and methods

4.2.1 Materials

Bisphenol A diglycidyl ether (DGBEA) epoxy resin (Araldite LY 564) was purchased from Huntsman Ltd; sebacic acid (SA) and 1,5,7-triazabicyclo[4.4.0]dec-5-ene (TBD) were supplied by Tokyo Chemical Industry Ltd Be. Elicarb premium grade graphene powder was purchased from Thomas Swan. GO dispersed in water was purchased from Graphenea (0.4 wt. % concentration). rGO powder were kindly furnished by Tirupati Graphite Plc. 1,2,4-Trichlorobenzene (TCB), ethylene glycol (EG), acetone, and 3-glycidoxy-propyltrimethoxysilane (3GPTS) was purchased from Sigma Aldrich. The chemical structure of nanoparticles can be seen in Figure B-1. Table B-1 shows the chemical structure of the epoxy resin, SA, TBD, EG and 3GPTS. Table B-2 summarises the manufacturer data of the GNP and GO dispersion. All chemicals were used without further purification.

4.2.2 Nanoparticles preparation

GNP and rGO were used as received. GO were dry on a hot plate at 90°C for one day, the resulting powder were further crushed into a grinder. The powder was then left in a vacuum oven at 120°C overnight. Finally, the powder was grinded a second time to insure that most of agglomeration due to the hot plate drying was removed.

GPTS-GO were produced using the former GO. Firstly, 1 g of GO was dispersed in 4 ml of acetone by ultrasonication for 1 h. Then, 14.25 g of 3GPTS were added and the mixture was stirred overnight at 90°C under reflux (Figure B-2). The resulting mixture was centrifuged repeatedly at 8000 rpm for 10 min with water and acetone after which the wet powder was vacuum dried overnight at 60°C.

4.2.3 Sample preparation

Neat sample (*i.e.* without nanoparticles) was prepared with a 1:1 molar equivalent (meq) ratio of epoxy and SA, and 5% meq TBD of the epoxy groups. SA and TBD were added to the epoxy, and mixed for 24 h at 50°C until a white homogeneous liquid was obtained. The final mixture was then placed into a mould creating rectangular 60 mm × 60 mm × 5 mm and dog-bone specimens of dimensions 115 mm × 33 mm × 6 mm, according to ASTM standard 638 Type IV. The samples were degassed under vacuum for 2 h at 90°C to ensure removal of possible air bubbles created during mixing. Samples were then cured at 145°C for 8 h (ramp 1.7°C/min from room temperature to 145°C) and post-cured at 160°C for 8 h.

For nanocomposite samples, nanoparticles were first weighted and mix manually in the epoxy for 2 min. The mixture was sonicated for 30 min at 50°C and shear mixed for 2 h at 3000 rpm. After this step, the mixture epoxy-graphene was left to cool down before being mixed with SA as neat samples. For each type of particles a loading of 0.1, 0.5, and 1 wt. % was manufactured, their labelling is shown in Table 4-1. A schematic of the manufacture process is shown in Figure 4-1. To ensure minimum bubble amount within the final composites, GO samples required a longer time (4 h instead of 2 h) to fully degas due to high viscosity.

Table 4-1 Samples denomination.

Sample labels				
	GNP	GO	GPTS-GO	rGO
0.1 wt. %	01GNP	01GO	01GPTS	01rGO
0.5 wt. %	05GNP	05GO	05GPTS	05rGO
1 wt. %	1GNP	1GO	1GPTS	1rGO

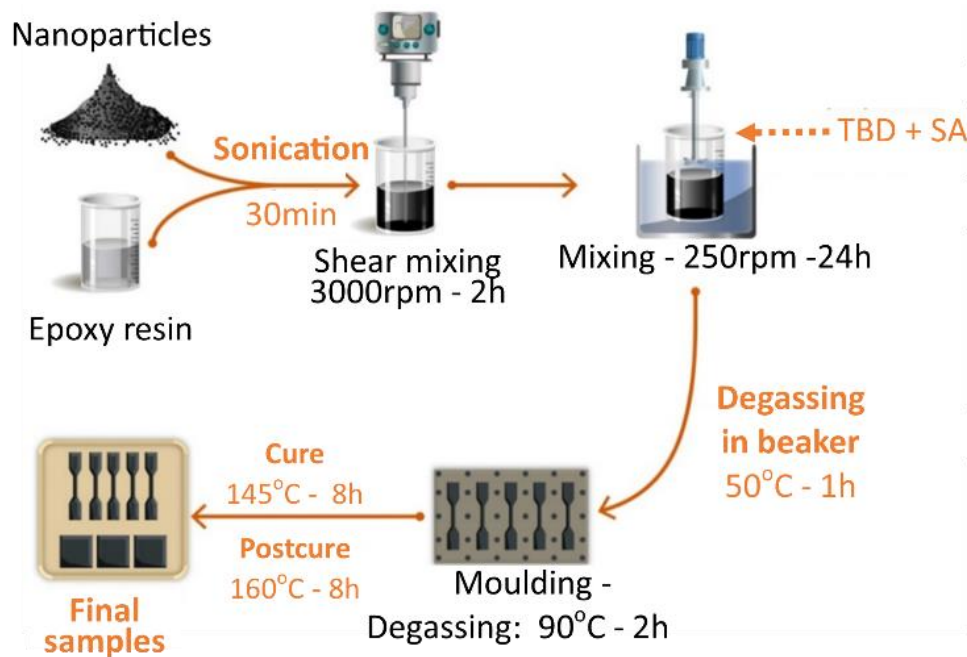


Figure 4-1 Schematic of the manufacture process to make GNP/GO/GPTS-GO/rGO samples. Neat samples was made from step 3 (Mixing at 250rpm for 24 h) of the process. Adapted from [56].

4.2.4 Nanoparticles recycling

Nanocomposite vitrimers were immersed in excess ethylene glycol at 180°C, after 2 h the resulting solution was sonicated for 2 h at 80°C and then heated at 180°C for 2 h. The resulting mixture was left to cool down at room temperature (RT), transferred into centrifuge tubes and acetone was added to the mix (ratio 50:50 acetone:solution). The samples were then centrifuged at 10 000 rpm for 10 min and all liquid was removed leaving only the particles at the bottom of the centrifuge tube. This step was repeated 3 times to ensure proper washing of particles. Acetone was then added to the particles and the solution was sonicated for 2 h at 50°C. Finally, the particles were vacuum dried at 80°C for 12 h (Figure 4-2). To calculate the yield of recycled particles, theoretical nanoparticles weight was calculated using the samples mass related to the loading of particles (*e.g.* for 1GNP $m_{sample} = 5g$ then $m_{particles} = 5 \times 00.1 = 50 \text{ mg}$).

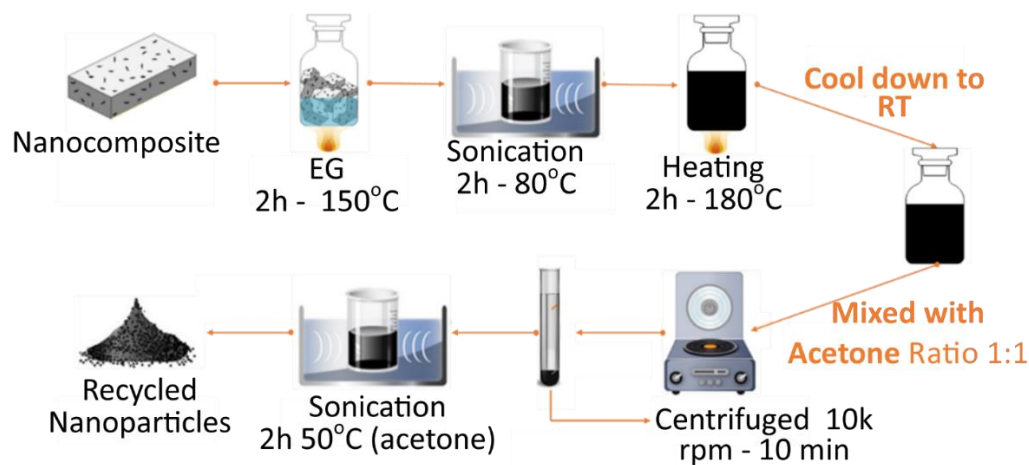


Figure 4-2 Schematic of the process to recycle graphene based nanoparticles from a vitrimer matrix. Adapted from [56].

4.2.5 Swelling and soluble fraction

Swelling studies were performed on samples measuring approximately 5 mm × 5 mm × 3 mm. Samples were weighed and their dimensions measured before being immersed in 1,2,4 trichlorobenzene (TCB). After one week immersion at 135°C (above T_g), the sample surfaces were wiped with fabric and stabilised at RT overnight to avoid any thermal expansion effects; weight was then recorded. Solvent was subsequently vacuum removed at 160°C overnight and samples were weighed again.

4.2.6 Mechanical test methods

Dynamic mechanical analysis (DMA), stress relaxation and creep experiments were performed using a Q800 DMA (TA Instruments, USA).

Measure of the glass transition temperature, T_g of samples were operated in the single cantilever mode on rectangular samples (35 mm × 15 mm × 4 mm) with a heating range of -50°C to 200°C at a rate of 3°C/min, and a measurement frequency of 1 Hz.

Creep was performed on rectangular samples (5 mm × 5 mm × 4 mm) cut from larger plates to observe bulk relaxation. For all samples, creep measurements were performed at several temperatures (from 100°C to 210°C). Samples were heated and left at 100°C for 5 min before applying a force of 0.1 MPa for 45 min. Samples were then left to relax for 15 min and heated to the next temperature, and measurement was then repeated.

Stress relaxation was performed on disk samples (10.15 mm × 4 mm) cut from larger plates. For all samples, stress relaxation measurements were performed at several

temperatures (from 100°C to 220°C). Samples were heated and left at 100°C for 5 min before applying a strain of 1% for 500 min. Samples were then heated to the next temperature, and measurement was then repeated.

Quasi-static tensile tests were performed on 3 dog-bone specimens (115 mm × 33 mm × 6 mm) using an Instron 5969 model testing machine and 2 kN load cell, following the ASTM standard 638 Type IV. Samples were tested at 20°C and a 3 mm/min test rate.

4.2.7 Spectral characterisation - XRD, Raman, ATR-FTIR, SEM, and XPS

X-ray Diffraction (XRD) was performed using a PANalytical X'Pert Pro Diffractometer (XRD5) in the 2θ range between 5 and 80° at a voltage of 40 mV and a current of 40 mA at a wavelength of 1.54 nm.

Raman spectroscopy was performed on a Renishaw RL633 class 3B Helium-Neon laser where 532 nm wavelength laser light was used. Three repeats were conducted on the powders where each scan consisted of 3 accumulations. Calculation of the average sp^2 cluster size L_D or rather the average distance between defects [57] is given in Equation B-1 and the defect density n_D with Equation B-2.

Attenuated total reflection infrared spectroscopy (ATR-FTIR) experiments were performed on samples using an INVENIO S Bruker spectrometer. Spectra were formed between wavenumbers 400 cm^{-1} and 4000 cm^{-1} and 64 scans were conducted per spectra.

Scanning electron microscopy (SEM) was performed on the same samples to allow comparison. Nanoparticles were suspended in acetone and sonicated for 15 min, to ensure an evenly dispersed solution. To ensure a more representative observation of graphene in the vitrimer, the time of sonication was limited to observe “semi-agglomerate” particles. Samples were pipetted onto mounted single crystal silicon chips. A SEM Tescan MIRA3 was used with a 10kV incident electron beam.

X-ray photoelectron spectroscopy (XPS) was carried out using an Axis Ultra Hybrid spectrometer (Kratos Analytical, Manchester, United Kingdom), with a monochromated Al $K\alpha$ X-ray radiation at 1486 eV (10 mA emission at 15 kV, 150 W), under ultra-high vacuum at a base pressure of 1×10^{-8} mbar. Samples were pressed onto conductive copper tape. A charge neutraliser was used to remove any differential charging at the sample surface. Parameters for calibration of binding energy (BE) scale, and spectral deconvolution follows procedure developed in previous work [13], [58]. To confirm functionalisation of GO to

GTPS (addition of silane epoxy bearing function), Si content was calculated from survey data on all samples. However, due to the low content of Si atoms, analysis of high resolution (C1s) spectra was made without Si-C bonds to limit fitting and convolution artefacts.

4.3 Results and discussions

4.3.1 Properties of nanoparticles

Nanoparticle atomic compositions was obtained by XPS, the survey spectra are shown in Figure 4-3 and the atomic content for each particle is given in Table B-3. Some differences are observed with the manufacturer data (Table B-2). GNP have a lower carbon content ($\approx 94\%$) possibly due to some oxygen contamination during transport and storage. GO particles exhibit a much lower oxygen content than the manufacturer data ($\approx 25.7\%$ compared to 49-56%). The thermal reduction that GO undergoes while being dried from the water solution could explain this variation. Nonetheless, the oxygen content remains high enough compared to GNP and rGO (5.5% and 7.2%, respectively). GPTS-GO exhibits a higher oxygen content (34.5%) and a Si content of 7.5% confirming that functionalisation of GO by the silane epoxy bearing compound was successful. The high resolution of C1s is discussed later when comparing neat particles and their recycled counterparts.

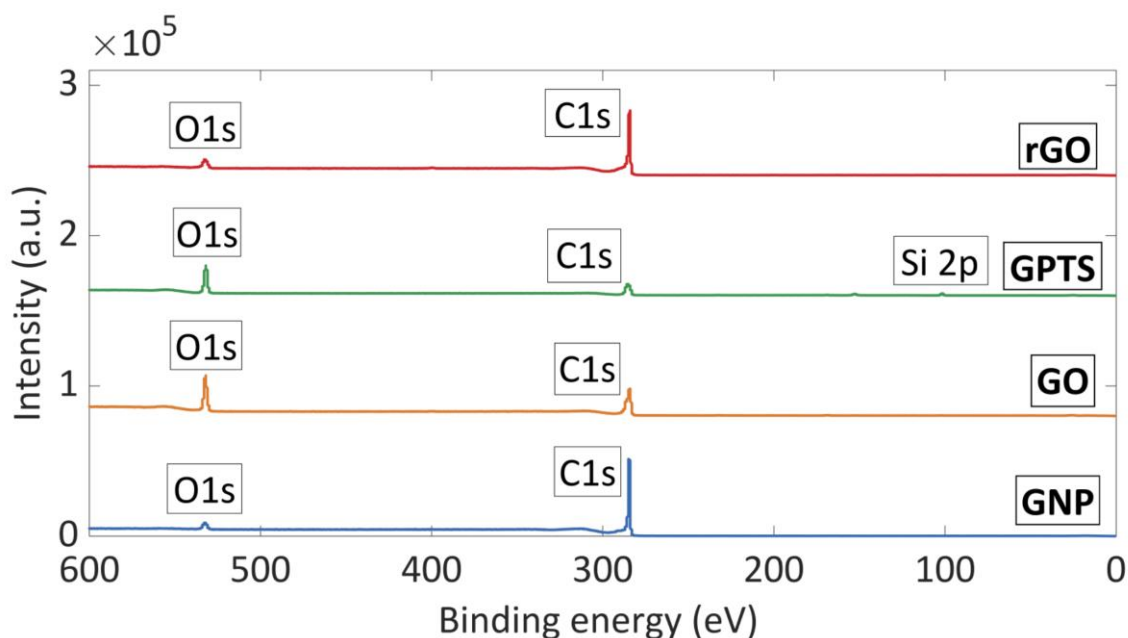


Figure 4-3 Wide survey XPS spectra of neat particles used in this study (GNP, GO, GPTS-GO, and rGO).

Crystalline structure of neat particles obtained by XRD is shown in Figure 4-4. GNP particles exhibit the characteristic peak of graphitic material at 26.41° , corresponding to the (002) plane crystalline structure attributed to the presence of sp^2 hybridised carbon. The other peaks 42.2° , 44.35° and 56.6° correspond to the (100), (101) and (004) planes, respectively [59]. GO exhibits a strong peak at 10.4° indicating higher d spacing between layers of graphene due to the introduction of oxygen and hydrogen atoms. A broad (002) peak is observed between 16° and 25° possibly due to some thermal reduction as also suggested by XPS data during the drying of GO. The small peak observed at 26.4° further confirm this assumption. The neighbouring peak at $\approx 25.3^\circ$ is attributed to graphitic impurity usually found in commercial GO [60]. GPTS-GO data show similar peaks to the GO pattern with the exception of the quenching of the (001) peak plane, indicating grafting of the GPTS function was achieved [61]. rGO exhibits typical reduced graphene oxide peaks at 26.41° (002) and 42.2° (100) [62].

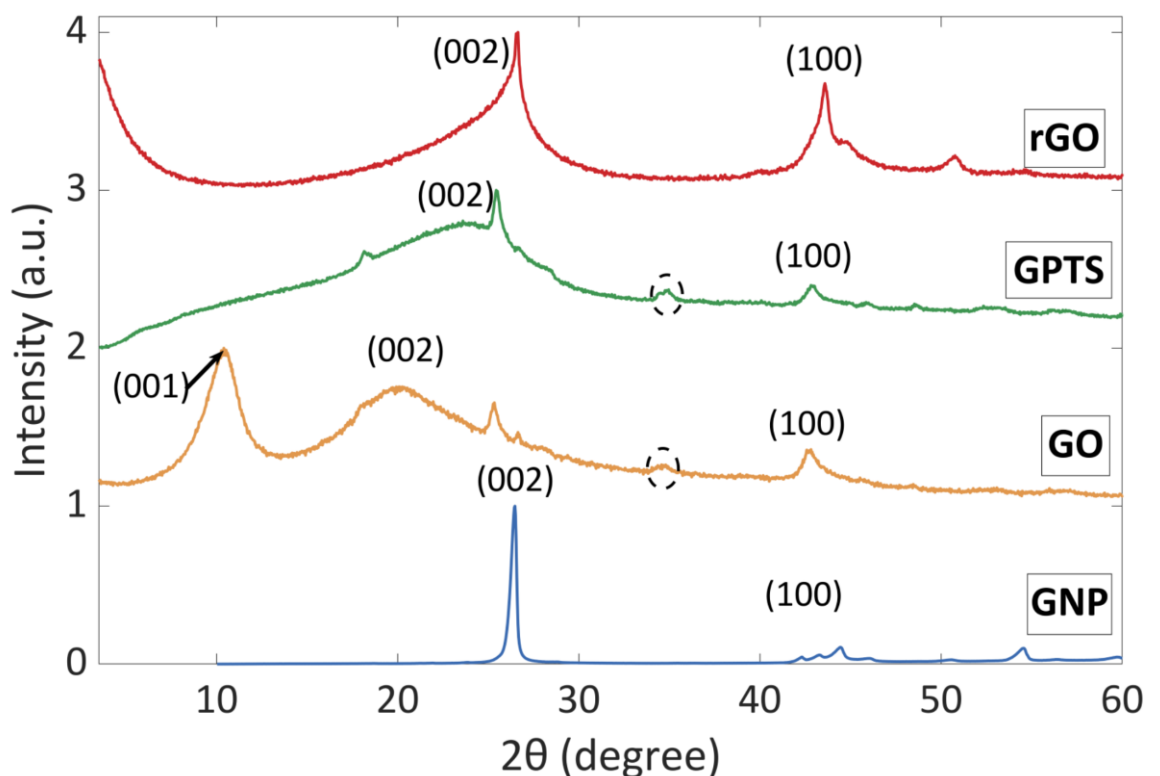


Figure 4-4 XRD pattern of neat particles used in this study - graphitic impurity of GO and GPTS-GO are indicated by dashed circle.

4.3.2 Properties of nanocomposites

Crystallinity of enhanced graphene vitrimer is shown in Figure 4-5. The only crystalline peak observed is the (002) plane at 26.41° for all GNP samples (Figure 4-5a) and for 1GO sample (Figure 4-5b). GNP samples (Figure 4-5a) exhibit a shift to the left of the peak compared to the neat vitrimer, however, the shift remains the same for any loading (0.1, 0.5, and 1 wt. %). For functionalised nanoparticles (GO, GPTS-GO, and rGO), this shift is translated progressively to the right concomitantly with increased content of reinforcements (Figure 4-5b, c and d).

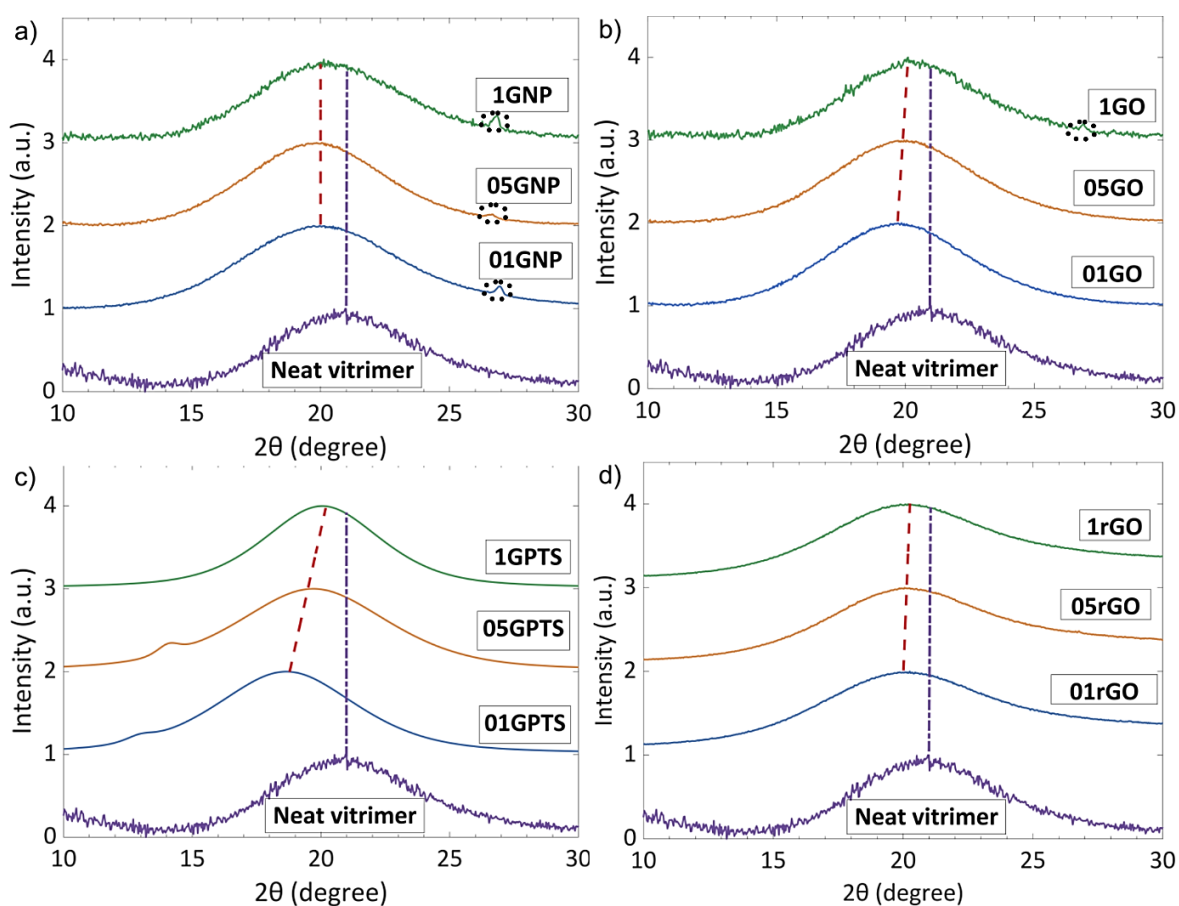


Figure 4-5 XRD pattern of manufactured nanocomposites: a) GNP samples, b) GO samples, c) GPTS-GO samples and, d) rGO samples – Red dotted lines shows the trend of amorphous polymer shift peak for nanocomposites samples, Purple dotted lines shows the position of the top of the amorphous peak of the neat vitrimer, (002) plan is shown by dashed circle; for colours code, reader should refer to online version of this thesis.

The amorphous polymer peak shift gives some indications towards bonding between nanoparticles and matrix. A peak shift in XRD patterns can be associated to several causes: stress/strain state [63]–[65], composition change [66]–[69], phase change [66],

[70], or crystallographic orientation [71]. Usually, these variations are observed for nanoparticles structure changes or crystalline structures (*i.e.* semi crystalline polymer) and not for amorphous polymer peak. The vitrimer area is a recent research field with limited literature related to nanocomposites and use of functionalised particles. Therefore, the current results can be analysed carefully to assume possible bonding between vitrimer matrix and nanoparticles. A change in crystallographic orientation is not possible in an amorphous polymer matrix and composition or phase change is not observed in FTIR data (Figure B-4). Hence, in this study, an amorphous polymer shift is assumed to be induced only by residual stress/strain occurring during the manufacture process (*e.g.* heating/cooling). For the particles with the lowest functionality (rGO) the amorphous peak shift is barely visible with increasing particles content. This indicates that residual stress within the nanocomposites is dependant of (functionalised) particles loading. As the functionalisation of nanoparticles is supposed to enable bond exchanges between nanoparticles and the polymer matrix, it is likely that a higher concentration of these (functionalised) particles allows a faster relaxation of residual stress (induced by the nanoparticles inclusion) during the cooling stage of the nanocomposites manufacture. Therefore, functionalisation of nanoparticles (GO and GPTS) led to proper covalent bonding with the vitrimer matrix as the shift is enhanced with increased loading. GNP sample amorphous peak remain at the same angle with different loadings demonstrating no bonding with the vitrimer. However, this analysis would require more studies concerning vitrimers, the functionalisation of nanoparticles and their weight loading to be confirmed.

Swelling and gravimetry for crosslinking confirmation

Swelling ratios of nanocomposites are shown in Figure B-3. The initial value of the neat sample is $\approx 61\%$. GNP samples show similar swelling behaviour: from $\approx 55\%$ to $\approx 60\%$ for 05GNP and 1GNP. GO samples exhibit a wider change with particles loading, 01GO has a swelling ratio of $\approx 65\%$, 05GO decreases to $\approx 51\%$, and 1GO exhibits the highest value of all samples at $\approx 72\%$. GPTS samples exhibit a similar trend than GO samples and GNP. However, the decrease is less significant with values from $\approx 61\%$ (01GPTS) to $\approx 57\%$ (1GPTS). Swelling ratio of rGO samples range from $\approx 67\%$ (01rGO) to $\approx 58\%$ (05rGO) and $\approx 57\%$ (1rGO). All samples - except 1GO - show a similar swelling ratio than the neat vitrimer (61%).

Soluble fraction of nanocomposites is shown in Figure 4-6. The initial value of neat sample is $\approx 25.5\%$. GNP samples show a decreasing trend of solubility with value from $\approx 32.5\%$ (01GNP) to $\approx 22.5\%$ (1GNP). GO, GPTS, and rGO samples exhibit a similar trend, increasing their solubility with particles content. GO samples display the widest change with particles loading from $\approx 23\%$ to $\approx 34\%$ from 01GO to 1GO. GPTS samples solubility evolution is more stable ranging from $\approx 27\%$ (01GPTS) to $\approx 31\%$ (1GPTS). rGO samples displays the lowest value of soluble fraction with a value of $\approx 16\%$ (01rGO) increasing to $\approx 26.5\%$ for 1rGO. Further confirmation that the nanocomposites chemical composition is similar to the pristine vitrimer is shown using FTIR spectroscopy (Figure B-4).

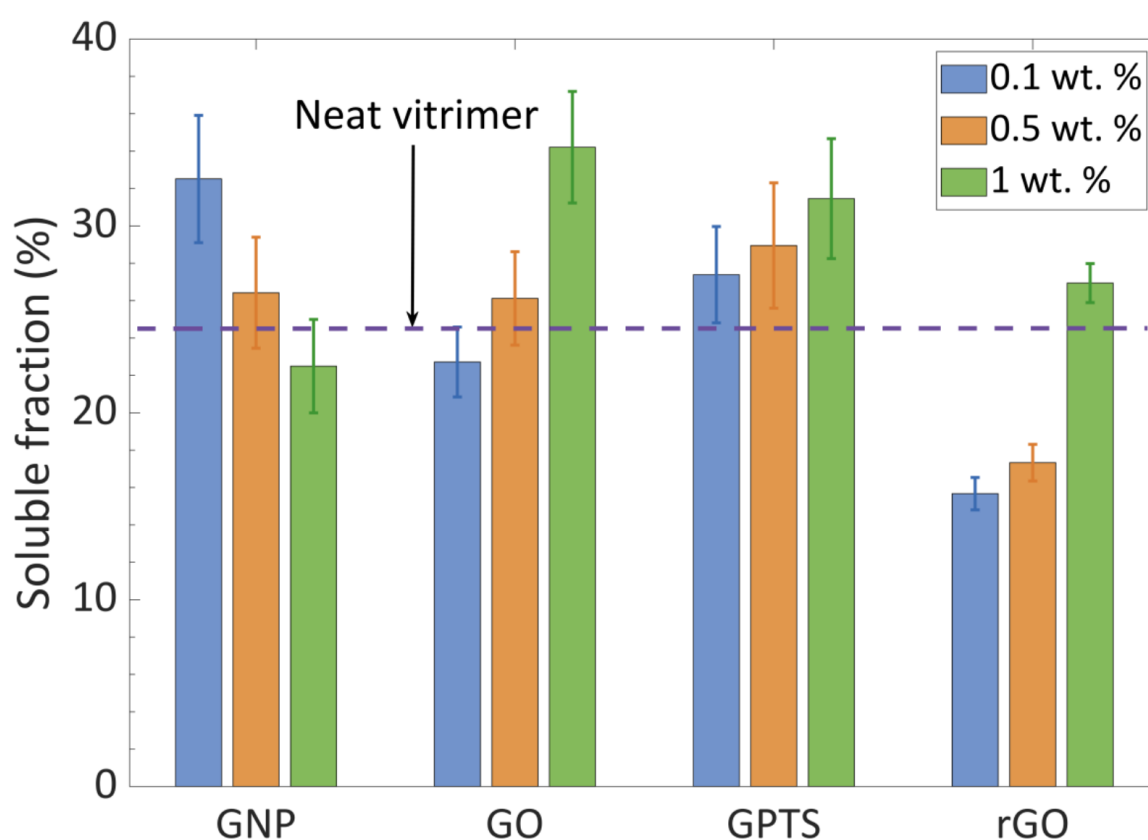


Figure 4-6 Soluble fraction of nanocomposites compared to swelling ratio of vitrimer without nano-reinforcement (purple dotted line) - samples were left at 135°C in TCB for 7 days.

Soluble fraction results suggest that the network is less cross-linked with increasing amount of GO, GPTS and rGO, all these particles have a possibility to react with epoxy and SA used in this study as suggested by XRD data. It is possible that unreacted monomers concentration are getting higher with increasing amount of nanoparticles or the amount of network defects (*i.e.* dangling chains, isolated microgel fragments, *etc.*) is increasing. GNP

samples follows an opposite trend with particles loading increasing, acting as an unreactive thermal diffuser which improve the heat distribution during polymerisation. Swelling ratio do not follow the same trend than the soluble fraction, meaning that the crosslink density varies with increased amount of functionalised graphene (GO, GPTS-GO and rGO). However, these variations remain close to the neat vitrimer's swelling ratio indicating a network with similar crosslink density with the embedded nanoparticles.

Stress relaxation to confirm strong former glass behaviour

The networks capacity to relax stress was assessed to determine the impact of graphene on the system. All samples exhibit full stress relaxation as shown in Figure 4-7a, b and Figure B-5 to Figure B-8. The relaxation time $\tau(G/G_0)$ is determined by fitting through a single exponential decay. For example, at 180°C, τ is about 286 s for 1GNP, 35 s for 1GO, 47 s for 1GPTS, 55 s for 1rGO and $\tau \approx 90$ s for neat sample (Figure 4-7a). Values of τ depending on graphene type and loading are disparate compared to the neat vitrimer with temperature change. GO samples, 01GPTS, 1GPTS and 1rGO have shorter relaxation time than the former vitrimer (Figure 4-7b) at 160°C and 180°C. The highest relaxation time at these two temperatures are for 01GNP, 1GNP, 05GPTS, and 05rGO.

Energy activation (E_a) has been calculated from stress relaxation experiments through Arrhenius plot (Figure 4-7c) and values are displayed in Figure 4-7d while experimental results are shown in Figure B-5 to Figure B-8. Sample 01GNP has a higher E_a than the former vitrimer value (122 kJ.mol⁻¹ compared to 111 kJ.mol⁻¹). 05GNP has a similar value with 124 kJ.mol⁻¹ and 1GNP decreases to 104 kJ.mol⁻¹. Contrary to GNP samples, GO samples have thermal stability with loading of particles (128 kJ.mol⁻¹, 128 kJ.mol⁻¹ and 121 kJ.mol⁻¹ for 01, 05, and 1GO, respectively). The activation energy of GPTS samples is higher with 133 kJ.mol⁻¹, 137 kJ.mol⁻¹ and 118 kJ.mol⁻¹ for 01, 05, and 1GPTS, respectively. The energy activation of rGO samples is overall lower than other samples depending of particles loading starting 119 kJ.mol⁻¹ for 01rGO, 101 kJ.mol⁻¹ for 05rGO and finally 115 kJ.mol⁻¹ for 1rGO. Creep test confirm that the network can flow faster while increasing temperature, data are shown in Figure B-9 to Figure B-12.

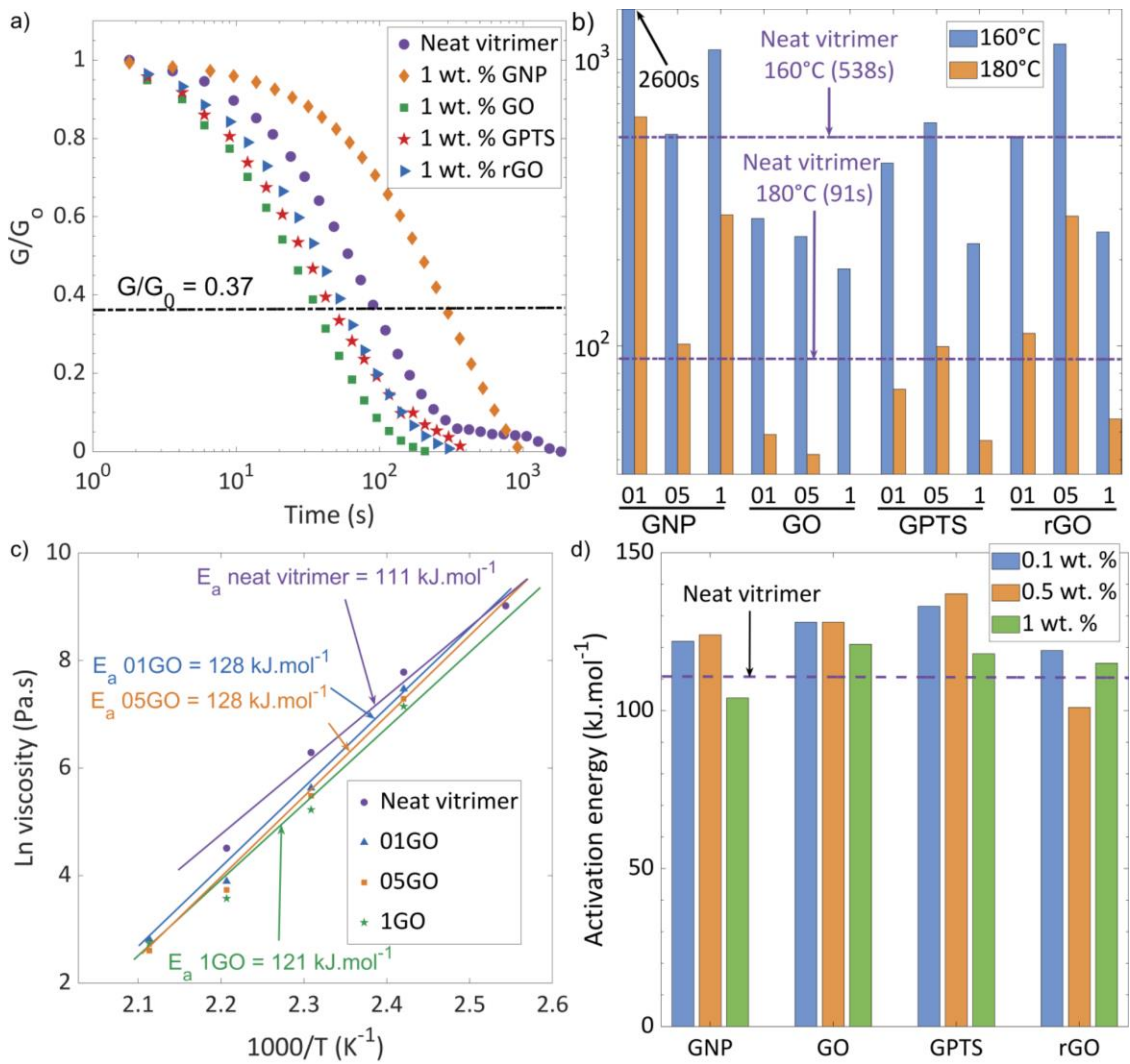


Figure 4-7 Stress relaxation of different nanocomposites: a) relaxation of 1wt. % samples compared to neat vitrimer at 180°C, b) Relaxation time τ for all samples at 160°C and 180°C, y axis is at log scale, c) Arrhenius plot for GO samples and neat vitrimer, and d) bar chart of activation energy for all nanocomposites compared to neat vitrimer (purple dotted line).

The inclusion of nanoparticles on the energy activation and capacity to relax stress of vitrimers samples has shown disparate/varying results. E_a is generally decreasing when increasing loading content. It is believed that the inclusion of nanoparticles act as a local heat transfer point, helping to reduce the energy barrier to achieve the bond exchange between ester and acyl functions. In the case of high functionality with covalent bonds between the matrix and nano-reinforcements (GO and GPTS-GO), a higher energy barrier must be overcome to exchange bonds between particles/matrix, rising the overall energy activation of nanocomposites. It should be noted that despite covalent bonding between nanoparticles and the vitrimer, the network remains mainly composed of β -hydroxyesters between epoxy and SA. E_a is mainly dependant of the network nature (structure, type of

bond, and catalyst), so the inclusion of low amount of nanoparticles (1 wt. %) does not show any particular impact of the sample reactivity. Nonetheless, as the particles act as a heat transfer point in a system which requires thermal energy to initiate its activity, it would be expected that nanocomposites relaxes stress faster. This time should be enhanced by the addition of free functional groups when particles are highly functionalised. Raw results showed faster relaxation in some samples at certain temperatures (*e.g.* GO samples at 160°C and 180°C). Other samples were taking longer time to relax the stress than the neat vitrimers, notably 05GPTS and 05rGO. As stress relaxation is linked with the mechanical properties of the network (*i.e.* stiffer material would have more difficulties to relax stress), the time τ of each samples was divided by their own Young's modulus and compared to the neat vitrimers values (Figure 4-8) and called τ' (which is corresponding to the inverse of viscosity).

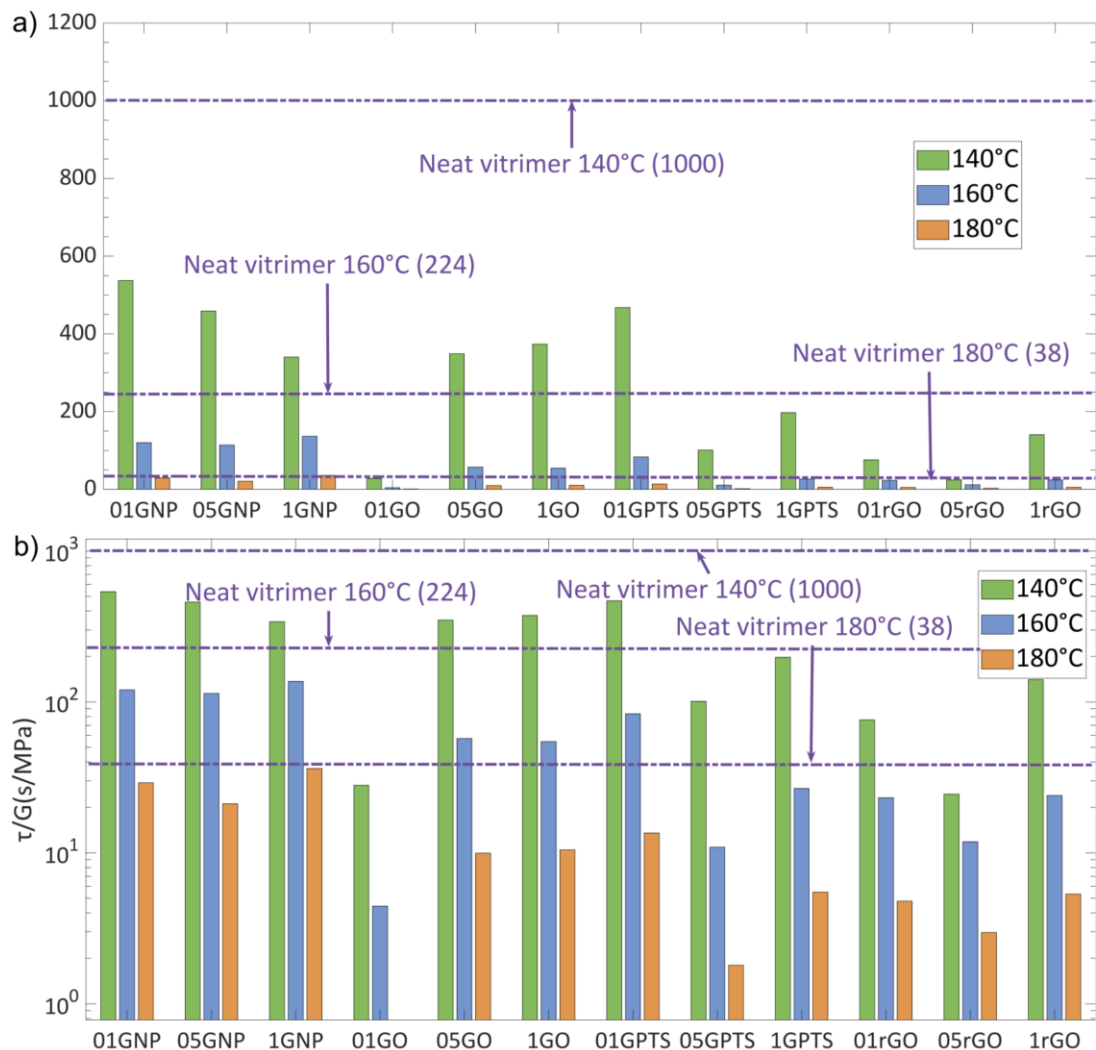


Figure 4-8 Relaxation time of nanocomposites divided by their own Young's modulus: a) Standard scale, b) y axis in log scale for comparison. 01GO time of relaxation at 180°C is not visible due to its small value (49 s).

From this figure, it becomes evident that the network has a faster relaxation time when nanoparticles are added to the matrix. The relative time τ' is faster for all nanocomposites at the same temperature compared to the neat vitrimers. This shows that the particles actually contribute to help a faster bond exchange due to their thermal impact (and also their functionalisation). From Figure 4-8b, it can be seen that the GNP and rGO samples displays barely any change in relaxation time with particles loading. On the other hands GO samples increase their relaxation time between 0.1 and 0.5 wt. % loading to then stabilise between 0.5 and 1 wt. % loading. GPTS samples exhibits an inverse initial trend by decreasing τ' between 01GPTS and 05GPTS. The duration of time then increases between 05GPS and 1GPTS. This shows that the functionality of particles and the introduction of free radicals impacts the capacity of the vitrimer to relax stress. The increased time τ' of GO samples can be related to a previous study showing that increasing particles loading hinder the chains motion and may make relaxation more difficult [72]. GPTS samples exhibit a particular behaviour. Whereas GO are not supposed to agglomerate as much as GNP or rGO, GPTS samples can agglomerate when not stored in solvent (*e.g.* acetone) [73]. Agglomeration and the bi-functionality of these particles (silane epoxy bearing and hydroxyl functions), could explain an initial decrease by introducing more epoxy and acyl functions. A possible agglomeration with higher particle loading is likely to slightly increase the relaxation time τ' . Nevertheless, from stress relaxation, it is confirmed that the network has an Arrhenius behaviour at high temperature while being cross-linked.

Mechanical properties at small and large deformations

DMA results for all samples are displayed in Figure 4-9, and Figure B-13 shows the measured glass transition temperature from the tan delta peak. The glass transition temperature of samples remain close (33°C to 40°C) to the neat matrix (≈ 40 °C). Overall the damping properties for the functionalised particles (GO, GPTS and rGO) appear to be stable (compared to its initial value of 1.3) as shown in the insets of Figure 4-9. However, GNP samples exhibit the highest change in damping compared to other samples ranging from 1.4 to 0.7.

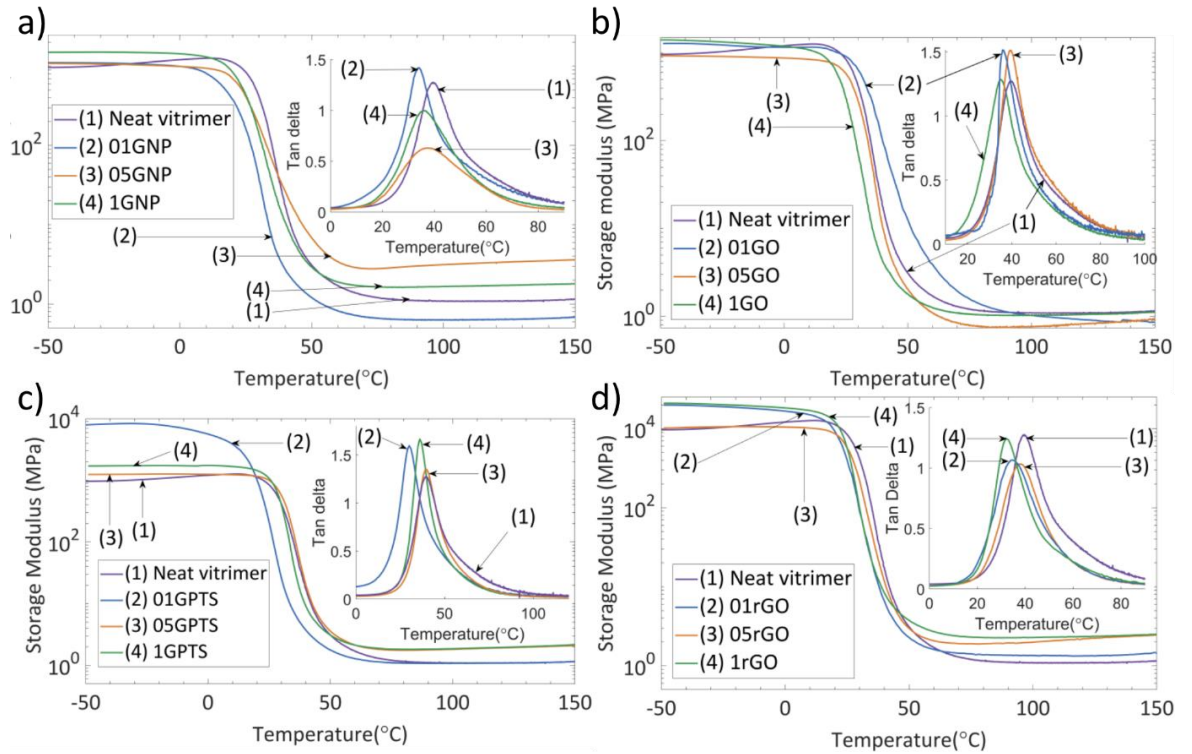


Figure 4-9 DMA results for all samples compared to raw vitrimer: a) GNP samples, b) GO samples, c) GPTS-GO samples, and d) rGO samples.

Tensile test were performed to measure the mechanical properties improvement of nanocomposites. Young's modulus has been calculated between 60-100% strains (Figure 4-10). All samples exhibit a higher Young's modulus than the neat vitrimer ($E_{\text{neatvitrimer}} \approx 0.5$ MPa), however, noticeable difference are observed between particles type and loadings. The best improvement observed for GNP samples is with a 0.1wt. % and 1wt. % loading, doubling the neat vitrimer Young's modulus value (from ≈ 0.5 MPa to ≈ 1 MPa). GO samples display similar behaviour with a higher increase with 0.1 wt. % (1.3 MPa). Whilst GTPS and rGO samples highest Young's modulus values are found with 0.5 wt. % loading (1.4 MPa and 1.5 MPa, respectively).

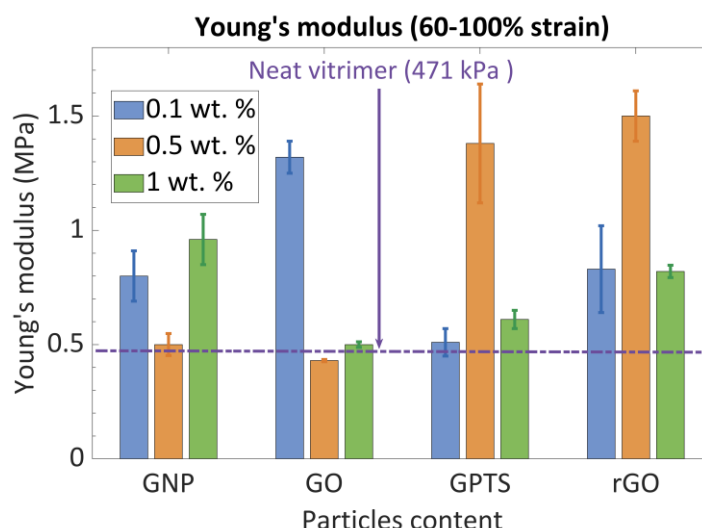


Figure 4-10 Young's modulus of nanocomposites calculated between 60-100% strain.

Breaking strain and ultimate tensile strength (UTS) are presented in Figure 4-11, typical stress strain curves can be found in Appendix B Figure B-14 and calculated values in Table B-4 to Table B-7. All nanocomposites exhibit lower breaking strain value than the neat vitrimer ($\approx 320\%$), ranging from $\approx 100\%$ (1GNP and 01GO) to $\approx 200\%$ (1GPTS). UTS (Figure 4-11.b) is increased compared to neat vitrimer (≈ 0.8 MPa) except for samples 05GO (≈ 0.8 MPa) and 1GO (≈ 0.7 MPa). The maximum increase is measured for 05GPTS (≈ 2.7 MPa) and 05rGO (≈ 3 MPa).

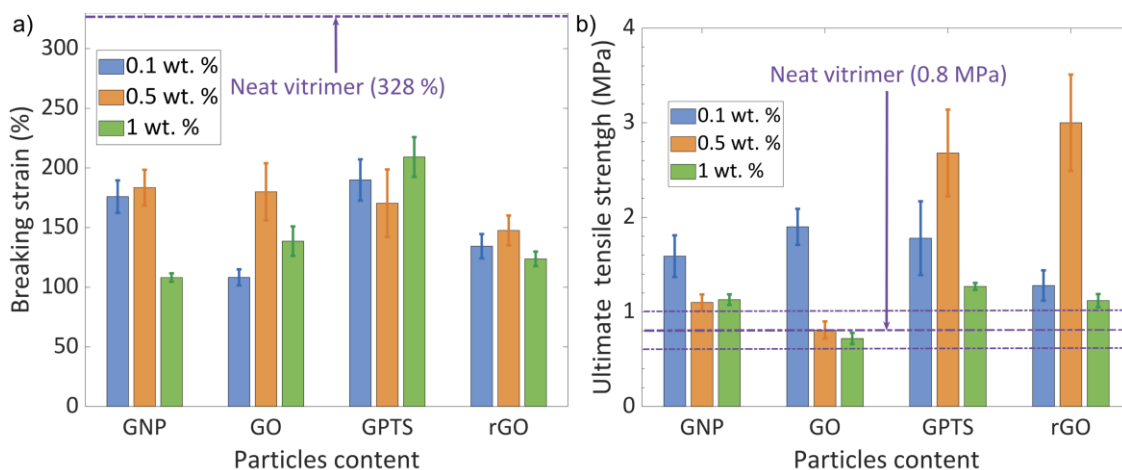


Figure 4-11 a) Breaking strain of nanocomposites, b) Ultimate strength of nanocomposites - smaller dotted line have been added for the UTS of neat vitrimer to show that lower UTS of nanocomposites (01GO and 05GO) are included in the measured errors of the neat vitrimer's UTS.

It is known that adding nanoparticles to a polymer matrix initially increases the Young's modulus, then reach a maximum value and then decreases as the reinforcements act as local stress points within the material [74]. In this study, the best enhancement for

GNP and GO are close to 0.1 wt. %, and 0.5 wt. % for GPTS and rGO. GNP particles, without functionalisation, are more prone to agglomerate and poorly transfer load, showing the lowest improvement among reinforcement type. As 01GO, 05GPTS, and 05rGO present the highest Young's modulus value, and likely have the better dispersion among samples, the load transfer between matrix and nano-reinforcements is optimal, giving as well the highest UTS results. It should be noticed that 1GPTS has also the higher UTS among all 1 wt. % loading (1.3 MPa vs 1.1 MPa, 0.72 MPa, and 1.1 MPa for 1GNP, 1GO, and 1rGO, respectively). The GPTS samples display the overall highest UTS improvement, as the nanoparticles possess both hydroxyl and epoxide functional group, they are likely to have the best bonding with the matrix. A decrease of the breaking strain is expected when increasing the material stiffness, however, GPTS and rGO samples display a better stability in breaking strain values due to the covalent bonding with the network. Possible chemical side reactions during samples manufacturing with GO samples might explain some heterogeneity on their mechanical behaviour. As mentioned in the experimental section, a longer time was required to degas the GO samples. Initially associated to be due to a higher viscosity, the probable reduction of GO followed by agglomeration under the TBD (strong base) influence is another possibility to consider. This behaviour requires further study to understand GO chemical stability during the cure of base catalysed polymerisation in this kind of polyester networks (chemical reduction, water bi-product impacting the mechanical properties of the final polymer, etc.).

4.3.3 Properties of recycled particles

Yield of recycled particles

After recycling, the efficiency of the method was determined by calculating the yield of recovered particles (Table 4-2). Yield of GNP and rGO particles is $\approx 92\%$ and $\approx 93\%$ respectively, showing that almost all nanoparticles were recovered from the nanocomposites. GO and GPTS-GO yield is much lower with values of 73% and 48% respectively. SEM micrograph (Figure B-15) shows that recycled particles do not have any residues of vitrimer. Further explanation of the yield values are developed with the help of spectroscopy.

Table 4-2 Calculated yield of recycling for nanoparticles - same recovery yield for GNP and rGO can be found in [75].

Samples	Mass of composite (g)	Wt. % of particles	Theoretical mass of particles (g)	Recycled mass (g)	Yield (%)
GNP	32.25	1	0.3225	0.2978	92
GO	30.73	1	0.3073	0.2243	73
GPTS-GO	21.98	1	0.2198	0.1055	48
rGO	30.32	1	0.3032	0.2814	93

X-ray photoelectron spectroscopy for recycled nanoparticles

Atomic compounds (at. %) of nanoparticles (original and recovered) have been calculated using survey spectra (Figure B-16) and are given in Table B-8. It is noticeable that in all recovered particles, nitrogen is found, however, the increase between original and recovered particles is a maximum of $\approx 1.8\%$ (for GO and GPTS-GO). GPTS-GO particles have a lower silicon atom content (1.5% compared to 7.5% initially) after recovery, while GO particles display an increase of 0.9% silicon atoms content. To limit artefacts, C_{1s} spectra analysis were performed without the inclusion of C-Si and C-N bonds. The deconvolution of C_{1s} spectra is shown in Figure 4-12, and contribution of individual chemical moieties are given in Table S9. GNP nanoparticles show a 32.8% decrease in C=C bonds while increasing its C-C and C-O compounds (+18.3% and +12.3% respectively). A slight increase in C=O and π - π stacking (+0.9% and +1%) is observed. GO particles demonstrate an increase in C=C (+5.2%) and C-O (+4.8%) compounds while their C-C component decreases of 10.7%. GPTS-GO shows an increase of 39.2% in C=C component and decreasing their C-C and C-O components by 4.8% and 13.8%. rGO particles shows a decrease in C=C (-27.4%), and π - π^* interaction (-4.2%) while increasing its C-C (+19%), C-O (+12.5%) chemicals moieties. The C=O interaction remains similar (+0.3%).

The low amount of nitrogen, from XPS data, found in all recovered particles is likely due to some doping of the graphene surface from the transesterification catalyst (*i.e.* TBD) [76], [77]. On the other hand, the Si content found in recovered GO is possibly due to some glass pollution from samples storage. The C_{1s} analysis of recovered GNP (higher oxygen content) associated with the slight increase in C=O and π - π^* stacking lead to the conclusion

that some hydroxyl functionalisation happened on their edges during recycling without impacting their surface and structure. Further analysis of XPS data are given with help of XRD data.

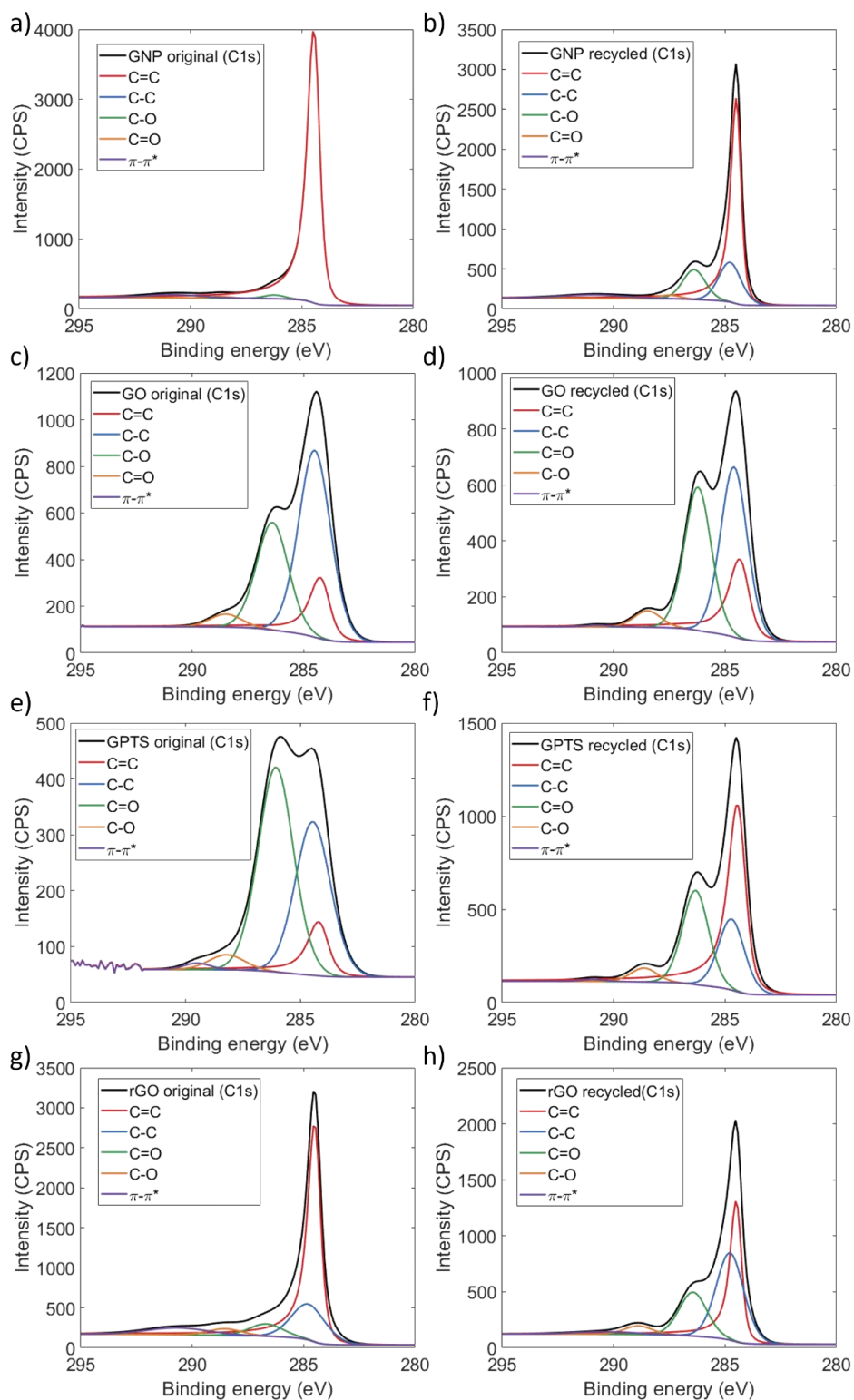


Figure 4-12 High-resolution core-level C_{1s} of original and recycled nanoparticles: a) original GNP, b) recycled GNP, c) original GO, d) recycled GO, e) original GPTS-GO, f) recycled GPTS-GO, g) original rGO, h) recycled rGO - for colours code, reader should refer to online version of this thesis.

X-ray diffraction spectroscopy for recycled nanoparticles

To further understand and confirm XPS data, XRD patterns are shown in Figure 4-13; distances (d) between graphene layers are given in Table 4-3, calculated from Bragg's law using the angle for the (002) plane direction. GNP patterns of original and recovered (Figure 4-13.a) look remarkably similar, and distance calculated between graphene layers remains the same. GO patterns (Figure 4-13.b) display radical changes with full quenching of the (100) peak of original GO and show a broader (002) plane peak. Interlayer distance is decreased by 0.6 nm. GPTS patterns (Figure 4-13.c), as for GO patterns, exhibit changes from original to recovered particles. The main peaks of original GPTS are found in the recycled pattern, an apparition of some crystalline structure can be perceived (peaks at 29.5°, 43.5° and 57.5°). The interlayer distance increases from 0.36 nm to 0.41 nm. rGO patterns are fairly similar between original and recycled particles, a disorder is introduced by the broadening of the (002) plane peak.

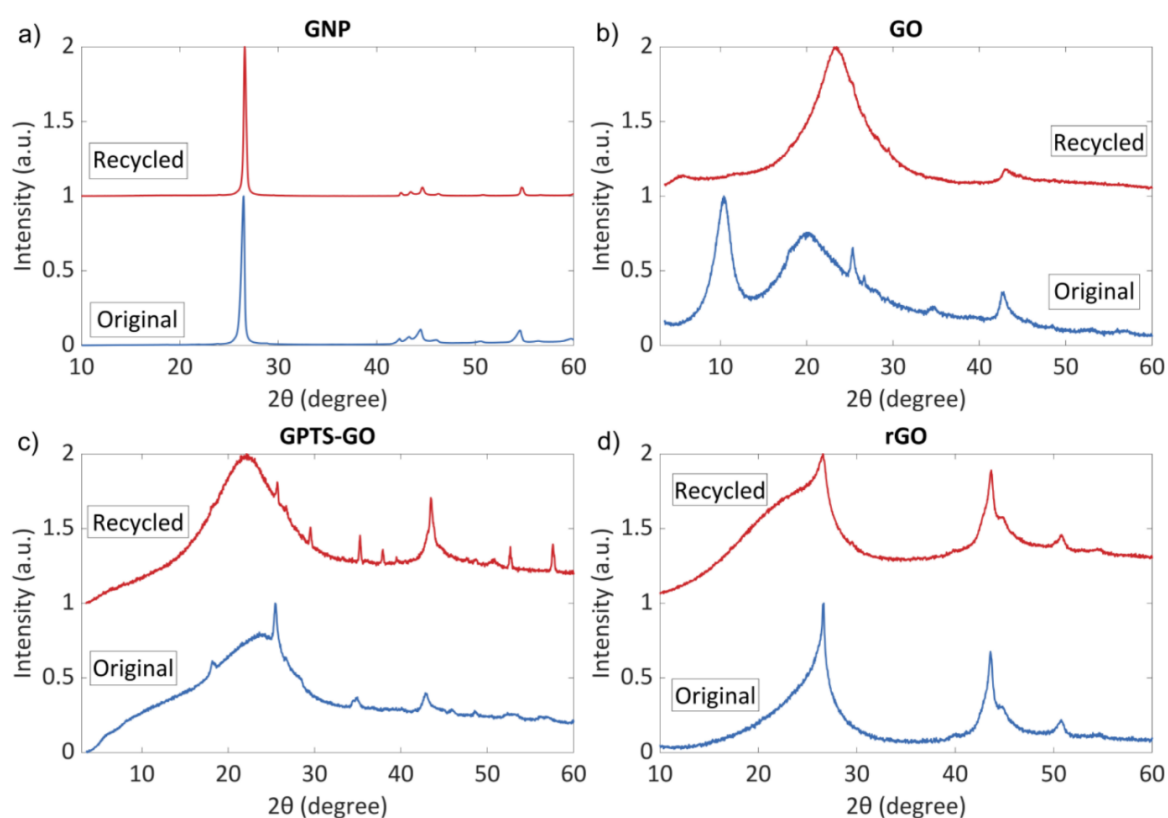


Figure 4-13 XRD patterns for original and recycled nanoparticles: a) GNP, b) GO, c) GPTS-GO and, d) rGO.

Despite a higher oxygen content (Table B-8), it is likely that edges functionalisation remains at too low concentration to be detected *via* XRD (Figure 4-13). A partial reduction of GO was found after extraction from vitrimer. The quenching of the (001) plane in the

XRD pattern confirms this assumption – these pattern matches similar results from literature where GO were partially reduced while keeping an oxygen content above 20% [78].

The decrease of silicon content for GPTS suggests that the functionalisation is pulled off from the particle during recycling and further chemical reduction is achieved as for GO particles. The increase of graphitic peak (002) and (100) in XRD data, confirms that most of the GPTS functions were removed from original GPTS during recycling with further chemical reduction. Remaining silicon atoms at the particles surface have likely bonded with some of the oxygen content. During this reduction, some layers of GPTS stacked together with Si atoms between sheets which is confirmed by the increased in the interlayer distance (from 0.36 nm to 0.41 nm). Similar peaks at 29.5°, 43.5° and 57.5° have been observed in literature for Si functionalised graphitic particles [79]–[81]. For rGO particles, the decrease in C=C and π - π^* with the increase of oxidation indicates that hydroxyl are added to the edges and surface. A disorder is introduced by the broadening of the (002) plane XRD peak which results of a chemical reduction compared to a thermal reduction [62].

Table 4-3 Distance between graphene layers calculated using Bragg's law with the top of (002) plane peak.

	GNP		GO		GPTS-GO		rGO	
	Original	Recycled	Original	Recycled	Original	Recycled	Original	Recycled
d (nm)	0.35	0.35	0.45	0.39	0.36	0.41	0.34	0.35

RAMAN spectroscopy to compare original and recycled particles

Raman spectroscopy was performed, and spectra are shown in Figure 4-14. From these data I_d/I_g , I_{2d}/I_g ratios, average sp^2 cluster size L_D (average distance between defects) and the defect density n_D were calculated and presented in Table 4-4. GNP and rGO nanoparticles (both original and recycled particles), exhibit the three known peaks at $\approx 1333\text{ cm}^{-1}$ (D band, associated to the crystal structure of carbon), $\approx 1582\text{ cm}^{-1}$ (G band, associated with amorphous carbon material, corresponding to the C-C planar breathing mode) and at $\approx 2660\text{ cm}^{-1}$ (2D band second order of two phonon process and gives structural information on carbon based materials) [82], [83]. The D' band located around

1620 cm^{-1} , also visible for these particles, is associated to the same phenomenon than the D band [84]. GO and GPTS-GO particles exhibit D, G and 2D bands such as GNP and rGO, although the 2D is barely visible. The G+D band appears in these spectrum but remains close to zero. All ratios I_{2D}/I_G and I_D/I_G decrease compared to original particles, n_D follows the same trend, while L_D increases (Table 4-4).

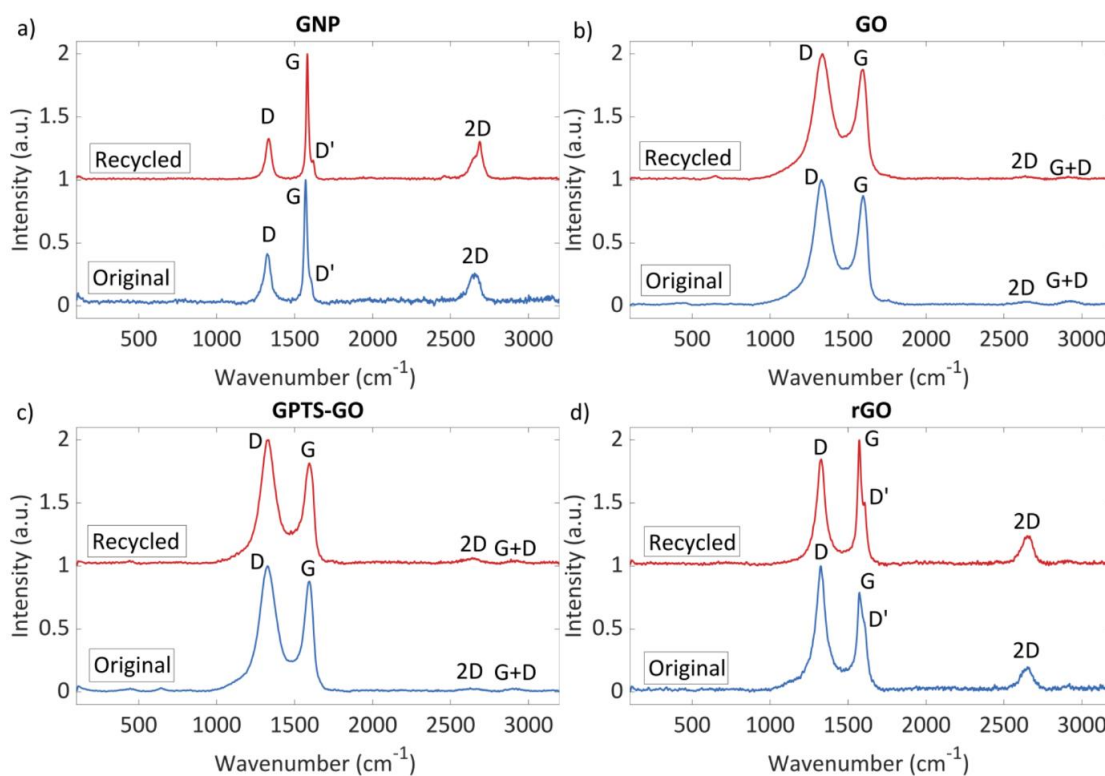


Figure 4-14 Raman spectrum of original and recycled nanoparticles: a) GNP, b) GO, c) GPTS-GO and d) rGO.

All Raman spectrum between original and recycled particles have similar pattern indicating that the particles have not undergone important structural changes during recycling. The overall increase of ratios I_{2D}/I_G indicates that some exfoliation was achieved after recycling except for GNP. The ratio I_D/I_G always decreases, demonstrating that the recycled particles have lower defects than their original counterpart. Initially contradictory with XPS data for GNP and rGO, one should consider that the Raman spectroscopy has an average of penetration within the samples 10 times higher than XPS spectroscopy. Therefore, if the addition of hydroxyl functions happens to the particles edges or surfaces, this will be magnified by XPS data. Nonetheless, Raman data will measure the defect density over several layers. Raman spectrum show that their average defect density (and mainly interlayer defects) is decreased (confirmed *via* the calculation of n_D and L_D given in

Table 4-4) which confirms that the hydroxyl function are added to the contour of GNP and rGO.

Table 4-4 Calculated I_d/I_g , I_{2D}/I_g ratios, average sp² cluster size L_D (average distance between defects) and the defect density n_D for original and recycled nanoparticles.

		I_D/I_g	I_{2D}/I_g	L_D (nm)	n_D (cm ⁻²)
GNP	Original	0.91	0.71	12.47 ± 1.77	2.04 × 10 ¹¹ ± 0.57 × 10 ¹¹
	Recycled	0.75	0.5	13.76 ± 1.95	1.68 × 10 ¹¹ ± 0.47 × 10 ¹¹
GO	Original	2.49	0.09	7.53 ± 1.07	5.60 × 10 ¹¹ ± 1.57 × 10 ¹¹
	Recycled	2.37	0.18	7.72 ± 1.09	5.33 × 10 ¹¹ ± 1.48 × 10 ¹¹
GPTS	Original	2.77	0	7.15 ± 1.01	6.23 × 10 ¹¹ ± 1.73 × 10 ¹¹
	Recycled	2.45	0.1	7.60 ± 1.08	5.50 × 10 ¹¹ ± 1.53 × 10 ¹¹
rGO	Original	2.30	0.33	7.84 ± 1.11	5.16 × 10 ¹¹ ± 1.43 × 10 ¹¹
	Recycled	1.99	0.50	8.43 ± 1.19	4.47 × 10 ¹¹ ± 1.24 × 10 ¹¹

As demonstrated above, the covalent bonding between highly functionalised graphene (GO and GPTS) and vitrimer matrix make separation between those harder. The loss of chemical functions decreases the average weight of single nanoparticles. These latter parameters, added to loss of particles on glassware edges and during filtration lead to a lower yield for GO and GPTS when compared to original particles. The particles with low functionality - as shown in Table B-9 (GNP and rGO) - exhibit a high yield (Table 4-2), and are considered to be fully extracted from the matrix when counting for the loss of particles during the developed recycling process.

4.4 Conclusion

The incorporation of carbon based nanoparticles in epoxy-based vitrimer has been studied and demonstrated that their unique behaviour is preserved. Indeed, the network keeps its crosslinked structure while being able to relax stress at higher temperature like a strong former glass material. It was confirmed that the functionalisation by either acyl or epoxy functions leads to covalent bonding between nano-reinforcement and nanoparticles. The time of relaxation τ , is impacted by the free radical inclusion from nanoparticles functionalisation, while it shows that low functionality particles (GNP and

rGO) only decreases τ' (τ/E) due to their thermal properties. If the functionality decreases τ' compared to neat vitrimer, the faster values are observed at relatively low amount of nanoparticles (01GO and 05GPTS), increasing particles loading then hinder chains motion which ultimately increases τ' . If the relaxation time can be considered faster relative to the materials stiffness, the activation energy of nanocomposites remains overall similar to the neat vitrimer. This value is due to the intrinsic chemical nature of the network and should not be impacted to a high degree by relatively small particle loading (*e.g.* 1wt. %). The mechanical properties of vitrimer are improved by the covalent bonding of nano-reinforcements with the matrix, however, these improvements are variable with particle loading and type. The behaviour of mechanical properties displays similar results that on traditional epoxy based samples leading to think that most previous work realised on classical thermoset would give similar results on alike vitrimer. This confirms that nanoparticles can be integrated to the vitrimer network without quenching their properties. Their integration strongly increase vitrimers mechanical behaviours. Young's modulus increased by at least one order of magnitude for any particles, and kept an elongation > 150%. Furthermore, the time required to relax internal stress is reduced which is a key properties to facilitate their reprocessing (*i.e.* lower time and temperature) [45].

Combined spectroscopy techniques show that nanoparticles can be successfully recycled from epoxy based vitrimer. The functionalisation of nanoparticles and their covalent bonding to the vitrimer lead to severe structural change during recycling: removal of functionalisation and possible edges functionalisation. Only low functionality particles (GNP and rGO) exhibit a yield higher than 90% when recycled. The recycling of these particles is achieved and could avoid potential release in the environment of nano-wastes at the end of the nanocomposite lifespans. Vitrimer matrices, compared to classic thermoset polymers, have therefore the possibility to bring sustainability in the use of nano-reinforcements, opening the path to close-loop recyclability [85]. The development and improvement of nanomaterials recyclability is an important step towards a wider use of multi-functional/smart materials. It has been demonstrated that the extraction of these nanoparticles from vitrimer is possible, with limited impact on their core structures. Further studies are needed to assess the re-use of recycled particles in new polymer matrices, the authors believe that the path used to recover nanoparticles from epoxy matrices has an

extensive interest for many nanocomposites application and vitrimers are proven to be excellent candidates towards full close-loop recyclability of multifunctional materials.

4.5 Conflicts of interest

There are no conflicts to declare.

4.6 Acknowledgement

The authors thank the Aerospace Research Institute (ARI) for its financial support. The department of Materials X-ray Diffraction Laboratory and the Electron Microscopy Faculty of Science and Engineering from the University of Manchester for its technical support. Dr Ben Spencer for its knowledge and support towards XPS data analysis and Harry Coppock for its preliminary work towards the recycling methodology developed in this paper.

4.7 References

- [1] K. S. Novoselov *et al.*, “Electric Field Effect in Atomically Thin Carbon Films,” *Science*, vol. 306, no. 5696, pp. 666–669, 2004.
- [2] Y. Yao *et al.*, “Three-Dimensional Printable High-Temperature and High-Rate Heaters,” *ACS Nano*, vol. 10, no. 5, pp. 5272–5279, 2016.
- [3] A. C. Ferrari *et al.*, “Science and technology roadmap for graphene, related two-dimensional crystals, and hybrid systems,” *Nanoscale*, vol. 7, no. 11, pp. 4598–4810, 2015.
- [4] S. Duan *et al.*, “Fabrication of Highly Stretchable Conductors Based on 3D Printed Porous Poly(dimethylsiloxane) and Conductive Carbon Nanotubes/Graphene Network,” *ACS Appl. Mater. Interfaces*, vol. 8, no. 3, pp. 2187–2192, 2016.
- [5] A. C. De Leon, Q. Chen, N. B. Palaganas, J. O. Palaganas, J. Manapat, and R. C. Advincula, “High performance polymer nanocomposites for additive manufacturing applications,” *React. Funct. Polym.*, vol. 103, pp. 141–155, 2016.
- [6] W. Li, A. Diciara, J. Zha, Z. Su, and J. Bai, “On improvement of mechanical and thermo-mechanical properties of glass fabric/epoxy composites by incorporating CNT-Al₂O₃ hybrids,” *Compos. Sci. Technol.*, vol. 103, pp. 36–43, 2014.
- [7] A. E. Jakus, E. B. Secor, A. L. Rutz, S. W. Jordan, and M. C. Hersam, “Three-Dimensional Printing of High-Content Graphene Scaffolds for Electronic and Biomedical Applications,” *ACS Nano*, vol. 9, no. 4, pp. 4636–4648, 2015.
- [8] F. Bonaccorso, A. Bartolotta, J. N. Coleman, and C. Backes, “2D-Crystal-Based Functional Inks,” *Adv. Mater.*, pp. 6136–6166, 2016.
- [9] A. Carlson, A. M. Bowen, Y. Huang, R. G. Nuzzo, and J. A. Rogers, “Transfer printing techniques for materials assembly and micro/nanodevice fabrication,” *Adv. Mater.*, vol. 24, no. 39, pp. 5284–5318, 2012.
- [10] R. Narayan, J. E. Kim, J. Y. Kim, K. E. Lee, and S. O. Kim, “Graphene Oxide Liquid Crystals: Discovery, Evolution and Applications,” *Adv. Mater.*, vol. 28, no. 16, pp. 3045–3068, 2016.
- [11] Q.-A. Poutrel, Z. Wang, D. Wang, C. Soutis, and M. Gresil, “Effect of pre and Post-Dispersion on Electro-Thermo-Mechanical Properties of a Graphene Enhanced Epoxy,” *Appl. Compos. Mater.*, vol. 24, no. 2, pp. 313–336, 2017.

- [12] A. Manta, M. Gresil, and C. Soutis, "Infrared thermography for void mapping of a graphene/epoxy composite and its full-field thermal simulation," *Fatigue Fract. Eng. Mater. Struct.*, vol. 42, no. 7, pp. 1441–1453.
- [13] C. Vallés *et al.*, "PMMA-grafted graphene nanoplatelets to reinforce the mechanical and thermal properties of PMMA composites," *Carbon*, vol. 157, pp. 750–760, 2020.
- [14] S. R. Ahmad, C. Xue, and R. J. Young, "The mechanisms of reinforcement of polypropylene by graphene nanoplatelets," *Mater. Sci. Eng. B*, vol. 216, pp. 2–9, 2017.
- [15] M. Klüppel *et al.*, "Characterization and Application of Graphene Nanoplatelets in Elastomers," in *Designing of Elastomer Nanocomposites: From Theory to Applications*, Springer International Publishing, 2017, pp. 319–360.
- [16] M. Gresil, Z. Wang, Q.-A. Poutrel, and C. Soutis, "Thermal Diffusivity Mapping of Graphene Based Polymer Nanocomposites," *Sci. Rep.*, vol. 7, no. 1, p. 5536, 2017.
- [17] S. G. Prolongo, R. Moriche, A. Jiménez-Suárez, A. Delgado, and A. Ureña, "Printable self-heating coatings based on the use of carbon nanoreinforcements," *Polym. Compos.*, vol. 41, no. 1, pp. 271–278, 2020.
- [18] H. Kim, A. A. Abdala, and C. W. Macosko, "Graphene/Polymer Nanocomposites," *Macromolecules*, vol. 43, no. 16, pp. 6515–6530, 2010.
- [19] D. Montarnal, M. Capelot, F. Tounilhac, and L. Leibler, "Silica-Like Malleable Materials from permanent organic network," *Science*, vol. 334, pp. 965–968, 2011.
- [20] C. J. Kloxin and C. N. Bowman, "Covalent adaptable networks: smart, reconfigurable and responsive network systems.," *Chem. Soc. Rev.*, vol. 42, no. 17, pp. 7161–73, 2013.
- [21] C. J. Kloxin, T. F. Scott, B. J. Adzima, and C. N. Bowman, "Covalent Adaptable Networks (CANs): A Unique Paradigm in Cross-Linked Polymers," *Macromolecules*, vol. 43, no. 6, pp. 2643–2653, 2010.
- [22] F. I. Altuna, C. E. Hoppe, and R. J. J. Williams, "Shape memory epoxy vitrimers based on DGEBA crosslinked with dicarboxylic acids and their blends with citric acid," *RSC Adv.*, vol. 6, no. 91, pp. 88647–88655, 2016.
- [23] F. I. Altuna, C. E. Hoppe, and R. J. J. Williams, "Epoxy vitrimers: The effect of transesterification reactions on the network structure," *Polymers*, vol. 10, no. 1, p. 43, 2018.

- [24] Y. Yang, E. M. Terentjev, Y. Wei, and Y. Ji, "Solvent-assisted programming of flat polymer sheets into reconfigurable and self-healing 3D structures," *Nat. Commun.*, vol. 9, no. 1, p. 1906, 2018.
- [25] Z. Ma, Y. Wang, J. Zhu, J. Yu, and Z. Hu, "Bio-based epoxy vitrimers: Reprocessability, controllable shape memory, and degradability," *J. Polym. Sci. Part A Polym. Chem.*, vol. 55, no. 10, pp. 1790–1799, 2017.
- [26] L. Li, X. Chen, K. Jin, and J. M. Torkelson, "Vitrimers Designed Both To Strongly Suppress Creep and To Recover Original Cross-Link Density after Reprocessing: Quantitative Theory and Experiments," *Macromolecules*, vol. 51, no. 15, pp. 5537–5546, 2018.
- [27] F. I. Altuna, U. Casado, I. E. Dell'Erba, L. Luna, C. E. Hoppe, and R. J. J. Williams, "Epoxy vitrimers incorporating physical crosslinks produced by self-association of alkyl chains," *Polym. Chem.*, vol. 11, no. 7, pp. 1337–1347, 2020.
- [28] Q.-A. Poutrel *et al.*, "Dicarboxylic acid-epoxy vitrimers: Influence of off-stoichiometric acid content on cure reactions and thermo-mechanical properties," *Polym. Chem.*, vol. 11, pp. 5327–5338, 2020.
- [29] Z. Liu, C. Zhang, Z. Shi, J. Yin, and M. Tian, "Tailoring vinylogous urethane chemistry for the cross-linked polybutadiene: Wide freedom design, multiple recycling methods, good shape memory behavior," *Polymer*, vol. 148, pp. 202–210, 2018.
- [30] I. Azcune and I. Odriozola, "Aromatic disulfide crosslinks in polymer systems: Self-healing, reprocessability, recyclability and more," *Eur. Polym. J.*, vol. 84, pp. 147–160, 2016.
- [31] F. Meng, R. H. Pritchard, and E. M. Terentjev, "Stress Relaxation, Dynamics, and Plasticity of Transient Polymer Networks," *Macromolecules*, vol. 49, no. 7, pp. 2843–2852, 2016.
- [32] Q. Yu *et al.*, "Vanillin-based degradable epoxy vitrimers: Reprocessability and mechanical properties study," *Eur. Polym. J.*, vol. 117, pp. 55–63, Aug. 2019.
- [33] S. Zhang *et al.*, "Preparation of a lignin-based vitrimer material and its potential use for recoverable adhesives," *Green Chem.*, vol. 20, no. 13, pp. 2995–3000, 2018.
- [34] J. J. Lessard *et al.*, "Catalyst-Free Vitrimers from Vinyl Polymers," *Macromolecules*, vol. 52, no. 5, pp. 2105–2111, 2019.
- [35] F. Romano and F. Sciortino, "Switching Bonds in a DNA Gel: An All-DNA Vitrimer,"

Phys. Rev. Lett., vol. 114, no. 7, p. 78104, 2015.

- [36] T. Stukenbroeker, W. Wang, J. M. Winne, F. E. Du Prez, R. Nicolaÿ, and L. Leibler, "Polydimethylsiloxane quenchable vitrimers," *Polym. Chem.*, vol. 8, no. 43, pp. 6590–6593, 2017.
- [37] B. Hendriks, J. Waelkens, J. M. Winne, and F. E. Du Prez, "Poly(thioether) Vitrimers via Transalkylation of Trialkylsulfonium Salts," *ACS Macro Lett.*, vol. 6, no. 9, pp. 930–934, 2017.
- [38] X. Huang, H. C. Liu, Z. Fan, H. Wang, G. S. Huang, and J. R. Wu, "Hyperbranched polymer toughened and reinforced self-healing epoxy vitrimer," *Acta Polym. Sin.*, vol. 50, no. 5, pp. 535–542, 2019.
- [39] Z. Yang, Q. Wang, and T. Wang, "Dual-Triggered and Thermally Reconfigurable Shape Memory Graphene-Vitrimer Composites," *ACS Appl. Mater. Interfaces*, vol. 8, no. 33, pp. 21691–21699, Aug. 2016.
- [40] G. kang Chen, K. Wu, Q. Zhang, Y. cen Shi, and M. geng Lu, "Dual-Responsive Shape Memory and Thermally Reconfigurable Reduced Graphene Oxide-Vitrimer Composites," *Macromol. Res.*, vol. 27, no. 6, pp. 526–533, Jun. 2019.
- [41] Y. Liu, Z. Tang, Y. Chen, S. Wu, and B. Guo, "Programming dynamic imine bond into elastomer/graphene composite toward mechanically strong, malleable, and multi-stimuli responsive vitrimer," *Compos. Sci. Technol.*, vol. 168, pp. 214–223, Nov. 2018.
- [42] Y. Yang, Z. Pei, X. Zhang, L. Tao, Y. Wei, and Y. Ji, "Carbon nanotube–vitrimer composite for facile and efficient photo-welding of epoxy," *Chem. Sci.*, vol. 5, no. 9, pp. 3486–3492, 2014.
- [43] H. Zhang and X. Xu, "Improving the transesterification and electrical conductivity of vitrimers by doping with conductive polymer wrapped carbon nanotubes," vol. 99, pp. 15–22, Aug. 2017.
- [44] R. H. Pritchard, A.-L. L. Redmann, Z. Pei, Y. Ji, and E. M. Terentjev, "Vitrification and plastic flow in transient elastomer networks," *Polymer*, vol. 95, pp. 45–51, 2016.
- [45] J. Chen *et al.*, "Vitrimer Chemistry Assisted Fabrication of Aligned, Healable, and Recyclable Graphene/Epoxy Composites," *Front. Chem.*, vol. 7, p. 632, Sep. 2019.
- [46] Y. Yuan *et al.*, "Multiply fully recyclable carbon fibre reinforced heat-resistant covalent thermosetting advanced composites," *Nat. Commun.*, vol. 8, p. 14657, 2017.

- [47] S. Wang *et al.*, "Facile *in situ* preparation of high-performance epoxy vitrimer from renewable resources and its application in nondestructive recyclable carbon fiber composite," *Green Chem.*, vol. 21, no. 6, pp. 1484–1497, 2019.
- [48] A. Li, J. Fan, and G. Li, "Recyclable thermoset shape memory polymers with high stress and energy output *via* facile UV-curing," *J. Mater. Chem. A*, vol. 6, no. 24, pp. 11479–11487, 2018.
- [49] X. Kuang, Y. Zhou, Q. Shi, T. Wang, and H. J. Qi, "Recycling of Epoxy Thermoset and Composites *via* Good Solvent Assisted and Small Molecules Participated Exchange Reactions," *ACS Sustain. Chem. Eng.*, vol. 6, no. 7, pp. 9189–9197, 2018.
- [50] I. Khan, K. Saeed, and I. Khan, "Nanoparticles: Properties, applications and toxicities," *Arabian Journal of Chemistry*, vol. 12, no. 7. Elsevier B.V., pp. 908–931, Nov. 01, 2019.
- [51] A. P. Gondikas, F. Von Der Kammer, R. B. Reed, S. Wagner, J. F. Ranville, and T. Hofmann, "Release of TiO₂ nanoparticles from sunscreens into surface waters: A one-year survey at the old danube recreational lake," *Environ. Sci. Technol.*, vol. 48, no. 10, pp. 5415–5422, 2014.
- [52] S. N. A. Shah, Z. Shah, M. Hussain, and M. Khan, "Hazardous Effects of Titanium Dioxide Nanoparticles in Ecosystem," *Bioinorg. Chem. Appl.*, vol. 4101735, 2017.
- [53] X. Yuan, X. Zhang, L. Sun, Y. Wei, and X. Wei, "Cellular Toxicity and Immunological Effects of Carbon-based Nanomaterials," *Particle and Fibre Toxicology*, vol. 16, no. 1. Particle and Fibre Toxicology, 2019.
- [54] G. H. Lee, K. H. Ahn, and I. J. Yu, "Testing of nanoparticle release from a composite containing nanomaterial using a chamber system," *J. Vis. Exp.*, vol. 2016, no. 117, pp. 1–10, 2016.
- [55] F. Zhou *et al.*, "Preparation of self-healing, recyclable epoxy resins and low-electrical resistance composites based on double-disulfide bond exchange," *Compos. Sci. Technol.*, vol. 167, pp. 79–85, 2018.
- [56] Y. Baghdadi, "Enhancement of the Mechanical Properties of Vitrimers using Functionalised Graphene Nanoplatelets," Manchester, 2018.
- [57] A. Ferrari and J. Robertson, "Interpretation of Raman spectra of disordered and amorphous carbon," *Phys. Rev. B - Condens. Matter Mater. Phys.*, vol. 61, no. 20, pp. 14095–14107, 2000.

- [58] A. Theodosiou, B. F. Spencer, J. Counsell, and A. N. Jones, "An XPS/UPS study of the surface/near-surface bonding in nuclear grade graphites: A comparison of monatomic and cluster depth-profiling techniques," *Appl. Surf. Sci.*, no. August, p. 144764, 2019.
- [59] Q. Wang *et al.*, "Preparation of high antistatic HDPE/polyaniline encapsulated graphene nanoplatelet composites by solution blending," *RSC Adv.*, vol. 7, no. 5, pp. 2796–2803, 2017.
- [60] T. N. Blanton and D. Majumdar, "X-ray diffraction characterization of polymer intercalated graphite oxide," *Powder Diffr.*, vol. 27, no. 2, pp. 104–107, 2012.
- [61] P. Haghdadeh, M. Ghaffari, B. Ramezanzadeh, G. Bahlakeh, and M. R. Saeb, "The role of functionalized graphene oxide on the mechanical and anti-corrosion properties of polyurethane coating," *J. Taiwan Inst. Chem. Eng.*, vol. 86, no. March, pp. 199–212, 2018.
- [62] H. S. Maharana, P. Kumar Rai, and A. Basu, "Surface-mechanical and electrical properties of pulse electrodeposited Cu-graphene oxide composite coating for electrical contacts," *J. Mater. Sci.*, vol. 52, no. 2, pp. 1089–1105, 2017.
- [63] B. Nasiri-Tabrizi, "Thermal treatment effect on structural features of mechano-synthesized fluorapatite-titania nanocomposite: A comparative study," *J. Adv. Ceram.*, vol. 3, no. 1, pp. 31–42, 2014.
- [64] M. Al-Qadhi, N. Merah, K. Mezghani, Z. Khan, Z. M. Gasem, and R. Sougrat, "Effect of high shear mixing parameters and degassing temperature on the morphology of epoxy-clay nanocomposites," *Adv. Mater. Res.*, vol. 652–654, no. January, pp. 159–166, 2013.
- [65] S. G. Prolongo, A. Jimenez-Suarez, R. Moriche, and A. Ureña, "In situ processing of epoxy composites reinforced with graphene nanoplatelets," *Compos. Sci. Technol.*, vol. 86, pp. 185–191, 2013.
- [66] M. Selvaraj, V. Venkatachalapathy, J. Mayandi, S. Karazhanov, and J. M. Pearce, "Preparation of meta-stable phases of barium titanate by Sol-hydrothermal method," *AIP Adv.*, vol. 5, no. 11, 2015.
- [67] K. Kanimozhi, P. Prabunathan, V. Selvaraj, and M. Alagar, "Mullite-reinforced caprolactam-toughened DGEBA epoxy nanocomposites: Preparation and characterization," *High Perform. Polym.*, vol. 27, no. 7, pp. 833–841, 2015.

- [68] A. Chandramohan, M. Mandhakini, K. Dinakaran, and M. Alagar, "Thermal, electrical and morphological properties of DGEBA/DDM and TGDDM/DDM epoxies modified by a flexible diepoxide and octaphenylamine-POSS," *J. Reinf. Plast. Compos.*, vol. 32, no. 9, pp. 602–611, 2013.
- [69] Y. J. Wan, L. X. Gong, L. C. Tang, L. Bin Wu, and J. X. Jiang, "Mechanical properties of epoxy composites filled with silane-functionalized graphene oxide," *Compos. Part A Appl. Sci. Manuf.*, vol. 64, pp. 79–89, 2014.
- [70] K. Zaitso, S. Lee, K. Ishibe, T. Sekitani, and T. Someya, "A field-cycle-induced high-dielectric phase in ferroelectric copolymer," *J. Appl. Phys.*, vol. 107, no. 11, 2010.
- [71] J. R. Connolly, "Diffraction Basics, Part 2," *Introduction to XRay Powder Diffraction*, vol. 2, pp. 1–12, 2009.
- [72] A. Legrand and C. Soulié-Ziakovic, "Silica-Epoxy Vitrimer Nanocomposites," *Macromolecules*, vol. 49, no. 16, pp. 5893–5902, 2016.
- [73] B. Ahmadi-Moghadam *et al.*, "Functionalization of Graphene Nanoplatelets on the Mechanical Response of Graphene/Epoxy Composites," *Mater. Des.*, vol. 66, pp. 142–149, 2015.
- [74] G. Gkikas, N. M. Barkoula, and A. S. Paipetis, "Effect of dispersion conditions on the thermo-mechanical and toughness properties of multi walled carbon nanotubes-reinforced epoxy," in *Composites Part B: Engineering*, 2012, vol. 43, no. 6, pp. 2697–2705.
- [75] A. Souvignet, "Reprocessing of vitrimer composites and recycling of graphene nanoparticles," Manchester, 2019.
- [76] Y. E. Shin *et al.*, "An ice-templated, pH-tunable self-assembly route to hierarchically porous graphene nanoscroll networks," *Nanoscale*, vol. 6, no. 16, pp. 9734–9741, 2014.
- [77] J. Ederer *et al.*, "Determination of amino groups on functionalized graphene oxide for polyurethane nanomaterials: XPS quantitation vs. functional speciation," *RSC Adv.*, vol. 7, no. 21, pp. 12464–12473, 2017.
- [78] L. Stobinski *et al.*, "Graphene oxide and reduced graphene oxide studied by the XRD, TEM and electron spectroscopy methods," *J. Electron Spectros. Relat. Phenomena*, vol. 195, pp. 145–154, 2014.
- [79] V. Chung, S. Tony, C. Hong, C. Chuan, B. Ying, and S. Chandra, "Effective Synthesis of

- Silicon Carbide Nanotubes by Microwave Heating of Blended Silicon Dioxide and Multi-Walled Carbon Nanotube,” *Mater. Res.*, vol. 20, no. 6, pp. 1658–1668, 2017.
- [80] Y. Chen, X. Zhang, Y. Tian, and X. Zhao, “Synthesis and characterization of silicon nanoparticles inserted into graphene sheets as high performance anode material for lithium ion batteries,” *J. Nanomater.*, vol. 2014, 2014.
- [81] S. Drewniak, R. Muzyka, A. Stolarczyk, T. Pustelny, M. Kotyczka-Morańska, and M. Setkiewicz, “Studies of reduced graphene oxide and graphite oxide in the aspect of their possible application in gas sensors,” *Sensors*, vol. 16, no. 1, 2016.
- [82] V. T. Nguyen *et al.*, “Synthesis of multi-layer graphene films on copper tape by atmospheric pressure chemical vapor deposition method,” *Adv. Nat. Sci. Nanosci. Nanotechnol.*, vol. 4, no. 3, pp. 2–7, 2013.
- [83] A. Raja *et al.*, “Visible active reduced graphene oxide-BiVO₄-ZnO ternary photocatalyst for efficient removal of ciprofloxacin,” *Sep. Purif. Technol.*, vol. 233, p. 115996, 2020.
- [84] Z. Yan and A. R. Barron, “Characterization of Graphene by Raman Spectroscopy,” in *Physical Methods in Chemistry and Nano Science*, M. V. Raja and A. R. Barron, Eds. LibreTexts library, 2019.
- [85] H. Memon *et al.*, “Vanillin-Based Epoxy Vitrimer with High Performance and Closed-Loop Recyclability,” *Macromolecules*, vol. 53, no. 2, pp. 621–630, 2020.

Appendix B. Supplementary information - Chapter 4

Quentin-Arthur Poutrel^{a,b}, Yasmine Baghdadi^b, Aline Souvignet^b, Matthieu Gresil^{c,*}

^a Aerospace Research Institute, The University of Manchester, Manchester, UK

^b Department of Materials, The University of Manchester, Oxford Road, Manchester, UK

^c i- Composites Lab, Department of Materials Science and Engineering, Monash University, 20 Research Way, Clayton, Australia

*corresponding authors: matthieu.gresil@monash.edu

B.1. Chemical structure of monomers and nanoparticles used in this study

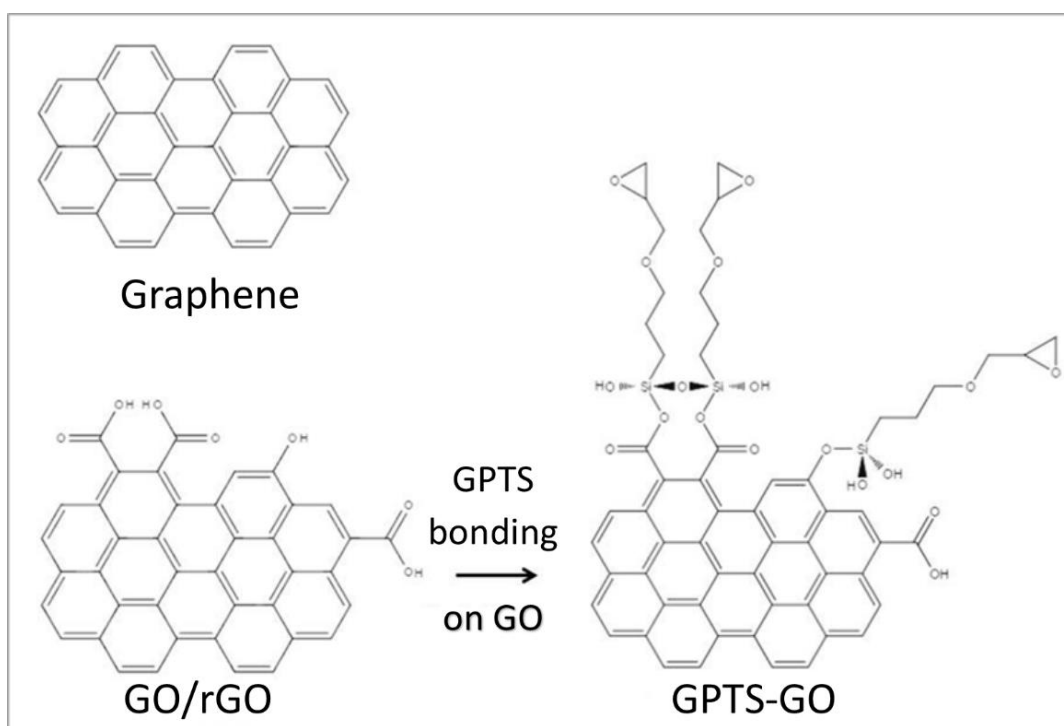


Figure B-1 Chemical structure of nanoparticles: GNP as stack of graphene layers (6-8), Graphene oxide and GPTS-GO - rGO have a similar structure than GO particles but should display lower functionality (acyl and carbonyl function).

Adapted from [1].

Table B-1 Reactant used in this study; eew: epoxy equivalent weight, mw: molecular weight.

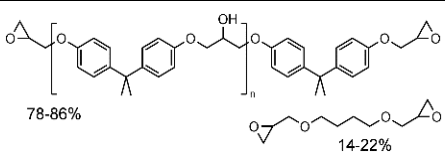
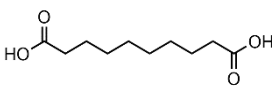
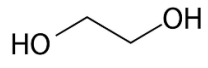
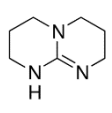
Chemical structure	Compound	Acronym	M (g/mol)
	Diepoxide monomer (LY564)	DE	172-176 (eew)
	Diacyl monomer (sebacic acid)	SA	202.2 (mw)
	Solvent for dilution (Ethylene Glycol)	EG	62.1 (mw)
	Transesterification catalyst (1,5,7-triazabicyclo[4.4.0]dec-5-ene)	TBD	139.2 (mw)

Table B-2 Properties of purchased GNP and GO.

	GNP	GO Dispersion (4 mg/mL)
Lateral size (μm)	0.5-1	15
Sheet resistance (Ω/sq)	10	-
Surface area ($\text{m}^2 \text{g}^{-1}$)	30-50	-
sp^2 carbon content (%w/w)	98	49-56
Oxygen content (%w/w)	-	41-50

B.2. Complementary experimental schematics and equations

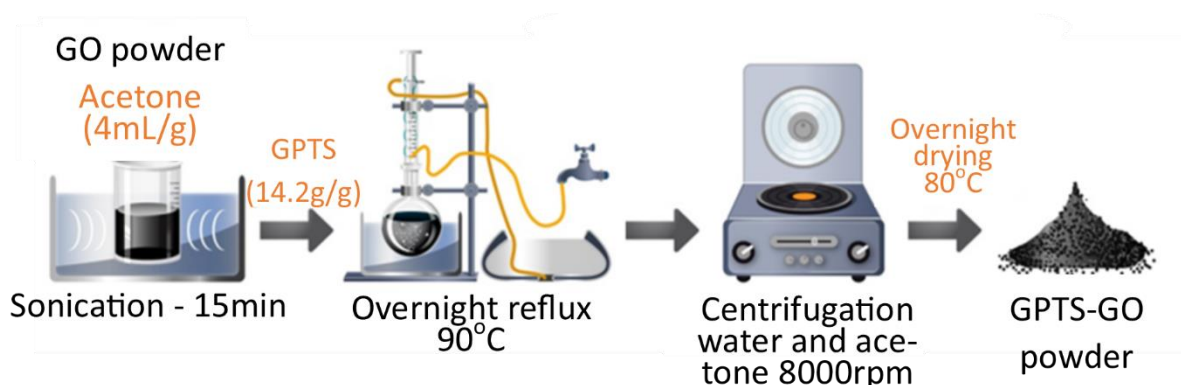


Figure B-2 Scheme of functionalisation of GO with GPTS - adapted from [2].

Equations to calculate the average sp^2 cluster size L_D (Equation B-1) and the defect density n_D (Equation B-2):

$$L_D (nm) = \sqrt{(1.8 \pm 0.5) * 10^{-9} \lambda_L^4 \left(\frac{I_D}{I_G}\right)^{-1}}$$

Equation B-1 Calculation for average sp^2 clusters size.

$$n_D (cm^{-2}) = \frac{10^{14}}{\pi L_D^2} = \frac{(1.8 \pm 0.5) * 10^{22}}{\lambda_L^4} \left(\frac{I_D}{I_G}\right)$$

Equation B-2 Calculation for the defect density.

Where λ_L is the wavelength of the incident laser light, I_D and I_G the intensities of the D and G peaks, respectively.

B.3. Complementary data for XPS survey of neat particles

Table B-3 Summary of the elemental composition determined via XPS survey analysis. The reader would acknowledge that total does not add up to 100% - N_{1s} peak was included in calculation to compare with survey graph of original and recycled particle (results developed later in this manuscript) however N_{1s} content is not relevant for neat particles.

	GNP	GO	GPTS-GO	rGO
O_{1s} (%)	5.5	25.7	34.5	7.2
C_{1s} (%)	94.2	73.4	58	91.8
Si_{2p} (%)	0.05	0.45	7.5	0.15

B.4. Swelling samples before and after being soaked in TCB at 135°C for 7 days

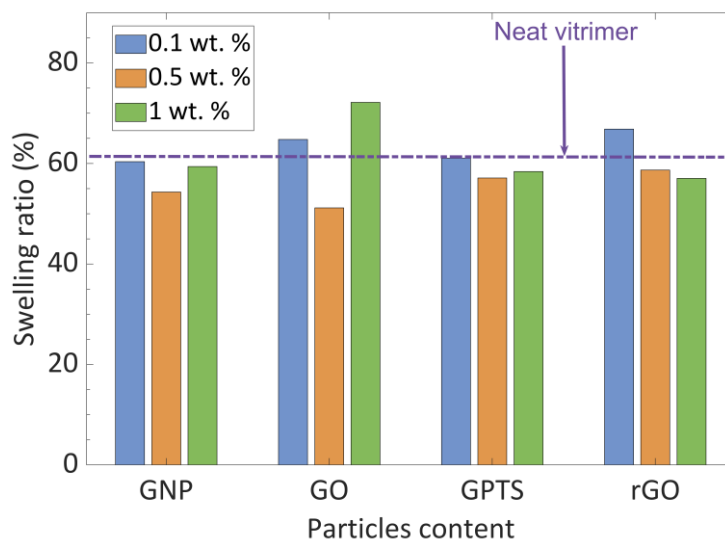


Figure B-3 Swelling ratio of nanocomposites compared to swelling ratio of vitrimer without nano-reinforcement (purple dotted line) - samples were left at 135°C in TCB for 7 days.

B.5. Complementary information: FT-IR data

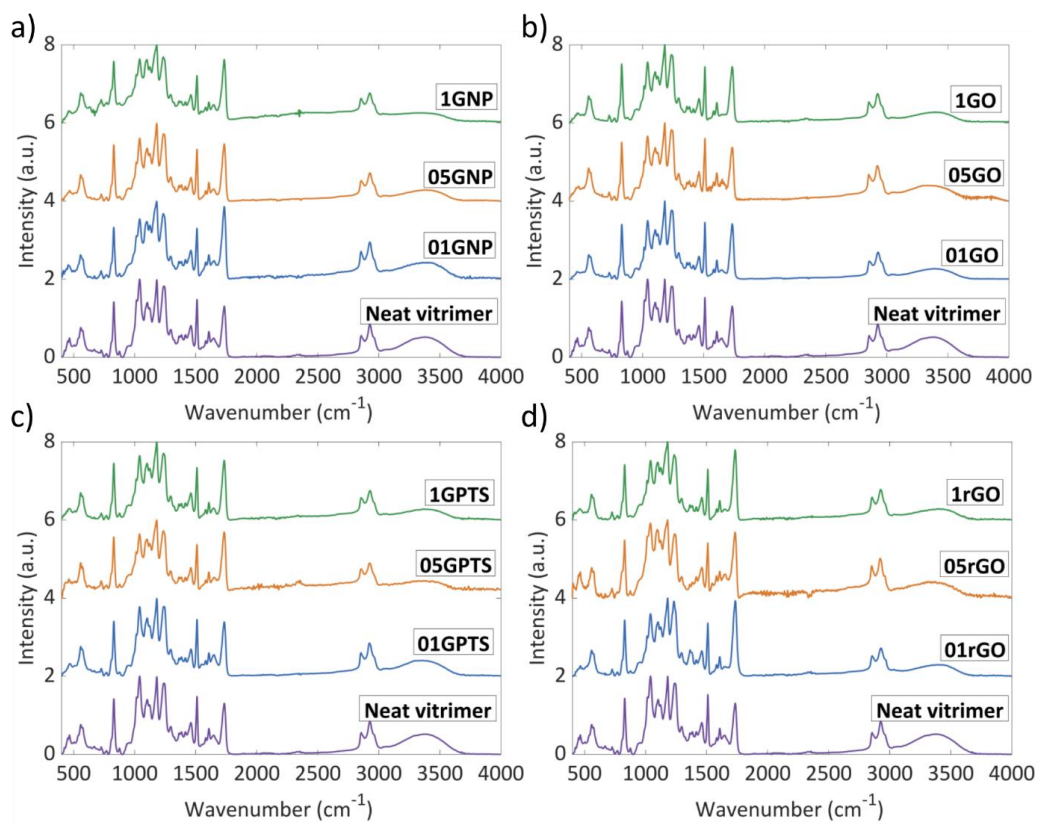


Figure B-4 FT-IR spectra of nanocomposites: a) GNP samples, b) GO samples, c) GPTS samples, d) rGO samples - chemicals species are not impacted by nanoparticles addition.

B.6. Stress relaxation and Creep data: experimental results

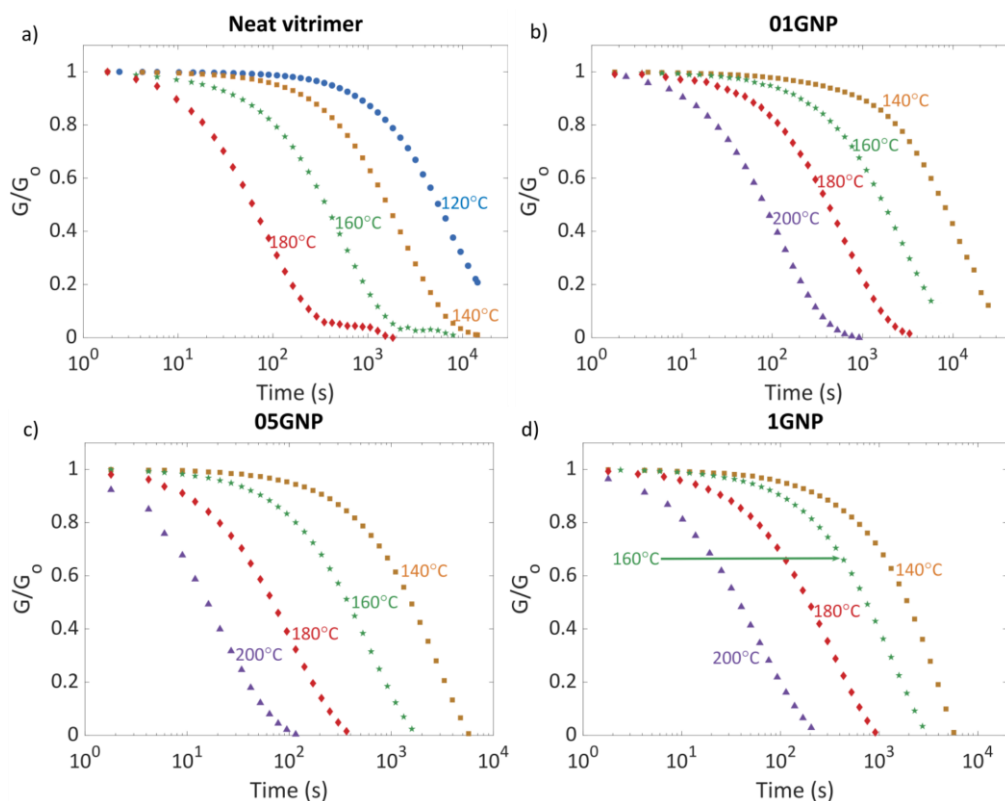


Figure B-5 Stress relaxation results at different temperature for GNP samples: a) Neat vitrimer, b) 0.1 wt. % GNP, c) 0.5 wt. % GNP, d) 1 wt. % GNP.

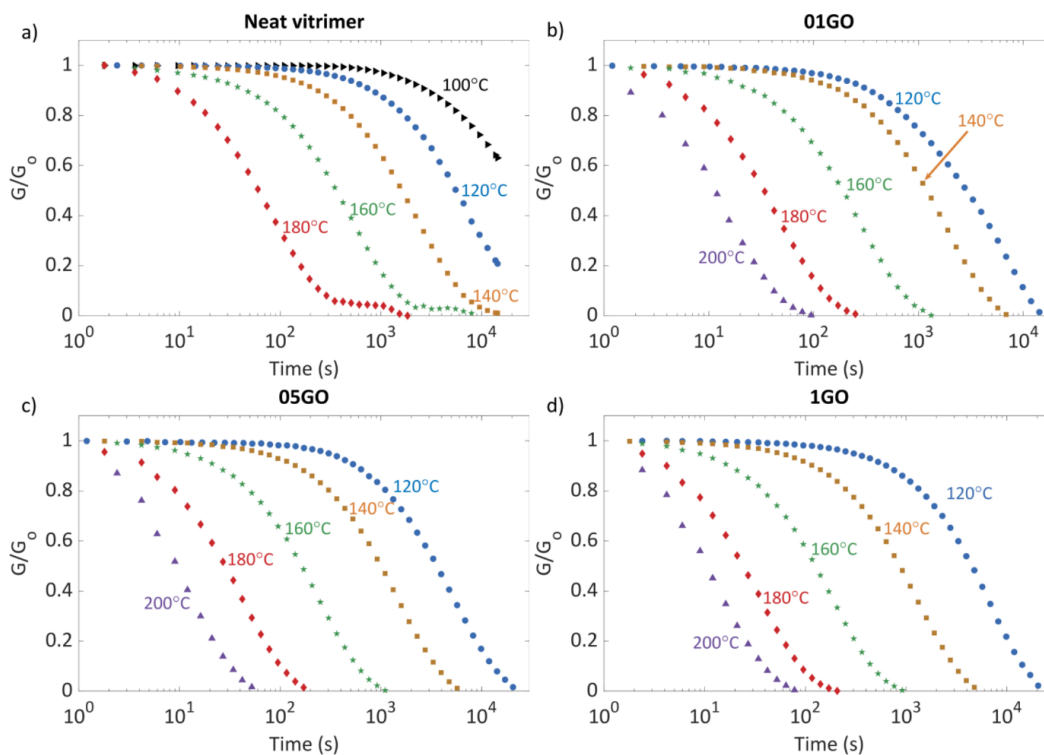


Figure B-6 Stress relaxation results at different temperature for GO samples: a) Neat vitrimer, b) 0.1 wt. % GO, c) 0.5 wt. % GO, d) 1 wt. % GO.

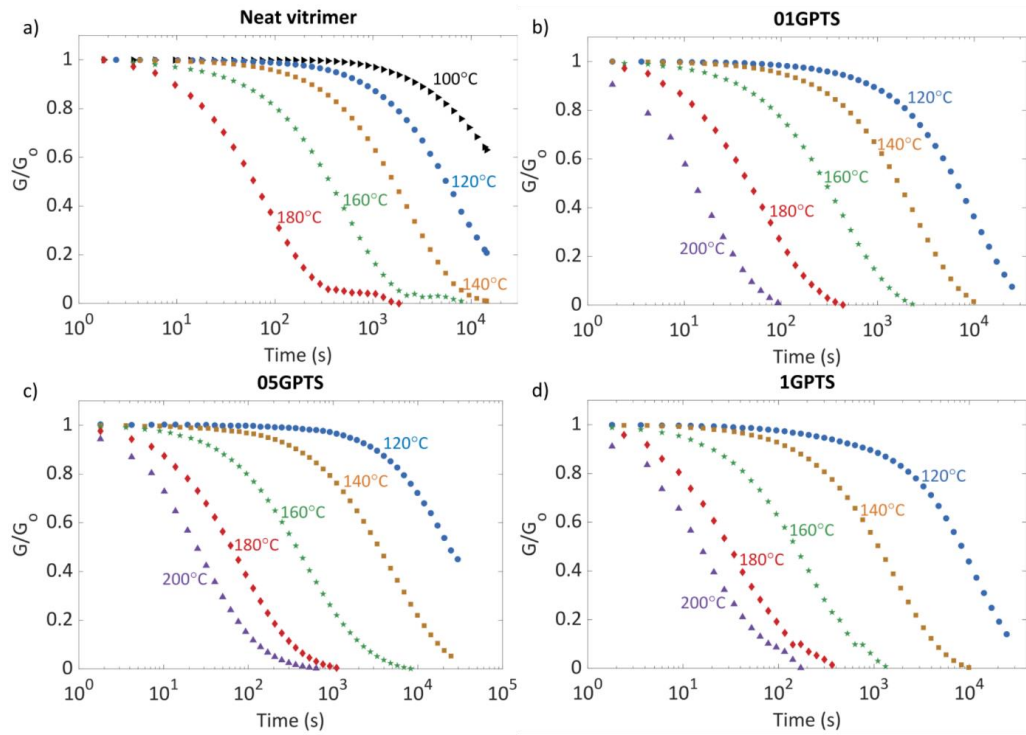


Figure B-7 Stress relaxation results at different temperature for GPTS samples: a) Neat vitrimer, b) 0.1 wt. % GPTS, c) 0.5 wt. % GPTS, d) 1 wt. % GPTS.

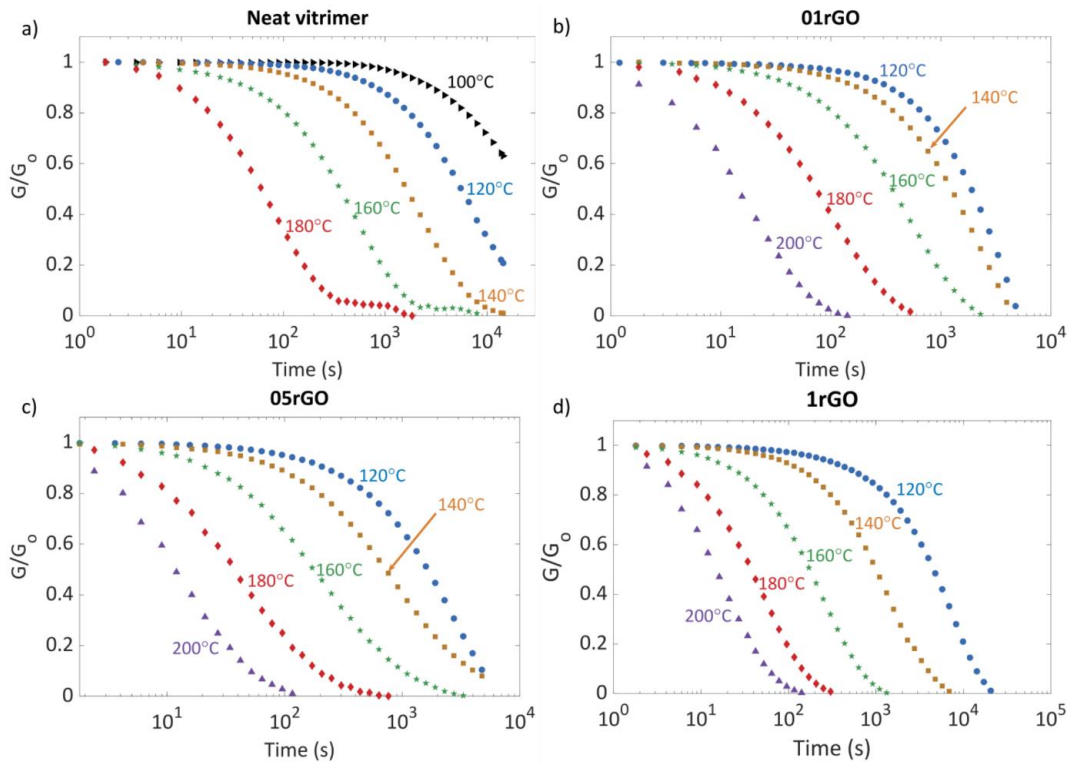


Figure B-8 Stress relaxation results at different temperature for rGO samples: a) Neat vitrimer, b) 0.1 wt. % rGO, c) 0.5 wt. % rGO, d) 1 wt. % rGO.

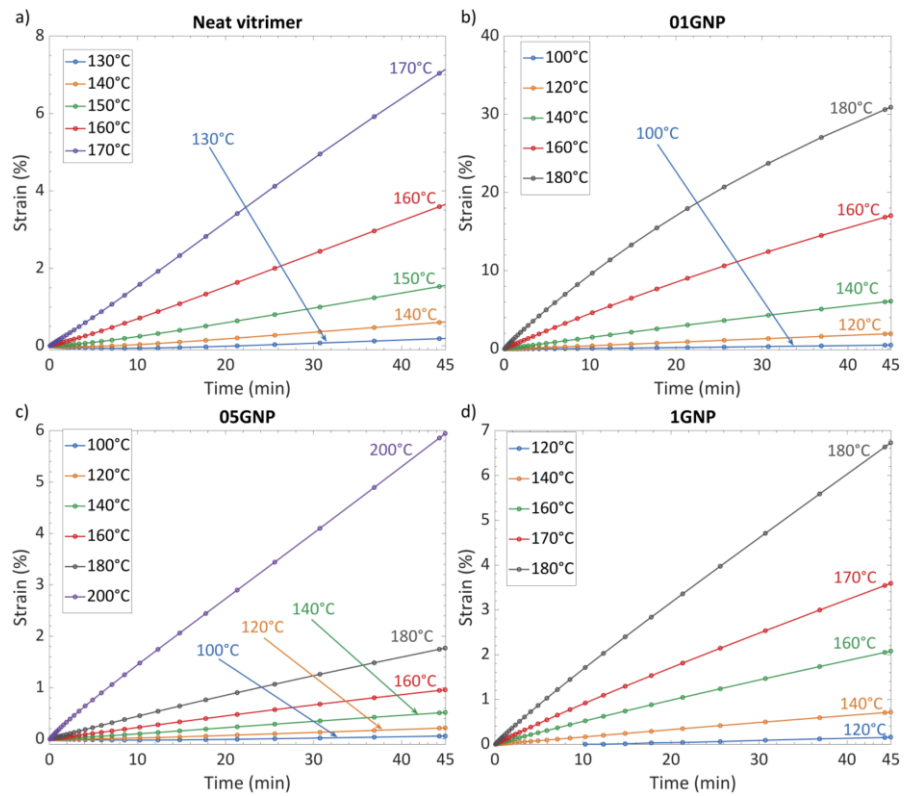


Figure B-9 Creep results after removal of initial elastic strain removal at different temperature for GNP samples: a) Neat vitrimer, b) 0.1 wt. % GNP, c) 0.5 wt. % GNP, d) 1 wt. % GNP.

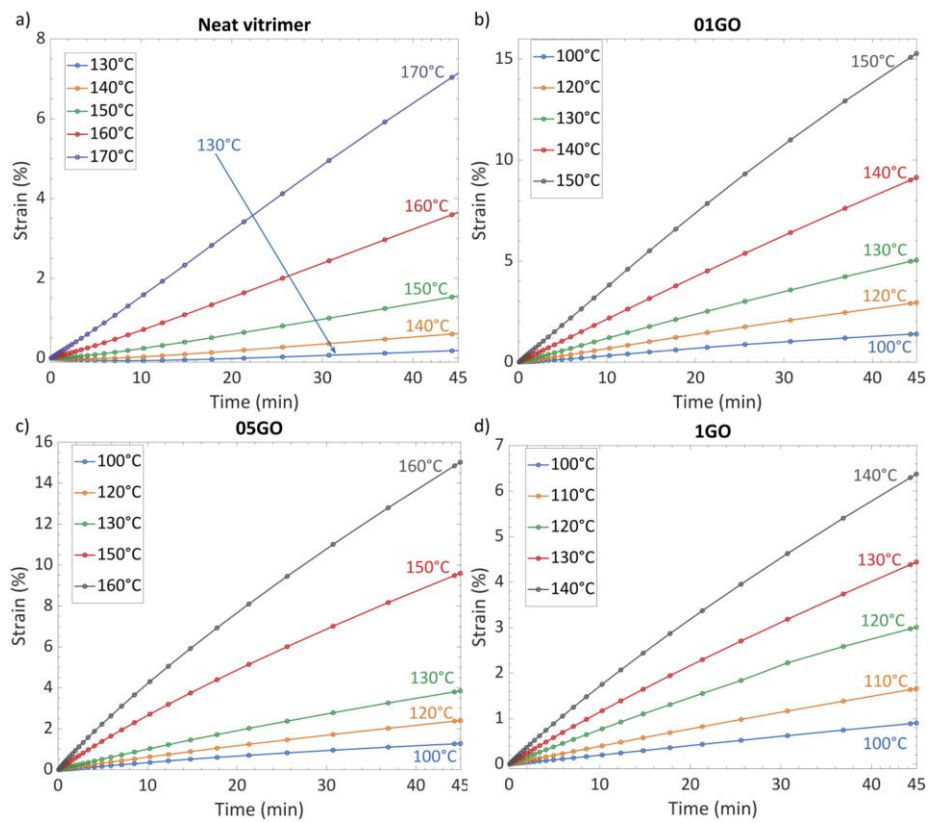


Figure B-10 Creep results after removal of initial elastic strain removal at different temperature for GO samples: a) Neat vitrimer, b) 0.1 wt. % GO, c) 0.5 wt. % GO, d) 1 wt. % GO.

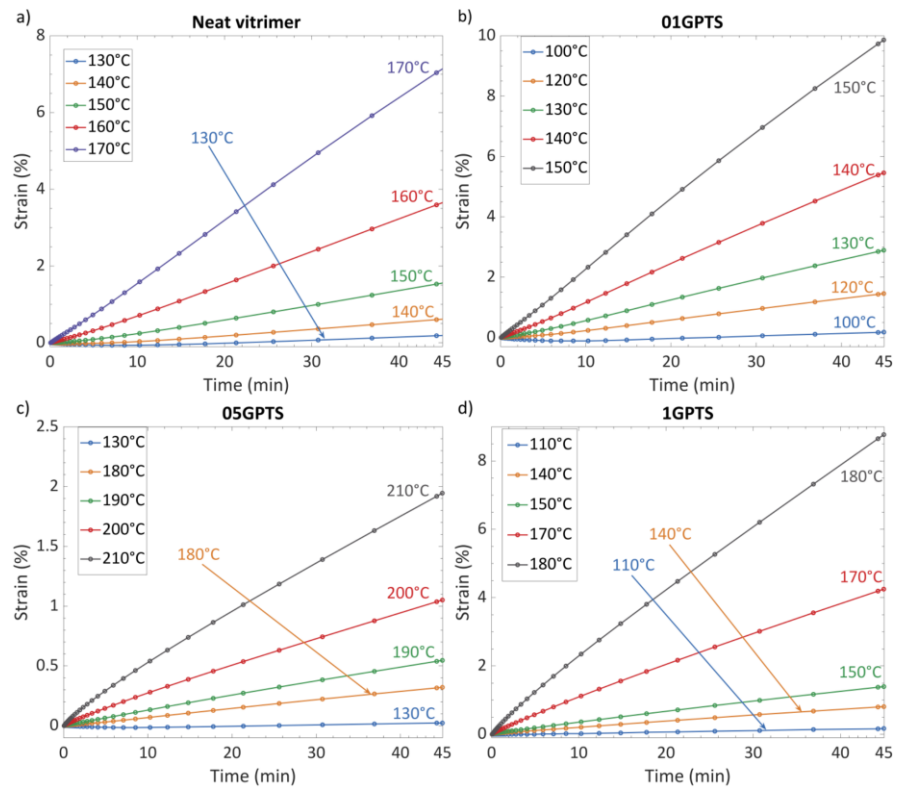


Figure B-11 Creep results after removal of initial elastic strain removal at different temperature for GPTS samples: a) Neat vitrimer, b) 0.1 wt. % GPTS, c) 0.5 wt. % GPTS, d) 1 wt. % GPTS.

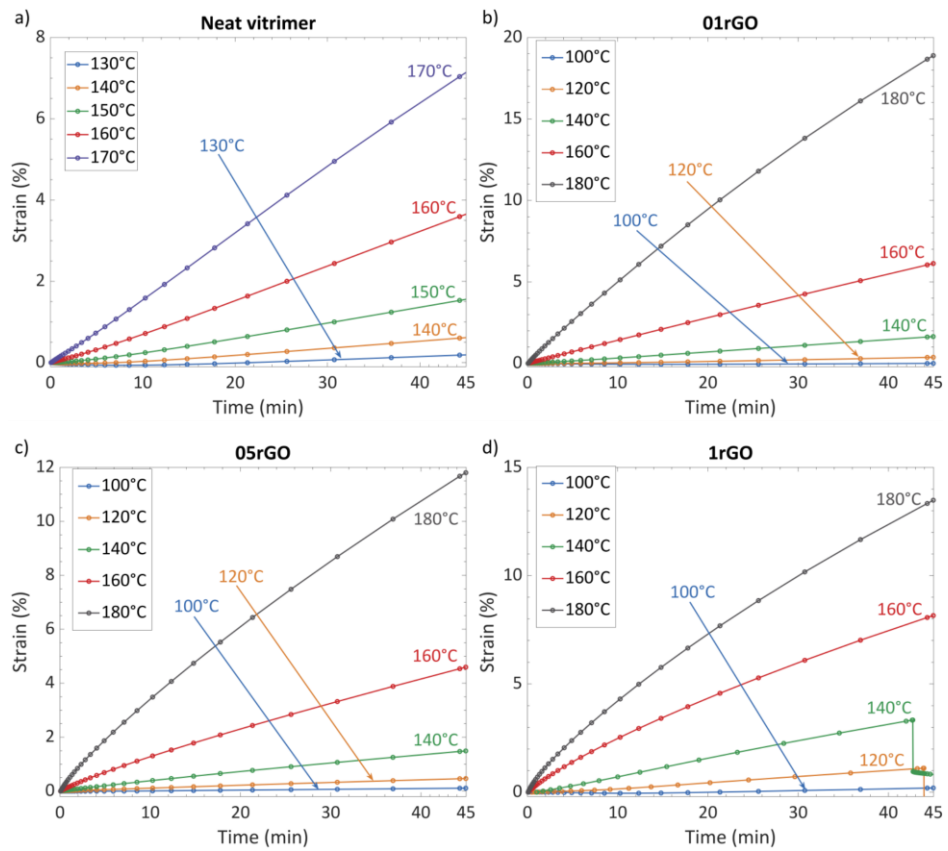


Figure B-12 Creep results after removal of initial elastic strain removal at different temperature for rGO samples: a) Neat vitrimer, b) 0.1 wt. % rGO, c) 0.5 wt. % rGO, d) 1 wt. % rGO.

B.7. Dynamical mechanical analysis results for nanocomposites samples

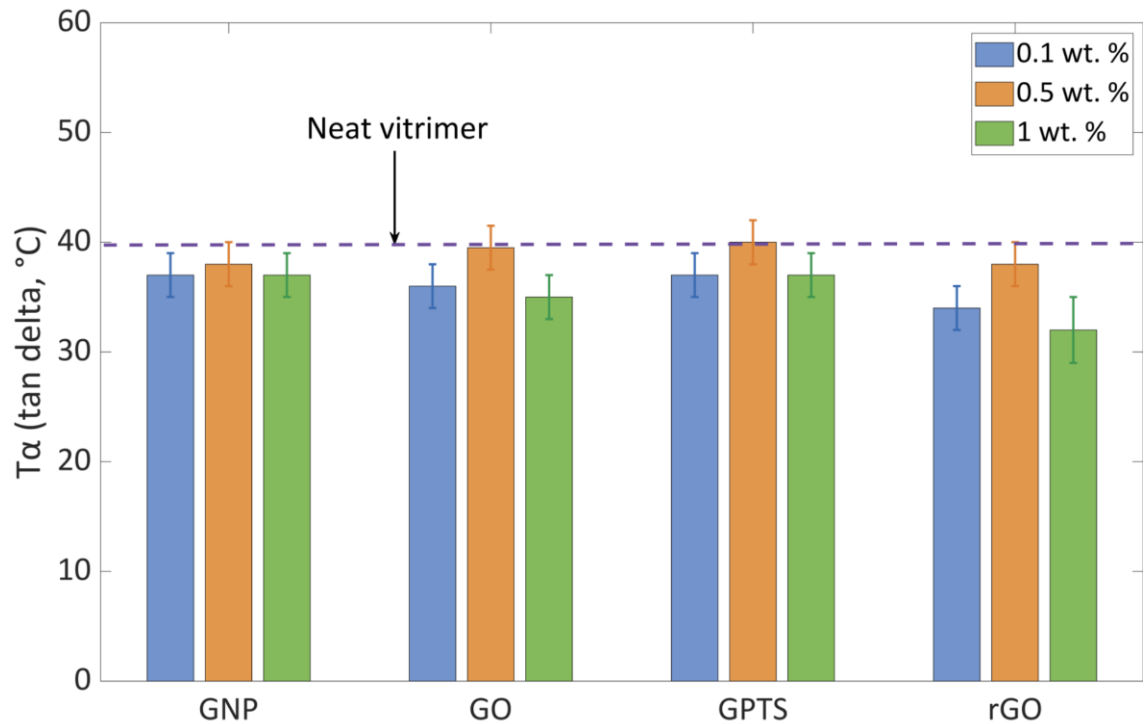


Figure B-13 Bar chart showing the glass transition temperature of the samples depending of the particles loading type and percentage.

B.8. Complementary information for tensile results

Table B-4 Summary of mechanical results for GNP samples.

	Neat vitrimer	01GNP	05GNP	1GNP
Young's modulus (0-0.1% strain, MPa)	2.4 ± 0.3	21.6 ± 4.7	4.8 ± 1.3	7.9 ± 0.7
Young's modulus (60-80% strain, MPa)	0.47 ± 0.14	0.8 ± 0.1	0.50 ± 0.04	1.0 ± 0.1
Breaking strain (%)	328 ± 19	176 ± 14	184 ± 15	108 ± 4
Ultimate strength (MPa)	0.83 ± 0.2	1.6 ± 0.2	1.1 ± 0.1	1.1 ± 0.1

Table B-5 Summary of mechanical results for GO samples.

	Neat vitrimer	01GO	05GO	1GO
Young's modulus (0-0.1% strain, MPa)	2.4 ± 0.3	62.7 ± 15.3	4.2 ± 1.5	3.4 ± 0.7
Young's modulus (60-80% strain, MPa)	0.47 ± 0.14	1.32 ± 0.07	0.43 ± 0.01	0.49 ± 0.01
Breaking strain (%)	328 ± 19	108 ± 7	180 ± 24	139 ± 12
Ultimate strength (MPa)	0.83 ± 0.2	1.90 ± 0.19	0.81 ± 0.09	0.72 ± 0.06

Table B-6 Summary of mechanical results for GPTS-GO samples.

	Neat vitrimer	01GPTS	05GPTS	1GPTS
Young's modulus (0-0.1% strain, MPa)	2.4 ± 0.3	5.2 ± 0.8	55.2 ± 6.8	8.5 ± 1.4
Young's modulus (60-80% strain, MPa)	0.47 ± 0.14	0.51 ± 0.06	1.4 ± 0.3	0.60 ± 0.04
Breaking strain (%)	328 ± 19	190 ± 17	170 ± 28	197 ± 17
Ultimate strength (MPa)	0.83 ± 0.2	1.8 ± 0.4	2.7 ± 0.5	1.3 ± 0.1

Table B-7 Summary of mechanical results for rGO samples.

	Neat vitrimer	01rGO	05rGO	1rGO
Young's modulus (0-0.1% strain, MPa)	2.4 ± 0.3	23.1 ± 3.7	95.5 ± 13.6	10.4 ± 1.9
Young's modulus (60-80% strain, MPa)	0.47 ± 0.14	0.8 ± 0.2	1.5 ± 0.1	0.82 ± 0.02
Breaking strain (%)	328 ± 19	134 ± 10	148 ± 13	124 ± 6
Ultimate strength (MPa)	0.83 ± 0.2	1.3 ± 0.2	3.0 ± 0.5	1.1 ± 0.1

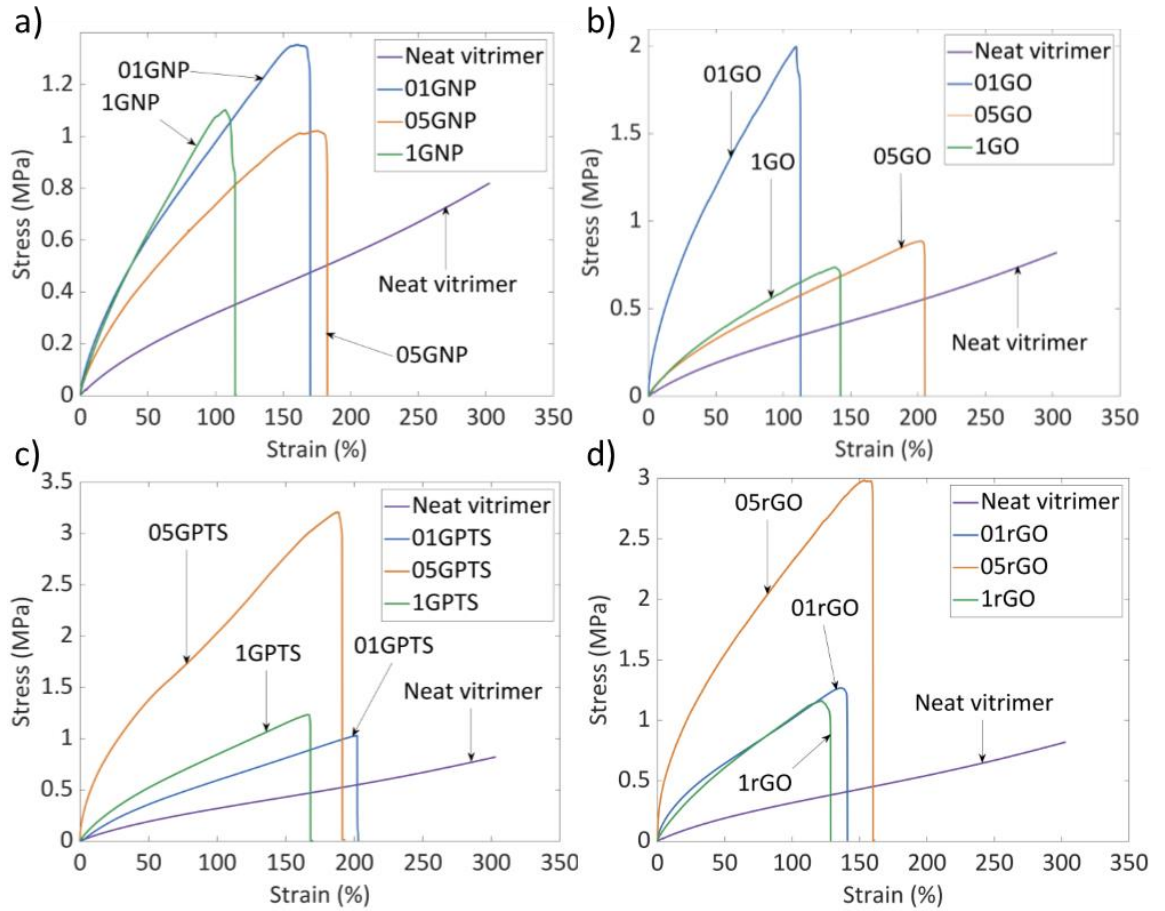


Figure B-14 Typical strain-stress curve for nanocomposites: a) GNP samples, b) GO samples, c) GPTS samples, d) rGO samples.

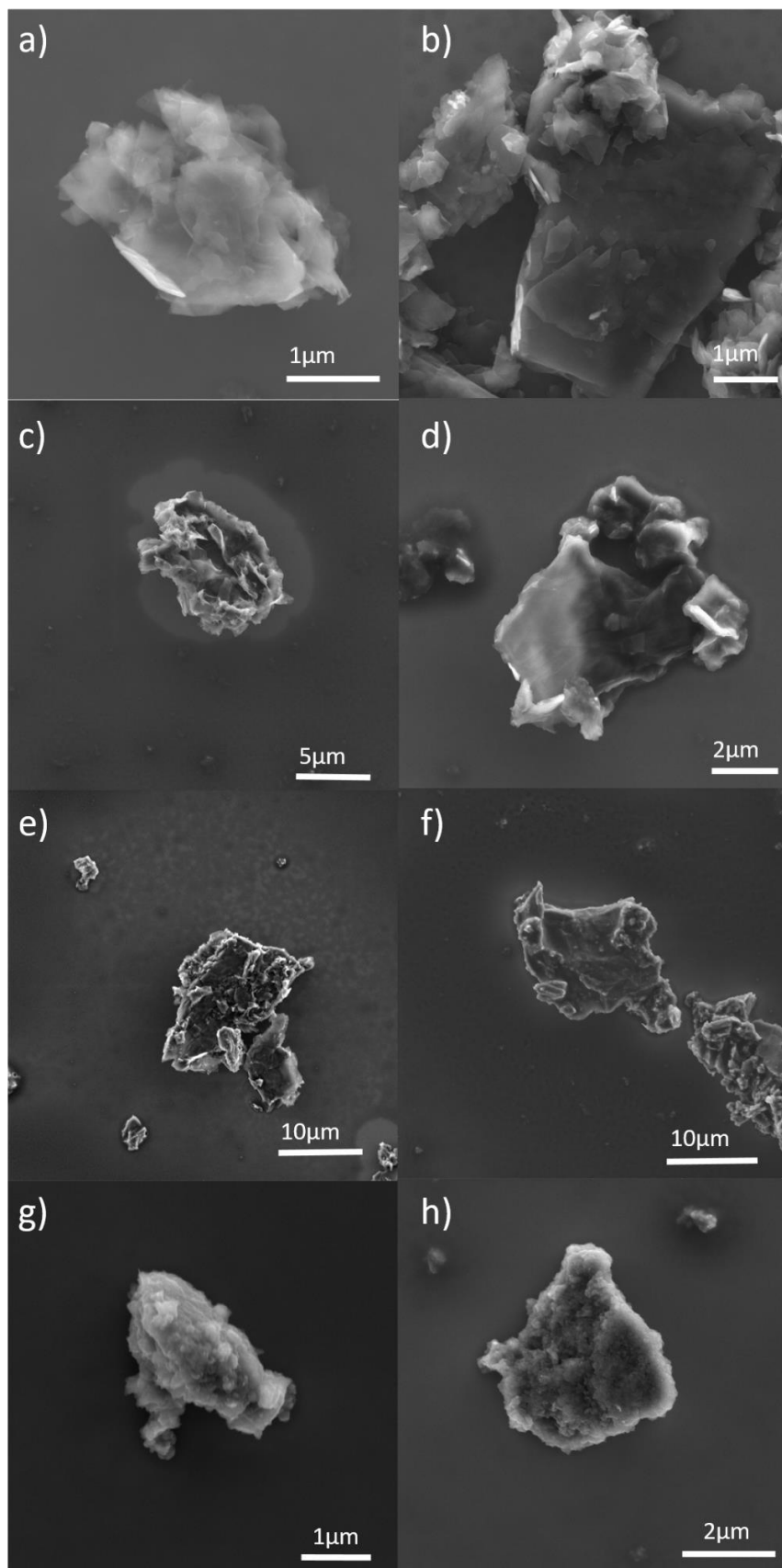


Figure B-15 SEM micrograph of original and recycled nanoparticles: a) original GNP, b) recycled GNP, c) original GO, d) recycled GO, e) original GPTS-GO, f) recycled GPTS-GO, g) original rGO, and h) recycled rGO.

B.9. Complementary data for XPS

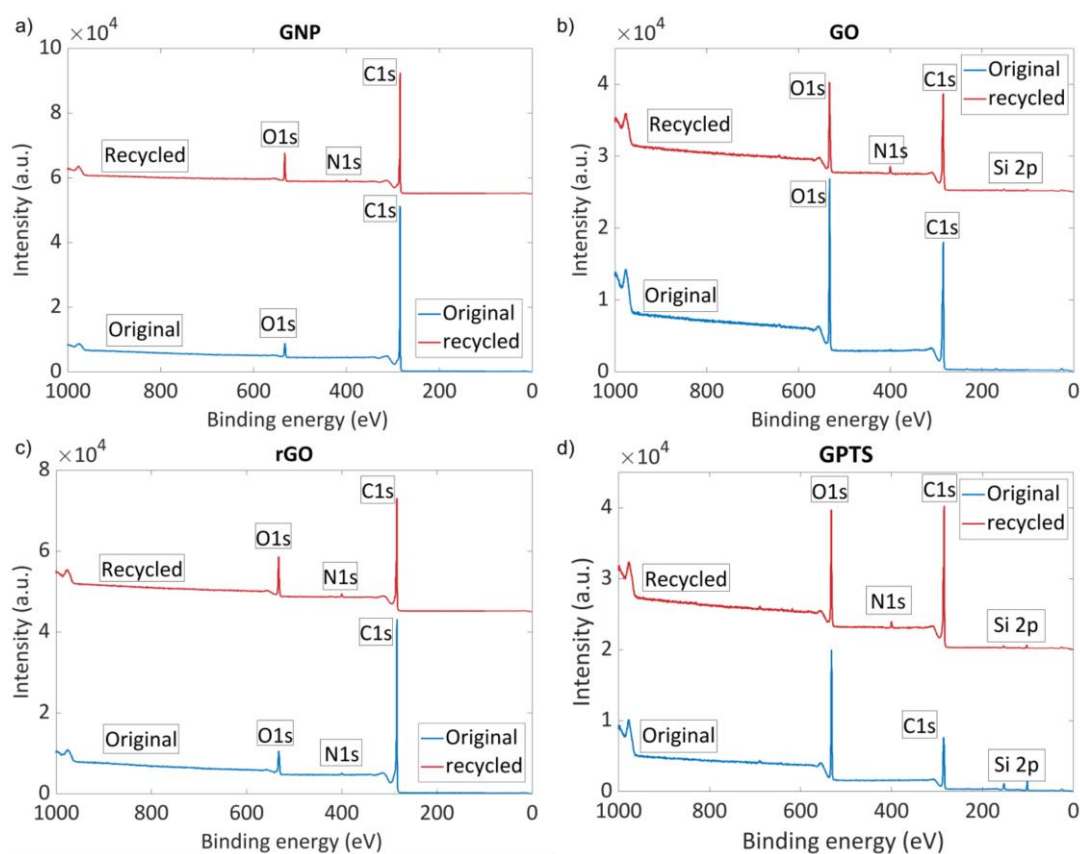


Figure B-16 XPS survey for original and recycled nanoparticles: a) GNP, b) GO, c) GPTS-GO and d) rGO.

Table B-8 Summary of the elemental composition calculated from survey XPS data with nitrogen and silicon compounds.

	GNP		GO		GPTS-GO		rGO	
	Original	Recycled	Original	Recycled	Original	Recycled	Original	Recycled
O_{1s} (%)	5.5	9.1	25.7	21.6	34.5	19.5	7.2	12.2
C_{1s} (%)	94.2	89.6	73.4	74.8	58	77.1	91.8	86.3
Si_{2p} (%)	0.05	0.2	0.45	1.34	7.5	1.5	0.15	0
N_{1s} (%)	0.3	1	0.4	2.34	0	1.8	0.8	1.5

Table B-9 Contributions of individual chemical moieties in the high-resolution C 1s spectra of original and recycled GNP, GO, GPTS-GO and rGO nanoparticles - nitrogen and silicon were removed for fitting to limit artefact.

	GNP		GO		GPTS-GO		rGO	
	Original	Recycled	Original	Recycled	Original	Recycled	Original	Recycled
C=C (%)	94.6	61.8	15.4	20.6	10.8	50	64.1	36.7
C-C (%)	0	18.3	51.5	40.8	36.2	19.6	19	38
C-O (%)	1.5	13.8	29.6	34.4	48.2	26.1	6.6	19.1
C=O (%)	0.6	1.7	3.6	3.9	3.6	3.8	3.5	3.8
π-π*	3.3	4.4	0	0.3	1.2	0.5	6.7	2.5

B.10. References

- [1] A. Souvignet, "Reprocessing of vitrimer composites and recycling of graphene nanoparticles," Manchester, 2019.
- [2] Y. Baghdadi, "Enhancement of the Mechanical Properties of Vitrimers using Functionalised Graphene Nanoplatelets," Manchester, 2018.

CHAPTER 5 - PRELIMINARY STATEMENT

This chapter comes from an original idea of Mathieu Gresil, Christopher Blandford and Quentin-Arthur Poutrel (QAP) from the University of Manchester to use enzyme as catalyst for vitrimer. Some research done by QAP suggested that lipases would be the best candidate and the work started to develop enzymatic materials under MG's and Jonny Blaker's (JB) supervision. Initial results quickly led to interest from the University of Manchester which resulted in this material to be patented under the reference: Blandford, CF, Gresil, M, Poutrel, Q-A & Malone, K Jan. 02 2020, Vitrimer containing a biocatalyst, Patent No. WO2020002904A1.

Therefore, this work is currently planned to be submitted as a communication to *Green Chemistry*. However, a communication length was judged not suitable by the author (QAP) to be an acceptable format for a thesis submission. Therefore more information has been added to the main chapter (Chapter 5), and will be transferred to electronic supplementary information (Appendix C) for submission to *Green Chemistry*.

This chapter is a collaboration between QAP and the MSc student AB (see declaration for full name) supervised by MG. In this chapter, samples manufacture was performed by QAP while enzyme activity assay, UV-visible data and FTIR of bulk samples were performed and collected by AU. DSC, DMA, swelling, soluble fraction data were collected as a team between AU and QAP; TGA samples were left to the University of Manchester service by AU. Creep data were collected by QAP and shared with AU for her report. Healing and reprocessing pictures were used to fill the patent report. Lorna Hepworth (LH) kindly realised the 3D structure of the lipase used in the graphical abstract. Rest of non-mentioned data are from QAP. All figures and analysis of this chapter are originated from QAP.

Chapter 5. Enzymer: sustainable enzymatic catalysis to produce new supramolecular thermoset quenchable to vitrimer material

Authors: Quentin-Arthur Poutrel^{a,b,*}, Auriane Bagur^b, Jonny Blaker^b, Matthieu Gresil^{c,*}

^a Aerospace Research Institute, The University of Manchester, Manchester, UK

^b Department of Materials, The University of Manchester, Manchester, UK

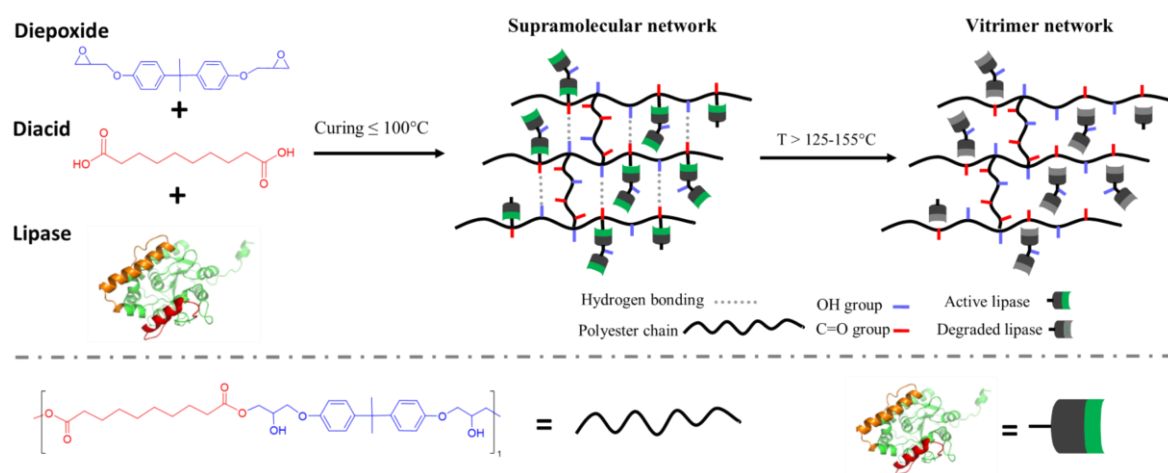
^c i-Composites Lab, Department of Materials Science and Engineering & Department of Mechanical and Aerospace Engineering, Monash University, Clayton, Australia

Corresponding authors: *quentin.a.poutrel@gmail.com *matthieu.gresil@monash.edu

Abstract

Lipases, as a transesterification catalysts, have been widely used in the production of bio-carburant, however, their use is still limited in the polymer field. This research focuses on the use of lipases as catalyst for epoxy-based polymer. The catalytic activity of lipases is used to: (i) enhance crosslink formation, (ii) produce sacrificial supramolecular interaction at low temperature (80°C) and, (iii) induce associative covalent bond exchanges after enzyme denaturation within the network. The produced network is able to flow like glass at higher temperature (185°C - 245°C) while remaining insoluble, exhibiting the vitrimer property. Contrary to classic catalysed vitrimer network, enzymers display a capacity to be healed and reprocessed at low temperature (80°C) via supramolecular behaviour. However, both of these properties are limited, once the enzymers is heated above 125°C, the supramolecular behaviour is sacrificed to obtain the vitrimer properties. This is the first reported case of bio-sourced catalyst used to produce a low temperature self-healable and reprocessable thermoset with vitrimer properties.

Graphical abstract



5.1 Introduction

Enzymes are proteins which present an active site, composed of a base, an acid, and a nucleophile, acting as a catalyst by bonding it with the substrate through non-covalent interactions including hydrogen bonds, ionic bonds, and hydrophobic interactions [1]. These proteins, and particularly lipases, have attracted considerable interest since the past three decades for their catalytic properties [2], [3]. The esterase activity of lipases have been found to successfully convert waste oils into esters (*via* transesterification) with results comparable to conventional catalysts, whilst avoiding any saponification [1], [4]. Therefore, biodiesel research led the development of various lipases types with improved regioselectivity, and temperature resistance [4], [5].

Reactions induced by lipases are not limited to transesterifications; they may also catalyse various synthesis reactions such as esterification, amidation, thioesterification, alcoholysis, aminolysis, or acidolysis [3]. For this reason, the use of lipases progressively moved towards monomers [6]–[8] and polymer synthesis [9]. Various polymers have been successfully produced with lipases as a catalyst, such polylactone [6], [10], polyester [11] or copolyester [12]. Their high regioselectivity have been used to design functional polyesters derived from glycerol [13]. Despite various approaches, the use of lipases in polymer networks has only scratched the surface of their potential to produce multifunctional materials. By their complex structures, interactions within polymer networks are often complex to understand and analyse. Lipases can be substrates for polymers but also interact together either by their backbones or active sites leading to

versatile behaviour [14], [15]. These interactions can be either covalent [16], [17] or in the ranges of supramolecular bonding [18], [19]. Recently, Amano lipases G were reported to co-catalyse the formation of a perfectly structured copolymer with laccase and forming supramolecular complexes [20].

Lately, the polymer field has seen the emergence of pioneering materials for multifunctional purposes. In 2011, Leibler and co-workers developed the first vitrimers [11], materials combining aspects of both thermoset and thermoplastic polymers (e.g. insoluble polymers flowing like former glass at high temperature). The permanently crosslinked, yet thermally reprocessable network, is capable of stress relaxation, self-healing, shape memory, and full recyclability [21]–[25]. The first vitrimer networks were based on epoxy-fatty acids system and, with the help of a transesterification catalyst, allows a crosslinked network to exchange its covalent bonds [26]. Since its development, many chemistries have been used to develop vitrimer materials such as disulphide bond [27], vinylogous urethane [28], [29], trialkylsulfonium salts [30] and others [31]–[34]. However epoxy thermosets are used widely in the industry for their improved stability and long lifespan, with usage in adhesives, coatings, and in transport applications as a composite matrix [35]. The epoxy-based polymer industry alone is worth over £6 billion [36] and is only expected to increase. As the market for epoxy resins is growing, so is the demand for environmentally-friendly processing and recycling. However, research concentrated on developing bio-based epoxy vitrimers [21], [27], [37] usually focus on monomers not widely used in the industry. Moreover, healing and reprocessing of vitrimers network usually induces creep of the materials or requires high temperature to active the bond exchange reactions [38]. Research has focused towards decreasing creep by including permanent crosslinks within the vitrimer network [38], [39], or including sacrificial supramolecular interactions (i.e. hydrogen bonds) to achieved healing at lower temperature [40]. The combination of supramolecular network and vitrimer properties is an interesting idea. Supramolecular networks have initially been designed to produce material with self-healing capability and easy processing over short amount of time [41], [42]. Usually, in polymer networks, the dominant mechanism used to achieve supramolecular properties is the formation and breaking of hydrogen bonding [41], [43]. However, the weak energy bonding related to this type of bond ($\approx 1\text{-}5 \text{ kcal.mol}^{-1}$) is limiting their application for high performance polymers [41]. On the other hand, catalysed

vitrimers often requires high temperature to be healed or reprocessed ($> 100^{\circ}\text{C}$, above their vitrification temperature, T_v). Therefore, the concept showed by Liu *et al.* [40] was highly relevant to develop vitrimer with lowered healing and processing temperature. Nevertheless, this solution requires creation of a copolymer with a portion of non-exchangeable bonds which limits the recyclability and reprocessability aspect of the vitrimer.

The present study proposes to tackle this issue by using lipases as a catalyst to produce a vitrimer polyester network based on a commercial epoxy (DGEBA LY564) and sebacic acid (SA) as a hardener. The polymerisation of various epoxy resins with dicarboxylic hardeners catalysed by lipases was previously studied and it was found that at 80°C , up to 99% monomers conversion was achieved (with a 5 wt. % lipases content) compared to no polymerisation without enzymes [44]. The epoxy network is cured at 100°C and its formation analysed by FTIR, reaching high conversion of epoxy and SA due to the enzymes active site. Conservation of mechanical properties and fast healing behaviour at low temperature (80°C) suggests supramolecular interactions induced by the lipases in the cured network. Vitrimer behaviour at high temperatures based on transesterifications is shown using creep study, stress relaxation, and dissolution/swelling experiments. Due to its relative difference with traditional vitrimer, the lipases catalysed network was named enzymmer.

5.2 Materials

The epoxy resin used was araldite LY564, bisphenol A diglycidyl ether (DGEBA) (174-176 *ew*) purchased from Huntsman advanced materials, Switzerland. Sebacic acid ($202.2 \text{ g}\cdot\text{mol}^{-1}$) was used as hardener and purchased from Tokyo chemical industry. Lipases TL[®] from *P. stutzeri* were purchased from Meito-Sangyo (Japan). 1,2,4-trichlorobenzene anhydrous $> 99\%$ (TCB), protease cocktail inhibitor tablets, 4-nitrophenylpalmitate (NPP), ethylene glycol (EG) and acetonitrile (AC) were purchased from Sigma Aldrich. 1,5,7-triazabicyclo[4.4.0]dec-5-ene (TBD) was purchased from Tokyo chemical industry. All chemicals were used without further modification.

5.3 Methods

5.3.1 Sample preparation

All samples were prepared using a 1:1 ratio of functional groups of epoxy to sebacic acid. Sebacic acid granules were ground into a fine powder manually using a mortar. It was then mixed with the epoxy DGEBA, and the enzymes were added subsequently to the mixture with a content of 3wt. % (TL3) of the total weight of the mixture. As enzymes are known to be degraded by temperature, the enzyme powder was put in an oven at 200°C for 2 h to degrade the active site (unfolding/denaturation of the proteins to deactivate them), and a sample was produced with 3 wt. % of this powder, namely TDL (thermally degraded lipases). A control sample was made without any enzyme loading (no catalyst, NC). Some data are compared with a vitrimer sample prepared from previous work [39] catalysed by TBD with 5% mol of the epoxy functions (curing conditions were different for this sample and can be found in [39]). The rough mixture was then transferred to a batch mixer to be mixed at 400 rpm, 60°C, for 24 h. The mixture was then degassed for 2 h at 50°C under vacuum. The final preparation was then transferred into mould for curing at 100°C for 72 h. Following initial results of dynamical mechanical analysis (DMA), one sample of TL3 was postcured at 200°C for 2 h for further characterisation, namely PTL3.

Table 5-1 Samples composition and labelling.

Catalyst	Content	Label
Raw Lipase	3 wt. %	TL3
Thermally-degraded lipase	3 wt. %	TDL
Raw lipase – postcured sample (2 h, 200°C for DMA analysis and cut healing)	3 wt. %	PTL3
None		NC
TBD	5 % meq	TBD

5.3.2 Lipase activity assay

Activity of lipases was measured by using UV-visible recording of the absorbance between 300 nm and 700 nm. Lipase was dissolved in water (0.5 mg/ml), and tested with

the help of a freshly made NPP solution in acetonitrile (10 mM), a known substrate for the enzyme active site [45]. The ratio NPP solution:lipase solution was fixed at 1:100.

5.3.3 IR monitoring of the curing process and cured samples

Attenuated total reflection Fourier-transform infrared spectroscopy (ATR-FTIR) was conducted using a Bruker INVENIO spectrometer equipped with a SPECAC high-temperature golden gate ATR accessory. Compounds were placed into a mortar and slowly ground/mixed together (with limited pressure applied) until a homogenous mixture was obtained. Resulting mixture was transferred directly on previously heated cell and curing was recorded at 100°C for 72 h. TL3 sample was then heated to 190°C with a 10°C stepwise to observe chemical change(s) in the network. For this study, most relevant information was found in the 900-2000 cm^{-1} and 3400-3800 cm^{-1} wavenumber range. The IR analysis method for integration and defined peak follows the procedure developed previously [39]. Hydroxyl groups (range 3590-3400 cm^{-1} for integration) were added in this study for a better understanding of the network formation catalysed by the enzymes. Spectrum of cured samples were performed at room temperature, scanned from 4000 to 400 cm^{-1} with a resolution of 4.0 cm^{-1} 64 times.

5.3.4 Swelling and soluble fraction analysis

Swelling behaviors were performed using samples measuring approximately 5 mm \times 5 mm \times 3 mm [8]. Samples were weighed and their dimensions measured before being immersed in 1,2,4-trichlorobenzene (TCB). After one-week immersion at 80°C, the sample surfaces were wiped with fabric and stabilised at room temperature for 2 days in order to avoid any thermal expansion effects; weight was then recorded. Solvent was then vacuum-removed at 170°C overnight and the samples were weighed again. After this process, samples were immersed again in TCB at 160°C for 3 days and previous experimental procedure was repeated to measure wet and dry weight.

5.3.5 Dissolution experiment

Dissolution tests were performed on enzymed samples. For each sample type, 2 cubes were cut from bigger plates measuring approximately 5 mm \times 5 mm \times 3 mm. Half of

these samples were put at 80°C in EG, the other half was heated up to 160°C in EG. All samples were left 24 h in solvent before heating was shut.

5.3.6 Thermomechanical characterisations

Differential scanning calorimetry (DSC) analyses were performed on TA DSC 2500 apparatus. Two heating cycles, from -40 to 100°C, were performed at 10°C.min⁻¹.

Thermogravimetric analyses (TGA) were conducted on a TA Q5000 SA. Samples were subjected to a heating ramp from 25°C to 1000°C at a speed of 10°C min⁻¹ under a nitrogen flow and an air flow.

Dynamic mechanical analysis (DMA) was operated in the dual cantilever mode on rectangular samples (55 mm × 15 mm × 4 mm) with a heating regime of -30°C to 200°C at 3°C min⁻¹, and a measurement frequency of 1 Hz following standard procedures to measure the glass transition temperature (T_g).

Crack healing was performed after freezing the sample at -18°C and applying a relatively light impact by hammer on the cold polymer. After formation of cracks, healing sample was performed at 80°C for 10 min.

Cut healing was performed after cutting the samples with a blade on a short distance (> 5 mm), samples (TL3 and PTL3) were put at 80°C for 10min in an oven without application of external pressure.

Polymer reprocessing was performed by grinding the frozen sample in a grinder; the ground polymer was then transferred to a steel mould and hot pressed at 80°C for 1 h with an applied pressure of 10 MPa.

Quasi-static tensile tests of original and reprocessed samples were performed on a rectangular samples (45 mm × 15 mm × 4 mm), using an Instron 5969 model testing machine, equipped with a 2 kN load cell. The samples were tested at 25°C at a displacement rate of 3mm.min⁻¹ to obtain the elastic modulus of these samples.

Stress relaxation experiments were conducted using a Q800 DMA (TA Instruments, USA) operating in the shear mode on rectangular samples (50 mm × 50 mm × 4 mm) with 1% strain applied and allowed to relax for 500min at each temperature. Stress relaxation was initially performed at 100°C, and following information from creep results, the samples was first heated to 200°C for 60min to ensure stabilization of network properties above

130°C. Stress relaxation was then performed at 150°C and 200°C for 500 min. TL3 sample was also tested at 250°C for 180 min.

Creep experiments were performed using a Q800 DMA (TA Instruments, USA) on round disk samples ($t = 5$ mm, $d = 10$ mm) cut from larger plates to observe bulk flow. The compression clamping system was chosen to minimise the noise due to measurement, artefacts due to samples breaking, and to minimise oxidation during the experiment. For all samples, creep measurements were performed at several temperatures (from 60°C to 250°C). Samples were heated and left at 60°C for 5 min before applying a force of 0.1 MPa for 30 min. Samples were then left to relax for 10 min and heated to the next temperature, and then the measurement was repeated. After the first cycle of creep, the same methodology was applied a second and third time between 125°C and 250°C. After the third cycle of creep, the sample was submitted to a last creep test between 60°C and 100°C.

5.4 Results and discussion

5.4.1 Preliminary information regarding NC sample

Throughout recording of FTIR measurement, NC sample showed no signals while recording ($\approx 0\%$ ATR on the measured range). The sebacic acid has a melting temperature of $\approx 135^\circ\text{C}$ and is only partially soluble in epoxy medium (source: sigma-Aldrich), therefore, when ground and mixed manually in a mortar, the SA had no possibility to react swiftly enough with the epoxy. Epoxy DGEBA LY564 is a low viscosity grade resin; at 100°C the small amount of compounds easily separate and the SA agglomerates on the FTIR cell. The solid white compound (SA) could not be measured for kinetic comparison with TL3 and TDL samples. For this reason, the kinetic analysis, but also DMA in dual cantilever geometry of NC, were not possible. However, it should be noted that these non-measurable data actually reinforce the fact that lipases TL are a good candidate to produce ester vitrimer network from ring opening polymerisation as it is demonstrated throughout this study.

5.4.2 Enzyme activity assay

To confirm that the thermal treatment of lipases had successfully degraded the active site of the protein, the UV-vis spectrum of both proteins was recorded. The enzyme active site performs hydrolysis of the NPP to 4-Nitrophenol (PNP), and using the acetonitrile

solution as buffer, the absorption peak at 400 nm confirms the presence of PNP [45]. Absence of absorbance peak confirms that the enzyme active is degraded. For the neat lipases TL, the peak is visible (Figure 5-1), however, thermally-degraded lipases a barely visible absorption band is seen, confirming that most the enzymes active site have been successfully degraded during the thermal treatment.

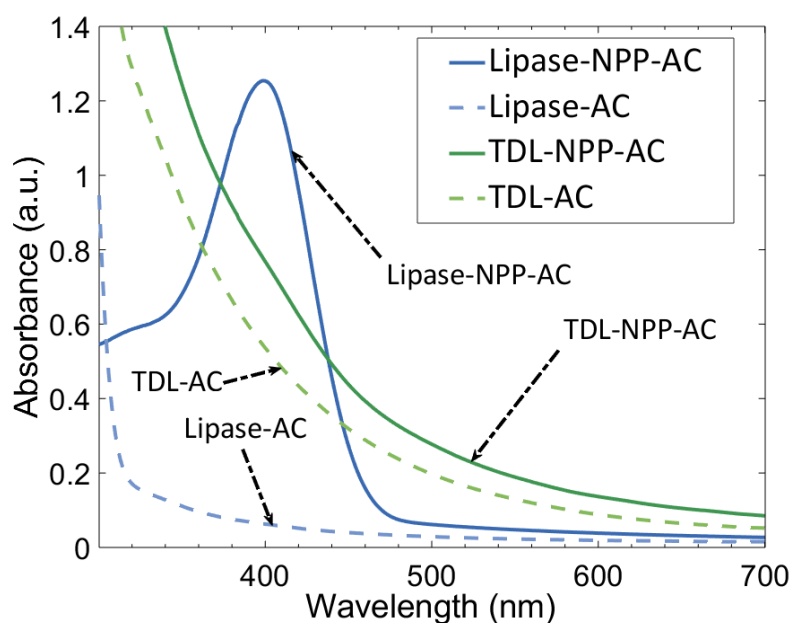


Figure 5-1 UV-Vis spectrum of lipase TL and thermally degraded lipase (TDL) - curve of lipases without NPP have been represented to show that no activity can be recorded without the use of NPP - adapted from [46].

5.4.3 Analysis of network formation via ATR-IR

Species evolution with raw enzymes and thermally degraded enzyme (3wt. %)

The evolution of ester and epoxy for TL3 and TDL samples are represented in Figure 5-2, and spectrum at $t = 0$ h and $t = 72$ h are presented in Figure C-1 with relevant peaks used for integration (as described in Chapter 3 and Appendix A). For both samples, the ester and epoxy curves follow complementary evolution demonstrating that both lipases (neat and degraded) are able to catalyse the esterification of the epoxy with SA. The TL3 sample shows a sharp increase of ester between 0 h and ≈ 12 h and reaches a plateau at ≈ 20 h. This result is consistent with previous studies of esterification between epoxy and carboxylic acid, where the reaction kinetic is initially fast, and slows down when available reactive groups (epoxy and carboxyl) are below $\approx 85\%$ of their initial concentration [47]–

[49]. Despite similar behaviour, TDL sample exhibits a much slower conversion rate, the sharpness of the initial increase is lowered and the time required to slow down the reaction is almost 3 times longer (≈ 34 h). After the 72 h curing cycle, the reaction still does not reach a plateau, indicating that the thermally-degraded lipases still catalyse the esterification (compared to the NC sample) but at a much slower pace than the neat lipases with an active site. The evolution of free hydroxyl signature follows (Figure C-2) the esters timing in both samples, confirming that the measured hydroxyl peak during curing of TL3 and TDL correspond to the formation of the ester network. However, the hydroxyl signature in TDL samples exhibits several plateaus compared to the TL3 one (which exhibits almost perfect linear matching of its related ester signature). From these and the UV-vis results it is likely that the small amount of remaining active sites from thermally-degraded lipases are responsible for the slower esterification of the network. The enzyme active site is effectively necessary for efficient catalysis of the esterification between epoxy and SA at 100°C .

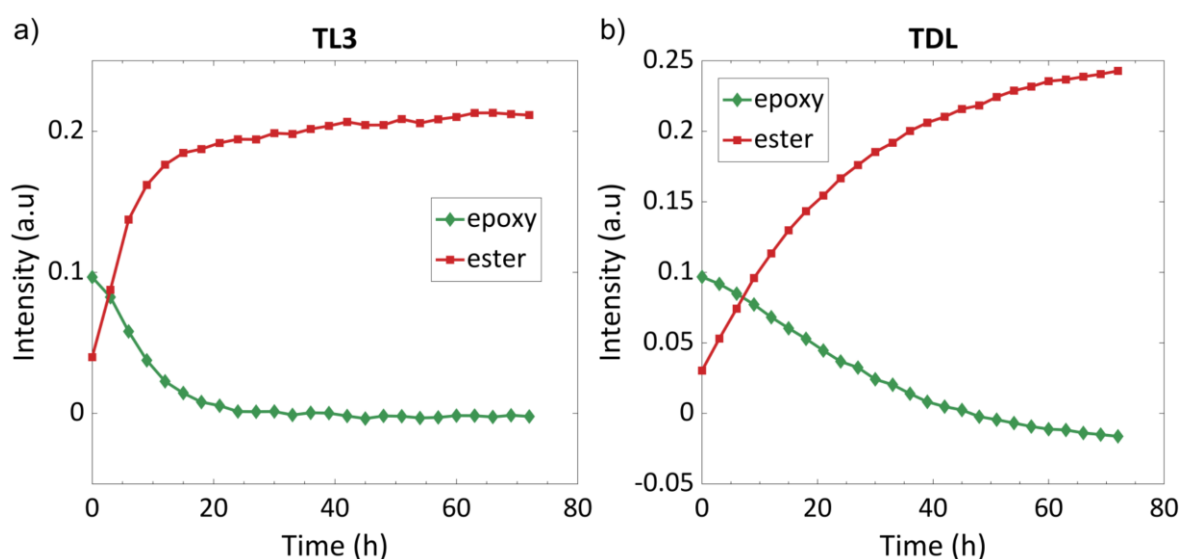


Figure 5-2 Evolution of ester (red square curve) and epoxy signature (diamond green curve) obtained via ATR-IR for: a) TL3 sample and, b) TDL sample. Values were normalised by the benzene epoxy peak located between $1490\text{-}1526\text{ cm}^{-1}$.

The acid and ether signatures evolution of TL3 and TDL are presented in Figure 5-3. The small values represented in the y-axis come from normalisation using the epoxy benzene ring peak ($1490\text{-}1526\text{ cm}^{-1}$) which is several orders bigger than the integrated peak of relevant species. This renders curves noisy but trends are conserved and can be analysed. Once again, both samples exhibit similar trend in their curing behaviour, with TDL

sample evolution being slower than TL3. However, a noticeable fact is that the acid and ether species initially increase (≈ 6 h for TL3 and ≈ 18 h for TDL) while it is expected that the acid signatures decrease concomitantly with the epoxy signature (while reacting together to form the ester network). After these maximum values, the acid curves decline, showing a plateau after ≈ 20 h for TL3 sample (matching the time of the epoxy plateau in Figure 5-2a) while the acid signature of TDL still declines after 72 h, confirming that the esterification is not finished with the degraded lipases. The ether curves exhibit a short plateau (to ≈ 15 h for TL3 and ≈ 35 h for TDL) and then an overall decreasing for the rest of the 72 h curing cycle. This fact is an interesting point for the vitrimer chemistry, as traditional catalysts usually also promotes network etherification between epoxy functional groups leading to permanent crosslinks [47], [50], [51]. Here the high regioselectivity of the lipase active site seems to promote only esterification of the network. However this area is known to be difficult to integrate in epoxy network [39], and the small values reported may also be influenced by artefacts induced through other C-O and O-H moieties within the $1000\text{-}1200\text{ cm}^{-1}$ range.

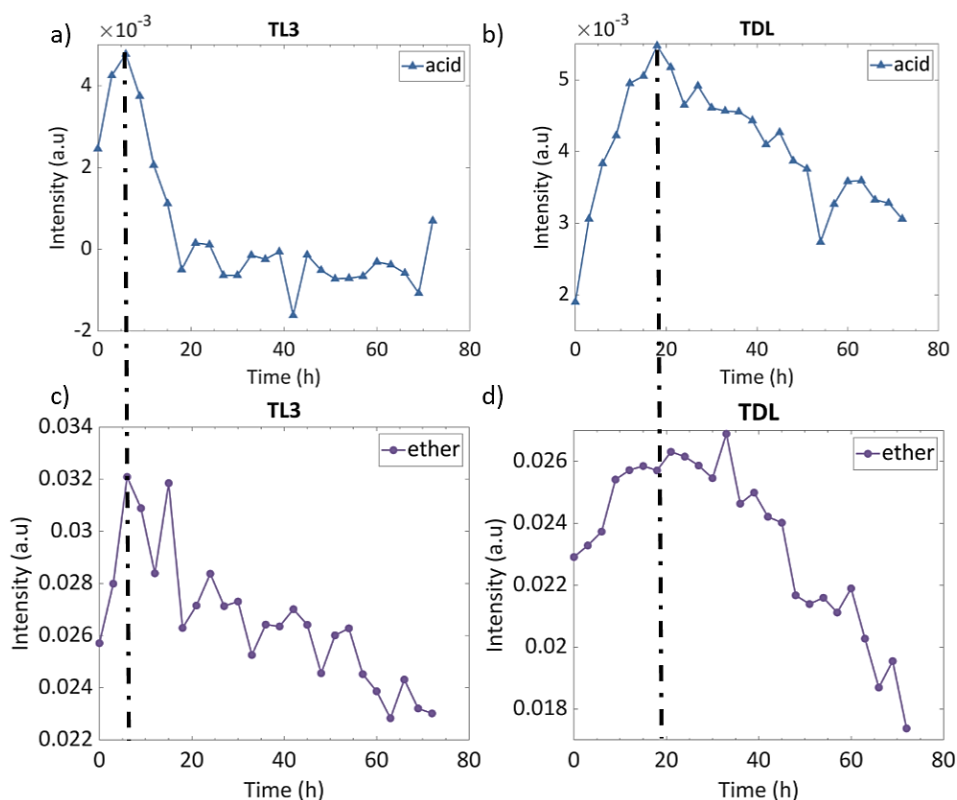


Figure 5-3 Evolution of acid (blue triangle curves) and ether species (purple circle curves) for TL3 sample (a, c) and TDL sample (b, d). The black dotted line represents the maximum peak of acid species and corresponding time in the ether signature evolution. Value were normalised by the benzene epoxy peak located between $1490\text{-}1526\text{ cm}^{-1}$.

Mechanism of epoxy ring opening via enzyme active site

To understand the behaviour of the acid signatures from TL3 and TDL samples, the reaction between only the neat lipases and epoxy was investigated over 72 h at 100°C. Initial and final spectrums are shown in Figure 5-4. Ester signal peak ($\tilde{\nu} \approx 1735\text{cm}^{-1}$) is not observed after 72 h because no polymerisation can occur. The epoxy peak ($\tilde{\nu} \approx 914\text{cm}^{-1}$) is still visible after 72 h, although the apparition of hydroxyl group (3000-3600 cm^{-1} range) shows that some reaction took place during the measurement.

A noticeable peak is seen at $t = 0$ h located at $\tilde{\nu} \approx 1105\text{cm}^{-1}$ (Figure 5-4), and was reported to be one of lipases' characteristic IR peaks [17]. At $t = 72$ h this peak is strongly reduced. This lipases peak is also present in TDL and TL3 samples at $t = 0$ h (but not in previous network studied with the epoxy SA study catalysed by TBD [39]) and seems to decrease at $t = 72$ h. This is an indicator that epoxy and lipases undergo some interactions with limited impact on the epoxy concentration (Figure C-3a) in the absence of SA. The ether signature (Figure C-3b) does not show an evolution between 0 h and 72 h except oscillation around a mean value (≈ 0.025 a.u.). The hydroxyl peak (Figure C-3c), in the meantime, shows a clear increase between 0 h and 16 h to reach a plateau for the rest of the measurement.

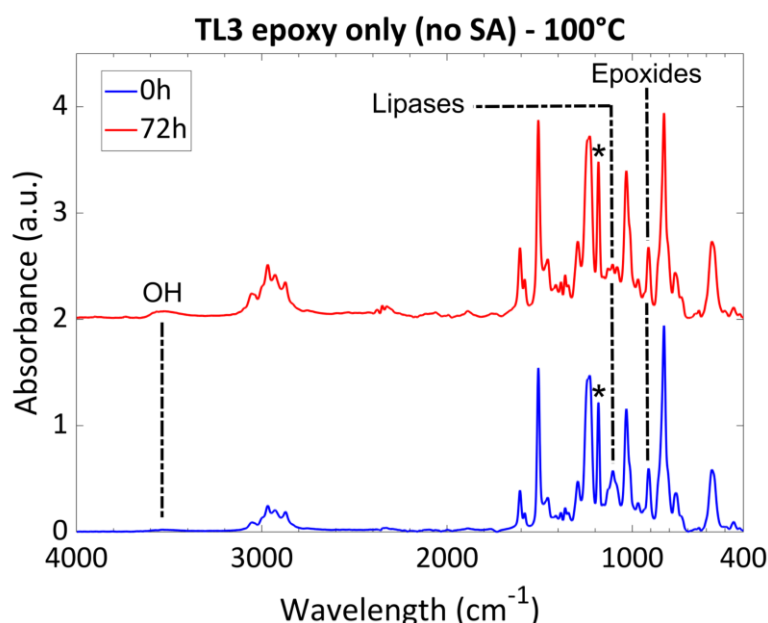


Figure 5-4 ATR-IR spectrums of lipases and epoxy at 100°C at a) $t = 0$ h (blue curve) and b) $t = 72$ h (red curve). The star shows the C-O stretching from epoxy. In samples with sebacic acid this peak increases due to the formation of esters, rendering the lipases peak nearly indiscernible.

To understand this behaviour, the chemical reactions catalysed by lipases have to be considered. The lipases from Meito-Sangyo group are from the class EC 3.1.1.3 and are known to catalyse a variety of synthesis reactions observable via FTIR [3]: (1) hydrolysis, (2) esterification, (3) amidation, (4) thioesterification, (5) transesterifications (comprising acidolysis, alcoholysis, aminolysis and interesterification – as these reactions produce similar compounds they cannot be differentiated by FTIR). They are also known to catalyse ring opening of various component such as lactone [52] or epoxy [16]. In our study, there is no thiol or amine group involved in the polymerisation so reactions (3), (4) are out of consideration.

The active site structure of lipases from Meito-Sangyo was investigated [53] and is comprised of the following amino acids: Tyrosine₅₄ (Tyr₅₄), Serine₁₀₉ (Ser₁₀₉) and Histidine₂₇₇ (His₂₇₇) bound via hydrogen bonding to a S-benzoin, with an Aspartate₃₃₃ (Asp₃₃₃) located below the His₂₇₇ (Figure C-4). It was also determined that without solvent, the catalytic triads responsible for reactions was the Ser₁₀₉, His₂₇₇ and Asp₃₃₃ [53].

The proposed mechanism of epoxy hydrolase *via* lipases shows that the Asp₃₃₃ is responsible for the epoxy ring opening via nucleophile attack of the oxyanion on the carbon's ring [16]. A molecule of water is then cleaving the Asp₃₃₃ and epoxy compound to fully hydrolyse it.

In regard to the epoxy lipases TL reaction (without SA), the production of hydroxyl without water production (absence of scissors band at $\tilde{\nu} \approx 1635\text{cm}^{-1}$) and the absence of full conversion of epoxy remove the possibility to fully hydrolyse of the epoxy. However, the initial mechanism can explain the apparition of the hydroxyl and limited decrease in the epoxy concentration. The Asp₃₃₃ attacks the epoxy ring allowing its opening and producing hydroxyl groups as presented in Figure 5-5. Without water in the medium, the reaction cannot continue towards the full epoxy hydrolysis. Therefore, the production of hydroxyl stops once all lipase active sites are bound with epoxy moieties.

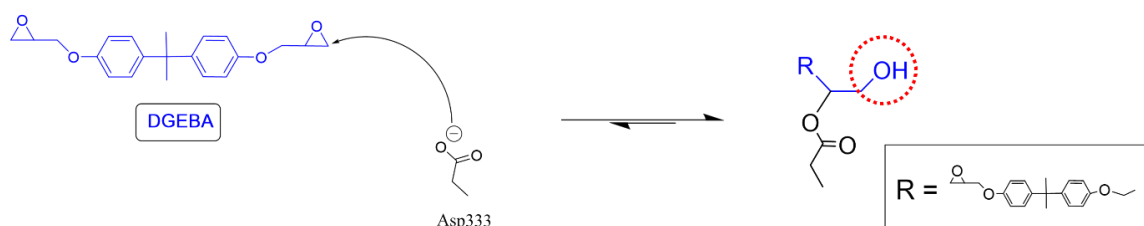


Figure 5-5 Nucleophile attack of the oxyanion from the Asp₃₃₃ on the epoxy ring. The red dotted circle indicates the free hydroxyl groups possibly detected in the IR curing of lipases and epoxy without dicarboxylic acid.

The initial increase of acids and ether signature seen in TL3 and TDL samples still remain to be determined. None of these signatures were detected in the lipases/epoxy curing and previously reported data of TBD catalysed epoxy/SA system show a constant decrease of acid signatures [39] (and slow but constant increase of ether function which was associated with ester formation in a stoichiometry epoxy:SA sets to 1:1). This increase is potentially due to the slow curing of the epoxy/SA system on the IR spectroscope, as the SA was manually grounded and mixed, it is likely that a small sedimentation happens on the ATR cell while performing the measurement. Once this agglomeration settles it can be seen that the SA reacts with the enzyme-acyl complex in order to form the ester network potentially via different hydrogen interaction within the enzyme active site which would need to be determined.

The continuous decrease of both ether signature after full acid consumption is still unclear. It was previously reported that the ether signature can correspond to the C-OH stretching of ester compound [39]. Decrease in the ether signature could be associated with crosslinking of the C=O bonds of a corresponding ester or potential hydrogen interactions between these two bonds. As both reactants are bifunctional, the production of a crosslink material would not be achieved without these intra-ester bonding. Therefore, the decrease of intensity and small variations among other area of the spectrum could be induced by the reaction of the OH from ester chains with either epoxy or SA monomers.

The studied mechanism would require further study (*e.g.* small molecules study, modelling of distance between compounds in the active site, fluorescence, HPLC, *etc.*) to be entirely understood. Many interaction can still be considered such as the hydrogen interaction between SA and histidine compound to favour the esterification and/or transesterification. However, the active site of the lipase TL is still confirmed to be a good catalyst of polyaddition for epoxy compound at low temperature ($\approx 100^{\circ}\text{C}$).

5.4.4 Polymer characterisation (general properties)

Once the kinetic study was performed, bulk polymers (NC, TDL and TL3) were produced in open moulds with a 5 mm thickness. Once unmoulded, it was clear that the neat lipases were catalysing the epoxy/SA esterification better compared to thermally degraded lipases. A biphasic sample was obtained after curing of the polymers for NC and

TDL with a sediment phase (bottom phase, $\approx 3\text{mm}$ white for NC and dark brown for TDL) and a clearer phase at the samples top half (top phase, $\approx 2\text{mm}$ transparent for NC and clear yellowish for TDL) as shown in Figure 5-6. TL3 sample was however quite homogenous despite a small gradient barely visible to the naked eye. The temperature of curing (100°C) does not allow a fast reaction between epoxy and SA. Moreover, as the SA was partially dissolved during the 24 h mechanical mixing, a possible de-solvation may happen once the mixture is left unagitated. With this in mind, it was clear that the slow reaction of epoxy/SA led to sedimentation of SA at the bottom of NC sample, and sedimentation of SA and most enzymes at the bottom of TDL sample. On the other hand, the homogenous colour of TL3 demonstrates that the faster polymerisation observed via FTIR was enough to catalyse the esterification reaction. During polymer characterisation, NC sample was not polymerised enough to be characterised by DMA in dual cantilever or other geometry. Therefore, in order to compare storage modulus, loss modulus and $T\alpha$, a sample previously studied catalysed with TBD was added to the analysis.

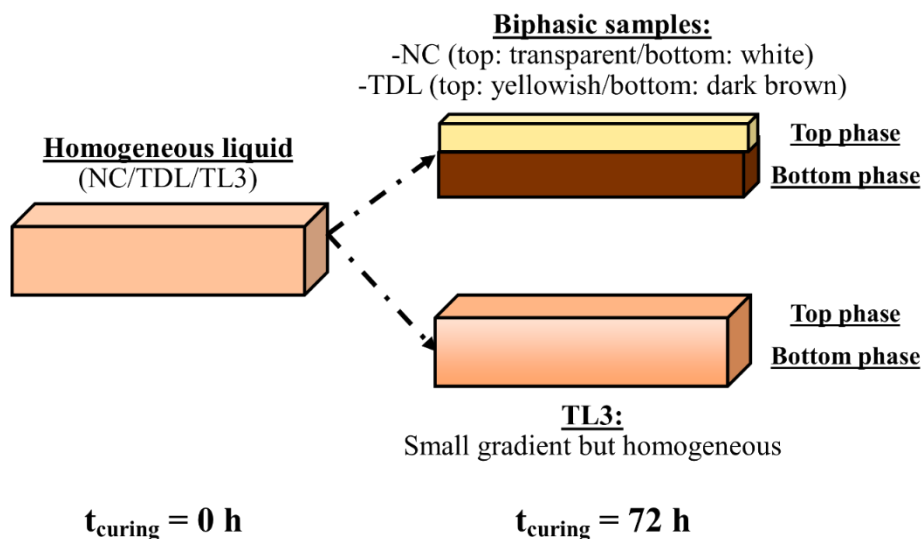


Figure 5-6 Schematic of sample phase separation after 72 h curing cycles: NC and TDL exhibit a sediment phase ($\approx 3\text{mm}$) and a clearer top surface ($\approx 2\text{mm}$) and TL3 sample exhibits a homogenous brown colour with a small gradient over its thickness.

Bi-phase polymer without catalyst and with TDL

The chemical nature of each face (top and bottom) was investigated by FTIR and are represented in Figure 5-7 for NC and TDL samples, and in Figure 5-8 for TL3 sample. In NC sample (Figure 5-7a), both faces exhibit remaining epoxy and acids signatures with a small

ester signature appearing on the left side of the acid one, confirming that the esterification of the network only partially started after the 72 h curing cycle. On the other hand, TDL sample (Figure 5-7b) exhibits two difference chemical structures between faces. The top spectrum is similar to the NC sample with unreacted acids and epoxides and few esters. However, the bottom face (with agglomeration of lipases and sebacic acid) of TDL sample has a single ester signature with a clear hydroxyl peak ($\tilde{\nu} \approx 3200\text{-}3600\text{ cm}^{-1}$) with no remaining epoxy and acid signatures. The phase separation proves that the catalysis was too slow to lead to a homogeneous curing of the polymer. However, the degraded lipases still achieved esterification on the network for the bottom phase of the sample.

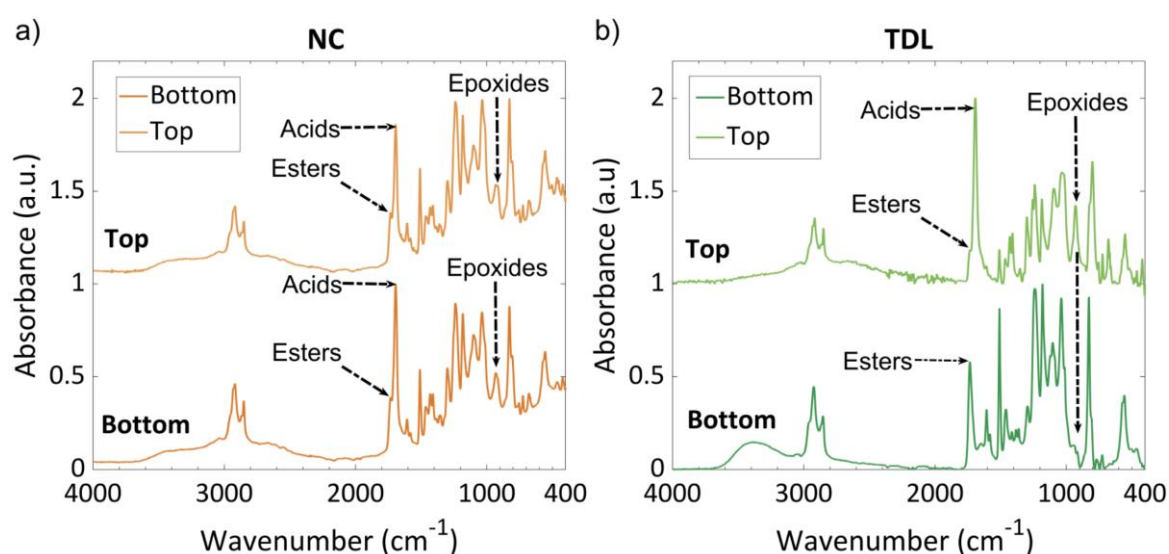


Figure 5-7 FTIR spectra of top and bottom and top surfaces for: a) NC sample, and b) TDL sample.

TL3 sample (Figure 5-8) has both faces with no acid or epoxy signatures remaining, exhibiting full esterification across the whole sample. The T_g of samples phases was determined using DSC as it allows to separate them easily for measurement. DSC results show that the T_g of the NC sample (Figure C-5a) is similar in both phases ($\approx -10^\circ\text{C}$) while the top phase of TDL (Figure C-5b) has similar T_g to NC sample but its bottom phase has a higher value ($\approx 4^\circ\text{C}$). The T_g of the bottom phase of TDL is equivalent to the T_g of TL3 sample (Figure C-6) showing that the crosslink density is higher in the presence of lipases and their active site plays a major role in the ring opening polymerisation reaction.

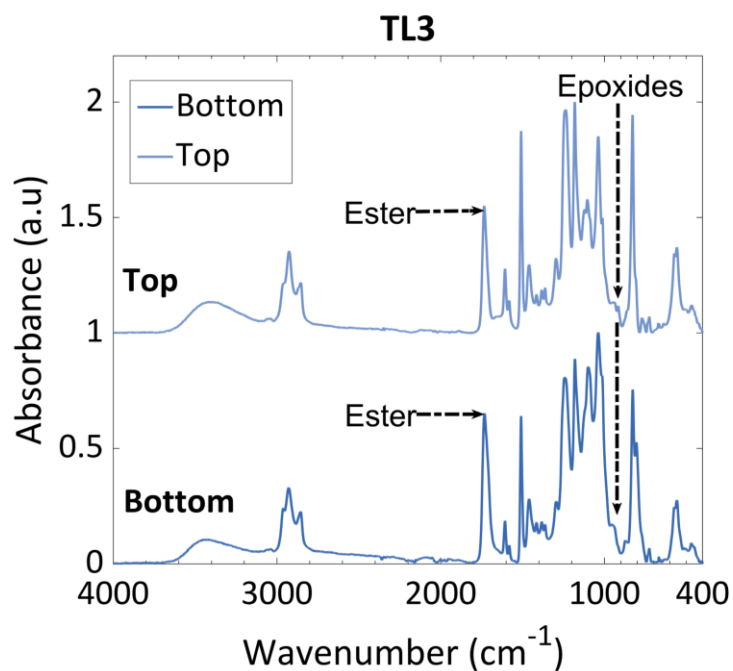


Figure 5-8 FTIR spectra of top and bottom and top surfaces for TL3 sample.

To determine the crosslink level of the resulting polymers, swelling studies were performed and picture of samples after swelling in TCB (7 days at 80°C, followed by 3 days at 160°C) are shown in Figure 5-9a-c. The soluble fraction of each sample is shown in Figure 5-9d and their corresponding swelling ratio in Figure C-7. After 10 days immersion, the NC has a soluble fraction close to 90%, showing a material poorly crosslink as shown from FTIR data, confirming that the esterification reaction was barely achieved without catalyst. TL3 sample has a soluble fraction $\approx 6\%$ after 10 days immersion in TCB, showing a high conversion of monomers to a crosslinked material with few soluble chemical moieties. TDL samples have an intermediate soluble fraction ($\approx 35\%$ after 10 days immersion) and the bottom phase shows almost no volume reduction with mainly the top phase being dissolved by TCB. In correlation with FTIR and DSC measurement, the bottom phase filled with lipases has similar thermomechanical properties than TL3 sample while the phase without lipases was not polymerised and behaves like the NC sample. The swelling ratio (Figure C-7) follows the same trend than the soluble fraction, with TL3 sample having the lowest value ($\approx 185\%$), TDL an intermediate value ($\approx 220\%$) and NC the highest value ($\approx 300\%$), confirming a light crosslinking density for the samples. The swelling of TL3 (and TDL) are higher than previously reported value of epoxy SA vitrimer catalysed by TBD [39], rather confirming that the lipases polymer has a lower crosslink density despite higher conversion

of monomers (lower soluble fraction of TL3 but similar soluble fraction of TDL). This confirms the high selectivity of the lipases to bond the epoxy/SA molecules and that crosslink between resulting ester occurs but in a lower concentration than with other catalyst types.

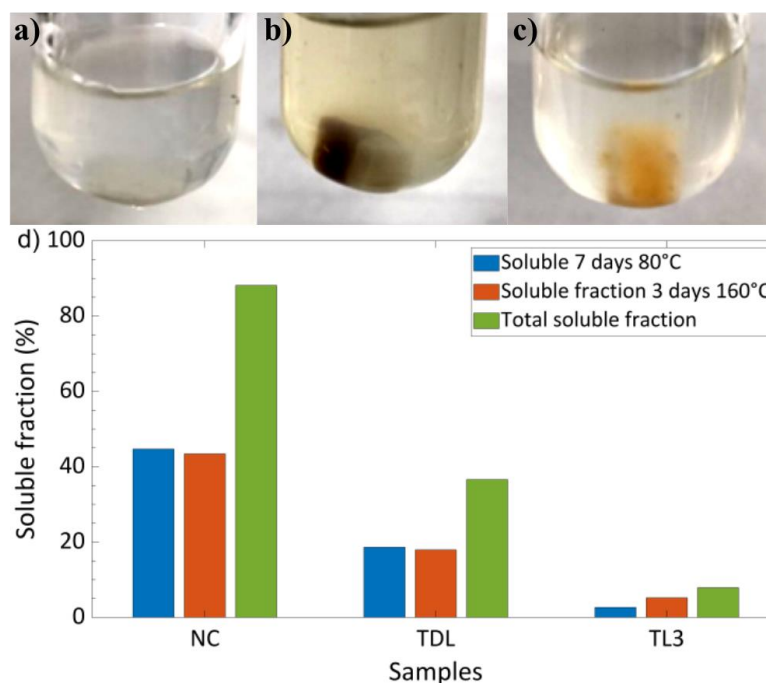


Figure 5-9 Samples after swelling in TCB (7 days at 80°C, followed by 3 days at 135°C): a) NC (delimited by black dotted line), b) TDL, c) TL3. d) Soluble fraction of NC, TDL and TL3 samples after 7 days at 80°C, followed by 3 days at 135°C and the total soluble fraction over 10 days.

DMA results for TDL and TL3 sample are presented in Figure 5-10 and compared to previous data of TBD sample (addition of PTL3 sample is discussed in the next paragraph). TL3 and TDL samples have a $T_{\alpha} \approx 26^{\circ}\text{C}$, PTL3 has a $T_{\alpha} \approx 31^{\circ}\text{C}$ (lower than previous sample catalysed by TBD with have a $T_{\alpha} \approx 40^{\circ}\text{C}$) confirming the ester network produced by lipases has a lower branching density as determined by IR and swelling experiment. However, TL3 and TDL sample exhibit an asymmetry after their T_{α} peak which is more pronounced in TL3 sample (up to 150°C compared to 120°C for TDL sample). At 125°C, both rubbery plateau of these samples exhibits a regular increase until 250°C. It should be noted that for TDL sample, a clear crosslink reaction is observed between 125°C and 170°C which correspond to the top phase of the sample where unreacted sebacic acid starts to melt to polymerise with the epoxy.

Asymmetrical T_{α} peak was previously reported in similar polymer comprised of citric acid which was partially crosslinked [54]; a postcure removed the asymmetry and the

storage modulus became stable at higher temperature. Moreover, a large increase (at least one order of magnitude) of the rubbery modulus was observed following post-cure, and was attributed to further crosslinking of unreacted functional groups [54]. Our previous data (combination of FTIR measurements and swelling experiment) suggested full conversion of epoxy and sebacic acid to ester. Therefore, a strip of TL3 was postcured at 200°C for 2 h and tested, results have been added to Figure 5-10 for comparison (PTL3 sample, red line in Figure 5-10). Effectively, the rubbery modulus becomes stable at higher temperature (with limited value increment compared to TL3 sample), and the tan delta only shows a single symmetrical peak with $T_{\alpha} \approx 31^{\circ}\text{C}$. Contrary to results reported in ref [54], the increase of rubbery plateau and T_{α} are too small to correspond in crosslink of unreacted monomers. This behaviour indicated more of an oxidation of the samples, potential reaction with the backbone of the lipases, or lipases denaturation. A noticeable point is that the TBD sample exhibits a higher value than PTL3 and TL3 of T_{α} (by $\approx 10\text{-}15^{\circ}\text{C}$) ($\approx 4^{\circ}\text{C}$), likely due to some etherification reaction induced by this catalyst type. This confirms the lipases' potential to only carry the network esterification without side reactions.

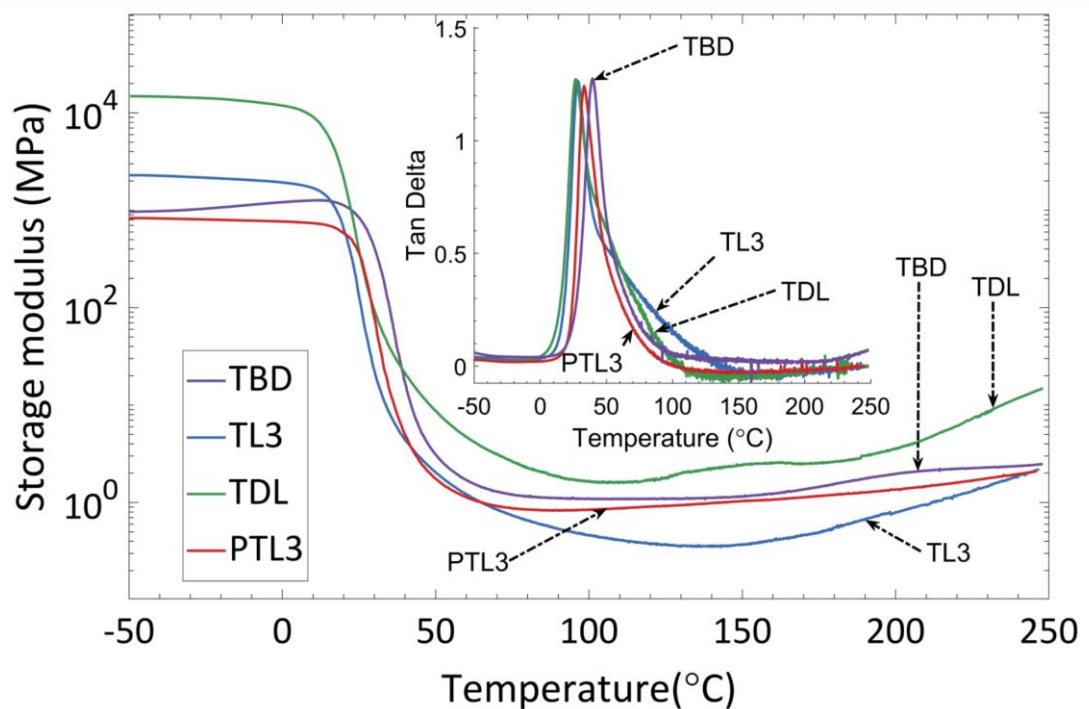


Figure 5-10 DMA results for samples TDL and TL3 compared to TBD and PTL3 (sample PTL3 was added after initial measures to investigate further crosslink mechanism). Inset shows the damping properties of the material with presence of a shoulder for TL3 and TDL sample.

TGA measurement of NC, TDL and PTL3 are shown in Figure 5-11 and degradation temperatures (5% weight) with maximum peak of the weight derivative (T_{dtg}) are outlined in Table 5-2. As the top phase of TDL is in every point similar to the NC sample, only the bottom phase (of TDL) was tested for proper comparison. NC samples exhibit the quickest degradation (330°C), followed by TDL (370°C) and finally TL3 which has the highest degradation temperature (420°C). The weight derivative for NC and TDL shows a small peak between 190°C and 290°C, and between 255°C and 355°C, respectively. This peak is not present for TL3 and is attributed, by deduction, to the unreacted epoxy monomers while the maximum peak degradation of NC samples corresponds to the degradation of unreacted sebacic acid [55]. The presence of this peak at higher temperature in TDL sample indicates that despite polymerisation by denatured lipases, even the bottom surface could not reach maximum conversion of monomers to esters. However, the higher crosslink density partially protects the unreacted sebacic acid against thermal degradation. TL3 sample exhibits a small shoulder at 460°C (barely visible, indicated in the inset of Figure 5-11), which may correspond to the small part of the network not crosslinked, determined by swelling ($\approx 6\%$). Both TDL and TL3 exhibit the highest T_{dtg} at 500°C corresponding to the crosslinked ester network.

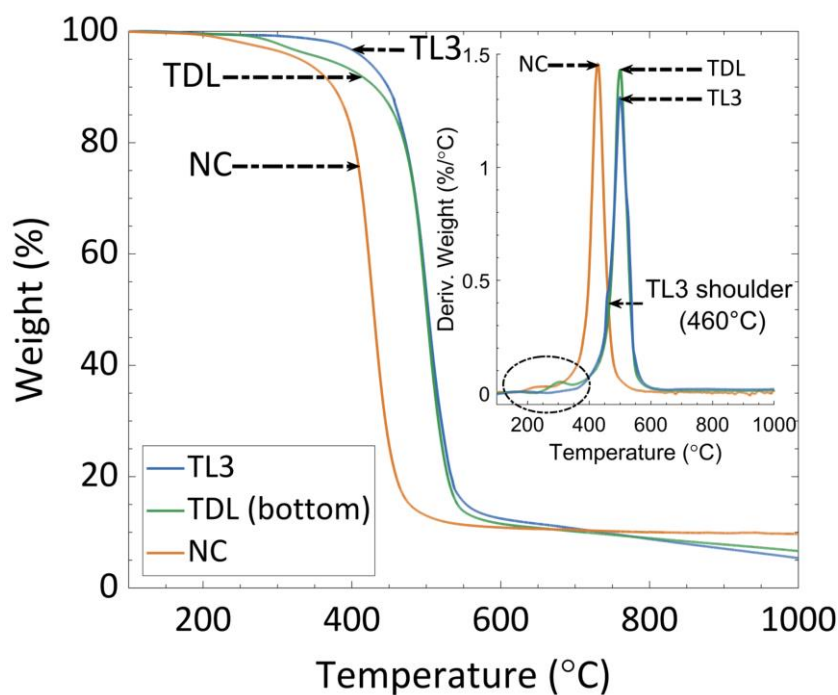


Figure 5-11 TGA results for NC, TDL and TL3 sample under nitrogen atmosphere. The inset represents the weight derivation of the measurement in function of temperature.

Table 5-2 Degradation temperature (5% weight) and maximum peak derivative weight temperature for NC, TDL and TL3 sample.

	$T_{d5\%}$	T_{dtg}
NC	330°C	428°C
TDL	370°C	500°C
TL3	420°C	500°C

5.4.5 Low temperature characterisation

The low temperature (< 100°C) characterisation of healing and reprocessing properties was solely carried out on TL3 sample. Indeed, both NC and TDL have proven to have a high part of unreacted monomers. It would have been impossible to determine if these properties were due to further curing of the polymer rather than its intrinsic properties. As the lipases TL can catalyse transesterification between ester compounds, producing, in theory, a vitrimer network (based on transesterification), the reprocessing, healing, creep, stress relaxation, and dissolution of the polymer bulk was assessed in the range of their activation temperature.

Lipases TL have a main activity peak at $\approx 50^\circ\text{C}$ (source: Meito-Sangyo) with activity decreasing until 80°C . However previous work with lipases on substrate showed an increase in thermal stability of CALB enzyme from 90°C to 160°C [56]. As the lipases TL react with epoxy moieties but also successfully catalyse the esterification of the network at 100°C , the assessment of healing capacity was performed at 80°C (below curing temperature to avoid potential secondary postcure reaction).

The reprocessing of the TL3 was carried out at 80°C for 1 h. After being crushed with a mixer, the mould was filled and placed under hot press. After 1 h (pressure 10 MPa), the sample was removed from the mould showing a homogenous sample despite patterning of the surface due to the peel ply used during the experiment (Figure 5-12). From this recycled sample and TL3 sample, three strips ($45\text{ mm} \times 15\text{ mm} \times 4\text{ mm}$) were cut after surface grinding of the sample and mechanically tested. The tensile curves for original and reprocessed TL3 samples are shown in Figure C-9. From the sample shape (not following standard ASTM), the only comparable data are the initial Young's modulus at low strain (0-0.1%). The original sample has an $E = 3.7 \pm 0.2\text{ MPa}$ and the reprocessed sample shows

a similar value at $E = 3.3 \pm 0.6$ MPa indicating that reprocessing was successfully achieved *via* crosslink of the crushed network.

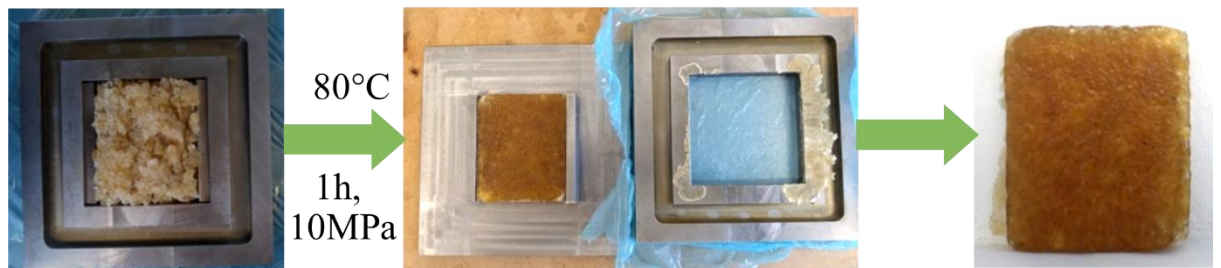


Figure 5-12 Reprocessing of TL3 samples at 80°C for 1h under 10MPa pressure - the rough surface observe of the reprocessed product has been induced by the blue peel ply used during the experiment, mould dimension are 55 x 45 x 5 mm.

Sample repairs were also assessed with internal cracks (Figure 5-13) and cut healing (Figure 5-14a,b). Healing of both cuts and cracks of sample TL3 are achieved within 10 min at 80°C, indicating that the network has a fast healing capacity. In order to confirm the role of the lipases active site in the healing and reprocessing of the sample, a piece of PTL3 sample (post-cured at 200°C for 2 h, allowing the enzymes to be degraded inside the network) was cut and put to heal following the same procedure than TL3. Results are shown in Figure 5-14c,d and no healing of the cracks is observed, confirming the essential role of the lipases in the repairs process.

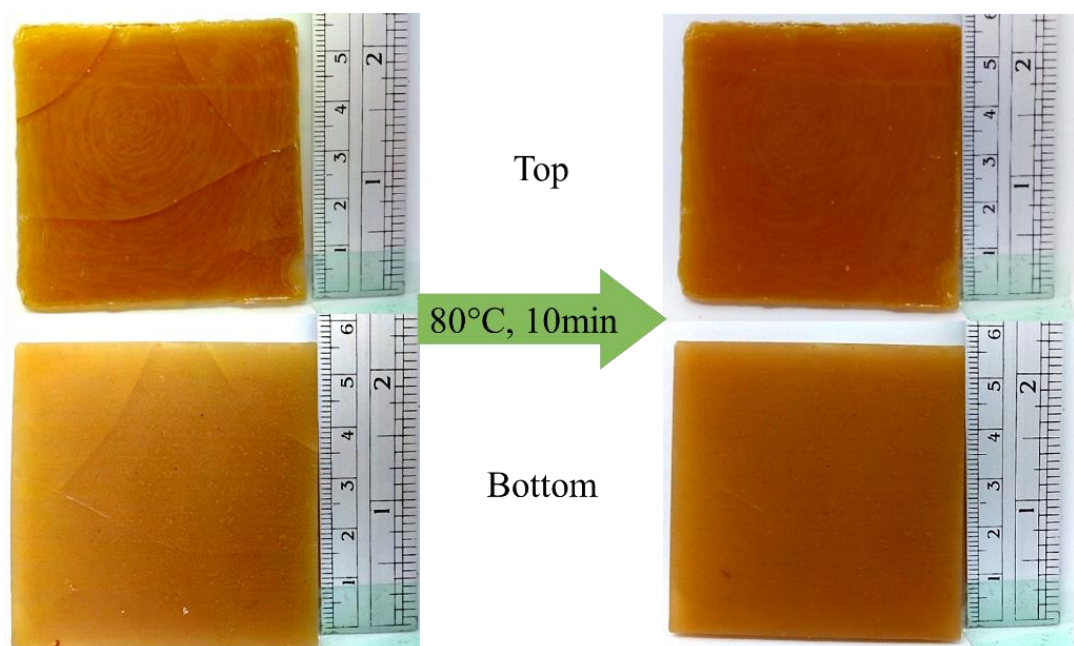


Figure 5-13 Cracks healing of original TL3 sample after 10 min at 80°C.

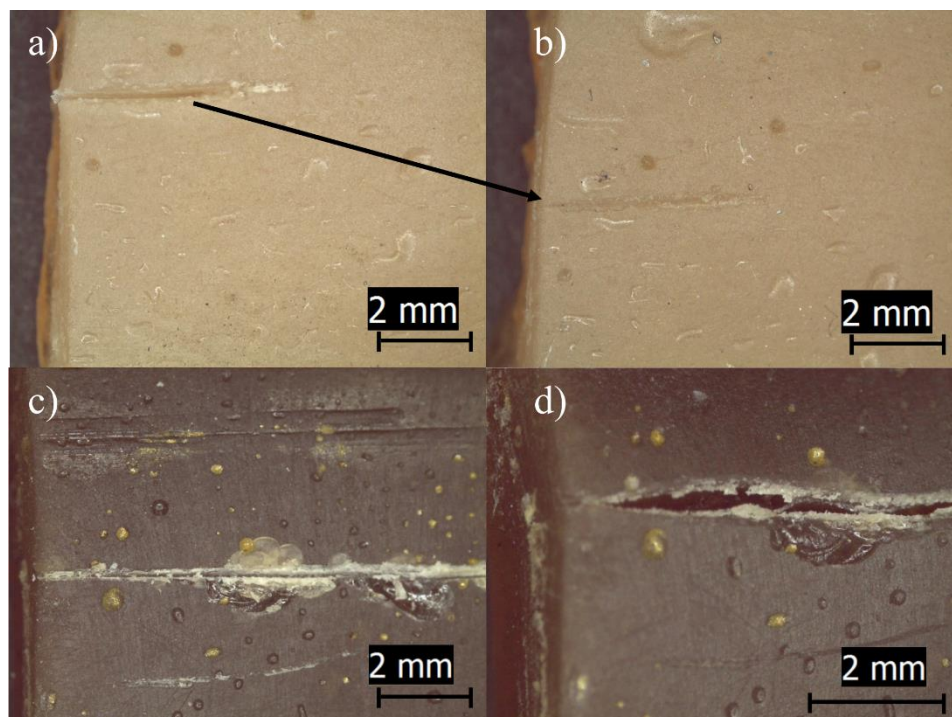


Figure 5-14 Cut healing: TL3 sample cut, b) TL3 sample after 10min at 80°C, c) PTL3 sample cut, d) PTL3 sample after 10min at 80°C - PTL3 shows no cut repair after lipases degradation in the polymer confirming the role of the active site in the healing process .

The question arises whether the transesterification is actually responsible for the healing mechanism of the enzymer. The FTIR is not able to detect this type of interaction, as both initial and end product have a similar chemical structure. In vitrimer characterisation, few techniques allow measurement of the bond exchange reaction such as creep study, stress relaxation, and dissolution in adapted solvent [57]–[59]. The stress relaxation of samples (NC, TL3, and TDL) was performed at 100°C and are presented in Figure 5-15a. The NC sample does not show any stress relaxation, and even some potential curing after 80 min (increase of initial relaxation modulus). Both TDL and TL3 sample show a partial stress relaxation with TL3 relaxing to $\approx 60\%$ of the stress after 8 h, while TDL to only $\approx 40\%$ of relaxation. TDL relax faster the stress maybe due to the interface of the double phased sample. For TL3, only $\approx 4\%$ of the stress is relaxed after 10 min. Creep data of these samples (Figure C-10) between 60°C and 80°C do not show any flow behaviour over 30 min, indicating that transesterifications are not measurable in this time scale. Furthermore, after immersion in ethylene glycol (reported to be a good solvent for vitrimer based on transesterification [59]) for 7 days, no dissolution is observable for sample NC, TDL, and TL3 (Figure 5-15b).

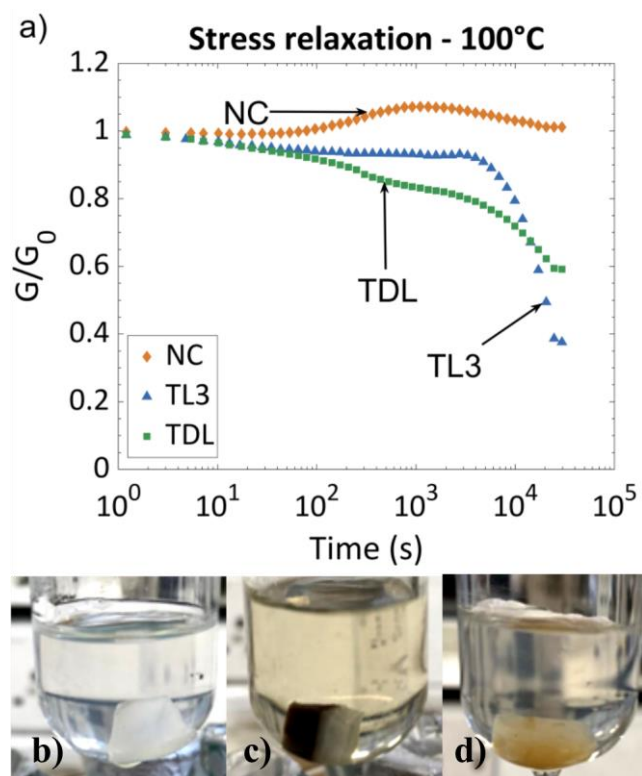


Figure 5-15 a) Stress relaxation of NC, TDL and TL3 samples, b-d) dissolution experiment at 80°C (7 days) in ethylene glycol for: NC (b), TDL (c), and TL3 (d) samples - NC sample does not exhibit any relaxation, TDL exhibits faster complex stress relaxation profile while TL3 only relaxes 4% of stress within 10 min. No sample exhibits full relaxation or dissolution in EG indicating that transesterification does not happen in between 80°C-100°C.

This indicates that the phenomenon responsible for the healing and reprocessing of the network was not based on transesterification. Fast healing (within 10 min) at low temperature (< 100°C) are usually seen in supramolecular network [41], [42], [60]. Enzymes are known to catalyse some of these interactions and have been recently reported to catalyse supramolecular assembly of copolymer blocks [20]. Evidence of fast healing and mechanical property conservation after reprocessing indicate that the lipases create alike interactions and potentially similar supramolecular assembly via hydrogen bonding or pi-pi stacking. However, it is still unclear where these interactions could be happening. The FTIR spectrum of epoxy and SA network covers most of the possible hydrogen signatures via C-O and/or C=O bonds. A likely mechanism would be enzyme fixation on the ester chains either on the C=O or C-OH groups. To investigate this mechanism several points would need to be defined, such as size of cluster (dissolution of the network and size characterisation of agglomerate, XRD, etc.) and proton interaction at different temperatures (solid state H-NMR at various temperature).

5.4.6 High temperature characterisation - determination of vitrimer properties

The capacity of lipases to catalyse *via* transesterification at higher temperature within the polyester network still remains. The creep behavior of samples (NC, TDL, TL3) was studied over several heating cycles: (1) from 60° to 250°C, (2) from 125°C to 245°C, (3) from 125°C to 245°C, and (4) from 60° to 100°C. The cycle (1) is shown in Figure C-11 for NC sample and Figure C-12 for TDL and TL3. NC samples do not creep over the whole cycle showing the behavior of a classic thermoset material. However, both TDL and TL3 samples shows an initial increase in their creep up to 125°C, without reaching a melt flow as defined in earlier vitrimer studies [57], which does not allow the enzymers to be defined as vitrimer at these temperatures and timescale. After 125°C and up to 245°C the creep decreases with temperature, which correlates with previous DMA data suggesting a possible lipases degradation/postcure of the material around 125-155°C. This degradation, although measurable by DMA does not affect the rubbery plateau of the samples significantly and suggests that the lipases denaturation (either full lipases for TL3 or remaining active of TDL), occurs in these temperature ranges, leading to some potential interaction with the polyester network. After this cycle, NC and TDL do not show any creep dependency with temperature for cycles (2) and (3) (Figure C-13), although TDL shows a small creep (< 0.5%) at extremely high temperature (230-245°C).

TL3 sample creep cycles (2) and (3) are shown in Figure 5-16. In both cycles the creep strain shows a linear temperature dependency (flow like a viscous liquid) and is high enough to allow calculation of the energy activation of the system. A small decrease in strain of the creep is observed for the third creep cycle attributed to oxidation/postcure of the network happening after long exposition at high temperature (degradation of the samples is not observed in TGA at these temperatures, see Figure 5-11). From these creep data the sample's viscosity was calculated and the Arrhenius plot is represented in Figure 5-17a. The second and third cycle exhibit relatively similar activation energy ($E_a = 73 \text{ kJ.mol}^{-1}$ and $E_a = 68 \text{ kJ.mol}^{-1}$ respectively), despite an increase in viscosity during the third cycle of creep (confirming some oxidation and polymerisation reaction during the experiment). In the creep cycle (4) (Figure C-14), all samples (NC, TDL, TL3) have exactly the same behavior showing that potential relaxation phenomenon was totally quenched following exposition

to temperature above the 125-155°C threshold. These results confirms that the supramolecular behavior at low temperature is suppressed by heating above this threshold once the enzyme are denatured and lead to the vitrimer properties.

The capacity of TL3 to fully relax stress was confirmed, after samples exposition to high temperature (Figure 5-17b and Figure C-15), only TL3 samples shows capacity to achieve stress relaxation at 150°C. TDL sample has some relaxation ($\approx 80\%$) but this relaxation is not dependent on the applied temperature. In order to obtain the activation energy of TL3 *via* stress relaxation, the sample was also tested at 250°C, and its $E_a \approx 55$ kJ.mol⁻¹. Difference of activation energy values between creep and stress relaxation measurements have been previously observed in vitrimer study [39], [57], [61], indicating either a heterogeneous material with several relaxation phenomenon or non-exchangeable crosslink units in the material.

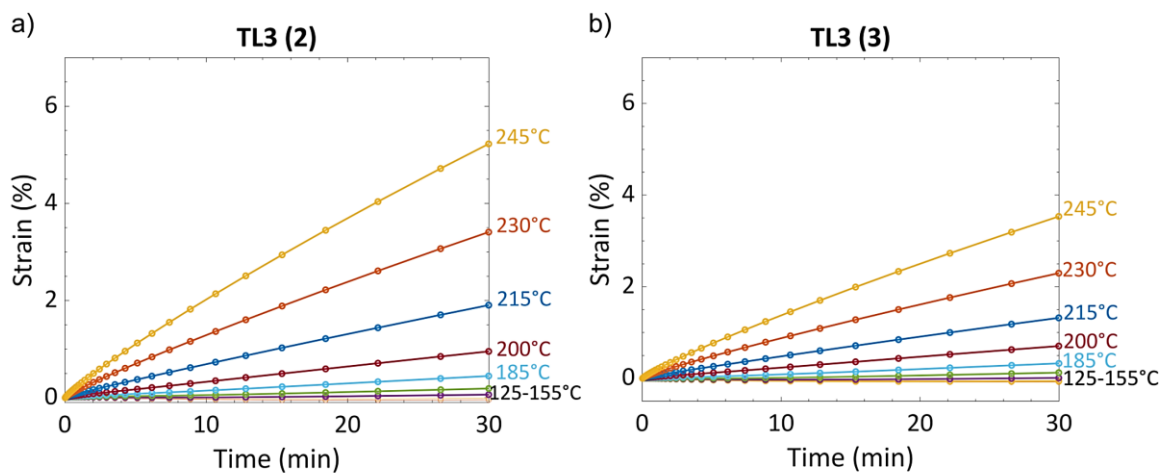


Figure 5-16 Creep profile of TL3 for: a) second heating cycle, and b) third heating cycle - both creep cycle exhibit a measurable flow to characterise the BER energy activation showing a vitrimer behaviour.

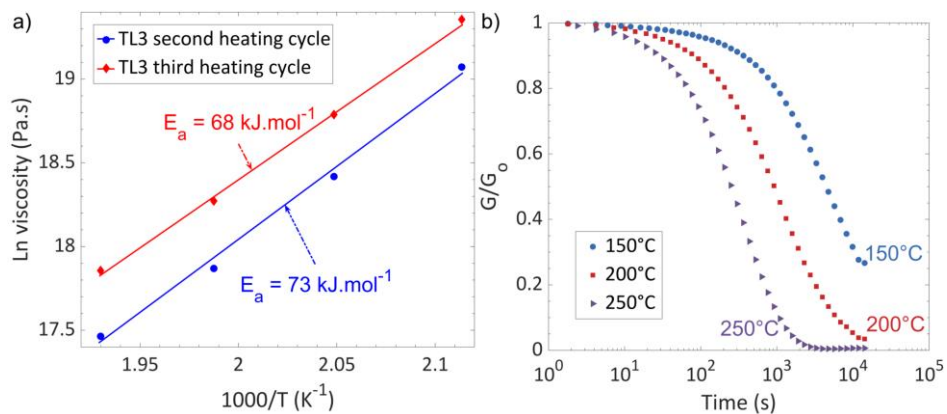


Figure 5-17 a) Arrhenius plot of second and third cycle of heating for TL3 sample, b) stress relaxation of TL3 sample ($E_a \approx 55$ kJ.mol⁻¹).

To confirm mechanism of transesterification is responsible for the material's stress relaxation, samples were immersed in EG for 24h at 135°C (above the temperature threshold), and dissolution results are shown in Figure 5-18. After this period of time, the NC sample did not dissolve. However, both TDL and TL3 samples are fully dissolved. Result for TL3 sample indicates that the transesterification mechanism is effectively responsible for its capacity to relax stress. TDL sample behaviour is less intuitive, but recent study showed that a classical thermoset could be recycled by swelling of catalyst and adapted solvent [62]. This phenomenon explains the dissolution of TDL sample, the small amount of initially non-degraded lipases can still catalyse partially the stress relaxation (as observed from creep and stress relaxation data). Once a part of the samples is dissolved, they can swell into the non-vitrimer part and progressively reach full sample dissolution.

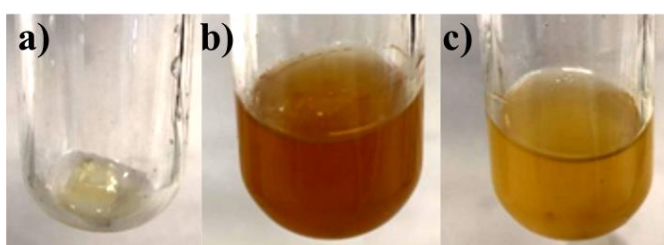


Figure 5-18 Dissolution of samples in ethylene glycol after 24h: a) NC (solvent removed to see sample), b) TDL (fully dissolve in solvent), and c) TL3 (fully dissolved).

It remains unclear how the transesterification BER can happen at higher temperature (threshold 125-155°C) and only after degrading the catalytic active site of the enzyme. In theory, the lipases denaturation should lead to a classical thermoset with no capacity to relax stress if the active site is only responsible for the bond exchange reaction (transesterifications). To understand this phenomenon, TL3 sample was submitted to FTIR measurement with progressive temperature increases after curing. Full spectrum range (400-4000 cm^{-1}) are shown in Figure C-16, and barely any change can be observed except appearance of C-O vibration due to atmospheric noises ($\approx 2100 \text{ cm}^{-1}$). A zoom-in of the 400-1790 cm^{-1} (Figure C-17) shows that no chemical change is observed in the samples in this area. The FTIR hydroxyl ranges (3300-4000 cm^{-1}) zoom-in is shown in Figure 5-19a. A peak located at 1700-1777 cm^{-1} (not mentioned previously) is present for both TDL and TL3 samples and not present in previous TBD catalysed network [39]. To confirm that this peak is non-related to the polyester formation, its integration was performed for the curing reaction for TDL and TL3 and results are presented in Figure 5-19b. These signatures are

similar for both samples and do not follow any of the previously studied trends corresponding to the esterification of epoxy and SA. As the signature is not related to this reaction nor to the enzyme active site presence, it is concluded that this peak corresponds to interaction between enzymes backbones leading to the formation of some free hydroxyl groups with lower binding energy than that of the polyester network. However, the hydroxyls groups signature of the polyester network undergoes a blueshift (shown by an arrow in Figure 5-19a) with temperature indicating a lower energy binding of these chemical moieties.

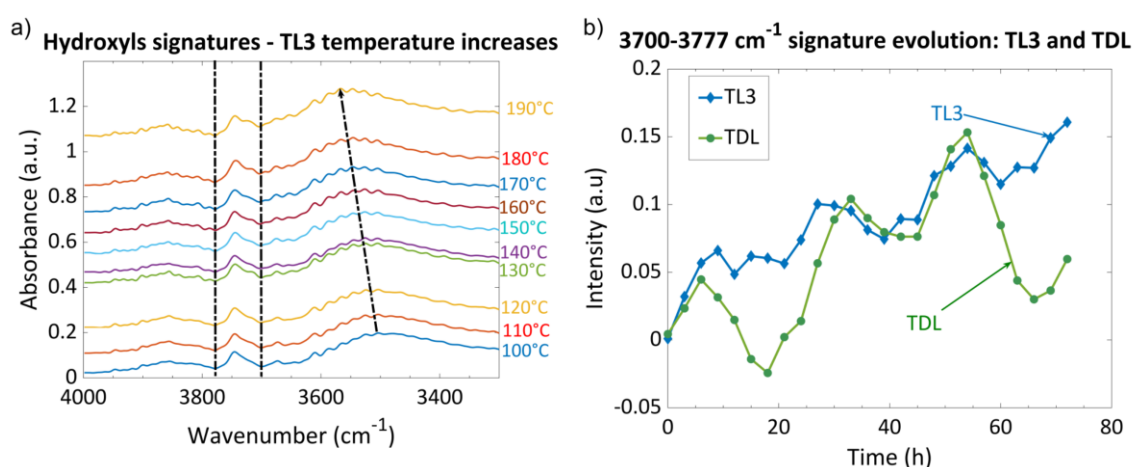


Figure 5-19 a) FTIR zoom-in of the hydroxyl range (3300-4000 cm⁻¹), b) evolution of the 1700-177 cm⁻¹ signature during curing for TLD and TL3. The hydroxyl signature (\approx 3400-3600 cm⁻¹) exhibits a redshift with temperature indicating less energy bonding of the esters' OH groups. The hydroxyl in the range 1700-177 cm⁻¹ (marked by the 2 dotted lines) coming from the enzymes displays change with temperature. The variation of this signature during the cure looks similar for TDL and TL3 indicating these groups are independent of the active site.

These hypothesis may be carefully taken to draw possible insights regarding the enzymes' behavior. A possible supramolecular organization at low temperature and transition to vitrimer after the temperature threshold is shown in Figure 5-20. The network formation suggests a high conversion of epoxy and SA monomers to form a polyester network. Its supramolecular behavior obtained by the presence of its active suggest a cluster-like structure proposed in a previous study [20], while the degradation of the active site allows production of a vitrimer based on transesterification between 125°C-155°C. Previous study showed that catalyst free transesterification can be achieved in polyester networks with an important portion of free hydroxyls groups [63]–[65]. The decrease of hydroxyl groups' binding energy with temperature indicates a possible degradation of hydrogen bonding within the network. It has been shown that some enzymes, such as

novozym45 [14] or other lipases [15], [66] can be subtracted on polymer, but that their backbones can also interact with each other or polymer chains to form some bonded clusters. On the other hand, nucleophile attack of some functional groups, such as carbonyl, by enzymes have shown a stabilise transition states of hydrogen bonds by forming tetrahedral intermediates [67]. In the case of enzymers, it is thought that after polyester formation, the lipases active site fixes on the carbonyl group of the polymer chains, while their backbones interact together to form some hydroxyls groups. The formation of tetrahedral complexes with the enzymes then enhances hydrogen bonds interactions, adding strength to the material (as previous measured values of Young's modulus for TBD sample was lower than the enzymers one, ≈ 2.1 MPa). These hydrogens bonds and possible re-polymerisation by the enzyme are then responsible of the healing and reprocessing of the network below the denaturation temperature. Once the lipases' active site is degraded at higher temperature ($\approx 125-155^\circ\text{C}$), these hydrogen bonds are suppressed. The suppression of the hydrogen bonds leads to a network with denatured enzyme connected together by the backbones with pendant hydroxyls groups embedded in a lightly crosslinked polyester network with a relatively high number of free hydroxyls groups. Self-catalysis of exchange mechanisms have been widely demonstrated to produce vitrimer network [28]–[30], [68], [69] by high proportion of free functional groups, and is believed to be responsible in the relaxation phenomenon observed in enzymers material. The difference of activation energy measured by creep and stress relaxation would then be explained by the presence of “dead” enzymes cluster helping to activate the transesterification but also acting as resistive “defect” in the relaxation process.

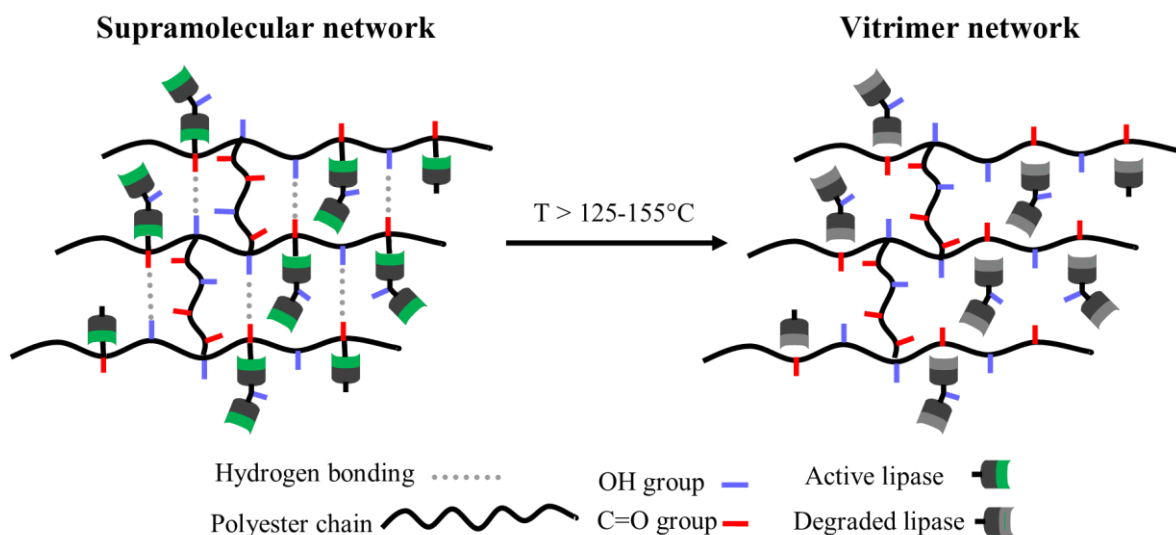


Figure 5-20 Schematic of enzymatic network representing the supramolecular network (left) formed by the lipases active site attacking carbonyl groups to form tetrahedral complex favouring hydrogen bonding with hydroxyl groups. After lipases denaturation ($T > 125-155^{\circ}\text{C}$, right side), the hydrogen bonds are suppressed leading to a polyester network with high proportion of free hydroxyl groups able to reorganise via transesterification.

5.5 Conclusions

Lipases TL from Meito-Sangyo have proved to be an excellent catalyst for the esterification of epoxy and carboxylic acid (SA). FTIR analysis have shown a high degree of conversion to ester formation at low temperature (100°C). The active site of the lipases plays an essential role in the polymerisation reaction and in production of a homogenous sample. A careful examination of the FTIR signatures of acid and ether during curing cycle suggests a simultaneous amine acid-monomers complexes formation within the active site: esterification of epoxy with Asp₃₃₃ and alkylation of SA with free amine group (from Ser₁₀₉ or His₂₇₇) leading to water formation. The water is then used to hydrolyse the epoxy-Asp₃₃₃ complex which then reacts with the amide complex *via* aminolysis to release an ester and recover the lipases active site for further esterification reactions. In the meantime, the lipases are thought to bridge through their backbones to form some free hydroxyl groups. The high regioselectivity of the lipases leads to high conversion rate with light crosslinking density (from swelling and DMA measurement), and further postcure of the system at higher temperature suggest a lipases denaturation in the $125-155^{\circ}\text{C}$ temperature range without inducing further crosslinks or polymerisation of the polyester network.

Once the network is cured and before their denaturation, the lipases interact with the polyester network to create an organised supramolecular network with fast healing

and reprocessing properties (1 h reprocessing with full conservation of mechanical properties or 10 min for cracks and cut healing at 80°C). At these temperatures the network remains chemically resistant to harsh and soft solvent with a maximum soluble fraction of $\approx 3\%$ after immersion for 7 days.

After the denaturation of lipases in the polyester network, the supramolecular network is quenched, liberating a high number of free hydroxyl groups. These hydroxyl groups lead to the formation of a catalyst free vitrimer network based on transesterification with an $E_a \approx 70 \text{ kJ.mol}^{-1}$, able to flow between 185°C and 245°C. The network shows the ability to fully relax stress and is supposedly reprocessable and healable within this temperature range, as previous vitrimer networks. Once the vitrimer network is obtained, its crosslinked structure keeps it chemically resistant to harsh solvent (TCB), with a maximum of $\approx 3\%$ soluble fraction after 3 days at 135°C. However, the transesterification mechanism induced by the free hydroxyl groups allows the network to be dissolved in soft solvent, such as EG, within 24 h at 135°C showing the ability of the polymer to be recycled with ease.

Many aspects of the polymerisation and mechanism of enzymes still remain to be clarified. For example, potential interactions with other amino acids near the active site could be helping the polymerisation to ensure its high conversion rate. Determination of how the lipases backbones interact to create these hydroxyl groups, and whether hydrogen interaction effectively happens via a tetrahedral complex between lipases and carbonyl groups of the polyester chains is required. The involvement of the enzymes' hydroxyl moieties in the transesterification needs to be determined either by becoming a part of the network or just impacting the hindrance of the hydroxyl groups belonging to the polyester chains.

This specific behavior of quenchable supramolecular network becoming a catalyst-free vitrimer material (due to the enzyme catalytic properties and denaturation), led to this new polymer type to be named enzymers. The characteristic of enzymers definitely make them an excellent candidate to be included in the current research related to vitrimer chemistry and more widely, self-healing polymers. Lipases are known to be a great bio-sourced and ecological catalyst, while having various choice in their designs to obtain specific interactions with their surrounding environment. The vitrimer chemistry often looked for solutions to decrease creep of the material during the reprocessing or healing

process, often by including permanent crosslink or using high T_g polymers. Here, the supramolecular structure allows to keep a low crosslink density (low T_g) while obtaining full recovery of the mechanical properties. Other studies looked to remove catalyst to avoid potential degradation of the system at high temperature or unwanted secondary reactions. In the case of the enzymes, the network tends to be able to relax stress far below any degradation recorded ($T_{d5\%} \approx 420^\circ\text{C}$). As enzymes can be designed to catalyse various polymerisations (esterification, amidification, *etc.*), this demonstrates the potential of enzymes as ecological solutions for polymerisation of epoxy network at low temperature leading to crosslinked networks with healing, reprocessing and recyclable properties.

5.6 References

- [1] N. N. Gandhi, N. S. Patil, S. B. Sawant, J. B. Joshi, P. P. Wangikar, and D. Mukesh, "Lipase-Catalyzed Esterification," *Catal. Rev. - Sci. Eng.*, vol. 42, no. 4, pp. 439–480, 2000.
- [2] U. Schuchardt, R. Sercheli, and R. M. Vargas, "Transesterification of vegetable oils: A review," *Journal of the Brazilian Chemical Society*, vol. 9, no. 3. Sociedade Brasileira de Quimica, pp. 199–210, 1998.
- [3] L. Casas-Godoy, F. Gasteazoro, S. Duquesne, F. Bordes, A. Marty, and G. Sandoval, *Lipases: An Overview*, no. 1835. 2018.
- [4] B. Norjannah, H. C. Ong, H. H. Masjuki, J. C. Juan, and W. T. Chong, "Enzymatic transesterification for biodiesel production: A comprehensive review," *RSC Adv.*, vol. 6, no. 65, pp. 60034–60055, 2016.
- [5] A. Gog, M. Roman, M. Toşa, C. Paizs, and F. D. Irimie, "Biodiesel production using enzymatic transesterification - Current state and perspectives," *Renew. Energy*, vol. 39, no. 1, pp. 10–16, 2012.
- [6] W. Farhat, A. Biundo, A. Stamm, E. Malmström, and P. O. Syrén, "Lactone monomers obtained by enzyme catalysis and their use in reversible thermoresponsive networks," *J. Appl. Polym. Sci.*, vol. 137, no. 18, 2020.
- [7] M. B. Buendia, A. E. Dugaard, and A. Riisager, "Catalytic Transesterification Routes to Novel Vinyl Glycolate Derivatives of Polyhydric Alcohols," *Catal. Letters*, no. 0123456789, 2020.
- [8] C. Aouf *et al.*, "The use of lipases as biocatalysts for the epoxidation of fatty acids and phenolic compounds," *Green Chem.*, vol. 16, no. 4, pp. 1740–1754, 2014.
- [9] R. A. Gross, A. Kumar, and B. Kalra, "Polymer synthesis by in vitro enzyme catalysis," *Chem. Rev.*, vol. 101, no. 7, pp. 2097–2124, 2001.
- [10] Y. Poojari and S. J. Clarson, "Lipase catalyzed synthesis of poly(ϵ -Caprolactone)-poly(Dimethylsiloxane)-poly(ϵ -Caprolactone) triblock copolymers," *Silicon*, vol. 1, no. 3, pp. 165–172, 2009.
- [11] Q. Dong *et al.*, "Structure-guided engineering of a *Thermobifida fusca* cutinase for enhanced hydrolysis on natural polyester substrate," *Bioresour. Bioprocess.*, vol. 7, no. 1, 2020.

- [12] W. Wu, "Lipase - catalyzed synthesis and post - polymerization modification of new fully bio - based poly (hexamethylene γ - ketopimelate) and poly (hexamethylene γ - ketopimelate - co - hexamethylene adipate) copolyesters," *e-polymer*, no. 20, pp. 214–225, 2020.
- [13] F. Zeng *et al.*, "Functionalized polyesters derived from glycerol: Selective polycondensation methods toward glycerol-based polyesters by different catalysts," *J. Appl. Polym. Sci.*, vol. 137, no. 16, pp. 1–7, 2020.
- [14] C. Ortiz *et al.*, "Novozym 435: The 'perfect' lipase immobilized biocatalyst?," *Catal. Sci. Technol.*, vol. 9, no. 10, pp. 2380–2420, 2019.
- [15] J. J. Virgen-Ortíz, J. C. S. Dos Santos, Á. Berenguer-Murcia, O. Barbosa, R. C. Rodrigues, and R. Fernandez-Lafuente, "Polyethylenimine: A very useful ionic polymer in the design of immobilized enzyme biocatalysts," *J. Mater. Chem. B*, vol. 5, no. 36, pp. 7461–7490, 2017.
- [16] T. Yamada, C. Morisseau, J. E. Maxwell, M. A. Argiriadi, D. W. Christianson, and B. D. Hammock, "Biochemical evidence for the involvement of tyrosine in epoxide activation during the catalytic cycle of epoxide hydrolase," *J. Biol. Chem.*, vol. 275, no. 30, pp. 23082–23088, 2000.
- [17] M. F. C. Andrade, A. L. A. Parussulo, C. G. C. M. Netto, L. H. Andrade, and H. E. Toma, "Lipase immobilized on polydopamine-coated magnetite nanoparticles for biodiesel production from soybean oil," *Biofuel Res. J.*, vol. 3, no. 2, pp. 403–409, 2016.
- [18] A. Jain, S. Dhiman, A. Dhayani, P. K. Vemula, and S. J. George, "Chemical fuel-driven living and transient supramolecular polymerization," *Nat. Commun.*, vol. 10, no. 1, pp. 1–9, 2019.
- [19] M. Wimmerová, V. Siglerová, D. Šaman, M. Šlouf, E. Kaletová, and Z. Wimmer, "Improved enzyme-mediated synthesis and supramolecular self-assembly of naturally occurring conjugates of β -sitosterol," *Steroids*, vol. 117, pp. 38–43, 2017.
- [20] D. M. Scheibel and I. Gitsov, "Unprecedented Enzymatic Synthesis of Perfectly Structured Alternating Copolymers via 'green' Reaction Cocatalyzed by Laccase and Lipase Compartmentalized within Supramolecular Complexes," *Biomacromolecules*, vol. 20, no. 2, pp. 927–936, 2019.
- [21] X. Yang, L. Guo, X. Xu, S. Shang, and H. Liu, "A fully bio-based epoxy vitrimer: Self-healing, triple-shape memory and reprocessing triggered by dynamic covalent bond

- exchange,” *Mater. Des.*, vol. 186, p. 108248, Jan. 2020.
- [22] J. Huang, L. Zhang, Z. Tang, S. Wu, and B. Guo, “Reprocessable and robust crosslinked elastomers via interfacial C–N transalkylation of pyridinium,” *Compos. Sci. Technol.*, vol. 168, no. July, pp. 320–326, 2018.
- [23] S. Zhang, L. Pan, L. Xia, Y. Sun, and X. Liu, “Dynamic polysulfide shape memory networks derived from elemental sulfur and their dual thermo-/photo-induced solid-state plasticity,” *React. Funct. Polym.*, vol. 121, pp. 8–14, 2017.
- [24] Z. Pei, Y. Yang, Q. Chen, Y. Wei, and Y. Ji, “Regional Shape Control of Strategically Assembled Multishape Memory Vitrimers,” *Adv. Mater.*, vol. 28, no. 1, pp. 156–160, 2016.
- [25] S. Zhang *et al.*, “Preparation of a lignin-based vitrimer material and its potential use for recoverable adhesives,” *Green Chem.*, vol. 20, no. 13, pp. 2995–3000, 2018.
- [26] D. Montarnal, M. Capelot, F. Tounilhac, and L. Leibler, “Silica-Like Malleable Materials from permanent organic network,” *Science (80-.)*, vol. 334, pp. 965–968, 2011.
- [27] Z. Ma, Y. Wang, J. Zhu, J. Yu, and Z. Hu, “Bio-based epoxy vitrimers: Reprocessability, controllable shape memory, and degradability,” *J. Polym. Sci. Part A Polym. Chem.*, vol. 55, no. 10, pp. 1790–1799, 2017.
- [28] Z. Liu, C. Zhang, Z. Shi, J. Yin, and M. Tian, “Tailoring vinylogous urethane chemistry for the cross-linked polybutadiene: Wide freedom design, multiple recycling methods, good shape memory behavior,” *Polymer (Guildf.)*, vol. 148, pp. 202–210, 2018.
- [29] W. Denissen, G. Rivero, R. Nicolaÿ, L. Leibler, J. M. Winne, and F. E. Du Prez, “Vinylogous urethane vitrimers,” *Adv. Funct. Mater.*, vol. 25, no. 16, pp. 2451–2457, 2015.
- [30] B. Hendriks, J. Waelkens, J. M. Winne, and F. E. Du Prez, “Poly(thioether) Vitrimers via Transalkylation of Trialkylsulfonium Salts,” *ACS Macro Lett.*, vol. 6, no. 9, pp. 930–934, 2017.
- [31] H. Guo, L. Yue, G. Rui, and I. Manas-Zloczower, “Recycling Poly(ethylene-vinyl acetate) with Improved Properties through Dynamic Cross-Linking,” *Macromolecules*, vol. 53, no. 1, pp. 458–464, 2020.
- [32] M. Guerre, C. Taplan, R. Nicolaÿ, J. M. Winne, and F. E. Du Prez, “Fluorinated Vitrimer

- Elastomers with a Dual Temperature Response,” *J. Am. Chem. Soc.*, vol. 140, no. 41, pp. 13272–13284, 2018.
- [33] F. Lossada, D. Jiao, X. Yao, and A. Walther, “Waterborne Methacrylate-Based Vitrimers,” *ACS Macro Lett.*, vol. 14, pp. 70–76, 2020.
- [34] J. H. Chen, W. Q. Yuan, Y. D. Li, Y. X. Weng, and J. B. Zeng, “Malleable and Sustainable Poly(ester amide) Networks Synthesized via Melt Condensation Polymerization,” *ACS Sustain. Chem. Eng.*, vol. 7, no. 18, pp. 15147–15153, 2019.
- [35] F. L. Jin, X. Li, and S. J. Park, “Synthesis and application of epoxy resins: A review,” *J. Ind. Eng. Chem.*, vol. 29, pp. 1–11, 2015.
- [36] Businesswire, “Global Epoxy Resins Market, Forecast to 2025 - DGBEA Will Bring in Healthy Gains of Over \$2.9 Billion by 2025,” *Global-Epoxy-Resins-Market-Forecast-2025*, 2020. .
- [37] H. Memon *et al.*, “Vanillin-Based Epoxy Vitrimer with High Performance and Closed-Loop Recyclability,” *Macromolecules*, vol. 53, no. 2, pp. 621–630, 2020.
- [38] W. Liu, D. F. Schmidt, and E. Reynaud, “Catalyst Selection, Creep, and Stress Relaxation in High-Performance Epoxy Vitrimers,” *Ind. Eng. Chem. Res.*, vol. 56, no. 10, pp. 2667–2672, 2017.
- [39] Q.-A. Poutrel *et al.*, “Dicarboxylic acid-epoxy vitrimers: Influence of off-stoichiometric acid content on cure reactions and thermo-mechanical properties,” *Polym. Chem.*, vol. accepted m, 2020.
- [40] Y. Liu, Z. Tang, S. Wu, and B. Guo, “Integrating Sacrificial Bonds into Dynamic Covalent Networks toward Mechanically Robust and Malleable Elastomers,” *ACS Macro Lett.*, vol. 8, no. 2, pp. 193–199, 2019.
- [41] L. Voorhaar and R. Hoogenboom, “Supramolecular polymer networks: Hydrogels and bulk materials,” *Chem. Soc. Rev.*, vol. 45, no. 14, pp. 4013–4031, 2016.
- [42] A. Campanella, D. Döhler, and W. H. Binder, “Self-Healing in Supramolecular Polymers,” *Macromol. Rapid Commun.*, vol. 39, no. 17, pp. 1–19, 2018.
- [43] P. Cordier, F. Tournilhac, C. Soulié-Ziakovic, and L. Leibler, “Self-healing and thermoreversible rubber from supramolecular assembly,” *Nature*, vol. 451, no. 7181, pp. 977–980, 2008.
- [44] Y. Soeda, T. Okamoto, K. Toshima, and S. Matsumura, “Enzymatic ring-opening polymerization of oxiranes and dicarboxylic anhydrides,” *Macromol. Biosci.*, vol. 2,

- no. 9, pp. 429–436, 2002.
- [45] J. Guo, C. P. Chen, S. G. Wang, and X. J. Huang, “A convenient test for lipase activity in aqueous-based solutions,” *Enzyme Microb. Technol.*, vol. 71, pp. 8–12, 2015.
- [46] A. Bagur, “Bio-vitrimer,” Manchester, 2020.
- [47] F. I. Altuna, C. E. Hoppe, and R. J. J. Williams, “Epoxy vitrimers: The effect of transesterification reactions on the network structure,” *Polymers (Basel)*., vol. 10, no. 1, p. 43, 2018.
- [48] F. Snijkers, R. Pasquino, and A. Maffezzoli, “Curing and viscoelasticity of vitrimers,” *Soft Matter*, vol. 13, no. 1, pp. 258–268, 2017.
- [49] L. Matějka, S. Pokomý, and K. Dušek, “Network formation involving epoxide and carboxyl groups,” *Polym. Bull.*, vol. 7, no. 2, pp. 123–128, 1982.
- [50] B. G. G. Lohmeijer *et al.*, “Guanidine and amidine organocatalysts for ring-opening polymerization of cyclic esters,” *Macromolecules*, vol. 39, no. 25, pp. 8574–8583, Dec. 2006.
- [51] F. I. Altuna, U. Casado, I. E. Dell’Erba, L. Luna, C. E. Hoppe, and R. J. J. Williams, “Epoxy vitrimers incorporating physical crosslinks produced by self-association of alkyl chains,” *Polym. Chem.*, vol. 11, no. 7, pp. 1337–1347, 2020.
- [52] A. M. Gumel, M. S. M. Annuar, Y. Chisti, and T. Heidelberg, “Ultrasound assisted lipase catalyzed synthesis of poly-6-hydroxyhexanoate,” *Ultrason. Sonochem.*, vol. 19, no. 3, pp. 659–667, 2012.
- [53] A. Maraite, P. Hoyos, J. D. Carballeira, Á. C. Cabrera, M. B. Ansorge-Schumacher, and A. R. Alcántara, “Lipase from *Pseudomonas stutzeri*: Purification, homology modelling and rational explanation of the substrate binding mode,” *J. Mol. Catal. B Enzym.*, vol. 87, pp. 88–98, 2013.
- [54] F. I. Altuna, V. Pettarin, and R. J. J. Williams, “Self-healable polymer networks based on the cross-linking of epoxidised soybean oil by an aqueous citric acid solution,” *Green Chem.*, vol. 15, no. 12, pp. 3360–3366, 2013.
- [55] G. Sailakshmi, T. Mitra, and A. Gnanamani, “Engineering of chitosan and collagen macromolecules using sebacic acid for clinical applications,” *Prog. Biomater.*, vol. 2, no. 1, p. 11, 2013.
- [56] Y. Poojari and S. J. Clarson, “Thermal stability of *Candida antarctica* lipase B immobilized on macroporous acrylic resin particles in organic media,” *Biocatal.*

- Agric. Biotechnol.*, vol. 2, no. 1, pp. 7–11, 2013.
- [57] R. G. Ricarte, F. Tournilhac, M. Cloître, and L. Leibler, “Linear Viscoelasticity and Flow of Self-Assembled Vitrimers: The Case of a Polyethylene/Dioxaborolane System,” *Macromolecules*, p. acs.macromol.9b02415, Feb. 2020.
- [58] Q. Shi *et al.*, “Recyclable 3D printing of vitrimer epoxy,” *Mater. Horizons*, vol. 4, no. 4, pp. 598–607, 2017.
- [59] K. Yu, Q. Shi, M. L. Dunn, T. Wang, and H. J. Qi, “Carbon Fiber Reinforced Thermoset Composite with Near 100% Recyclability,” *Adv. Funct. Mater.*, vol. 26, no. 33, pp. 6098–6106, 2016.
- [60] Y. Yang and M. W. Urban, “Self-healing polymeric materials,” *Chem. Soc. Rev.*, vol. 42, no. 17, pp. 7446–7467, 2013.
- [61] F. Meng, R. H. Pritchard, and E. M. Terentjev, “Stress Relaxation, Dynamics, and Plasticity of Transient Polymer Networks,” *Macromolecules*, vol. 49, no. 7, pp. 2843–2852, 2016.
- [62] X. Kuang, Y. Zhou, Q. Shi, T. Wang, and H. J. Qi, “Recycling of Epoxy Thermoset and Composites via Good Solvent Assisted and Small Molecules Participated Exchange Reactions,” *ACS Sustain. Chem. Eng.*, vol. 6, no. 7, pp. 9189–9197, 2018.
- [63] Y. Shan *et al.*, “A renewable dynamic covalent network based on itaconic anhydride crosslinked polyglycerol: Adaptability, UV blocking and fluorescence,” *Chem. Eng. J.*, vol. 385, Apr. 2020.
- [64] J. Han, T. Liu, C. Hao, S. Zhang, B. Guo, and J. Zhang, “A Catalyst-Free Epoxy Vitrimer System Based on Multifunctional Hyperbranched Polymer,” *Macromolecules*, vol. 51, no. 17, pp. 6789–6799, 2018.
- [65] X. Huang, H. C. Liu, Z. Fan, H. Wang, G. S. Huang, and J. R. Wu, “Hyperbranched polymer toughened and reinforced self-healing epoxy vitrimer,” *Acta Polym. Sin.*, vol. 50, no. 5, pp. 535–542, 2019.
- [66] O. Barbosa, R. Torres, C. Ortiz, Á. Berenguer-Murcia, R. C. Rodrigues, and R. Fernandez-Lafuente, “Heterofunctional supports in enzyme immobilization: From traditional immobilization protocols to opportunities in tuning enzyme properties,” *Biomacromolecules*, vol. 14, no. 8, pp. 2433–2462, 2013.
- [67] S. M., *Comprehensive Biological Catalysis*, Vol 1. London: Academic Press, 1998.
- [68] J. Han *et al.*, “Hyperbranched Polymer Assisted Curing and Repairing of an Epoxy

Coating," *Ind. Eng. Chem. Res.*, vol. 58, no. 16, pp. 6466–6475, 2019.

- [69] T. Liu *et al.*, "Glycerol Induced Catalyst-Free Curing of Epoxy and Vitrimer Preparation," *Macromol. Rapid Commun.*, vol. 40, no. 7, pp. 1–6, 2019.

Appendix C. Supplementary information - Chapter 5

Authors: Quentin-Arthur Poutrel^{a,b,*}, Auriane Bagur^b, Jonny Blaker^b, Matthieu Gresil^{c,*}

^a Aerospace Research Institute, The University of Manchester, Manchester, UK

^b Department of Materials, The University of Manchester, Manchester, UK

^c i-Composites Lab, Department of Materials Science and Engineering & Department of Mechanical and Aerospace Engineering, Monash University, Clayton, Australia

Corresponding authors: *quentin.a.poutrel@gmail.com, *matthieu.gresil@monash.edu

C.1. Analysis of network formation via ATR-IR

C.1.1. Species evolution with raw enzymes and thermally degraded enzymes (3 wt. %)

Spectrums at 0 h and 72 h for TL3 and TDL are shown in Figure C-1. At $t = 0$ h (blue curves), the presence of a double peak in the 1690 cm^{-1} - 1760 cm^{-1} corresponds to the C=O stretching bands of carboxyl functional groups. The left peak at $\tilde{\nu} \approx 1735\text{ cm}^{-1}$ corresponds to solvated carboxyl groups by epoxy compounds (interacting with the surrounding ether group of epoxy *via* hydrogen bonding) [1] and the right peak at $\tilde{\nu} \approx 1705\text{ cm}^{-1}$ corresponds to the conventional signal of carboxylic acid. The presence of the characteristic epoxy peak is located at $\tilde{\nu} \approx 914\text{ cm}^{-1}$. At $t = 72$ h (red curves), both TL3 and TDL samples exhibit extinction of the epoxy and molten state of the carboxylic acid peak. However, the peak at $\tilde{\nu} \approx 1735\text{ cm}^{-1}$ increases and becomes more defined, corresponding to the formation of the esters formation after polymerisation of epoxy and SA. The apparition of the peak in the $3000\text{-}3600\text{ cm}^{-1}$ range corresponds to the free hydroxyl groups of the ester chains at the junction where epoxy and SA react.

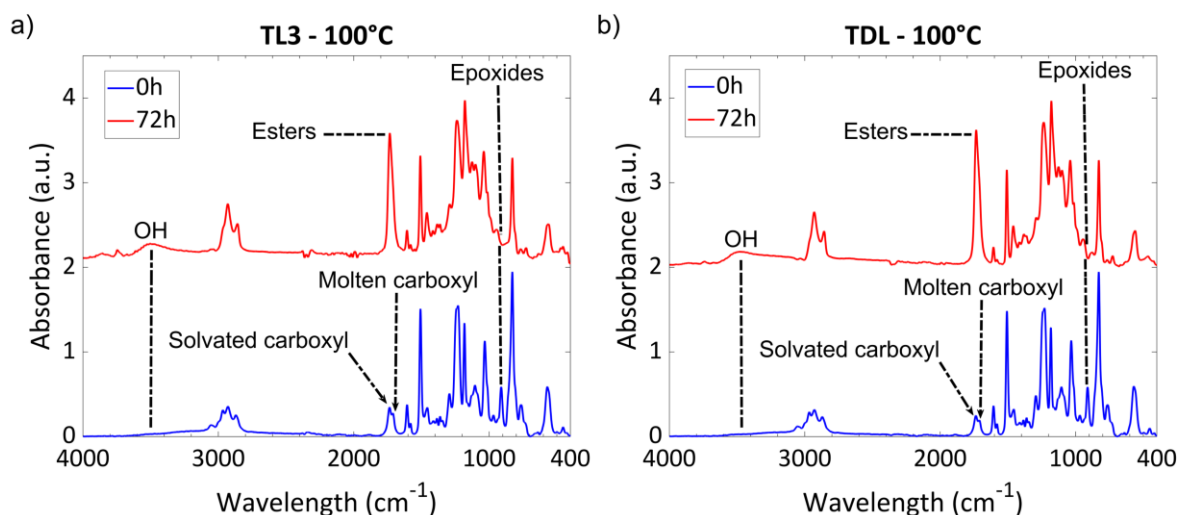


Figure C-1 Spectrum of curing cycle at $t = 0\text{h}$ (blue curves) and $t = 72\text{h}$ (red curves) for: a) TL3 sample, and b) TDL sample.

The evolution of hydroxyl groups of TL3 and TDL are presented in Figure C-2. As stated in the main text, the evolution of TL3 OH groups is fast and linear before reaching a plateau at $\approx 20\text{ h}$, and also exhibiting the highest value ($\approx 0.45\text{ a.u.}$). For TDL sample, the evolution is stepped and slower, and does not reach a stable value after 72 h meaning that the esterification reaction has not been completed (reinforced by the smaller maximum value, peaking at 0.38 a.u. despite the same amount of initial compound).

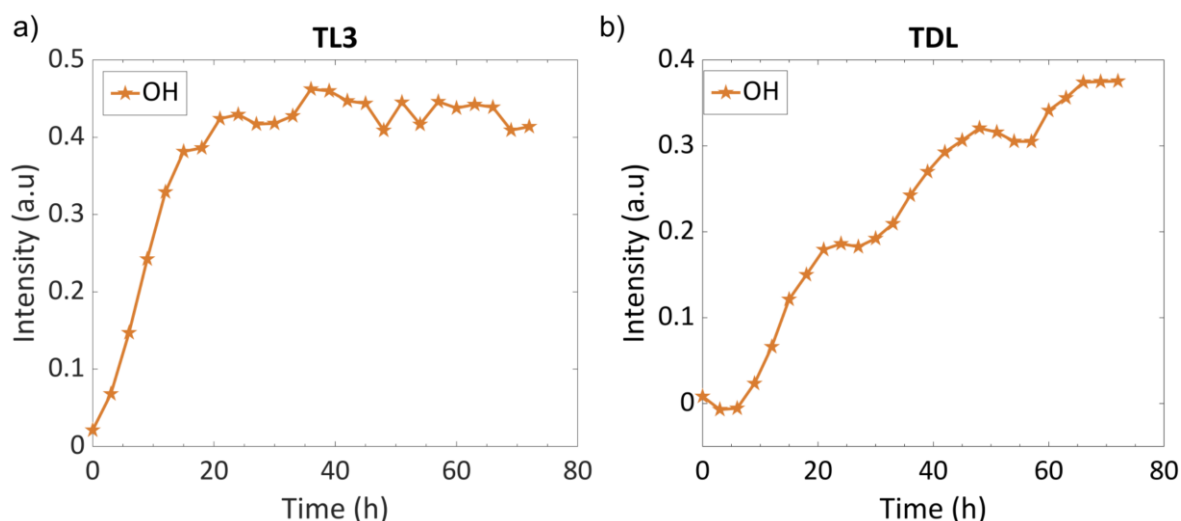


Figure C-2 Evolution of hydroxyl groups for: a) TL3 sample, and b) TDL sample.

C.1.2. Mechanism of epoxy ring opening via enzyme active site

The evolution of epoxy, ether and hydroxyl signatures for the lipase epoxy reaction are shown in Figure C-3. It is possible to see that the epoxy and ether signatures show few changes in values, with the epoxy oscillating between 0.098 a.u. and 0.096 a.u. despite

some tendency to decrease after ≈ 16 h. The ether signature has an overall stable value. On the hand, the hydroxyl has a clear and fast increase over ≈ 16 h to then reach a stable plateau for the rest of the 72 h of monitoring.

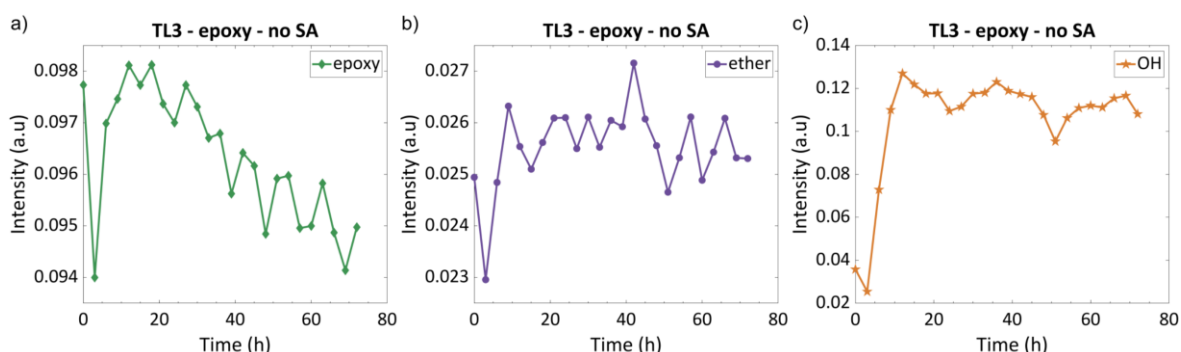


Figure C-3 Evolution of chemical species for the chemical reaction of epoxy and lipases without sebacic acid: a) epoxides, b) ether, and c) hydroxyl groups.

The lipase TL active site adapted from the previous modelling work [2] is represented in Figure C-4. The S-benzoin links by hydrogen bonding Tyrosine₅₄ (Tyr₅₄), Serine₁₀₉ (Ser₁₀₉, red dotted circle), and Histidine₂₇₇ (His₂₇₇, clear blue dotted circle). Aspartate₃₃₃ (Asp₃₃₃) is located below the S-benzoin complex near the His₂₇₇. The catalytic triad is comprised of the trio: Asp₃₃₃, His₂₇₇, and Ser₁₀₉ (with their developed structure). With this structure and FTIR data, the oxyanion of the Asp₃₃₃ is most likely to open up the epoxy ring via one of its carbon groups (possible interactions with the His₂₇₇ on the oxygen atom may help the ring opening by the Asp₃₃₃ [3]). In the meantime, the sebacic acid may react with the amine group of the His₂₇₇ or Ser₁₀₉. The production of water leads to hydrolysis of the ester product of the epoxy ring opening leading to an aminolysis between the SA/Ser₁₀₉ bond, producing the ester.

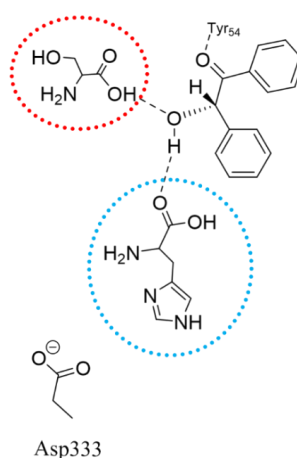


Figure C-4 Scheme of the lipase TL active site adapted from [2]. The Ser₁₀₉ is located in the red dotted circle and the His₂₇₇ is located in the blue dotted circle.

C.2. Polymer characterisation (general properties)

C.2.1. Bi-phase polymer without catalyst and with TDL

The FTIR of NC and TDL bulk sample is shown in Figure C-5. Both sides of NC sample shows a T_g below 0°C indicating a low crosslink achieved in the whole surface. The top surface (with no lipases) has also a temperature below 0°C indicating similar crosslinks formation that the NC sample. The bottom phase (sediment lipases) shows a higher T_g ($\approx 3^\circ\text{C}$) indicating that the crosslink of the network is higher in this part of the sample.

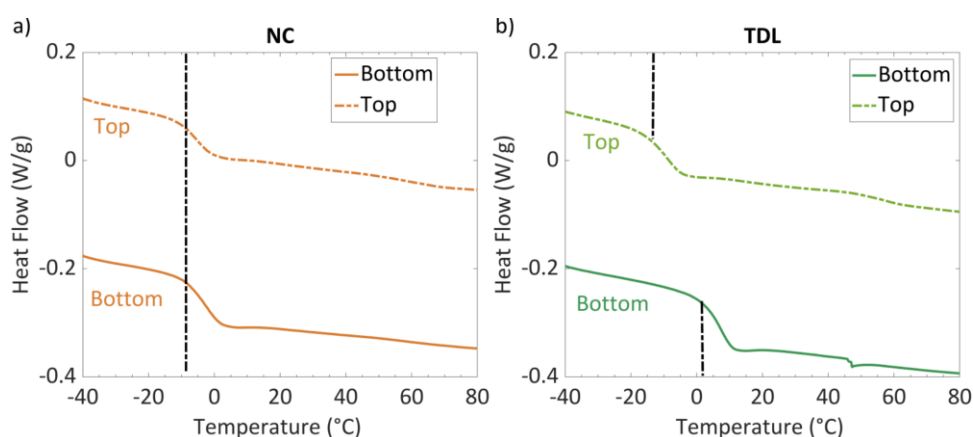


Figure C-5 DSC of top and bottom faces for: a) NC sample, and b) TDL sample.

The top phases of NC and TDL are compared to TL3 in Figure C-6a, and their top phases compared to TL3 in Figure C-6b. It can be seen that TL3 has a higher T_g ($\approx 6^\circ\text{C}$) than both top phases of the biphasic samples. The bottom phases of TDL is however closer to TL3 value, confirming that TDL bottom phase has achieved higher crosslink formation than its top phase due to the lipases presence.

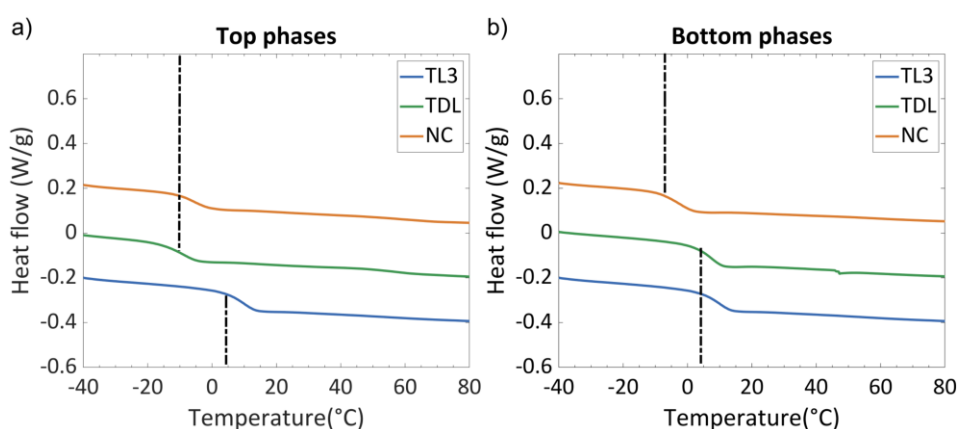


Figure C-6 Comparison of TL3 DSC measurement with: a) top phases of NC and TDL samples, and b) bottom (sediment) phase of NC and TDL sample - data for NC and TDL are the same that in Figure C-5.

The swelling results for all samples (NC, TDL and TL3) is shown in Figure C-7. The swelling ratio of NC sample is limited due to his high soluble fraction, however TL3 exhibits a high swelling ratio which confirms the formation of a light crosslink density.

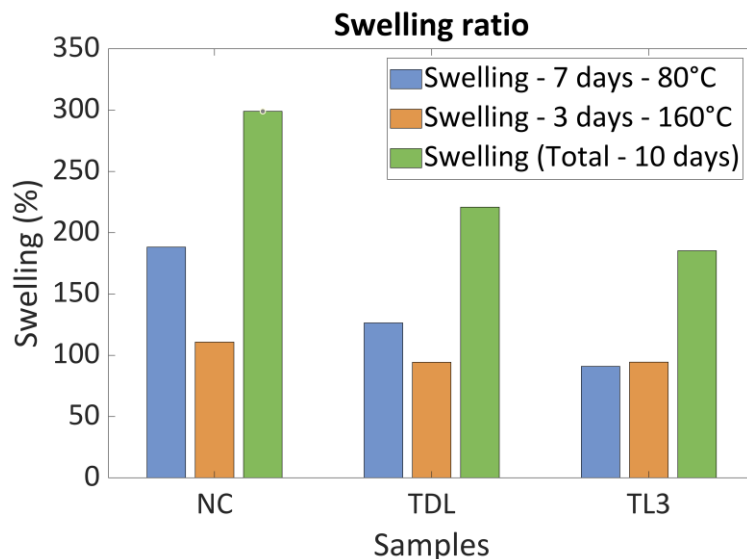


Figure C-7 Swelling ratio of NC, TDL and TL3 samples after 7 days at 80°C, followed by 3 days at 135°C and the total swelling over 10 days. Solvent: TCB.

The TGA result for all samples under air is shown in Figure C-8. The trend follows the one observed under nitrogen atmosphere, however an additional peak ($\approx 580^{\circ}\text{C}$) is seen for TDL and TL3 sample indicating some sensitivity to oxygen degradation.

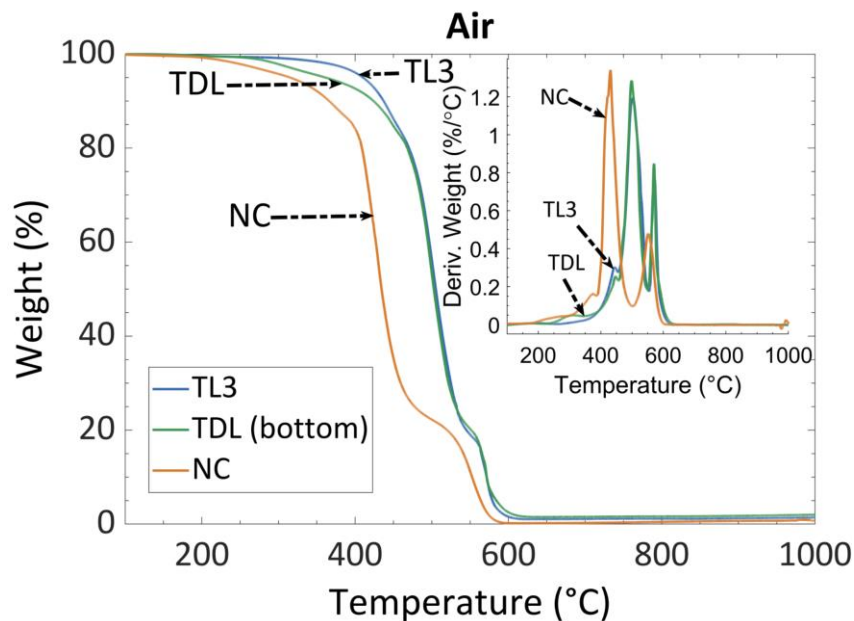


Figure C-8 TGA results for NC, TDL and TL3 sample in air. The inset represents the weight derivation of the measurement in function of temperature.

C.3. Supramolecular properties

The typical tensile properties of original and reprocessed TL3 sample are shown in Figure C-9.

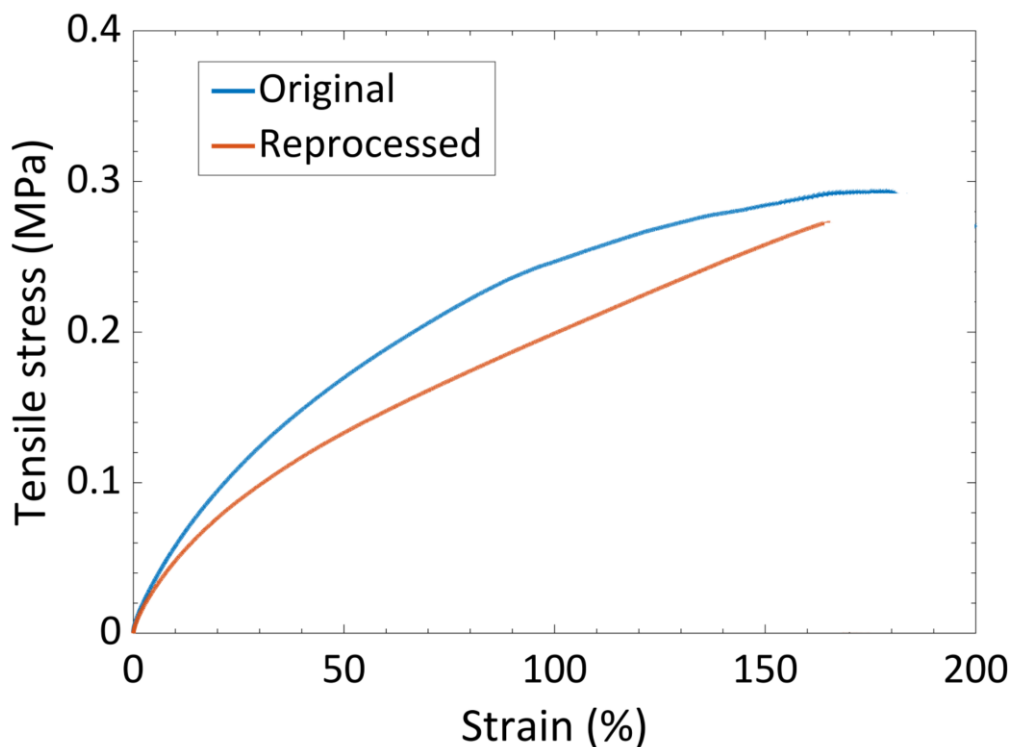


Figure C-9 Typical tensile curve of original TL3 sample and reprocessed TL3 sample.

Creep results of TDL and TL3 samples between 60°C and 80°C are shown in Figure C-10. Both sample exhibit some fast increases in their primary region, however, the secondary region show little creep indicating no permanent deformation is achieved.

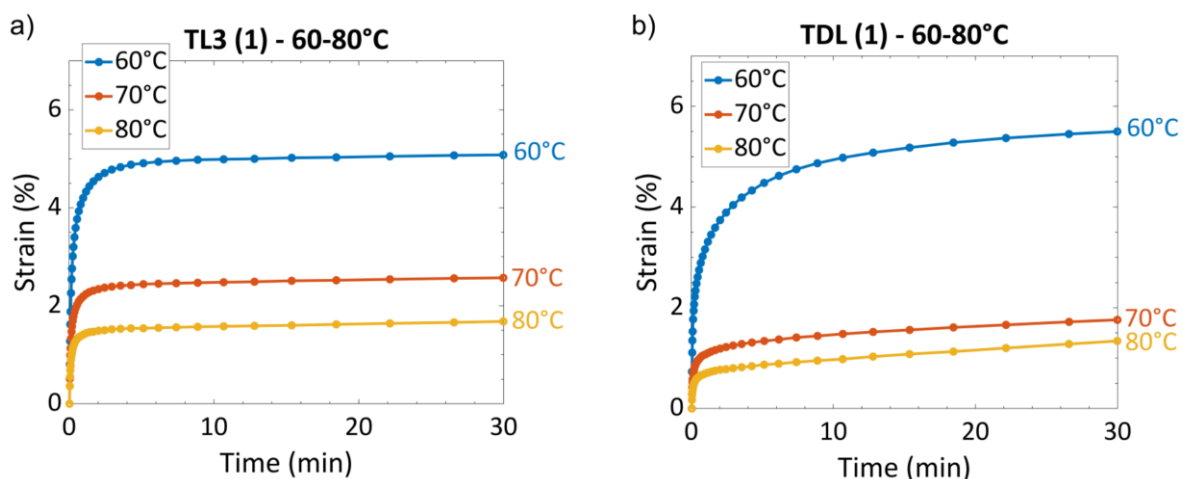


Figure C-10 Creep result between 60°C and 80°C for: (a) TL3 samples, and (b) TDL sample - The networks do not show any flow behaviour due to transesterification at these temperature.

C.4. Vitrimer properties

Creep results of first heating cycle (between 60°C and 245°C) for NC sample are shown in Figure C-11. On the overall cycle, no creep is observed showing the behavior of a traditional thermoset.

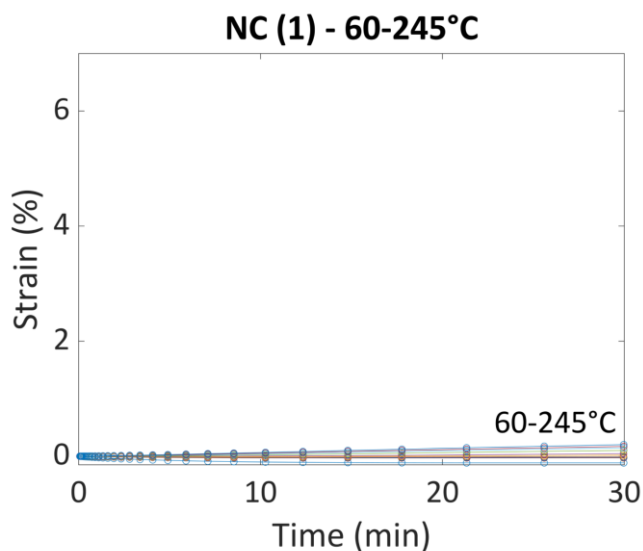


Figure C-11 First heating cycle of creep for NC sample - The sample do not exhibit any creep behaviour behaving like a thermoset material.

Creep results of first heating cycle (90-245°C) of TDL and TL3 samples are shown in Figure C-12. Both samples exhibit a complex behavior with initial increase of creep up to 140°C, which then decreases up to 245°C (re-increases from 215°C for TL3 sample). This indicates potential lipases degradation and of their interactions with the polyester network, competing with the relaxation mechanism of potential transesterification.

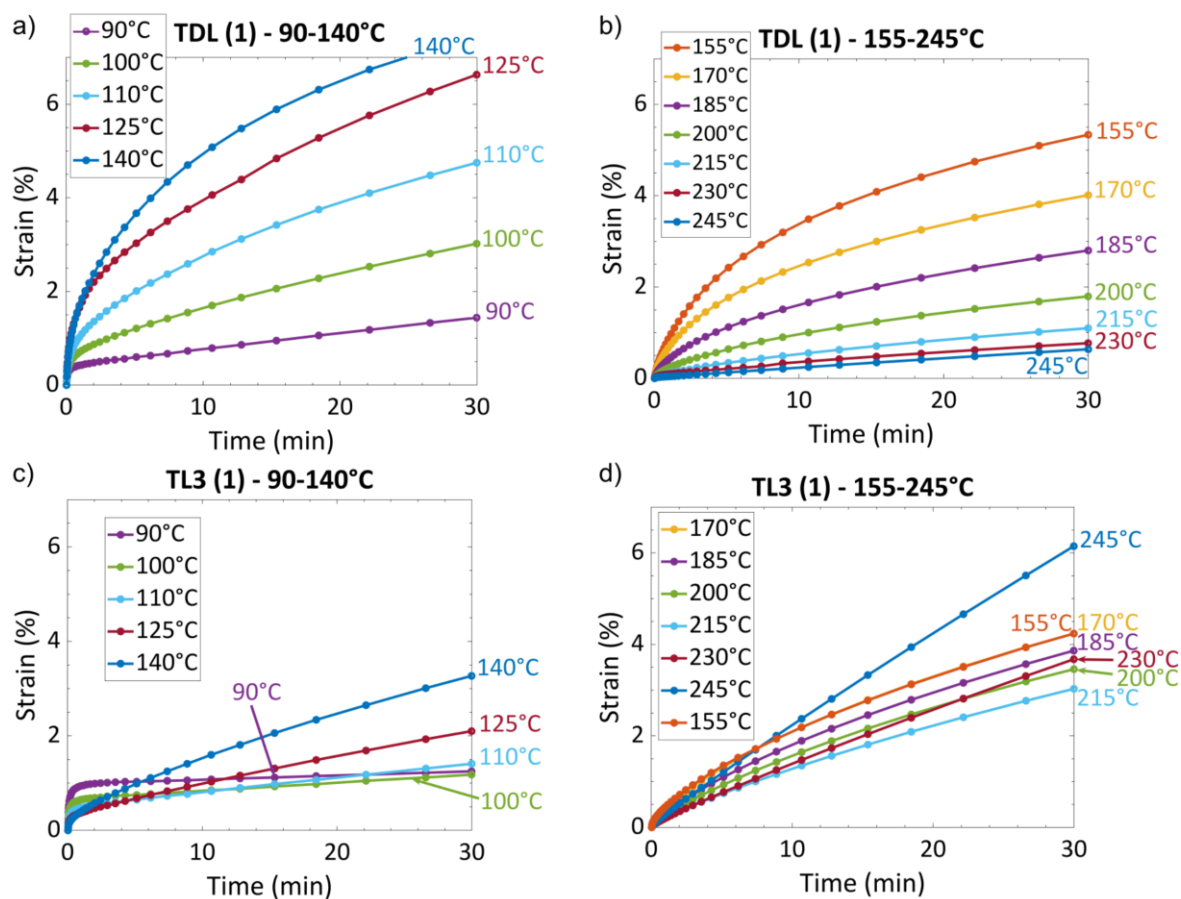


Figure C-12 Creep profile of first heating cycle for: a-b) TDL, and c-d) TL3 - The initial increase of creep between 90°C and 140°C corresponds to potential relaxation phenomenon but the material do not flow enough to be characterised the transesterification. Between 140°C and 245°C, the material creep decreases corresponding to complex degradation of lipases and interaction with the polyester network.

Creep results of second and third heating cycle (125-245°C) of NC and TDL samples are shown in Figure C-13. Both samples exhibit a thermoset behavior with no flow observed at these temperature, although TDL show a little increase at extreme temperatures (230-245°C), possibly from partial relaxation induced from the bottom phase of the sample. However, this relaxation cannot be quantify to be characterize as a vitrimer.

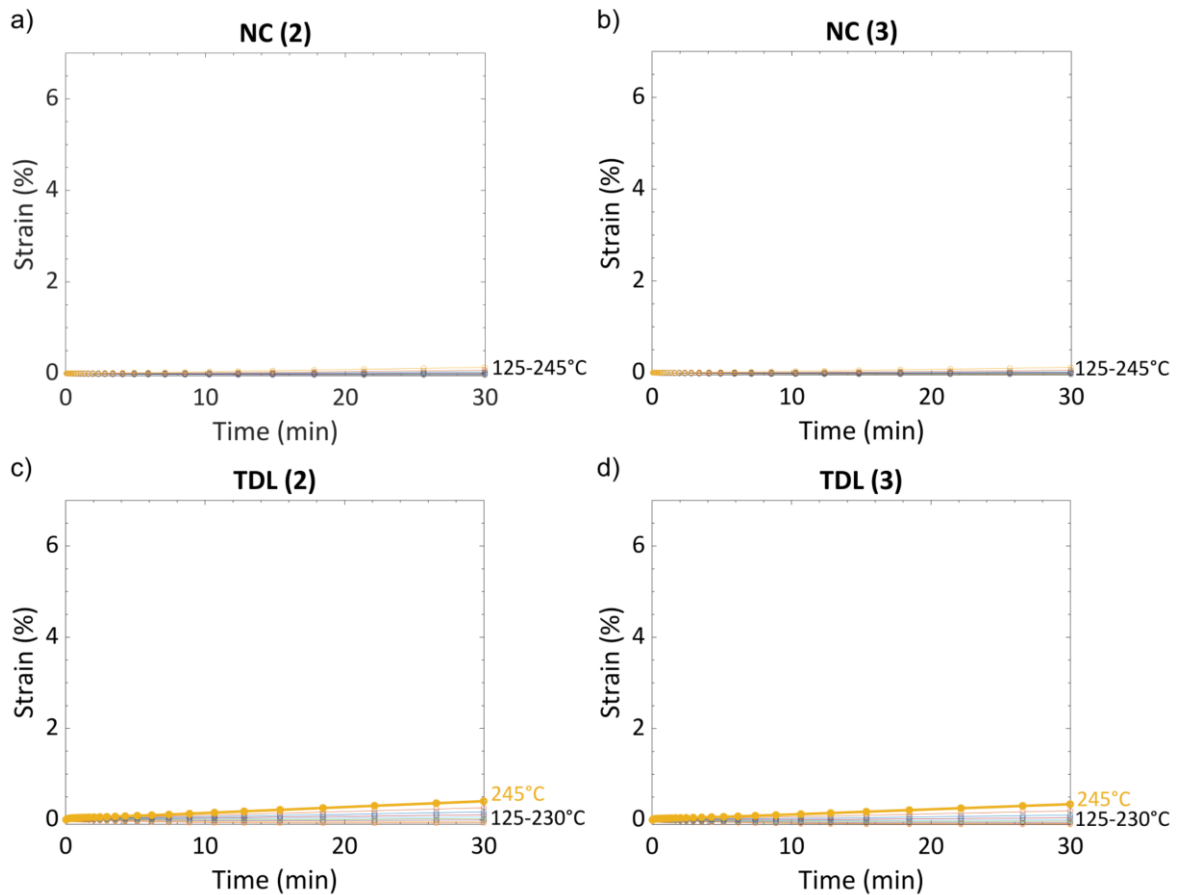


Figure C-13 Second and third creep cycle for NC and TDL samples: a) NC (2), b) NC (3), c) TDL (2), and d) TDL(3). - NC samples behaves fully like a classical thermoset, TDL shows little increase of creep at extremely high temperature probably to the amount of initial active lipases.

The fourth heating creep cycle (60-100°C) of all samples (NC, TDL, and TL3) is presented in Figure C-14. All samples behave the same, indicating there is no further difference between lipases samples and NC sample at these temperatures after thermal treatment and lipases denaturation.

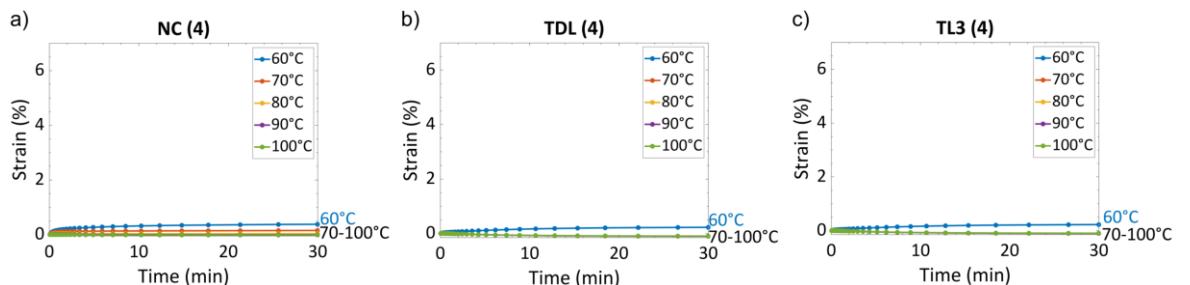


Figure C-14 Fourth creep cycle for samples: a) NC, b) TDL, and c) TL3 - all samples shows similar behaviour indicating that the lipases do not have any impact in this temperature range.

The stress relaxation results of all samples after exposition to high temperature (< 150°C for 2 h) are presented in Figure C-15. Only TL3 sample shows a relaxation time faster

with increased temperature, the calculated E_a ($\approx 55\text{kJ}\cdot\text{mol}^{-1}$) is lower than the creep calculated value. The relaxation curves were not fitting perfectly with a single exponential decay suggesting a possible heterogeneous material or different relaxation phenomenon happening in parallel to the transesterification reaction [4].

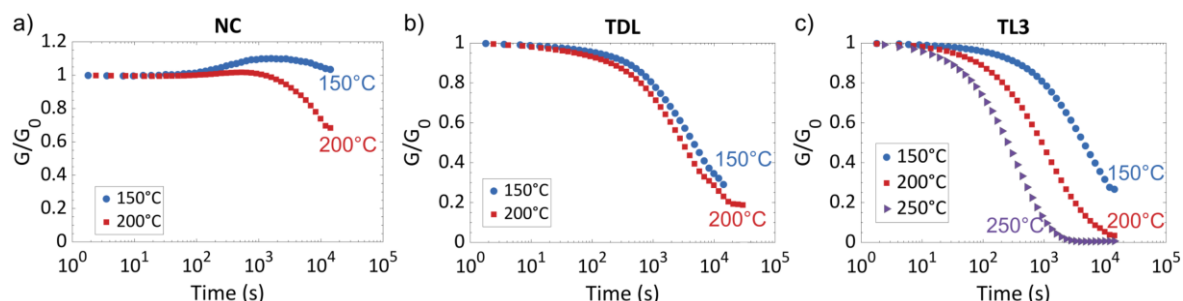


Figure C-15 Stress relaxation of samples at higher temperature for: a) NC, b) TDL, and c) TL3 - Only TL3 is able to achieved full stress relaxation and show a faster stress relaxation with increased temperature; a higher temperature (250°C) was added for TL3 in order to calculate the energy activation of the sample - $E_a \approx 55\text{ kJ}\cdot\text{mol}^{-1}$.

The FTIR data for TL3 sample with increased temperature from 100°C to 190°C are presented in Figure C-16. The only changes clearly observed is $\approx 2100\text{ cm}^{-1}$, corresponding to the C-O vibration from potential atmospheric noises. A zoom-in of these data in the 400cm^{-1} - 1790 cm^{-1} is presented in Figure C-17. No chemical structures changes can be observed in this area while the temperature is increased.

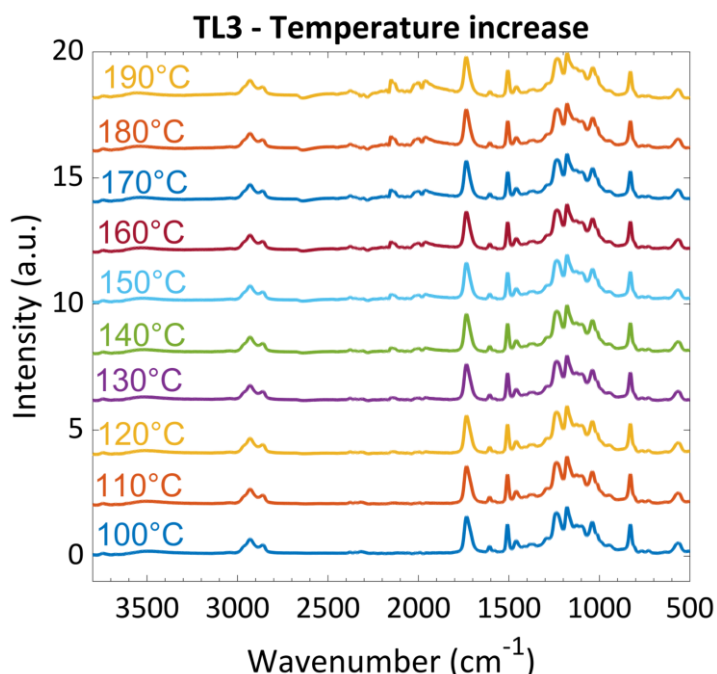


Figure C-16 FTIR spectrum of TL3 sample from 100°C to 190°C after the 72 h curing cycle - Only difference visible except from hydroxyl groups undergoing a redshift are the C-O vibration $\approx 2100\text{ cm}^{-1}$ due to atmospheric noise.

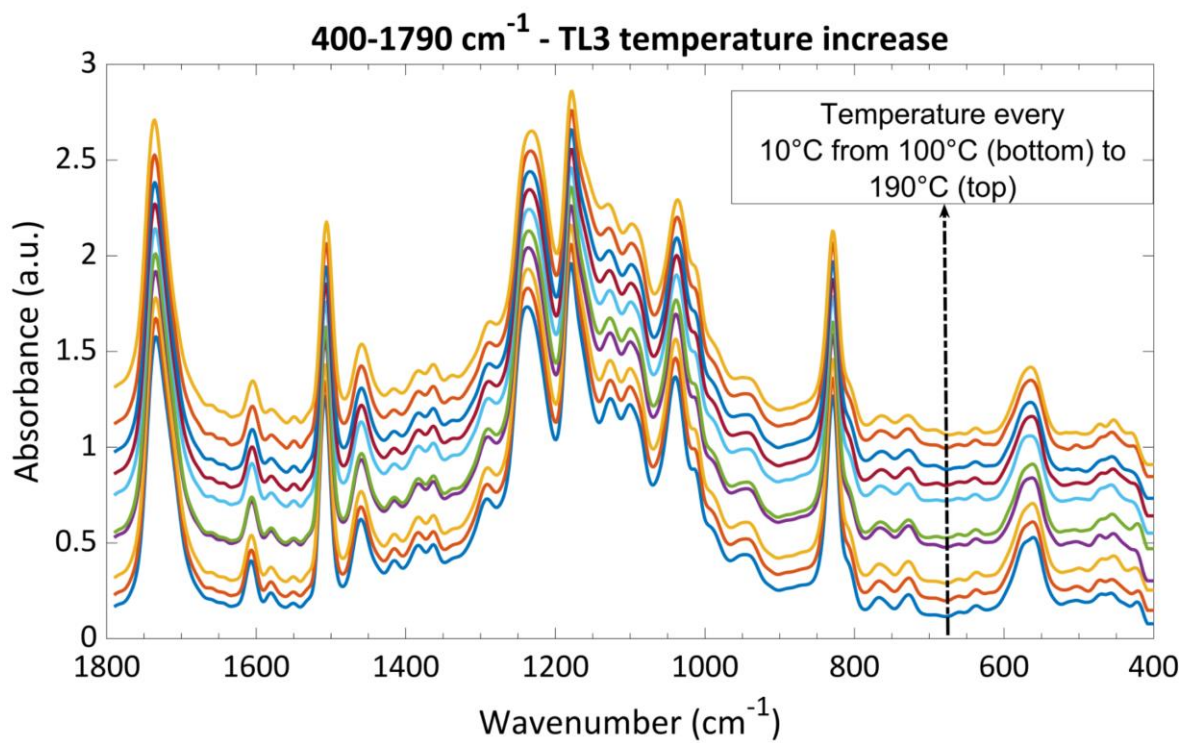


Figure C-17 Zoom-in in the 400-1790 cm^{-1} of the FTIR spectrum of TL3 sample from 100°C up to 190°C after the 72 h curing cycle - no chemical changes is observed.

C.5. References

- [1] E. Cazares-Cortes, B.C. Baker, K. Nishimori, M. Ouchi, F. Tournilhac, Polymethacrylic Acid Shows Thermoresponsivity in an Organic Solvent, *Macromolecules*. 52 (2019) 5995–6004.
- [2] A. Maraite, P. Hoyos, J.D. Carballeira, Á.C. Cabrera, M.B. Ansorge-Schumacher, A.R. Alcántara, Lipase from *Pseudomonas stutzeri*: Purification, homology modelling and rational explanation of the substrate binding mode, *J. Mol. Catal. B Enzym.* 87 (2013) 88–98.
- [3] T. Yamada, C. Morisseau, J.E. Maxwell, M.A. Argiriadi, D.W. Christianson, B.D. Hammock, Biochemical evidence for the involvement of tyrosine in epoxide activation during the catalytic cycle of epoxide hydrolase, *J. Biol. Chem.* 275 (2000) 23082–23088.
- [4] R.G. Ricarte, F. Tournilhac, M. Cloître, L. Leibler, Linear Viscoelasticity and Flow of Self-Assembled Vitrimers: The Case of a Polyethylene/Dioxaborolane System, *Macromolecules*. (2020) [acs.macromol.9b02415](https://doi.org/10.1021/acs.macromol.9b02415).

Chapter 6. General conclusions

This thesis set out to explore the polymerisation mechanisms and sustainable potential of a catalysed epoxy-sebacic acid vitrimer system *via* three different routes: The study of off-stoichiometric ratio with excess of epoxy, the addition of functionalised graphitic nanoparticles with their recovery (extraction and structural characterisation) and the novel formulation of vitrimer based on a biocatalyst.

The first route explored (Chapter 2) demonstrated the possibility to manufacture various epoxy:acyl ratios (1:1, 1:0.75, 1:0.6, 1:0.5, 1:0.3) catalysed by 5% meq of TBD without changing experimental parameters (nature of monomers, temperature and processing time), leading to the formation of epoxy-sebacic acid bulk polymers with a wide range of thermomechanical properties. The glass transition (T_g) of the network is tuned from $\approx 40^\circ\text{C}$ (ratio 1:1) to $\approx 100^\circ\text{C}$ (ratio 1:0.3) and the T_g of the network can be fitted with the Fox-Flory equation (with $T_{g1} = 39^\circ\text{C}$ and $T_{g2} = 160^\circ\text{C}$) which shows the possibility to predict the network properties ahead of its manufacture. Meanwhile the tensile properties of the network display a huge increase starting at ≈ 0.5 MPa up to ≈ 2.4 GPa showing the possibility to increase the network properties by epoxy homopolymerisation when the feeding ratio is in epoxy excess. This fact is further confirmed by damping and soluble fraction; when the epoxy is fed in excess, both of these parameters progressively decrease, indication of lower defect density in the network (*i.e.* dangling chains, oligomers, *etc.*). These results concluded that the sebacic acid for this system should be more accurately called “soft hardener” rather than hardener.

The kinetic study of the polymerisation by TBD with the different ratios (of [epoxy]/[acyl]), compared with 2-PI, showed that the anionic polymerisation of vitrimer network was not an issue during their formulation. Indeed, the results clearly show a step by step mechanism: the esterification of the network is happening prior to epoxy homopolymerisation. This indicates that the catalyst favours the vitrimer network formation (β -hydroxyesters) to then realise reinforcement *via* anionic ROP (*i.e.* epoxy homopolymerisation leading to ether without BER capability). Moreover, the study also demonstrates the limitation of such a technique to obtain a vitrimer network. Indeed, creep and stress relaxation capacity decrease with an increase of ether content. The ratio 1:1 and 1:0.75 both exhibit full relaxation; however, the energy activation (E_a) of sample

1:0.75 differs between creep and stress relaxation data ($E_{\text{acreep}} \approx 100\text{kJ}\cdot\text{mol}^{-1}$ and $E_{\text{astressrelaxation}} \approx 90\text{kJ}\cdot\text{mol}^{-1}$) while the ratio 1:1 has an $E_a \approx 100\text{kJ}\cdot\text{mol}^{-1}$ for both experimental measurements. This indicates different mechanisms are involved in the relaxation process due to the insertion of non-exchangeable bonds within the vitrimer formulation which decreases the thermo-responsivity of the sample 1:0.75. Going further in epoxy excess (1:0.6) leads to samples only partially relaxing stress ($\approx 70\text{-}95\%$). At this point stress relaxation curves cannot be fitted *via* a mono-exponential and the material is described as “vitrimer-like”. Further epoxy excess (1:0.5, 1:0.3) do not show the capability to relax enough or to have a temperature dependency which demonstrates the vitrimer behaviour is lost and transits to classical thermoset one.

It is believed that this study contributes to the understanding of the polymerisation mechanisms of vitrimer but also gives input into the behaviour of “vitrimer-like” materials. Moreover, the sebacic acid, being a sustainable and safe hardener (or “soft crosslinker”), displayed mechanical properties similar to commercial epoxy formulation without the need to alter the chemical formulation of the polymer which could be interesting for the development, at a bigger scale, of vitrimer materials and their derivatives.

The second route explored (Chapter 4) the effect of nanoparticles functionalisation and their recovery from vitrimer matrices. The use of four types of graphitic nanoparticles (GNP, GO, GPTS-GO, and rGO) were explored with different loading: 0.1 wt. %, 0.5 wt. %, and 1 wt. %. The same aforementioned technique was used to develop these materials with previous dispersion of the nanoparticles inside the epoxy resin. XRD data shows that a high functionalisation of nanoparticles (GPTS-GO and GO) induced a shift in the amorphous polymer peak attributed to potential bond within the matrix. Thermomechanical analysis shows that the T_α of the polymer is not greatly influenced by the nanoparticles ($T_\alpha \approx 33\text{-}40^\circ\text{C}$). Tensile results associated with stress relaxation data display disparate results; however, an improvement of mechanical properties was overall observed with the nanoparticles addition. The best improvement of Young’s modulus (calculated between 0% and 0.1%, E) for each particle type was found for 01GNP ($E \approx 22\text{ MPa}$), 01GO ($E \approx 63\text{ MPa}$), 05GPTS ($E \approx 55\text{ MPa}$) and 05rGO ($E \approx 95\text{ MPa}$) compared to the neat vitrimer $E \approx 2\text{ MPa}$. The lowest improvement reached by GNP particles is attributed to the poor interfacial bonding between the vitrimer and the non-functionalised nanoparticles which leads to lower load transfer when a force is applied to the

nanocomposites. GO and GPTS both exhibit a higher improvement due to their functionalisation, and the highest improvement obtained by rGO was attributed to potential charge transfer from remaining functionality. The highest overall at any loading strength (UTS) improvement was observed for GPTS samples which is believed to be the nanoparticles having both acyl and epoxide functions leading to a better bonding with the vitrimer matrix. In terms of vitrimer properties, the E_a of the nanocomposites is overall increased and oscillates between 100 kJ.mol^{-1} (1GNP) to 138 kJ.mol^{-1} (05GPTS) indicating the nanoparticles can slow the relaxation process. For further investigation, the relaxation time τ (taken at $G/G_0 = 0.37$) normalised by the modulus of each samples (E) was compared for all samples at 140°C , 160°C , and 180°C . It is apparent that the relaxation times are faster with particles addition due to a better thermal transfer and the functionalised nanoparticles (GO, GPTS-GO, and rGO) display more efficient relaxation due to introduction of free radicals such as hydroxyl and epoxides functions. However the TBD influence during cure of the polymer and potential agglomeration of the nanoparticles requires further investigation to clarify the disparate results of the bulk vitrimers.

The potential sustainable recovery of nanoparticles used in vitrimers matrix was then explored *via* network dissolution using mild condition (150°C in ethylene glycol), followed by washing in acetone and water. Both low functionality nanoparticles (GNP and rGO) exhibit a high recovery yield (calculated by recovered weight which is 92% and 93%, respectively) while high functionality nanoparticles (GO and GPTS) exhibit lower yield (73% and 48% respectively) and SEM characterisation does not show any residual vitrimer on the recovered nanoparticles. The structural changes of the nanoparticles were investigated by XPS, XRD, and Raman spectroscopy. XPS data suggest a small pollution of nitrogen due to TBD and silicon due to glassware manipulation on the recovered particles. The combination of XPS and XRD data reveal that the GNP and rGO have undergone some hydroxyl functionalisation on the edge of the nanoparticles. GPTS-GO and GO display a reduction of their functionality due to a decrease of their C-C moieties content ($\approx -11\%$ for recovered GO and $\approx -16\%$ for recovered GPTS-GO). The Raman data further confirm that the functionalisation of GNP and rGO happened on the nanoparticle edges and that GO and GPTS-GO have undergone chemical reduction of their functionality. The lower yield for these two latter nanoparticles type was attributed to the chemical reduction and the

nanoparticles were all considered to be recoverable without changing the graphitic structures.

This study has shown that the nanoparticles can be added to epoxy vitrimer matrix while producing improvement on the general polymer properties and keeping the vitrimer behaviour with various functionalisation. The improvements still require further study to confirm mechanisms of nanoparticles binding and agglomeration with the matrix for a better control of the nanocomposites' final properties. However, the sustainability of the use of particle in an epoxy vitrimer matrix is demonstrated and shows great potential for their recovery. It is believed that a careful balance needs to be maintained between functionalisation for improvement and minimal structural changes of the nanoparticles during recovery. Nevertheless, the mild condition of recovery shows an easy path to potentially recycle nanoparticles from crosslinked polymers for further use.

Eventually, the final route explored (Chapter 5) was to find a more sustainable catalyst for epoxy-carboxylic acid vitrimer formulations (sebacic acid as hardener in case of this project). The esterification of the network was successfully achieved by replacing TBD by a cheap and safe biocatalyst: lipase TL. The cure kinetic comparison between active lipase and denatured lipase shows that the active site of the lipase has a great impact on network esterification. Moreover, the lipases are required to be active to obtain a homogenous sample cure at 100°C (45°C lower than the network catalysed by TBD) using the same manufacture method developed in Chapter 3. The cure kinetic allows to propose a parallel polymerisation mechanism of the epoxy and carboxyl compound: the epoxy reacts with the amino acid Asp₃₃₃ to form an ester; meanwhile sebacic acid reacts with the rest of the active site *via* polyaddition and produces amide and water. The water is then used to hydrolyse the ester compound which can react *via* aminolysis with the amide compound. The ester is then released by the lipase active site to continue the polymerisation reaction. It is still unclear how the crosslink can be further achieved but an esterification of the hydroxyl from the produced ester are considered. The network soluble fraction is smaller than the network catalysed by TBD ($\approx 6\%$ compared to $\approx 24\%$ respectively), which indicates a higher degree of monomers conversion to ester and the higher swelling ratio ($\approx 180\%$) seems to confirm a very lightly crosslinked network. All these data confirm that the lipases TL are a much more efficient esterification catalyst than the

previously used TBD which could perform anionic homopolymerisation; and this behaviour is associated to the high regioselectivity of the enzyme.

The bulk polymer characterisation at low temperature ($< 100^{\circ}\text{C}$) interestingly demonstrated that the lipases do not perform transesterification at this temperature range, contrary to initial expectations. Instead the network shows a fast healing and reprocessing time characteristic to supramolecular networks. Reprocessing at 80°C showed a full recuperation of the tensile properties after 1 h under 10 MPa pressure ($E = 3.7 \pm 0.2$ MPa and $E = 3.3 \pm 0.6$ MPa for original and reprocessed samples respectively). These values being slightly higher than the TBD sample (2.4 ± 0.1 MPa) further confirms that some hydrogen bonding is reinforcing the material's strength as they both have the same chemical structure. A threshold temperature ($125\text{-}155^{\circ}\text{C}$) is found to denature the enzyme once they are embedded in the vitrimer. Past this threshold, the supramolecular behaviour is lost revealing a vitrimer behaviour with lower activation energy than the TBD-catalysed system (≈ 70 kJmol^{-1} compared to 100 $\text{kJ}\cdot\text{mol}^{-1}$ for TBD system). FTIR data suggest that the network does not undergo any chemical change during the switch from supramolecular to vitrimer network, and an additional hydroxyl peak (not present in any TBD and graphene formulations) was attributed to the enzyme backbone interacting together. It was concluded that, once the temperature is high enough, the network can undergo transesterification without the help of a catalyst due to the high amount of free hydroxyl functions within the network as previously reported for hyperbranched glycerol vitrimer formulations.

This study demonstrates the capability to use lipases as a biocatalyst for the esterification of epoxy and sebacic at low temperature (100°C) and create a vitrimer network. Moreover, the network displays new supramolecular properties compared to classic vitrimer allowing to heal and reprocess the network at 80°C . This added functionality entirely due to the enzyme complex nature still requires further understanding, but has led this new polymer network to be called 'enzymers'.

To conclude, this thesis demonstrated the sustainable potential of vitrimers using three distinct routes:

1. Using a safe and environmentally-friendly hardener (sebacic acid) to tune the mechanical properties of the vitrimer *via* a simple method taking advantage of the secondary reaction induced by the vitrimer catalyst
2. Showing the implementation and recovery of nanoparticles is feasible using mild condition with a high yield of recovery for low functionality nanoparticles. Despite structural changes, it is believed that these nanoparticles could be re-used as new reinforcements in other applications but can at least be safely remove from the crosslinked polymer at the end of its life
3. Using a lipase as biocatalyst, demonstrating the possibility to replace traditional Lewis acid or acid base in these formulations by a cheap and safe catalyst. The produced network is determined by the high regioselectivity of the enzyme and also has the capacity to be cured, healed or reprocessed at 100°C or below making it interesting for lower energy impact compared to traditional vitrimer formulations.

The author of this thesis strongly believes that this project, despite an already impressive interest from the scientific community, demonstrates vitrimers have still more to reveal and are only at the early stage of development of their incredible potential.

Chapter 7. Further work

As the vast majority of any research projects, this thesis has risen more questions to seek answers to than it answered. Therefore, this part is dedicated to suggestion routes to further understand and exploit some of these findings and questions. This chapter is organised following each experimental chapters: (i) the off-stoichiometric study of the epoxy-sebacic acid network formation and reinforcement, (ii) The effect of graphitic nanoparticles and their recovery, and (iii) the formation of enzymer *via* sustainable enzymatic catalysis.

7.1 Dicarboxylic acid-epoxy vitrimers: influence of the off-stoichiometric acid content on cure reactions and thermo-mechanical properties

The first study showed the capability to increase the T_{α} of the network *via* epoxy homopolymerisation when the epoxy was fed in excess compared to the acyl function and see the limitation to obtain a vitrimer network. It would be therefore, interesting to study the network formation in the other way of the spectrum (*i.e.* an acyl feeding excess compared to epoxy). This would determine if the T_{α} could be decreased compared to the 1:1 epoxy:acyl ratio and determine to which extent a vitrimer material can be obtained. Furthermore, the kinetic mechanism could reveal if other polymerisation mechanisms, such as Fischer esterification, take place. Moreover, the ratio threshold (1:0.6) determined with the sebacic acid system might be different with different hardener length (*e.g.* dodecanoid acid) and it would be interesting to study this behaviour on various hardener lengths or configuration. This also deserves to be thoroughly investigated with anhydride acid compounds as they have been mentioned to be more relevant in these kind of formulations (see section 2.8.1 for more information).

Interestingly the 2-PI catalyst, known to be an anionic ROP catalyst was found to perform in the same way as TBD in off-stoichiometric formulations: esterification of the network followed by reinforcement of the network *via* epoxy homopolymerisation. It would be worth studying a combination of the two catalysts (TBD and 2-PI) in various vitrimer systems to see if shorter curing time and/or lower curing temperature could be achieved and if the vitrimer properties could be obtained similar to those with TBD alone.

Finally, the stress relaxation was found to not be perfectly fit for 1:0.75 ratio and other vitrimer-like formulations. It would be beneficial for the vitrimer field to develop relaxation models adapted to these different mechanisms, in order to separate the vitrimer relaxation from other relaxation modes and be able to calculate, accurately, the energy activation of each vitrimer formulation.

7.2 Graphene epoxy based vitrimer: From matrix properties enhancement to sustainability via nanoparticles recovery

The graphene study revealed disparate results on tensile properties but also on the relaxation mechanisms associated with the vitrimer network. Despite an overall improvement, a thorough study of the impact of catalysts on chemical changes and agglomerations of nanoparticles during the cure is needed to further understand this behaviour. The nanoparticles structure should be investigated at each stage of the manufacture process (post dispersion, after mixing for 24 h, after degassing, and during cure before/during gelation of the network) in the same manner that they have been characterised in chapter 4 (XPS, XRD, Raman, and SEM) but also with FTIR, DLS, (dynamic light scattering), and AFM. Thermal characterisation of the bulk nanocomposites (homogeneity of the thermal diffusivity) should also be performed to study their agglomerations. The author would like also to point the idea to use SThM (scanning thermal microscopy) with AFM to measure the thermal energy of the bonds between vitrimer/nanoparticles and nanoparticles/nanoparticles. This technique can also be used to map surface and inside of the bulk nanocomposites to study potential agglomeration and build a 3D image of these types of nanocomposites. Once these parameters have been further understood, the use of a solvent and better dispersion technique could be adapted for each particle type - this solvent would have to be carefully chosen to lower its interaction with the vitrimer chemistry (if left during the components mixing stage).

As for chapter 3, the nanoparticles led to more complex relaxation modes in the vitrimer network. Therefore a thorough study of comparison between creep and stress relaxation experiments associated with some multi scale modelling or molecular dynamic of the bond energy is necessary to understand better the effect of these nanoparticles on the vitrimer matrix.

7.3 Enzymer: sustainable enzymatic catalysis to produce new supramolecular thermoset quenchable to vitrimer material

The last experimental chapter (chapter 5) is probably the most interesting regarding the questions risen for both its curing mechanism but also its bulk behaviour.

In the proposed polymerisation mechanism, it was suggested that either the His₅₄ or Ser₁₀₉ could react with the sebacic acid. A small molecules study using FTIR and also C-NMR could show and confirm this assertion that is responsible for the amidification of the sebacic acid. Furthermore, a modelling of the active site size and the distance between each reactant (active site, epoxy and sebacic acid), could give information on the polymerisation mechanism. This small molecule study could be performed with sebacic acid but also with other dicarboxylic acids with lower melting temperature ($\approx 100^{\circ}\text{C}$) in order to facilitate the study and also observe the FTIR evolution of the hardener with lipases alone. It would allow to manufacture enzymer with this new hardener and observe if similar properties are obtained for the bulk polymer with other hardener types. An H/C NMR study of dissolute bulk vitrimers will be required to see if the enzyme bonds between each and/or the vitrimer network.

The supramolecular behaviour requires further investigation to find out its origin. Various methods can be used such as solid state H-NMR compared to vitrimer catalysed by TBD. Additionally, a study of healing and reprocessing at various temperature ranges need to be performed to determine the role of the active site in the supramolecular behaviour (from RT to the lipases degradation temperature). A colorant can be added in the formulation to observe the interface evolution during reprocessing and healing. Curing at various temperatures (from 60°C to 155°C with a 5°C or 10°C step) needs to be performed to determine the threshold beyond which supramolecular behaviour can no longer be observed. Also, the lipases may be labelled with fluorescent markers and the agglomeration and bonding types may be observed *via* fluorescent microscopy. All these characterisations may be used for determining vitrimer behaviour at higher temperatures. It would be also interesting to use different enzymes to determine the impact of the potential free hydroxyl group generated by their backbones.

Other formulation also needs to be investigated; for example, a fully bio-based vitrimer could be produced using ESO. However, the most interesting part would be to

develop a vitrimer network to combine supramolecular and vitrimer behaviour below 100°C which would allow to keep the enzyme active site without losing supramolecular behaviour to obtain the vitrimer network. Further investigation of better enzyme stabilisation (i.e. enzyme not denaturing at 200°C) needs to be also considered to obtain high temperature network with both behaviours.

Questions arise regarding the kind of applications that enzymer could be most suited for. For example, the supramolecular network has the potential to be used for 3D printing of complex structures but this needs to be investigated. Moreover, epoxy and sebacic acid are both known to be biocompatible to some extent. The production of vitrimer network based on enzymatic catalysis should be considered for potential bio-applications such as stent or small implants.